

I. DETERMINATION OF ABSOLUTE CONFIGURATION OF CHIRAL 1,2-DIOLS
II. PROGRESS TOWARDS THE TOTAL SYNTHESIS OF NAPYRADIOMYCIN A1

By

Saeedeh Torabi Kohlboundi

A DISSERTATION

Submitted to
Michigan State University
in partial fulfillment of the requirements
for the degree of

Chemistry–Doctor of Philosophy

2022

ABSTRACT

- I. DETERMINATION OF ABSOLUTE CONFIGURATION OF CHIRAL 1,2-DIOLS
- II. PROGRESS TOWARDS THE TOTAL SYNTHESIS OF NAPYRADIOMYCIN A1

By

Saeedeh Torabi Kohlouni

This dissertation focuses on two parts. The first part introduces an operationally simple and microscale method for the absolute stereochemical determination of 1,2-diols. In situ derivatization of 1,2-diols with dinaphthyl borinic acid generates the induced helicity of the two naphthyl groups, which leads to an observable ECCD spectrum. The observed *P* or *M* helicity follows a predictable trend for *S* and *R* chiral 1,2-diols, respectively.

The Second chapter is the progress towards the asymmetric catalytic synthesis of napyradiomycin A1. The chapter is divided to three sections. The first section is installation of chlorine chiral center at C3. This goal is achieved using cinchona chiral catalyst, and DCDMH as chloronium source. The second section is the synthesis of the α -lapachone core of napyradiomycin A1, was accomplished using Diels-Alder/aromatization cascade reaction. The last section shows our effort toward the attachment of geranyl side chain.

I dedicate my dissertation to my dearest parents, my sisters, Somayeh and Zahra, my nephew, Nikan, and my lovely husband, Aliakbar, for all their support, love and always believing in me

ACKNOWLEDGMENTS

I would like to express my gratitude to my advisor for six years of support. I am also thankful to my committee members, Professor William Wulff, Professor Robert Maleczka and Professor Melanie Cooper for their help and suggestion during my graduate program in Michigan State University.

I would like to express my most sincere gratitude and appreciation to my Ph. D. advisor, Professor William Wulff, for his endless support, continuing encouragement, and kind guidance and advise.

I would like to thank all the members of the Borhan group for their invaluable help and support and friendship during my graduate school. I especially would like to thank Dr. Chrysoula Vasileiou for her limitless support and help. I have had the pleasure and privilege of working with most of the current and former members of Borhan group, to that extend, I am thankful to all of them. I am very thankful to all my talented undergraduate students, Ian, Natasha, and Adam for helping me with the research.

Saving best for last, I am thankful for my dad, my mom, my sisters, my nephew, and my lovely husband. Their unconditional love and support have been my driving force in my daily life. I would not be standing here if it was not because of their support and encouragements.

TABLE OF CONTENTS

LIST OF TABLES	x
LIST OF FIGURES	xi
Chapter I - Determination of Absolute Configuration of Chiral 1,2-Diol	1
I-1 Introduction.....	2
I-2 Conventional methods for the stereochemical determination of chiral molecules.....	5
I-2-1 X-ray crystallography	5
I-2-2 Mosher ester analysis	6
I-2-3 Chiroptical spectroscopy for stereochemical determination of chiral organic molecules	9
I-3 Exciton Coupled Circular Dichroism (ECCD)	18
I-4 Conventional method for stereochemical determination of vicinal diols	24
I-5 Absolute stereochemical determination of 1,2-diols via complexation with dinaphthyl borinic acid	28
I-6 Conformational analysis	38
I-7 Conclusion.....	41
Chapter II – Towards the Total Synthesis of Napradiomycin A1	43
II-2 A survey of previous total synthesis of napradiomycin	44
II-3 Enantioselective synthesis of napradiomycin A1	46
II-4 Enantioselective synthesis of azamerone	47
II-4 Divergent synthesis of napradiomycin family.....	49
II-5 Retrosynthesis of α -lapachone II-52	56
II-6 Synthesis of α -lapachone derivative	57
II-7 Synthesis of Ring A	71
II-8 Attachment of geranyl side chain	73
II-8-1 Prediction of diastereoselectivity using theoretical calculations	73
II-8-2 Experiment Investigating the geranyl side-chain attachment	75
II-8-3 Michael addition of allyl organocuprate to quinone	76
II-9 Semipinacol rearrangement as a possible solution for C10a allylation	83
II-9-1 1,2-Rearrangement of epoxides	85
II-9-2 1,2-migration of 2,3-epoxy alcohols.....	86
II-10 Rearrangement of allylic alcohols induced by chloronium ion.....	89
II-11 New pathway for attachment of the geranyl chain.....	91
II-12 Summary	92
Chapter III – Experimental Section	93
III-1 Materials and general instrumentations.....	94
III-2 CD measurements.....	94
III-3 CD spectra.....	95

III-4 Synthetic procedures	98
III-4-1 Di(1-naphthyl) borinic acid ¹¹⁴	98
III-4-2 Typical procedure for synthesis of chiral diols using Sharpless asymmetric dihydroxylation (SAE).....	99
III-4-3 1-Bromo-4-vinylbenzene (I-51).....	99
III-4-4 (<i>R</i>)-1-(4-Bromophenyl) ethane-1,2-diol (I-41).....	100
III-4-5 1-(Trifluoromethyl)-4-vinylbenzene (I-52).....	100
III-4-6 (<i>R</i>)-1-(4-(Trifluoromethyl) phenyl) ethane-1,2-diol (I-42).....	101
III-4-7 (<i>R</i>)-1-(Naphthalen-2-yl) ethane-1,2-diol (I-43).....	102
III-4-8 (<i>R</i>)-1-Cyclohexylethane-1,2-diol (I-44).....	102
III-4-9 (<i>S</i>)-2-Phenylpropane-1,2-diol (I-45).....	103
III-4-10 (<i>S</i>)-1-Phenylethane-1,2-diol (I-46).....	103
III-4-11 (<i>S</i>)-3-Methylbutane-1,2-diol (I-47).....	104
III-4-12 (<i>R</i>)-2-Phenylpropane-1,2-diol (I-53).....	104
III-4-13 (<i>R</i>)-2-Hydroxy-2-phenylpropyl 4-methylbenzenesulfonate (I-54).....	105
III-4-14 (<i>R</i>)-1-Azido-2-phenylpropan-2-ol (I-55).....	105
III-4-15 (<i>R</i>)-1-Amino-2-phenylpropan-2-ol (I-50).....	106
II-5 Extinction coefficient measurement	106
III-6 Napyradiomycin experimental section	115
III-6-1 6,4-Bromo-2,5-dimethoxybenzaldehyde (II-57).....	115
III-6-2 4-Bromo-2,5-dimethoxyphenol (II-59).....	116
III-6-3 1,1-Dimethyl-prop-2-ynyl methyl carbonate (II-61).....	117
III-6-4 1-Bromo-2,5-dimethoxy-4-((2-methylbut-3-yn-2-yl)oxy)benzene (II-62).....	118
III-6-5 5,5'-((6-Methylhepta-2,4-diyne-1,6-diyl)bis(oxy))bis(2-bromo-1,4-dimethoxybenzene) (II-63).....	119
III-6-6 1-Bromo-2,5-dimethoxy-4-((2-methylbut-3-en-2-yl)oxy)benzene (II-68).....	120
III-6-7 4-Bromo-3,6-dimethoxy-2-(3-methylbut-2-en-1-yl)phenol (II-69).....	121
III-6-8 4-Bromo-2,5-dimethoxyphenyl (2-methylbut-3-en-2-yl) carbonate (II-76).....	121
III-6-9 1-Bromo-2,5-dimethoxy-4-((3-methylbut-2-en-1-yl)oxy)benzene (II-155).....	122
III-6-10 Decarboxylative allylic etherification and tandem aromatic Claisen of II-76 carbonate.....	123
III-6-11 6-Bromo-3-chloro-5,8-dimethoxy-2,2-dimethylchromane (II-84).....	123
III-6-12 (<i>R</i>)-6-Bromo-3-chloro-2,2-dimethyl-3,4-dihydro-2 <i>H</i> -chromene-5,8-dione (II-85).....	125
III-6-13 Methyl (<i>E</i>)-3-methoxybut-2-enoate (II-156).....	126
III-6-14 (<i>E</i>)-((1,3-Dimethoxybuta-1,3-dien-1-yl)oxy)trimethylsilane (II-98).....	126

III-6-15 (<i>R</i>)-3-Chloro-6-hydroxy-8-methoxy-2,2-dimethyl-3,4-dihydro-2benzo[<i>g</i>]chromene-5,10-dione (II-99)	127
III-6-16 (<i>R</i>)-3-Chloro-6,8-dimethoxy-2,2-dimethyl-3,4-dihydro-2 <i>H</i> -benzo[<i>g</i>]chromene-5,10-dione (II-100)	128
III-6-17 (3 <i>R</i>)-10-Allyl-3-chloro-10-hydroxy-6,8-dimethoxy-2,2-dimethyl-2,3,4,10-tetrahydro 5 <i>H</i> -benzo[<i>g</i>]chromen-5-one (II-119/126).....	129
III-6-18 (3 <i>R</i> ,10 <i>R</i>)-10-Allyl-3-chloro-6,10-dihydroxy-8-methoxy-2,2-dimethyl-2,3,4,10 tetrahydro-5 <i>H</i> -benzo[<i>g</i>]chromen-5-one (II-133).....	132
III-6-19 (10-Allyl-3-chloro-6,10-dihydroxy-8-methoxy-2,2-dimethyl-2,3,4,10-tetrahydro-5 <i>H</i> -benzo[<i>g</i>]chromen-5-one (II-135).....	133
III-6-20 3a-Allyl-8-hydroxy-6-methoxy-2,2-dimethyl-1a,2-dihydro-1 <i>H</i> ,9 <i>H</i> -cyclopropa[<i>c</i>]naph -tho[2,3- <i>b</i>]furan-4,9(3a <i>H</i>)-dione (II-135)	133
III-6-21 1-Allyl-5'-chloro-1-hydroxy-4,6-dimethoxy-6',6'-dimethyl-5',6'-dihydrospiro[indene-2,2'-pyran]-3,3'(1 <i>H</i> ,4' <i>H</i>)-dione (II-141)	134
III-6-22 1-Allyl-1-hydroxy-4,6-dimethoxy-6',6'-dimethylspiro[indene-2,2'-pyran]-3,3'(1 <i>H</i> ,6' <i>H</i>) -dione (II-142).....	135
III-6-23 8-Allyl-6-bromo-3-chloro-8-hydroxy-2,2-dimethyl-2,3,4,8- tetrahydro-5 <i>H</i> -chromen-5-one (II-151).....	136
III-6-24 3-Methoxycyclohex-2-en-1-one (II-160)	137
III-6-25 Tert-butyl((5-methoxycyclohexa-1,5-dien-1-yl)oxy)dimethylsilane (II-161)	138
III-7 NMR spectra	139
REFERENCES	205

LIST OF TABLES

Table I-1 ECCD data for DBA -derivatives	32
Table I-2 ECCD data for DBA -derivatives	33
Table II-1 Optimization of the Claisen rearrangement	59
Table II-2 Effect of solvent and chloronium ion source	64
Table II-3 Effects of temperature and various additives.....	65
Table II-4 Solvent screening for chloroetherification reaction	68
Table II-5 Asymmetric chloroetherification in the presence of cinchona alkaloids.....	70
Table II-6 Optimization of Diels-Alder/Aromatization	73
Table II-7 Optimization of 1,2-allyl under basic condition	79
Table II-8 Optimization of 1,2-allyl migration of unprotected quinol under acidic and basic conditions	80
Table II-9 Nucleophilic ring opening of cyclopropane with the chloride ion	81

LIST OF FIGURES

Figure I-1 Different scenarios of molecular chirality. a. Point chirality. b. axial chirality. c. helical chirality.	2
Figure I-2 Representative enantiomers possess different properties.	3
Figure I-3 Synthesis of R- and S-Mosher esters.	5
Figure I-4 Representative conformers of Mosher diastereomer I-6S/R used to indicate the shielding effect of the phenyl group.	6
Figure I-5 Light as an electromagnetic radiation.	9
Figure I-6 a. Circularly polarized light. b. Left-handed circularly polarized light. c. Right-handed circularly polarized light.	10
Figure I-7 a. Left and Right components of the plain polarized light b. Generation of the elliptically polarized light due to the difference in absorption of the left and right circularly polarized light by chiral matters.	13
Figure I-8 a. Positive and b. negative CD spectra or Cotton effects.	14
Figure I-9 Pictorial description of "right hand rule" to determine the direction of magnetic dipole transition moment.	15
Figure I-10 Schematic representation of a CD spectropolarimeter.	16
Figure I-11 Splitting of the excited state of the isolated chromophores by exciton interaction.	18
Figure I-12 The a. UV and b. ECCD spectrum of two degenerate chromophores interacting through space.	19
Figure I-13 Exciton interaction of edtm of two chromophores (in-phase and out-of-phase) result in a bisignate CD curve.	20
Figure I-14 Derivatization of two enantiomeric diols result in ECCD spectra with two opposite signs.	21

Figure I-15 Stereochemical determination of threo diols.	24
Figure I-16 Steric configuration of molybdenum complex and its effect on dihedral angle of the cottonogenic derivative.	25
Figure I-17 Spiro dioxolane formation of chiral diols leads to CD active complex.	26
Figure I-18 Main transition dipoles of the <i>R</i> -configured phenyl substituted boronate complex.	27
Figure I-19 Conformational diastereomers of (<i>R,R</i>)-diols. The solid box represents the hydrogen above the ring while the dashed box indicates the hydrogen below the ring. 27	
Figure I-20 Use of porphyrin tweezers to interrogate the absolute stereochemistry of threo and erythro diols.	28
Figure I-21 a. Derivatization of chiral amines with BDN b. Esterification of di(1-naphthyl) methanol (DNM) with asymmetric carboxylic acid.	29

Chapter I - Determination of Absolute Configuration of Chiral 1,2-Diols

I-1 Introduction

The term "chirality" is originally from a Greek word that means hand. The general definition of chirality is that the object is chiral if it cannot be superimposed on its mirror image.¹ Our hands are one of the simple examples of chirality in nature. The definition of chirality at the molecular level extends from the same concept where mirror images of a structure are nonsuperimposable. Two mirror images of the non-superimposable molecules are called enantiomers. There are a number of ways to define a chiral molecule, but all of them follow the same rule, absence of plane of symmetry.

Molecular chirality is classified into two categories: point chirality and axial chirality. An example of point chirality is illustrated in Figure I-1. The carbon with sp^3 hybridization is attached to four different groups generating a chiral carbon center. The actual spatial arrangement of the groups around the chiral center is defined as configuration.

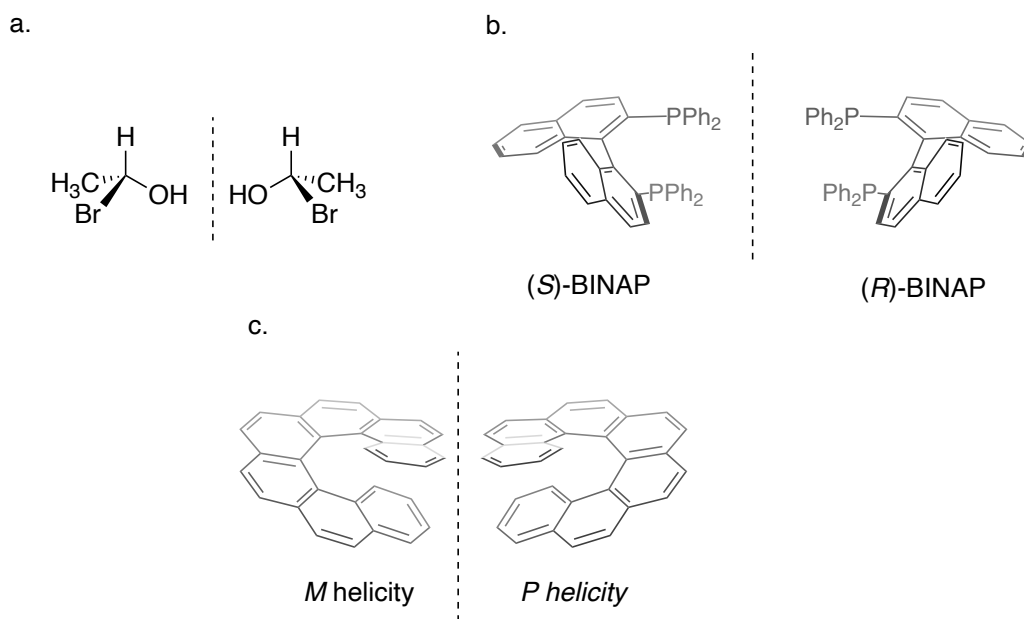


Figure I-1 Different scenarios of molecular chirality. a. Point chirality. b. axial chirality. c. helical chirality.

Configuration of the chiral center is determined using the letters *R* and *S*. Cahn-Ingold-Prelog priority rules are used to name the absolute configuration of the chiral center (Figure I-1a).²

The second category is classified as axial chirality. Axial chirality possesses a chiral axis instead of a chiral center. The spatial arrangement of the ligands around this axis generates a chiral molecule that is not superposable on its mirror image. One of the most common family of axially chiral compounds are substituted biaryl molecules. The rotation around the aryl-aryl ring is restricted due to the steric hindrance of substitution on the aryl rings. The two enantiomers of an axially chiral molecule are called atropisomers (Figure I-1b). Another class of chiral molecules is helical chirality. This chirality is induced by the spiral arrangement of the molecular frame.¹ Depending on the arrangement, the helix

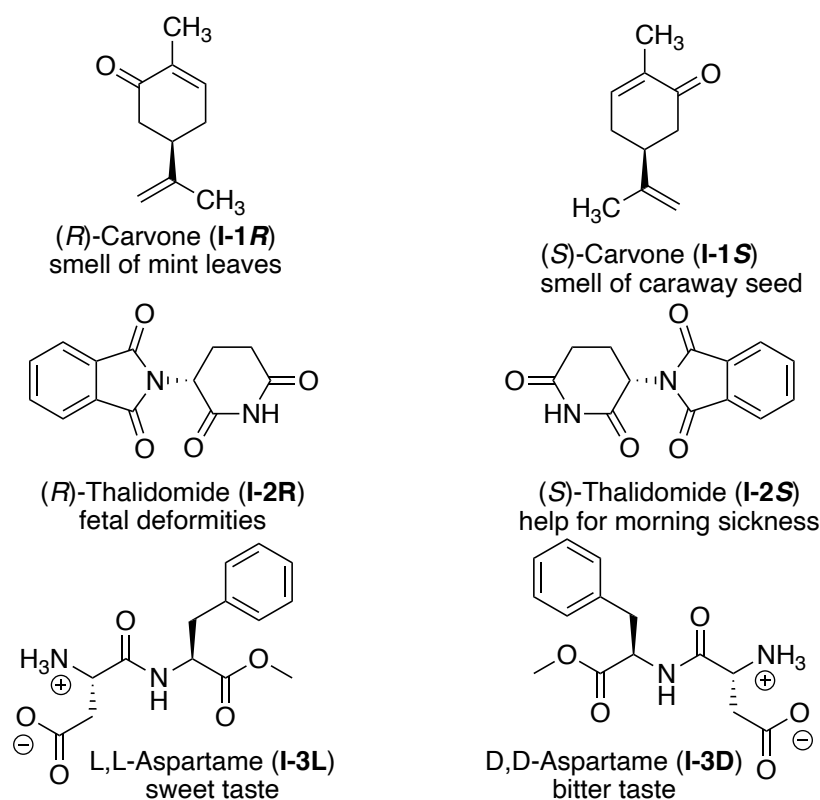


Figure I-2 Representative enantiomers possess different properties.

could be defined as either left-handed or right-handed. As shown in Figure I-1c, even though these molecules do not have asymmetric carbons, they are chiral due to the lack of a plane of symmetry.

Life is affected by chirality. The compounds of living organisms are exclusively in one form of chirality (homochirality). Most of the natural amino acids are in the L-form; however, the relevant active forms of the sugars are in their D-form. Enzymes are chiral, which means they provide an asymmetric environment for interaction.³ Two enantiomers of a chiral molecule can interact differently with a chiral environment. For example, they result in different tastes or smells. For instance, carvone exists in two enantiomeric forms. (*R*)-carvone is the major contributor to the smell of mint leaves, while (*S*)-carvone smells like caraway seed. Another example is L,L-aspartame, an artificial sweetening agent 200 times sweeter than sucrose, and yet, its enantiomer has a bitter taste.⁴ The importance of chirality is more significant when the chirality is embedded in pharmaceutical products. Major commercial pharmaceutical compounds are chiral. Drugs prepared from naturally occurring sources and material are in one form of the enantiomer. Nevertheless, the synthetically produced drugs from achiral starting material are in their racemic mixture. Until 1970, most chiral commercialized medicines were sold in their racemic format, even though their medicinal feature came from one of the enantiomers. Mostly, the other enantiomer did not show any biological activity. In the 1960s, a racemic mixture of thalidomide was sold and prescribed to pregnant women to help with their morning sickness. The *S* enantiomer showed the desired activity, but *R* enantiomer resulted in fetal deformities and abnormalities.⁵ Tragic events such as this led the pharmaceutical

industry to realize the importance of chirality and drug activity, and nowadays, most chiral drugs are developed as one enantiomer. Besides the pharmaceutical industry, other industries such as agriculture consider molecular chirality as a critical issue. As a result, finding a simple and effective method for determining the absolute configuration of chiral molecules has witnessed tremendous attention.

I-2 Conventional methods for the stereochemical determination of chiral molecules

I-2-1 X-ray crystallography

X-ray crystallography provides one of the most straightforward methods for defining the absolute stereochemistry of chiral molecules.⁶ A complete stereochemical analysis of the chiral molecule can be achieved in a single experiment using X-ray crystallography. Still, this method is accompanied with some drawbacks which are hard to overcome. One limitation is the necessary presence of heavy atoms such as bromine in the structure of the chiral substrate. Another issue that decreases the number of potential substrates for this analysis is that not all the organic compounds can be crystallized. Besides, not all of them generate a single crystal necessary for X-ray crystallography. One might be able to improve the crystal quality of the molecule using derivatizations. These requirements limit

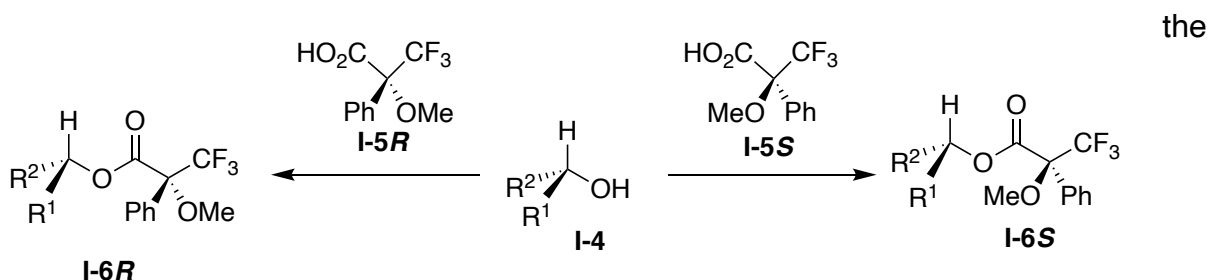


Figure I-3 Synthesis of R- and S-Mosher esters.

applicability of X-ray analysis for the determination of the absolute stereochemistry of chiral molecules. Therefore, new method development for assigning the configuration of chiral compounds is one of the research areas of interest.

I-2-2 Mosher ester analysis

A basic and essential property of the chiral compounds is the absolute configuration of the asymmetric center.⁷⁻¹⁰ One of the most common techniques to establish the absolute configuration of chiral molecules is the Mosher ester analysis. In this method, used for alcohols and amines, the chiral molecule with an unknown configuration is derivatized with two enantiomers of a chiral aryl carboxylic acid with a known

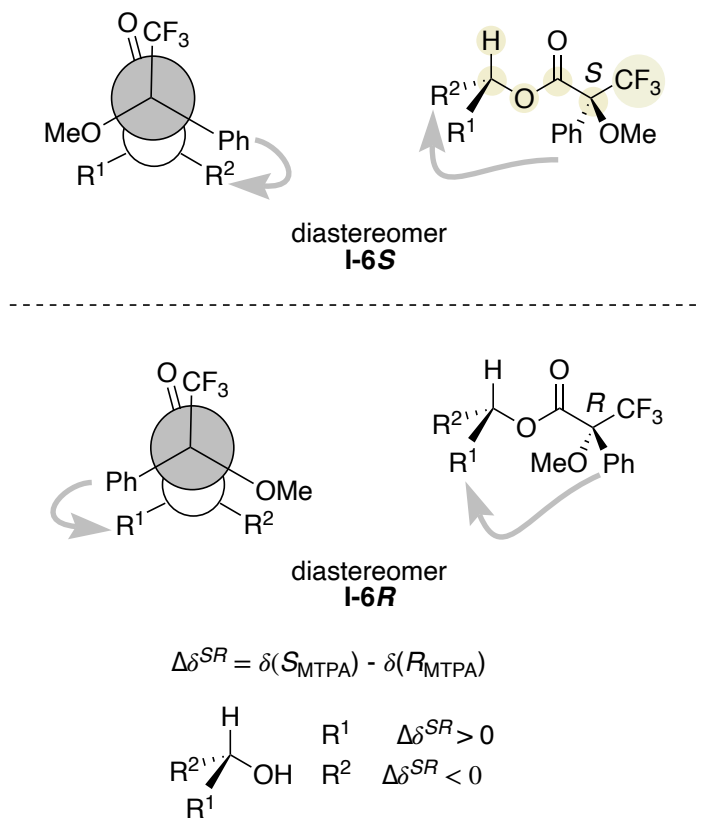


Figure I-4 Representative conformers of Mosher diastereomer **I-6S/R** used to indicate the shielding effect of the phenyl group.

configuration that generates two diastereomers. Although various chiral carboxylic acids have been employed to derivatize chiral 2° alcohols, α -methyl- α -trifluoromethylphenyl acetic acid (MTPA-OH), known as Mosher's acid, has been widely used for derivatization.¹¹⁻¹³ As mentioned before, Mosher ester analysis starts with the formation of two diastereomeric esters resulting from the coupling of the alcohol with both enantiomers of Mosher's acid. Diastereomers possess different spectroscopic properties, and their ¹HNMR spectra differ. Therefore, one could determine the absolute configuration of the chiral alcohol or amine using the difference in chemical shift of hydrogen atoms present on the substitutions (R₁, R₂) of the chiral center. This difference results from the anisotropic effect of the aryl group of the derivatization agent on the substituents of the chiral target molecules. The success of Mosher ester analysis in determining the absolute stereochemistry of chiral 2° alcohols or amines depends on a few assumptions regarding the conformation of each diastereomer. As illustrated in Figure I-4, some of the Mosher ester structural features include the *s-trans* conformation of the ester group (O-CO), *syn* arrangement of the less hindered group on the chiral center with the carbonyl of the ester, and the anti-periplanar arrangement of the trifluoromethyl group of the MTPA with C-O bond of the ester. As highlighted in Figure I-4, and based on the Mosher ester's structural feature, the CH-O-C(=O)-C-CF₃ are in the same plane. These assumptions are crucial for meaningful interpretation of the changes in NMR chemical shift and any deviation from the results in contradiction of Mosher ester analysis.^{10, 14, 15}

Aryl rings are known to induce an anisotropic shielding effect on hydrogens located above or below aromatic rings.¹⁶ The chemical shift of these proximal hydrogens would be affected by this magnetic shield and shift upfield. In the **I-6S** conformer, the R² group is eclipsed with the phenyl ring, which results in the higher shielding of the protons of the R² group (lower chemical shift (δ) in NMR spectra); on the other hand, protons of the R¹ group of diastereomer **I-6R** are upfield in the NMR spectra. In the end, the chemical shift difference (δ^{SR}) of hydrogens of substructures R¹ and R² in two diastereomers is measured. The sign of δ^{SR} is employed to properly place the R¹ and the R² group around the chiral center, which defines the absolute stereochemistry of the original target molecules. For the substrate indicated in Figure I-4, δ^{SR} for protons correspond to the R² group have a negative sign ($\delta^S - \delta^R$); conversely, δ^{SR} of those hydrogens at R¹ will be positive.¹⁷ Even though Mosher ester analysis has been widely used to assign the absolute configuration of chiral alcohols and amine, it has its own drawbacks. Requirement for milligram quantity of the chiral molecule for derivatization and the presence of several functional groups in the chiral substrate that could undergo derivatization are some of the limitations of this method. Moreover, the syn alignment of the ester carbonyl with the smallest group of the chiral center, and anti-periplanar alignment of CF₃ with C-O bond are necessary to provide predictable results. Deviation from any of these assumptions causes inconsistencies for the results of Mosher ester analysis.¹⁵

I-2-3 Chiroptical spectroscopy for stereochemical determination of chiral organic molecules

Chiroptical methods are used to discriminate between two enantiomers. Light consists of magnetic and electric field components that fluctuates perpendicular to one another in the direction of light's propagation, resulting in the right-handed coordinate system (Figure I-5).¹⁸

Light coming from the sun or any ordinary light source is unpolarized because the light waves propagate in all directions, and there is no preferred plane for propagation. On the other hand, linearly polarized light contains only waves with oscillations in one specific plane. As shown in Figure I-5, the electric field of a linearly polarized light fluctuates only in the z plane, while the magnetic field traverses on the y plane.¹⁹

When two electromagnetic plane-polarized waves with the same intensity and 90°

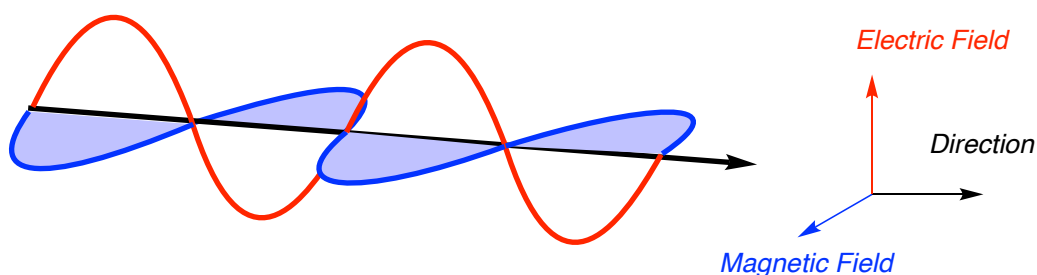


Figure I-5 Light as an electromagnetic radiation.

phase differences meet each other perpendicularly, they generate a new wave resulting from the overlay of two plane-polarized waves. The resulting new wave is called circularly polarized light. Suppose two plane-polarized light fluctuates with a 90° phase difference. In that case, the resulting circular polarized light is called right circularly polarized light since the electric vector of the circularly polarized light rotates clockwise while looking at the source (Figure I-6-a and -c). On the other hand, if two plane-polarized waves oscillate

with a -90° phase difference, the circularly polarized light is said to be left handed, and the vector of the electric field rotates counter-clockwise (Figure I-6-b).²⁰

Interaction of the light with matter might cause a change in its properties such as wavelength, velocity, polarization, amplitude, etc. For example, absorption (or extinction) and changing the velocity are two phenomena caused by the interaction of the electric field of the light with electrons of the substance. This interaction decreases the propagation velocity, which is called refraction and is defined by refraction index (n). Reducing the electronic vector of light is said to be absorption and is described by the molar absorption coefficient (ϵ). For the refraction and absorption to occur, there is no need for polarized light; however, the behavior of chiral molecules is sensitive to left or right circularly polarized light. Therefore, each enantiomer of chiral molecules shows different refraction indices and absorption coefficients for left and right circularly polarized light. When the polarized light passes through an asymmetric environment, changes in

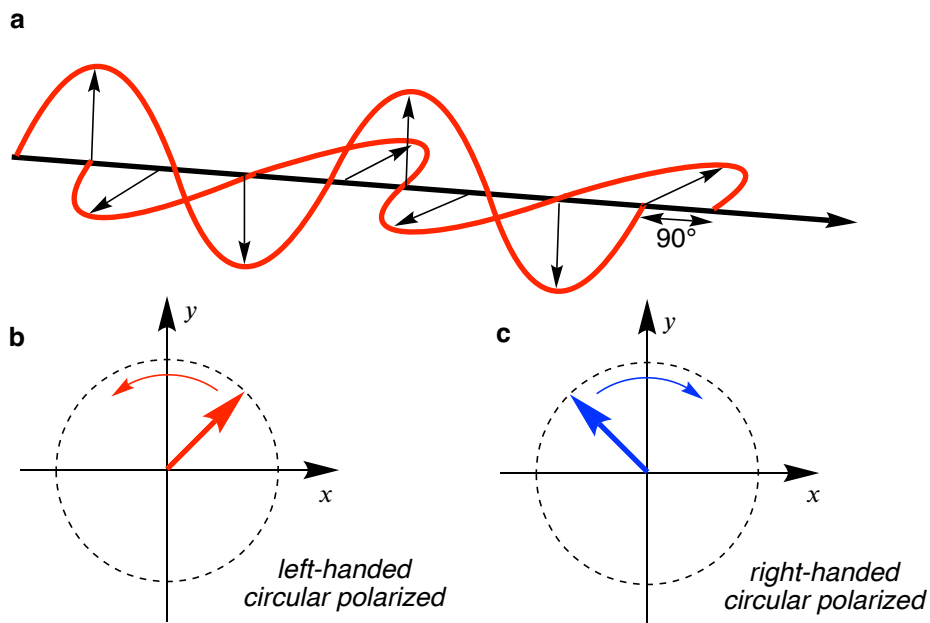


Figure I-6 a. Circularly polarized light. b. Left-handed circularly polarized light. c. Right-handed circularly polarized light.

the velocity and the absorbance of the circularly polarized are different. The difference in the velocity of the circularly polarized light is called optical rotatory dispersion (ORD).²¹

$$\Delta n = n_L - n_R \neq 0$$

Because the velocity of the left and right circularly polarized light that passes through the chiral environment differs, the combined left and right circularly polarized light's angle is different from the plane polarization of the occurrence wave. The amount of this deviation from the original plane is determined as α optical rotation. α and the refractive indices difference is quantitatively related to each other using the following equation. In this equation, n_L and n_R are refractive indices, l is the length of the path in decimeters and λ_0 is the wavelength of the light.

$$\alpha = (n_L - n_R)1800 l/\lambda_0$$

Specific rotation $[\alpha]$ is another property of chiral molecules which is measured in ORD spectroscopy and can be derived from observed rotation using the following equation:

$$[\alpha] = \alpha/cl$$

To convert an optical rotation to a specific rotation in degrees, the observed rotation is divided by the concentration in g mL^{-1} (c) and the path length in decimeters (l).

It was noted that specific rotation is affected by some external factors, and it depends on the wavelength and the solvent used to prepare the sample. As a result, specific rotation is commonly reported along with the temperature, solvent, concentration, and wavelength employed for the measurement.

It should be mentioned that all compounds with chirality show refraction at every wavelength of radiation. Since ORD is based on the refractive indices differences, ORD can be measured at a different wavelength. Nonetheless, the sodium D-line (589 nm) is

used to reveal and quantify optical activity. Measuring the specific rotation of chiral molecules and comparing the result with the reported specific rotation of the same molecule assigns the absolute stereochemistry of chiral molecules. However, if there is no reported value for the same compound, measuring the optical rotation of the chiral compound does not provide any information regarding the absolute configuration of the target compound.

Our focus so far was on the plane-polarized light's rotation with an angle α compared to the initial plane of polarization, which happens after the polarized light passes through an optically active substance. As was mentioned before, when polarized light passes through an optically active medium, not only is there a difference in the refractive indices of right and left circularly polarized light, but also a difference of absorbance between these two-component has been observed as well. Therefore, the optically active materials have different molar absorptivity coefficients ε for right and left polarized light. The difference in molar absorptivity is called Circular Dichroism (CD), as illustrated in the following equation where, ε_L and ε_R are the left and right molar absorption coefficients, respectively.²¹

$$\Delta\varepsilon = \varepsilon_L - \varepsilon_R \neq 0$$

CD is based on an absorptive process, and it occurs in the vicinity of an absorption band. Plotting the absorption difference of left and right circularly polarized light over the wavelengths that the chiral molecule absorbs light results in the CD spectrum. Consequently, for a CD spectrum to be observed, the presence of a chromophore in the chiral compound is necessary.

After passing through a chiral material, two circularly polarized lights are out of phase and have different amplitudes. Due to these differences, the geometry of the wave changes. As shown in Figure I-7, the superimposition of the two circular polarized light results in forming an electric field that does not oscillate over a straight line. It oscillates through an elliptical path (Figure I-7b) generates an ellipsoid polarized light.¹⁸

Circular dichroism can be described quantitatively, using Beer-Lambert-Bouguer law (see the following equation).

$$A = \log_{10} \left(\frac{I_0}{I} \right) = \epsilon cl$$

Where, A is the recorded absorbance, I_0 is the light's intensity before entering the cell, and I is its intensity after passing the cell. A is also proportional to c as concentration and l as the length of the cell. ϵ , as mentioned before, is molar absorptivity when c is in mol L⁻¹, and l is in centimeters. Two equations for absorption can be recorded for each circular component since the left, and right circularly polarized light have nonequivalent absorption for a chiral molecule.

$$A_L = \log_{10} \left(\frac{I_{0L}}{I_L} \right)$$

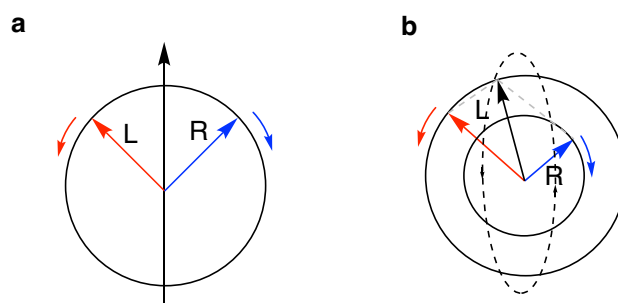


Figure I-7 a. Left and Right components of the plain polarized light b. Generation of the elliptically polarized light due to the difference in absorption of the left and right circularly polarized light by chiral matters.

$$A_R = \log_{10} \left(\frac{I_{0R}}{I_R} \right)$$

Because the initial intensity of both left and right circular polarized light is the same, we can remove the L and R index of I_0 . Thus, the difference of absorption of these two circular components can be used to arrive at the circular dichroism of the chiral medium.

$$\Delta A = A_L - A_R = \log_{10} \left(\frac{I_{0L}}{I_L} \right) - \log_{10} \left(\frac{I_{0R}}{I_R} \right) = \log_{10} \left(\frac{I_R}{I_L} \right)$$

Using Beer-Lambert-Bouguer law, circular dichroism can also be presented as a molar absorptivity difference.¹

$$A = \epsilon cl \rightarrow \Delta \epsilon = \frac{\Delta A}{cl}$$

Due to the fact that difference between A_L and A_R (or left and right molar absorptivity) are reflected in the CD spectrum, the sign of this spectrum might be positive or negative according to the chiral environment.

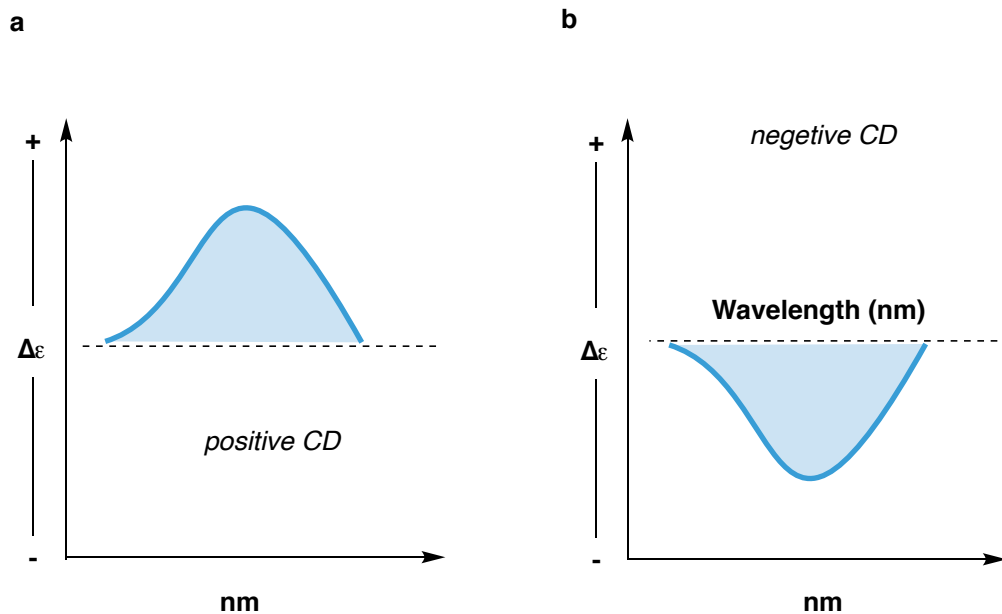


Figure I-8 a. Positive and b. negative CD spectra or Cotton effects.

Upon absorption of light by the molecule, accompanied by electron transfer from a ground state to an excited state, a momentary dipole called electric dipole transition moment (edtm) is generated. The electric transition dipole moment is denoted by μ , with the same direction of propagation as the direction in which electrons move during the transition. Interaction of the magnetic field of the electromagnetic radiation with substances generates a circular arrangement of the electron density, which results in the creation of a magnetic dipole transition moment (mdtm). The direction of the mdtm can be determined using the "right-hand rule." According to this rule, four fingers of the right

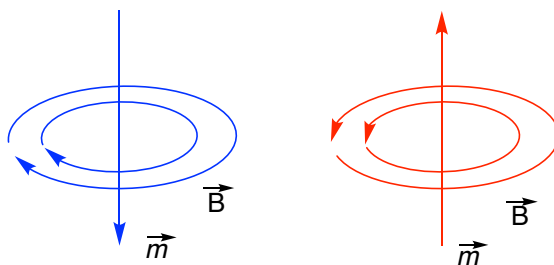


Figure I-9 Pictorial description of "right hand rule" to determine the direction of magnetic dipole transition moment.

hand curve to the direction of the electron flow in the magnetic field B , the thumb stretches out to the direction of magnetic dipole transition moment (Figure I-9).

In symmetric molecules, there is a net planar electron distribution. It is either linear or circular. In chiral molecules, the electron distribution is spiral; therefore, the interaction of the chiral molecule with the polarized light would generate a magnetic field and mdtm. The interaction of the edtm and mdtm forces a helical distribution of the electrons. The interaction of the electric field of the light with edtm and simultaneously interaction of the magnetic field of the light with mdtm have been summarized using the Rosenfield equation. This equation has been employed to depict the sign and strength of a CD signal

and ORD (Cotton effect) denoted by rotational strength, R . This parameter is driven by the scalar product of the electric and magnetic transition moment (see the following equation).¹

$$R = \mu \cdot m = |\mu||m| \cos \beta$$

Where β is defined as the angle between electric and magnetic dipole transition moments. When this angle is acute ($0 < \beta < 90^\circ$), the sign of the Cotton effect is positive, and it is negative when the angle is obtuse ($90^\circ < \beta < 180^\circ$). There is no Cotton effect when the electric and magnetic transition dipole moments are perpendicular to one another.

Both CD and ORD can be recorded using circular dichrometers. Figure I-10 shows the general composition of the CD spectropolarimeter. The source of light is typically a xenon lamp. First, linearly polarized light is produced by passing the generated light from several crystal prisms. Next, the linearly polarized light incident with the modulator, known as a wave plate, at 45° , generates two equal electric field components. One of these two components is retarded by a quarter wavelength, resulting in the 90° out of phase compared to each other. As a result, one of the two emerging components is always maximum while the other is zero—the effect mentioned above results in the formation of circularly polarized light. The 90° shift happens due to the specific thickness of the birefringent crystal. Due to the 90° shift, this plate is referred to as a quarter-wave plate. The circularly polarized light passes through the sample, and the transmitted light is

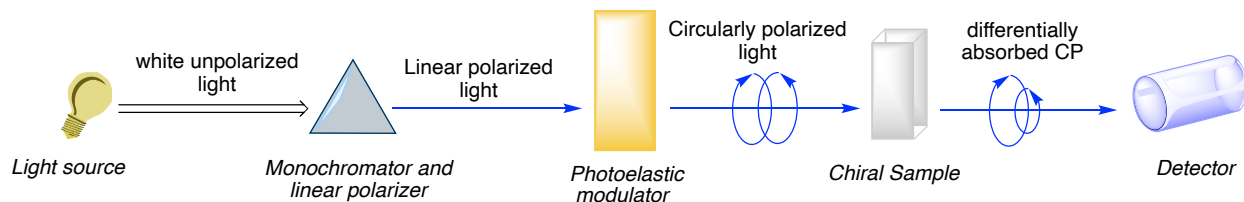


Figure I-10 Schematic representation of a CD spectropolarimeter.

measured using a photomultiplier tube which generates a current. The resulting current is detected and recorded by the polarimeter. The magnitude of produced current depends on the number of incident photons that pass through the multiplier.²²

ORD and CD can be employed to detect and quantify the enantiomeric excess of a sample. Nonetheless, they cannot lead to the direct determination of absolute stereochemistry of unknown samples. Extensive theoretical studies have been employed to compute and predict the ORD or CD of small molecules with specific stereochemistry to solve this issue.²³ However, the empirical feature of these theoretical methods leads to significant limitations. Furthermore, the accuracy of the results deriving from computational methods depends on the careful choice of various computational methods, which is a challenging task. The selection is more demanding when it comes to more complex molecules. Among different types of CD spectroscopy, vibrational circular dichroism (VCD) and electronic circular dichroism (ECD) have extensive applications in assigning the absolute stereochemistry of chiral compounds. VCD is the absorption in the infrared region, while ECD is based on the absorption in the UV-vis region.²⁴⁻²⁶

In the VCD case, the spectra of both enantiomers are calculated. Then, the calculated spectrum is compared with the experimental result to predict the stereochemistry of the chiral substrate.^{24, 27, 28} One of the limitations of VCD spectroscopy is its weak absorption. Because of this issue, VCD requires long acquisition times and concentrated samples to provide a trustable result. Also, electronic CD (ECD) like VCD is merged with theoretical and computational techniques to develop a tool for the configuration assignment. The

specific variant of the ECD technique is Exciton Coupled Circular Dichroism (ECCD), pioneered by Harada and Nakanishi in the 1980s.²⁹

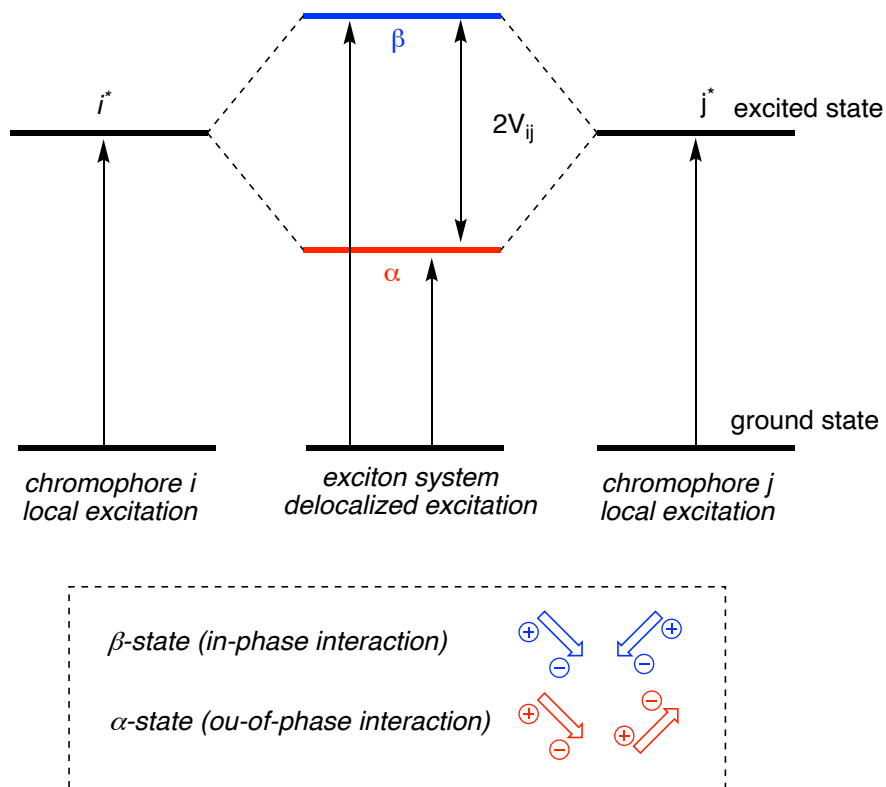


Figure I-11 Splitting of the excited state of the isolated chromophores by exciton interaction.

I-3 Exciton Coupled Circular Dichroism (ECCD)

An ECCD results from the coupling of the excited state of two or more chromophores, embedded in the chiral molecules. This phenomenon is called exciton coupling. In the excited state, chromophores gain an electric dipole transition moment, which has two directions for oscillation. The existence of the two chromophores results in the generation of the two electric transition dipole moments which interact with each other through space. The resultant excitation is delocalized between the chromophores at their excited states.³⁰ In order for this interaction to occur, it is required that both chromophores have the

transition with the similar or close energy. Due to the oscillation of transition moments of the chromophores, there are two possible scenarios: either both transition moments oscillate in-phase or transition moments are out-of-phase (Figure I-11). Thus, the two-phase interactions of edtm result in splitting the excited state into two energy states α and β . The energy difference between these two states is called the *Davydov split*.²⁹ The transitions from the ground state to either the α or β state causes two different UV-vis absorbances. The higher wavelength is responsible for out-of-phase interaction (stabilizing dipole-dipole interaction), while the lower wavelength results from in-phase interaction (destabilizing dipole-dipole interaction). Consequently, the UV-vis spectrum is detected as a two-component peak but usually appears as a single peak with double intensity. One should note that a spectrum with two peaks might become evident if there is a significant energy difference between two excited states.

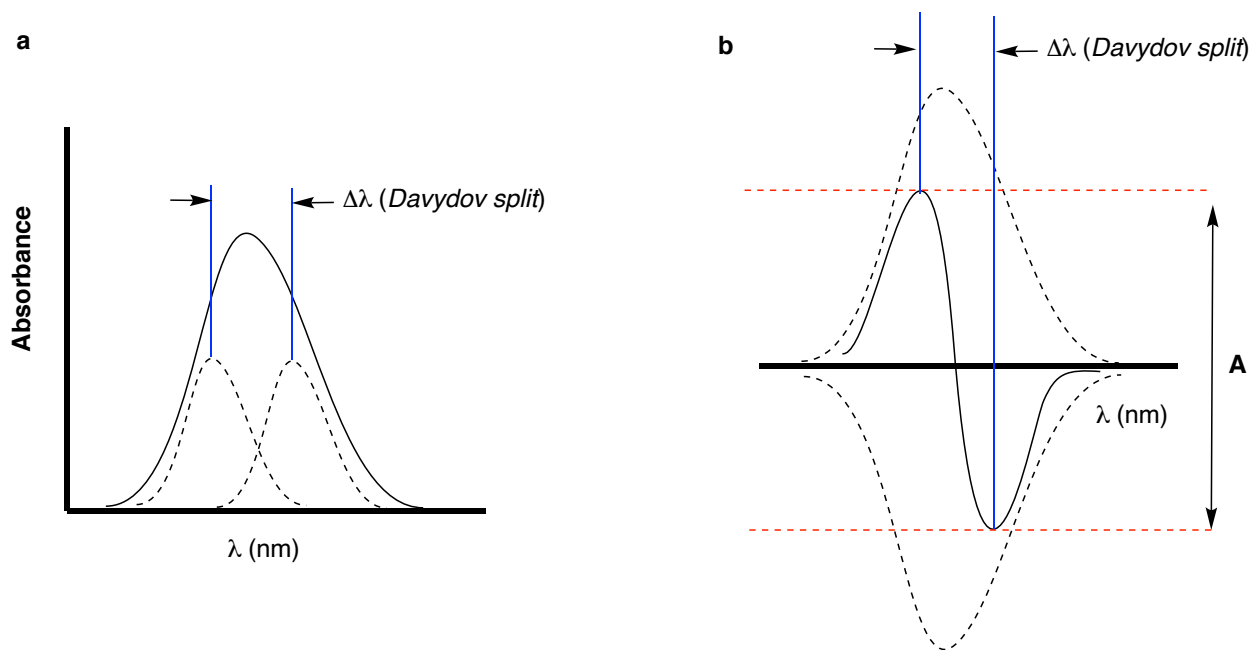


Figure I-12 The a. UV and b. ECCD spectrum of two degenerate chromophores interacting through space.

The absolute spatial orientation of the chromophores relative to each other leads to the existence of a CD detectable transition. Because CD spectroscopy is based on the difference in the absorption of the left and right circularly polarized light, the chromophores must have chiral orientation relative to each other. Thus, if the direction of the two edtm originating from two chromophores is parallel or both chiral orientations are presented simultaneously (non-chiral) in the medium, the interactions will be neutralized, and no CD signal will be detected. Therefore, the angular orientation of the edtms defines the appearance of the ECCD spectra. A CD active transition is perceived as a bisignate CD graph called the ECCD spectrum (Figure I-12).²⁹ The chromophores have two possible arrangements, clockwise (positive, *M* helicity) and counter-clockwise (negative,

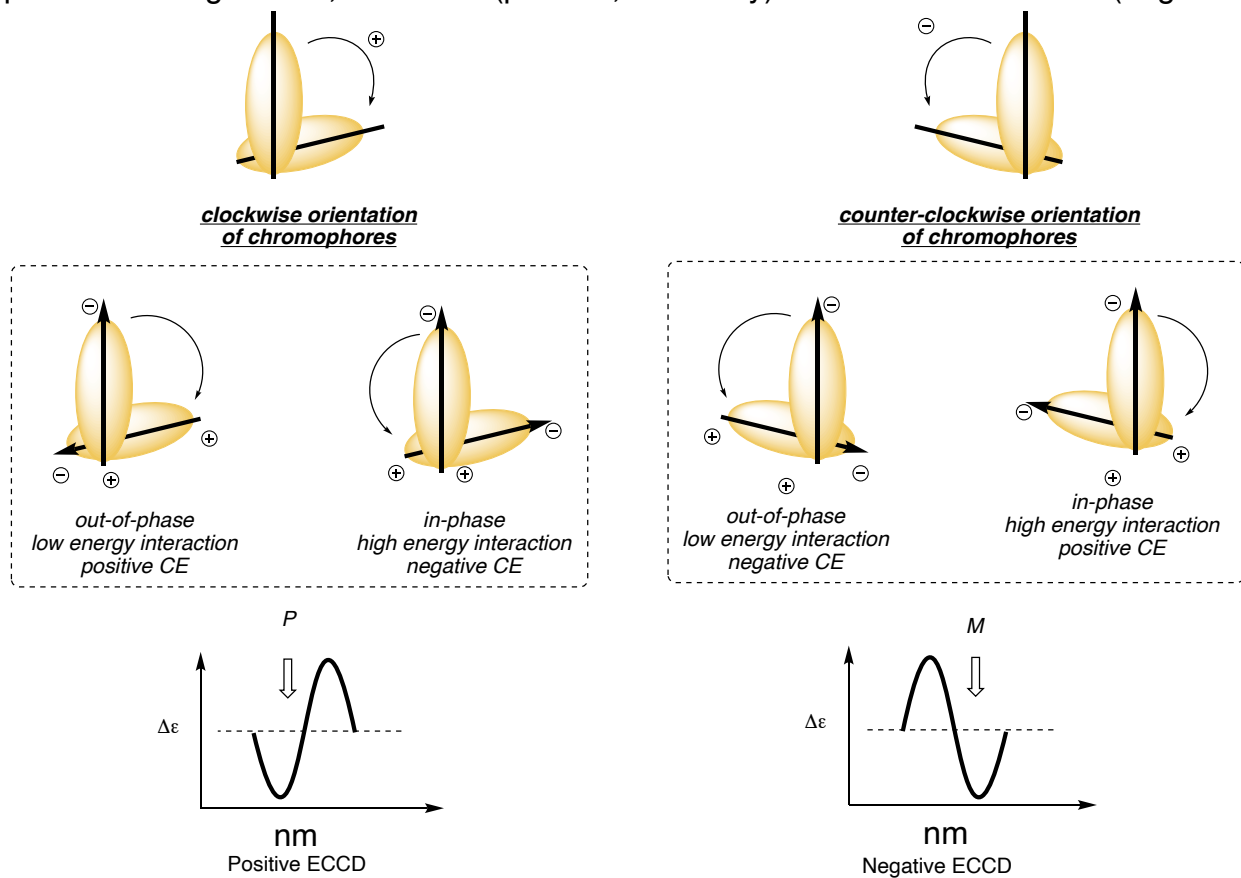


Figure I-13 Exciton interaction of edtm of two chromophores (in-phase and out-of-phase) result in a bisignate CD curve.

P helicity). Considering that each interaction of edtm involves symmetric (in-phase) and asymmetric (out-of-phase) exciton coupling, then every helical rearrangement of two chromophores has two sets of exciton coupling. Figure I-13 presents a detailed analysis of exciton coupling interaction of transition dipole moments leading to the bisignate CD spectrum for clockwise and counter-clockwise orientations. The oscillation of charge (minus to plus) in each transition generates either clockwise or counter-clockwise direction.³¹ For example, the in-phase interaction of clockwise orientation induces a

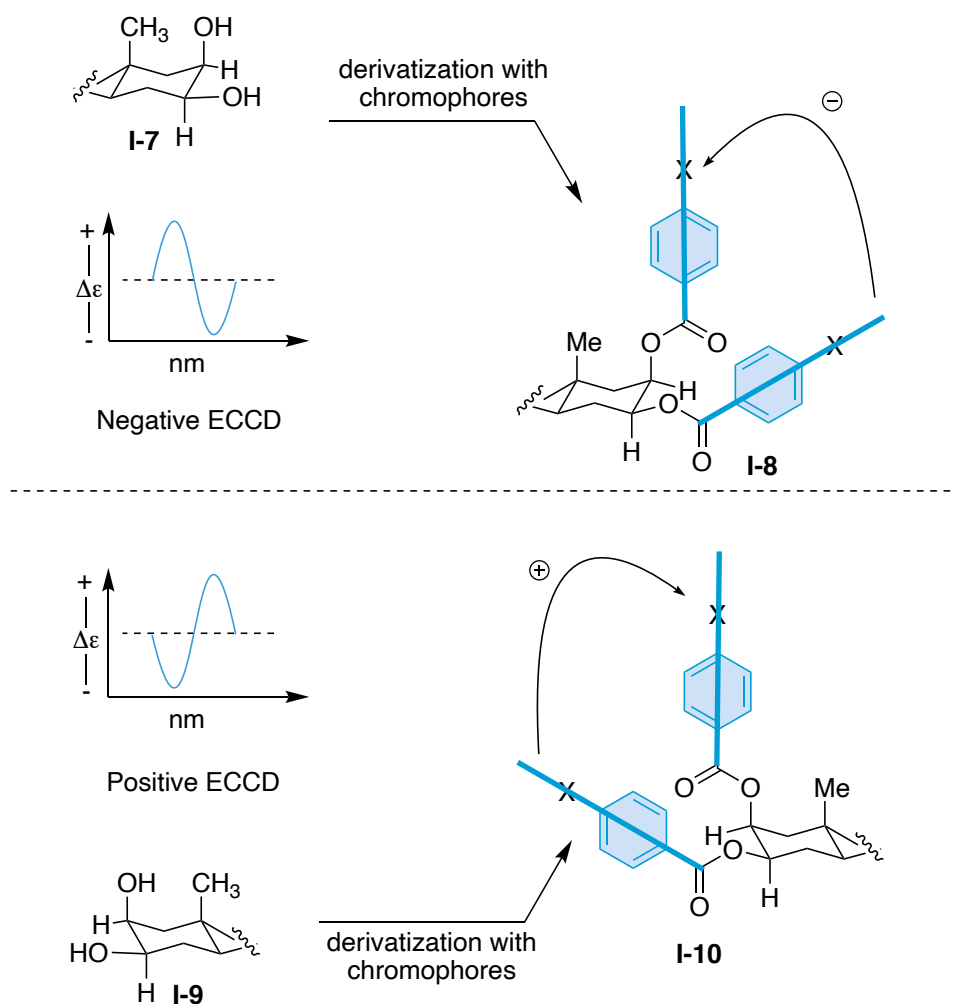


Figure I-14 Derivatization of two enantiomeric diols result in ECCD spectra with two opposite signs.

positive swinging of charge and yields a positive Cotton effect. On the other hand, the out-of-phase interaction in the same system causes a negative oscillation of charge and leads to a negative cotton effect. These two transitions have different energy due to the symmetry of the interaction.

Due to the repulsion between similar charges in symmetric in-phase interaction, this transition has higher energy and appears at a lower wavelength. The out-of-phase exciton will be detected at a higher wavelength because of the stabilization of the charges. Thus, the clockwise orientation of the chromophores will lead to the positive ECCD spectrum, with a positive Cotton effect at lower energy, followed by a negative CD of higher energy. A similar analysis could explain the ECCD spectrum coming from the counter-clockwise orientation of the chromophores. At the same time, higher wavelength leads to a negative Cotton effect, followed by positive CE at higher energy.

The ease of analysis of the observed ECCD signal and its correlation to the absolute orientation of chromophores results in the extensive application of the Exciton Coupled Circular Dichroism spectroscopy to determine the absolute stereochemistry of chiral molecules.

As mentioned before, ECCD arises from the excited coupling of chromophores set in the chiral substrates. Detection of a strong exciton coupling requires close UV-vis absorption of the chromophores. One of the significant issues regarding ECCD is that strong absorbing chromophores do not exist in the skeleton of all chiral molecules. Therefore, enormous efforts have been directed to design or introduce suitable chromophores into the structure of chiral molecules. One of the early methods was to

employ derivatization of the chiral molecules with two chromophores for absolute stereochemical determination. A classic example of this approach is shown in Figure I-14, where the diols were derivatized with 4- substituted benzoates as chromophores.³² The stereochemistry of the diol dictates the relative arrangement of the installed chromophores. The ubiquitous nature of the 1,2-diol functionality as a subunit of numerous natural products and as an invaluable asymmetric synthon in synthetic endeavors, signifies its centrally important role in organic chemistry and related fields. In fact, the Exciton Coupled Circular Dichroic methodology, pioneered by Nakanishi and Harada,²⁹ finds its genesis in the absolute stereochemical determination of 1,2-diols.³³ The dibenzoate method (Figure I-14), as it was referred to, not only demonstrated the non-empirical fashion by which the ECCD method reports absolute stereochemistry (a novel discovery at that time) but also laid the foundation for decades of research in the application of ECCD, establishing it as a mainstream method for stereochemical determinations.^{3, 34-37} Since 1969, the year in which the original paper on the dibenzoate process was published,³³ numerous strategies and methodologies have expanded on the utility of the ECCD method to address the absolute stereochemical determination of a large number of different functionalities.^{36, 38} Yet, the governing principle remains the same; orient two or more chromophores in space in a spiral arrangement, such that the coupling of their respective electric transition dipole moments leads to a predictable bisignate curve in the CD spectrum. In this chapter, an operationally simple and microscale determination of 1,2-diols is presented. Prior to that, we briefly go over the previous approaches reported for the stereochemical determination of chiral molecules.

I-4 Conventional method for stereochemical determination of vicinal diols

The absolute stereochemistry of *threo* diols is mainly determined using the benzoate derivatization methodology. Figure I-15 shows the application of derivatization for the absolute stereochemical determination of *threo* diols.³³ The *threo* benzoate derivatives rotamers with the highest population result in the positive ECCD signal irrespective of the R₁ or R₂ groups. However, the highest population of the rotamers of *erythro* diols is CD silent, and other rotamers with lower populations show opposite CD signals, which complicates the analysis. Therefore, no reliable conformers could be employed to indicate the absolute stereochemistry of the *erythro* using the derivatization strategy. One challenge of using ECCD to determine absolute stereochemistry is that the system should be robust enough to provide consistent results with compounds with various structures.²⁹

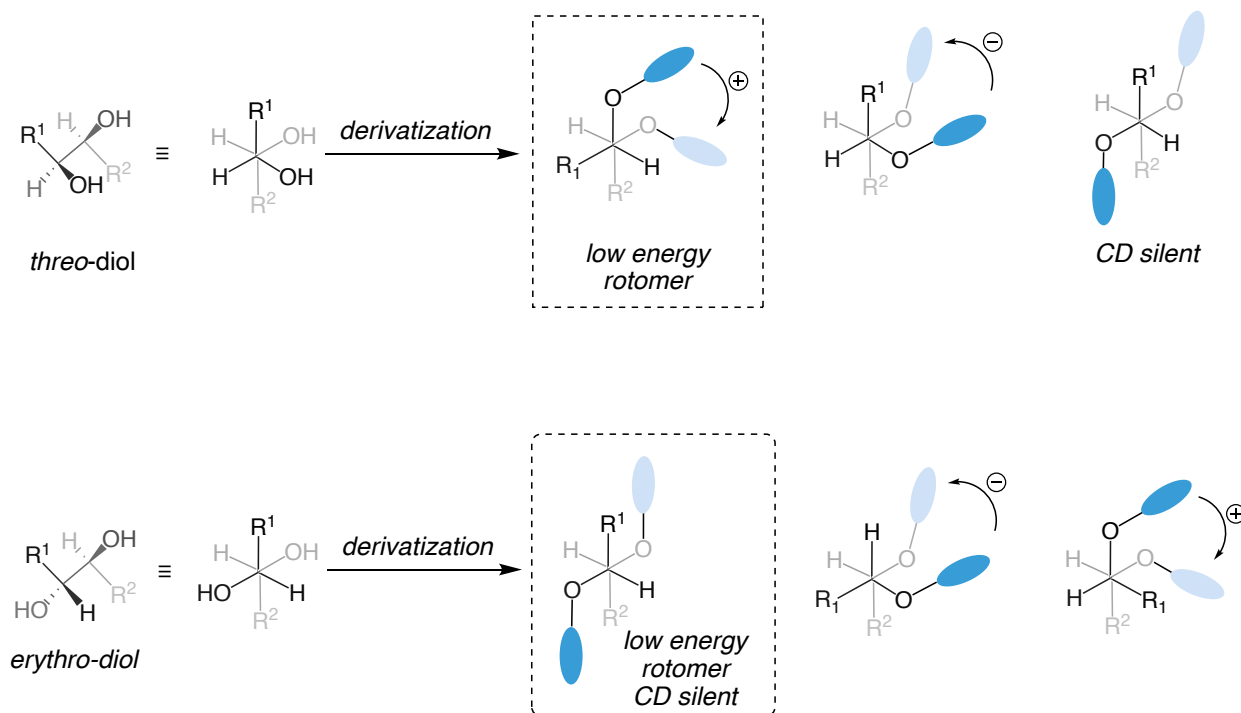


Figure I-15 Stereochemical determination of threo diols.

In general, applying the derivatization approach for determining the absolute stereochemistry of acyclic diols requires a detailed conformational analysis. Acyclic diols are conformationally mobile, which causes the application of the system mentioned above to become more difficult. There have been a number of other chiroptical strategies to address the absolute stereochemical determination of 1,2-diols. Most often, acyclic diols are converted to their corresponding cyclic, conformationally more rigid, and defined derivatives for stereochemical analysis.³⁹⁻⁴⁶ One alternative technique to remedy this issue is using transition metal complexes with optical activity.³⁹⁻⁴³

All the approaches using transition metals share several common points, such as (1) even though a stock solution of the metal complex is stable thermodynamically, it might be unstable kinetically; (2) the enantiopure compound acts as a ligand and coordinates to the metal; (3) due to the ligation, the substrate is conformationally more restricted; (4) the metal complex solution has a detectable absorption band in UV-vis region (d to d or f to f absorption of the metal, metal to ligand charge transfer electronic transition, etc.); (5)

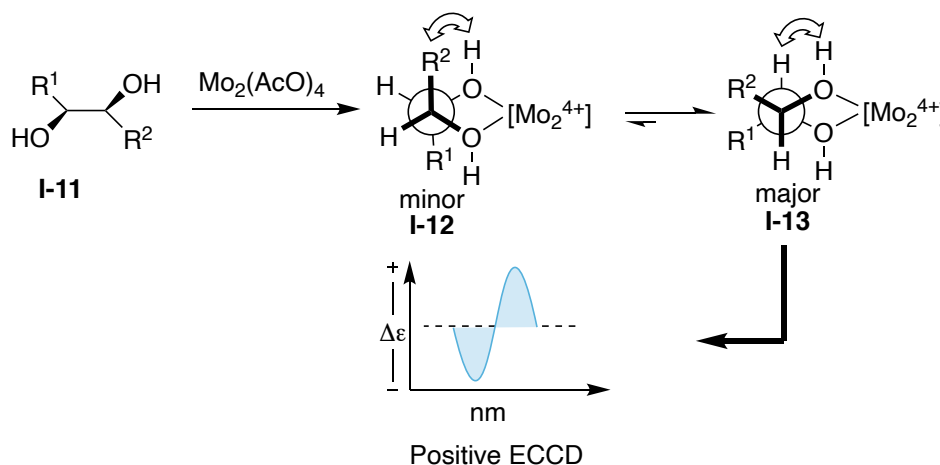


Figure I-16 Steric configuration of molybdenum complex and its effect on dihedral angle of the cottonogenic derivative.

the CD active compound simply forms by mixing metal and chiral substrates; (6) because of the restriction of conformational freedom of the complex, the sign of the Cotton effect can be linked to the structure and absolute configuration of chiral compounds. In 2001, Salvadori and coworkers illustrated the application of molybdenum tetraacetate in the assignment of the stereochemical configuration of chiral *threo* diols. They showed that after forming the complex between the chiral substrate and metal, diols are constrained into two possible chiral and gauche arrangements. One of these two diastereomers is more favored due to the less steric interaction between substituents. As shown in Figure I-16, the bulkier group prefers to occupy a *pseudo*-equatorial position and face away from the rest of the complex in the selected arrangement.⁴⁰

Rosini and coworkers report another approach for the determination of the absolute configuration of 1,2- and 1,3-diols. Their process was to convert chiral diols into spiro dioxolanes utilizing a bridge biphenyl system containing a ketal moiety (Figure I-17). The formation of spiro dioxolanes results in the biphenyl backbone's axial chirality, which is induced by the chirality of the diol substrates. The orientation of the aryl groups generates

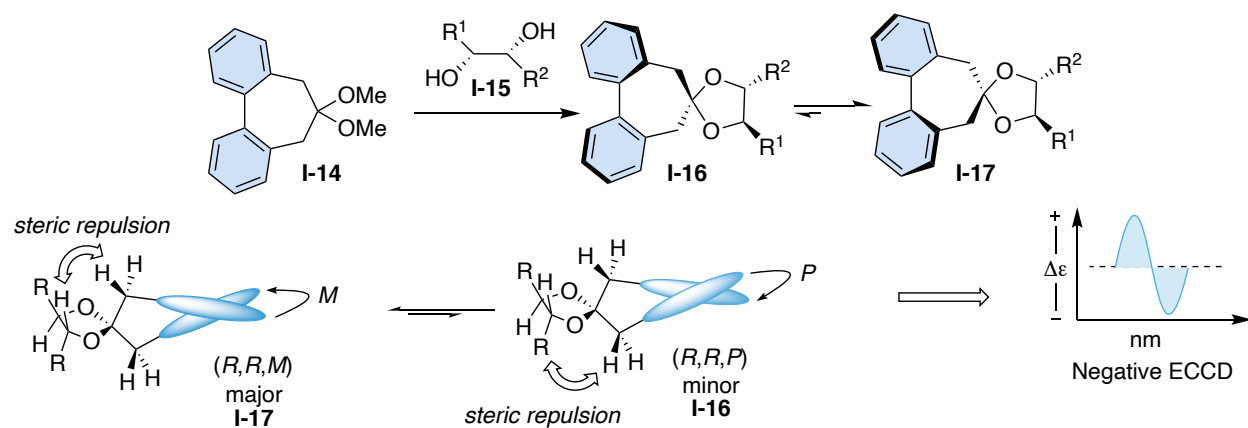


Figure I-17 Spiro dioxolane formation of chiral diols leads to CD active complex.

appropriate ECCD signal, which can be directly correlated to the chirality of the derivatized diols. This method provides an efficient procedure for presenting the chromophores to the diols without a detectable absorption band.⁴⁴

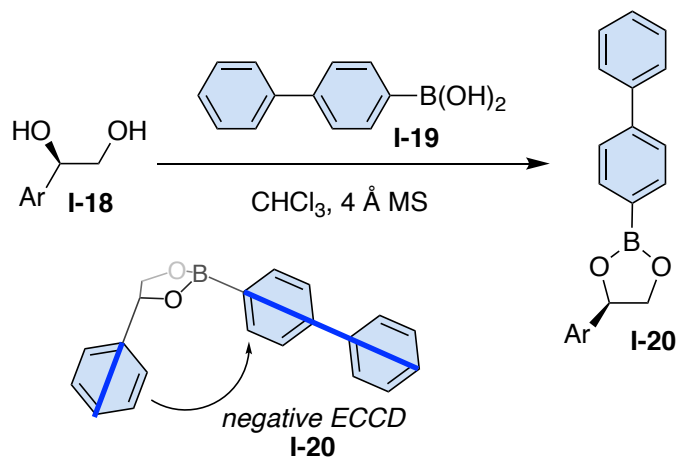


Figure I-18 Main transition dipoles of the *R*-configured phenyl substituted boronate complex.

In 2004, Rosini and coworkers reported a non-empirical and straightforward method to determine the absolute configuration of 1-aryl-1,2-diols. To record the CD spectra of the diols, it was necessary to produce the 4-biphenyl boronic acid ester of the diols. Using

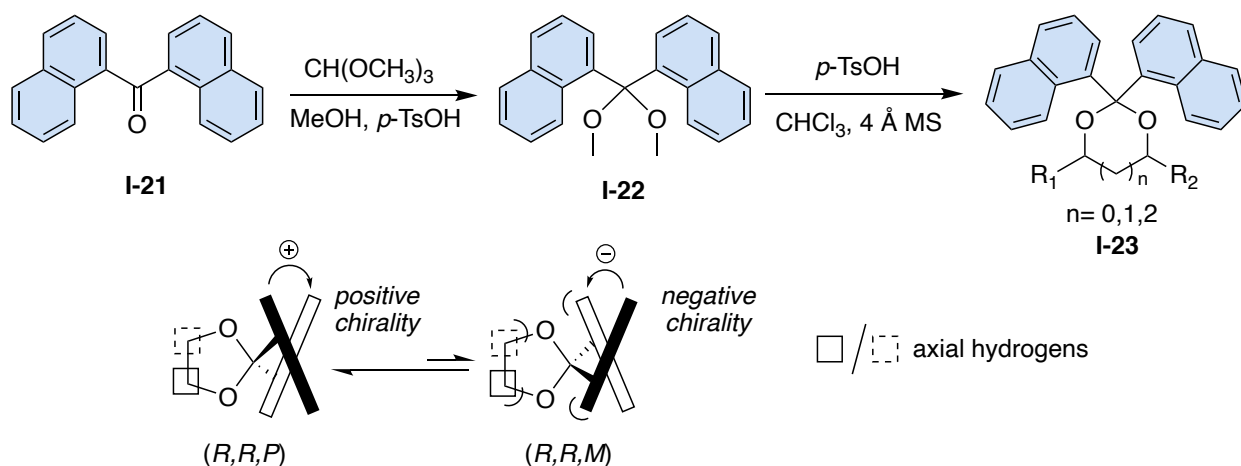


Figure I-19 Conformational diastereomers of *(R,R)*-diols. The solid box represents the hydrogen above the ring while the dashed box indicates the hydrogen below the ring.

the sign of CD spectra, they were able to assign the absolute configuration of the benzylic center. A negative sign was correlated to an *R* configuration of the chiral center (Figure I-18).⁴⁵ In 2008, the same group reported on a simple and new method for assigning the absolute configuration of acyclic aliphatic diols via transformation of the 1,*n*-diols into their corresponding di(1-naphthyl)ketals (Figure I-19).⁴⁶

Another effective strategy, especially for erythro 1,2-diols, is the porphyrin tweezer method which was reported previously by our group (Figure I-20).⁴⁷

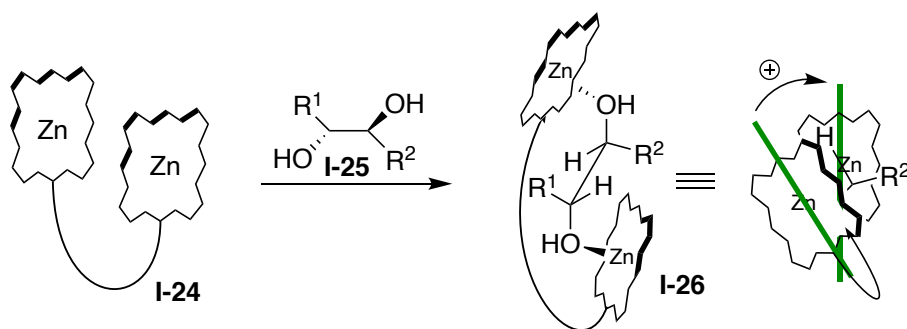


Figure I-20 Use of porphyrin tweezers to interrogate the absolute stereochemistry of threo and erythro diols.

I-5 Absolute stereochemical determination of 1,2-diols via complexation with dinaphthyl borinic acid

The inspiration for the present work finds its origins not only from the work of others discussed above (converting acyclic diols into a cyclic derivative) but also in our recent work in which 1,1'-(bromomethylene) dinaphthalene (**BDN**)⁴⁸ and di(1-naphthyl) methanol (**DNM**)⁴⁹ systems were used to determine the absolute stereochemistry of chiral amines and chiral carboxylic acids, respectively (Figure I-21). Derivatization of **BDN** and **DNM** with their respective asymmetric counterparts yields a system with a

preferential helical arrangement of the naphthyl groups on the reporter. The helicity of dinaphthyl chromophore is thus dictated by the nature of substituents on the chiral center, leading to either a positive or a negative ECCD signal. Low-cost conformer distribution analysis coupled with the observed ECCD spectra led to the prediction of absolute stereochemistry. We surmised that replacement of the central carbon in **BDN**

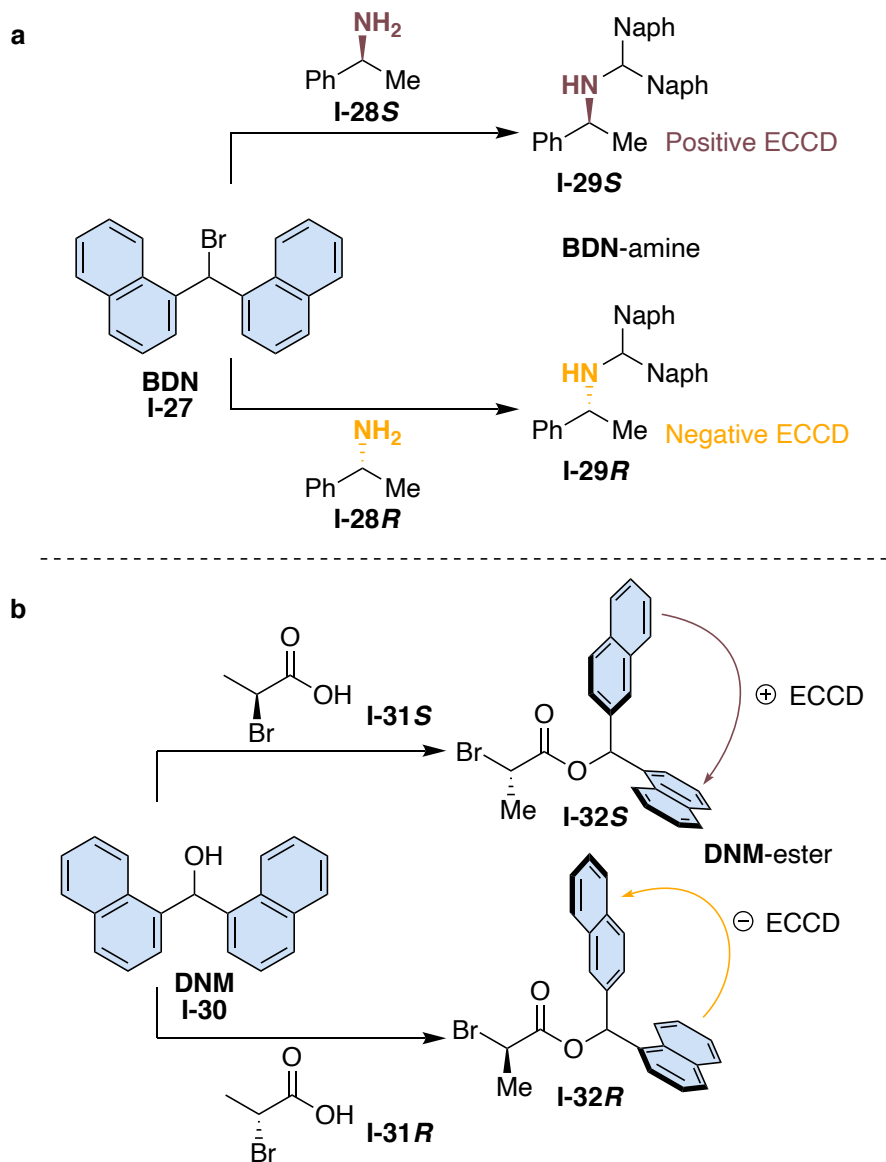


Figure I-21 a. Derivatization of chiral amines with **BDN** b. Esterification of di(1-naphthyl) methanol (**DNM**) with asymmetric carboxylic acid.

addition of a 1,2-diol (Figure I-22). Note, the term dioxaborolane refers to a tetracoordinated boron atom containing two oxygen substituents. In the following part of

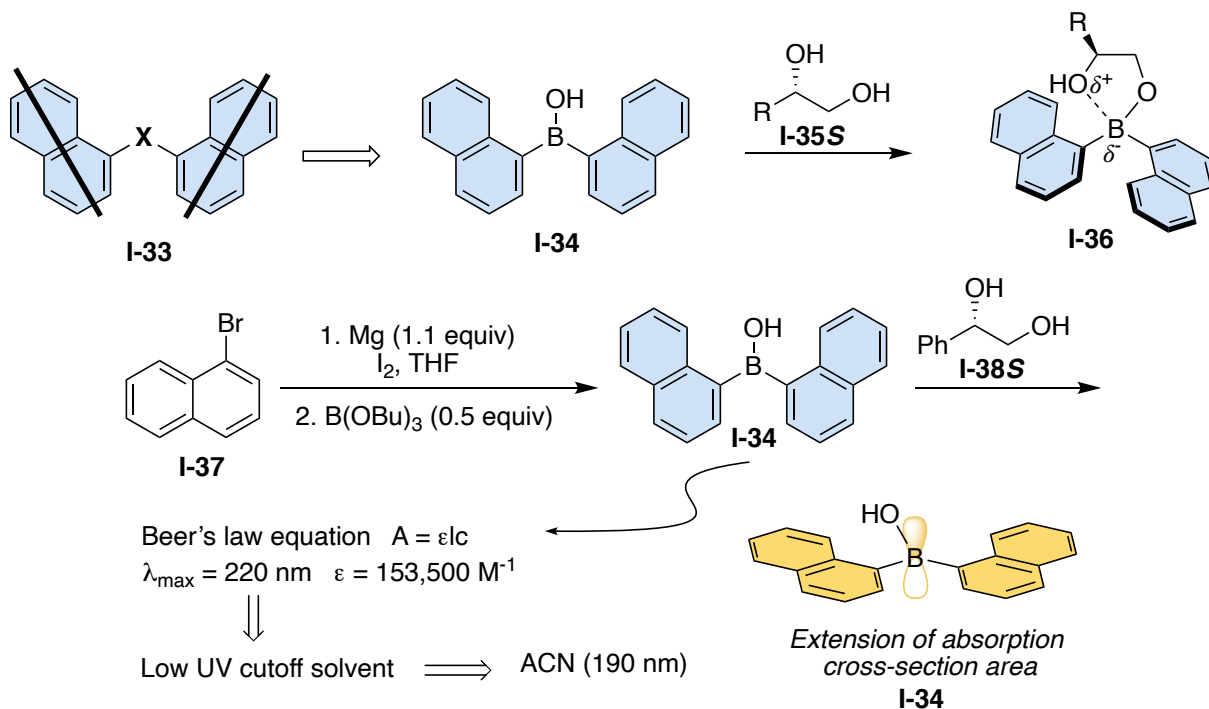


Figure I-22 Proposed DBA for stereochemical discrimination of chiral 1,2-diols.

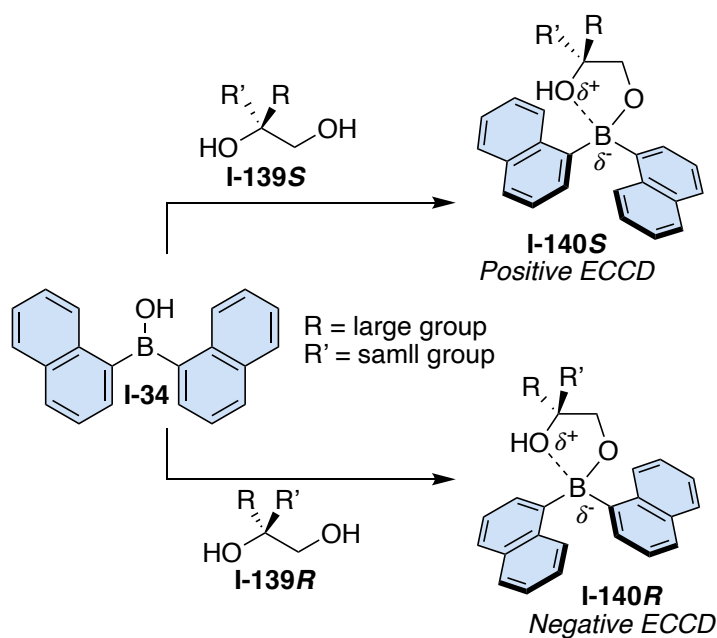


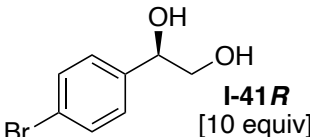
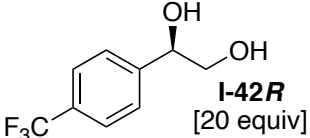
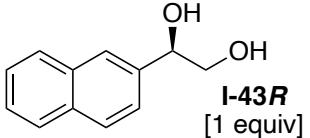
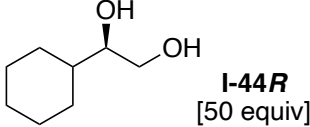
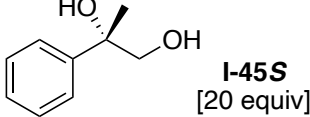
Figure I-23 Proposed mnemonic for the prediction of ECCD signal

and **DNM** with boron would enable the facile formation of a dioxaborolane **I-36** with the addition of 1,2-diol. In this chapter, we use the term dioxaborolane, somewhat loosely since the structure resembles a dioxaborolane, although we believe the second oxygen bond is dative and not covalent, *Vide infra*. To the best of our knowledge, the only similar system to the one proposed with **DBA** is the elegant studies by Rosini and coworkers, in which an aryl boronic acid was used to complex with an aryl containing 1,2-diol.^{45, 50} The coupling between the two aryl groups, one from the substrate and one from the boron source, led to CD spectra used for stereochemical analysis. In our case, the two coupling aryl substituents reside on the boron atom and thus do not require the presence of an aryl containing 1,2-diol. Dinaphthyl borinic acid (**DBA**) was prepared easily by addition of 2 equivalents of 1-naphthylmagnesium bromide to tributyl borate followed by hydrolysis of the resulting dinaphthyl boronic butyl ester **I-34** (Figure I-22). Physical properties for **DBA** are provided in the experimental chapter; however, the calculated extinction coefficient is noteworthy. The value of 153,500 M⁻¹cm⁻¹ for its λ_{\max} (220 nm) was determined via two independent routes (measured by weight and via NMR concentration determination). This is much larger than that anticipated since naphthalene has an $\epsilon \sim 13,000$ M⁻¹cm⁻¹. Nonetheless, we used the calculated value for our experiments and ascribed the unusually large value to the presence of the boron atom inserted between the two naphthyl rings, providing an electronic conduit through its empty P orbital to extend the cross-sectional area for absorption.

It was envisioned that addition of asymmetric 1,2-diols will result in a dioxaborolane depicted in Figure I-23, where the helicity of the naphthyl groups would be under the

steric influence of the substituents of the reacting diol. The induced helicity as a result of the preponderance of one helical population should result in an observable ECCD spectrum. In practice, 1,2-diols were mixed with DBA at

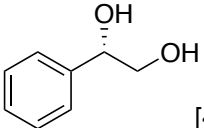
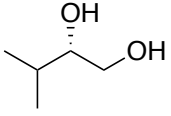
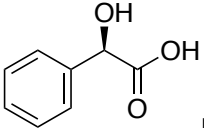
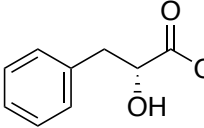
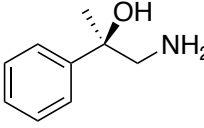
Table I-1 ECCD data for **DBA**-derivatives

Entry	Substrate (equiv) ^a	Predicted ECCD	$\lambda(\text{nm})$ $\Delta\epsilon^b$	A ^c
1	 <p>I-41R [10 equiv]</p>	Neg	233, -222	-222
2	 <p>I-42R [20 equiv]</p>	Neg	232, -93	-95
3	 <p>I-43R [1 equiv]</p>	Neg	234, -213	-360
4	 <p>I-44R [50 equiv]</p>	Neg	232, -35	-64
5	 <p>I-45S [20 equiv]</p>	Pos	233, 215	+360

^aAll CD measurement were recorded with 1 μM **DBA** derivative in acetonitrile at temperatures that maximized ECCD (see Chapter III for temperatures for each substrate). ^bThe reported $\Delta\epsilon$ is from the long wavelength portion of the couplet. ^cA refers to the amplitude of the ECCD couplet.

noted equivalents in the CD cell, and measurements were ensued in minutes following the complexation. Prior to analysis, it is important to note that the solvent of choice must have a low UV cutoff in order to avoid overlap of a strong absorption band with the absorption of the naphthyl group. We found that acetonitrile is a suitable solvent,

Table I-2 ECCD data for **DBA**-derivatives

Entry	Substrate (equiv) ^a	Predicted ECCD	$\lambda(\text{nm})$ $\Delta\epsilon^b$	A^c
6	 I-46S [40 equiv]	Pos	232, 220	+293
7	 I-47S [40 equiv]	Pos	233, 67	+102
8	 I-48R [1 equiv]	Neg	230, -188	-262
9	 I-49S [10 equiv]	Pos	231, 50	+69
10	 I-50R [4 equiv]	Neg	230, -883	-1350

^aAll CD measurement were recorded with 1 μM DBA derivative in acetonitrile at temperatures that maximized ECCD (see Chapter III (SI) for temperatures for each substrate). ^bThe reported $\Delta\epsilon$ is from the long wavelength portion of the couplet. ^cA refers to the amplitude of the ECCD couplet.

not only because it has a low UV cutoff, but also because all components for analysis were readily soluble (Figure I-22).

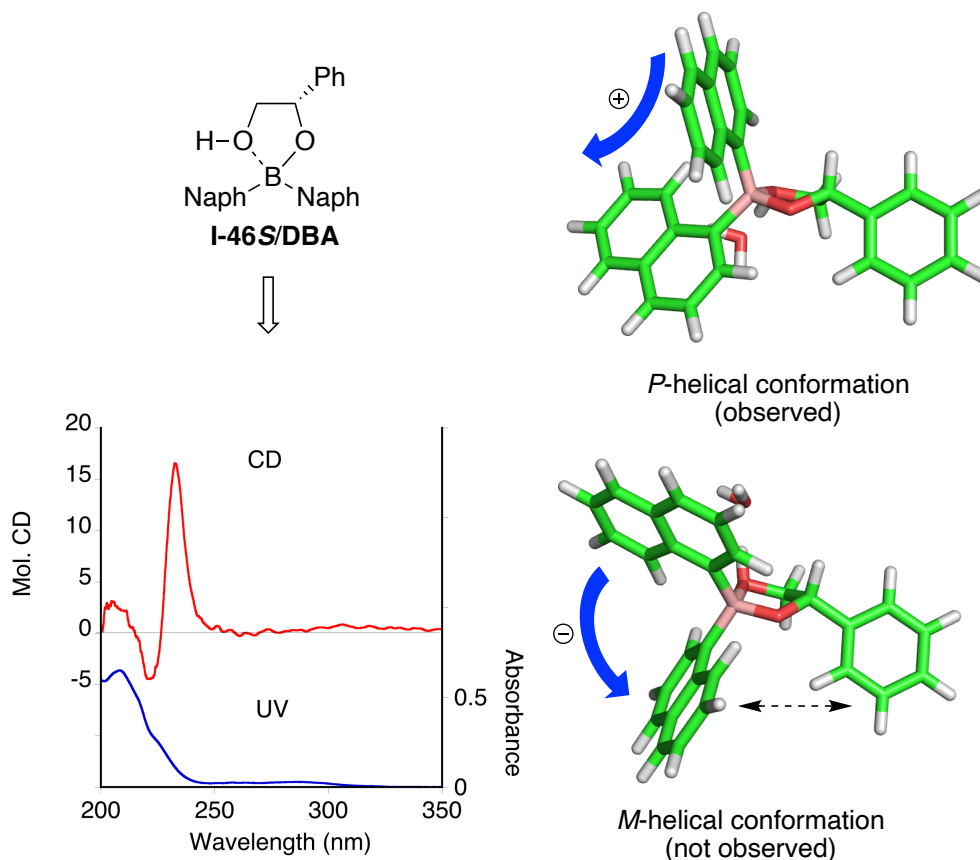


Figure I-24 UV-vis and CD spectra of I-46S complexed with DBA, along with energy minimized structures.

Dinaphthyl borinic acid (1 μL of a 1 mM solution in acetonitrile) was added to acetonitrile (1 mL) in a 1.0 cm cell to obtain a 1 μM **DBA** solution. The blank spectrum containing only solvent and **DBA** was obtained from 200 nm to 350 nm with a scan rate of 100 nm/min (at various temperatures depending on the substrate). Chiral substrate solution (up to 5 μL of a 10 mM solution in acetonitrile) was added into the prepared **DBA** solution (1 μM) to afford the host/guest complex. CD spectra of samples (10 scans) was

measured and was subtracted from the blank spectrum. Normalization of the resultant spectra considering the concentration of the **DBA** chromophore led to the reported results in molecular CD (Mol. CD).

Table I-1 and I-2 show a set of chiral 1,2-diols examined with **DBA**. In practice, the experiments were carried by addition of various equivalents of the diol to a 1 μ M solution of **DBA** in acetonitrile. No more than a 1 min incubation period was required prior to CD measurements, which were either carried out at room temperature or -4 $^{\circ}$ C, depending on the substrate examined. As expected, **DBA** is CD silent in acetonitrile. We were pleased to observe ECCD signals with the substrates tested. A consistent trend was observed, where a positive ECCD signal was observed for (*S*)-1,2-diols complexed with

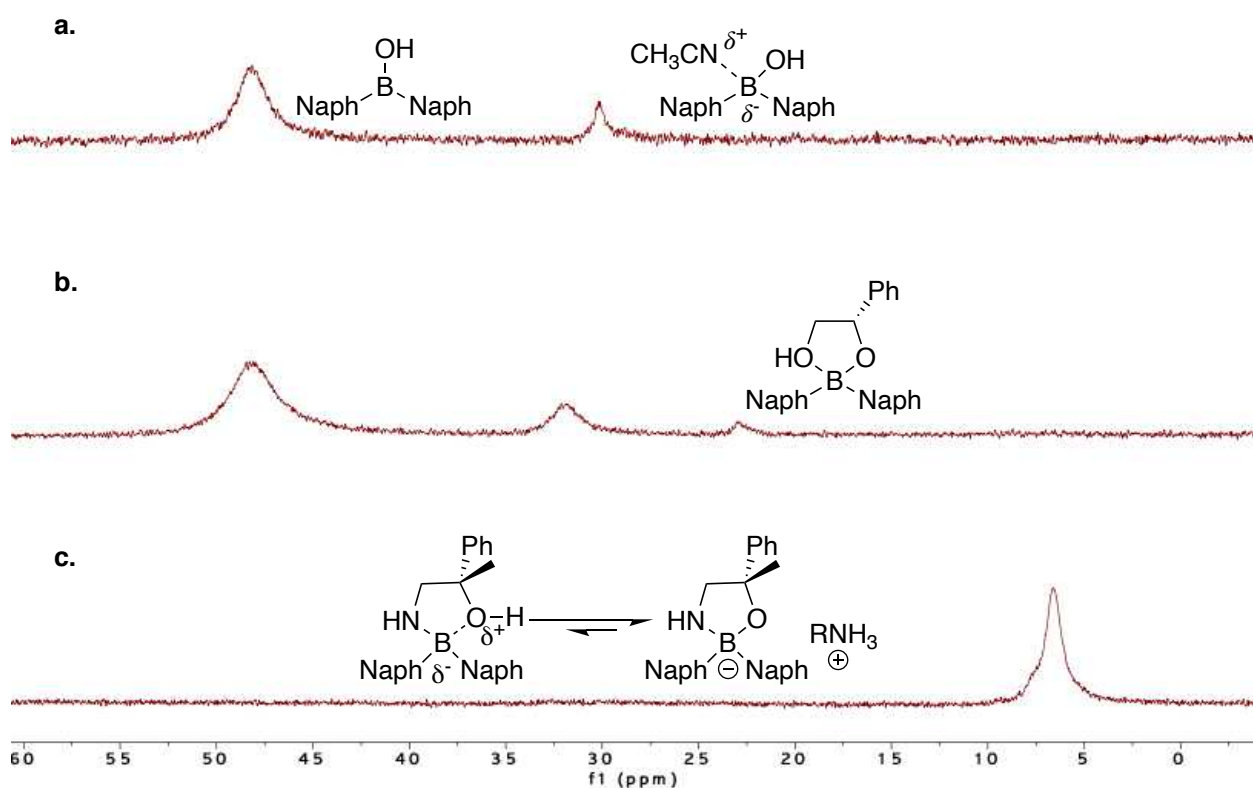


Figure I-25 ^{11}B -NMR of: a. **DBA** in acetonitrile. b. (*S*)-amino alcohol complexed with **DBA**. c. (*R*)-amino alcohol complexed with **DBA**.

DBA, while (*R*)-1,2-diols yielded a negative ECCD spectrum, irrespective of being substituted with an aryl or alkyl group (Figure I-23). Figure I-24 illustrates the UV-vis and ECCD spectra of **I-46S** complexed with **DBA**, demonstrating a common trend observed in all of the CD spectra obtained for this study, notably, the asymmetric nature of the couplet. In fact, this observed asymmetry for naphthyl groups has been reported on previously and is related to the coupled electric transition moments that lead to the Cotton effects. Furthermore, strong absorptions close to 200 nm, either from solvent and/or minute impurities, can diminish the short absorption band due to reduced signal/noise ratio. As observed in our previous studies with naphthyl substituted systems,^{48, 49} although two main transitions (1L_a ~270 nm and 1B_b ~220 nm) are present, there is no evidence of 1L_a in the ECCD spectra, and only the coupling from the more intense 1B_b band (long axis transition) is observed. The naphthyl substrate **I-43R** (entry 3) is noteworthy, as addition of more than 1 equiv led to a complex CD spectrum with diminished amplitude. This is presumably the result of coupling of the naphthyl group from the substrate with the naphthyl groups on **DBA**.

Figure I-24 depicts energy minimized models of **I-46S/DBA** complex in two different conformations. Structural optimization (DFT-B3LYP/6-31G*) were carried with a trivalent boron, assuming a dative bond of one of the hydroxyl groups of the diol with the boron atom. The calculations assumed a water molecule hydrogen bonded to the hydroxyl group that is coordinated to the boron atom. This ensured electrostatic compensation to avoid an energetic penalty by the over estimation of charged species in gas phase

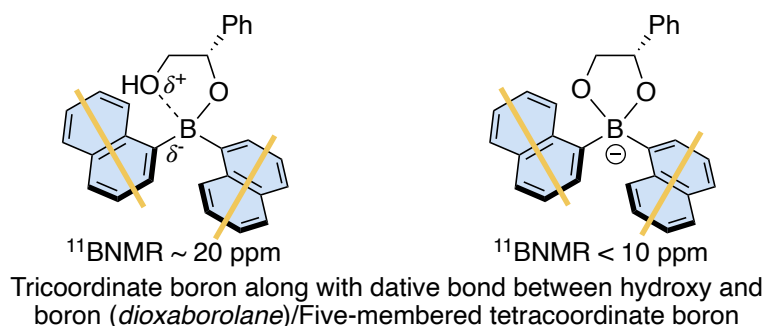


Figure I-26 Chemical shift of tri and tetracoordinate boron

calculations. In fact, without the water molecule, the dioxaborolane ring would fragment in calculations. The choice to have a dative bond between the hydroxyl and the boron atom is confirmed from NMR studies, where the boron is clearly tricoordinated, with a chemical shift (22.6 ppm) consistent with the latter assignment (see Figure I-25a,b for ^{11}B -NMR of **DBA** and **I-46S/DBA** complex and Figure I-26 for chemical shift of tri and tetracoordinate boron).⁵¹⁻⁵³ As expected, the five-member dioxaborolane ring adopts a chair conformation, placing the larger phenyl group in the pseudo equatorial position. It is anticipated that this geometry would dictate the favored helicity of the 1-naphthyl substituents, with the observed *P*-helical arrangement avoiding the more sterically congested rotameric position. The *M*-helicity would bring the equatorial naphthyl group in a closer proximity to the phenyl ring (see the double headed arrow that indicates the increased steric crowding in Figure I-24). Application of this simple mnemonic to the substrates in Table I-1 leads to the prediction of the anticipated ECCD.

Although not a focus of this project, we surmised that 1,2-amino alcohols should react with **DBA** in the same manner as 1,2-diols, adopt a similar conformation, and result in a preferred helicity of the naphthyl groups due to the presence of the stereogenic center.

In fact, we would predict that because of the stronger interaction of the amine with the boron center, a stronger complex, and thus a larger ECCD amplitude would be observed. As Figure I-27 depicts, complexation of (*R*)-1-amino-2-phenylpropan-2-ol (**I-50R**) with **DBA** does yield a negative ECCD, as predicted. Impressively, with only 4 equivalents of **I-50R** added (in comparison to 40 equivalents for 1,2-diols listed in Table I-1), the observed ECCD amplitude was in excess of 1300. ¹¹B-NMR of the **I-50R/DBA** complex is also markedly different as compared to the NMR of 1,2-diols complexed with **DBA** (see Figure I-25c). The ¹¹B chemical shift with the amino alcohol complex is shielded to 6.6 ppm (22.6 ppm for 1,2-diols), which along with its sharper profile indicates a tetracoordinate boron atom. This also would further rigidify the cyclic structure, leading to a larger discrimination of conformer populations, resulting in a stronger ECCD.

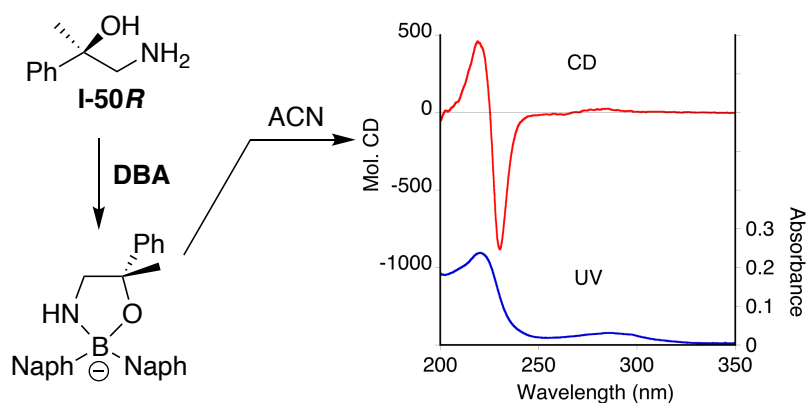


Figure I-27Complexation of amino alcohol **I-50R** with **DBA** leads to a strong ECCD active complex.

I-6 Conformational analysis

Calculations were performed with the Spartan'18 software package. Conformer distributions leading to the observed ECCD signals were modeled in the following three steps:

- 1) Initial conformational searches were carried out using Monte Carlo search algorithm with the starting temperature at 10,000 K. Molecular mechanics at the MMFF level of theory was implemented to quickly generate a library conformational minimum.
- 2) The entire library conformational minima were then subjected to further optimization using density functional theory B3LYP/6-31G* (gas phase). All structures were finally re-optimized using DFT-B3LYP/6-31G* level of theory in acetonitrile (SM8 solvation model).
- 3) Following structural optimization, Boltzmann weights were assigned to each structure to calculate the average contribution of the *P* vs *M* helicity for each system.

I-46S/DBA diol was chosen as the modeling candidate given its relatively small size and large ECCD signal amplitude ($A = +49$). Two tautomers of the dioxaborolane were considered for conformational analysis. The first tautomer has the 1° alcohol as the dative bond donor to the boron center and the second has the 2° alcohol as the donor (Figure I-28). Conformer distributions of both tautomers were considered for the Boltzmann analysis as they could be in rapid equilibrium in the solution. The deprotonated anionic borinate was however not considered for analysis, since NMR studies did not show any evidence of the existence this species in solution.

Nonetheless, conformational analysis of both **I-46S/DBA-1** and **I-46S/DBA-2** lead to ring opened structures (Figure I-28) as the lowest energy conformers. This is because the dative bond itself is insufficient in compensating for the resulting charge separation at

the sterically demanding tetra-coordinated boron. Nevertheless, conformational analysis of these two open forms suggested a 87.7:12.3 population ratio of *P* to *M* helical structures (top 2 kcal/mol), which did support the observed ECCD signal. We further investigated the possibility of a closed ring structure contributing to the ECCD signal.

Conformational analysis of the complex **I-46S/DBA-1** and **I-46S/DBA-2** with an additional water molecule favored closed ring structures (Figure I-29). This is because hydrogen bonding from the water to the hydroxyl sufficiently compensates for the charge separation and increased sterics generated from the dative bond. The presence of this

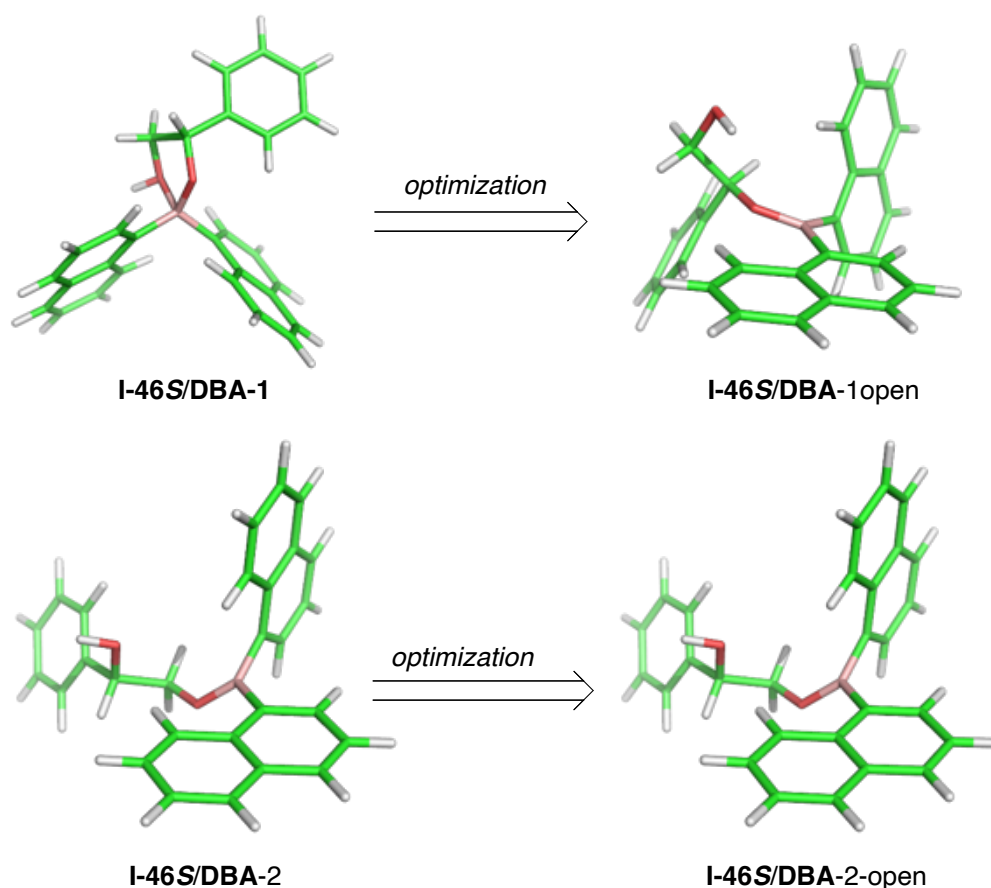


Figure I-28 Ring opened dioxaborolane structures (right) found from conformational search started from ring closed structures (left) and optimized with DFT-B3LYP/6-31G* (SM8-acetonitrile).

ring dioxaborolane system yields a mnemonic that follows the observed trend. Further studies to change the nature of the chromophore on the boron, not only to change its absorption profile (bathochromic), but also to force larger steric interactions, are underway. Also, continuing studies are in progress for application of the same strategy to other functional groups, such as amino alcohols, amino acids, and α -hydroxy carboxylic acid.

Chapter II – Towards the Total Synthesis of Napyradiomycin A1

I-Introduction

So far, nearly 5000 biogenic halogenated natural compounds have been discovered. This number increases as chemists investigate chloride- and bromide-rich environments for exploring new biologically active natural products. Almost all organohalogen natural products demonstrate a range of unique biological activities. Nearly half of the halogenated natural derivatives feature an sp^3 -hybridized carbon bonded to the halogen. As a result, stereochemical control in the installation of the halogen has to be considered as a critical component of any synthesis pathway.^{54, 55} Despite the abundance and biological activities of the halogenated natural products, synthetic methods for enantioselective installation of carbon-halogen bonds are scarce.

One class of halogenated natural products are the napyradiomycins. The napyradiomycins are a large set of unique meroterpenoids featuring various halogen substitution patterns, primarily seen with chlorine. A few examples of napyradiomycins have been synthesized in a racemic manner, and just one chemical asymmetric synthesis of napyradiomycins has been reported.⁵⁶ The critical challenge for the synthesis of napyradiomycins and other halogenated natural products is that the number of methodologies for the introduction of the halogenated stereocenters is limited. Of natural products containing brominated or chlorinated stereocenters, only 12 natural products have been synthesized.⁵⁷

II-2 A survey of previous total synthesis of napyradiomycin

A literature search shows that three chemical syntheses of the napyradiomycins have been reported so far. These syntheses include the racemic synthesis of napyradiomycin

A1 and the enantioselective synthesis of two members of this family, napyradiomycin A1 and azameron. A brief discussion of these syntheses will be provided below.

In 2002, Tatsuta and coworkers reported the first total synthesis of (\pm)-napyradiomycin A1 in 16 steps (Figure II-1).⁵⁸ The tricyclic core was made starting from commercially available 2,4-dihydroxy benzoic acid in eight steps. Installation of the chlorine atoms and geranyl side chain in a regio- and stereoselective fashion were the critical steps in their

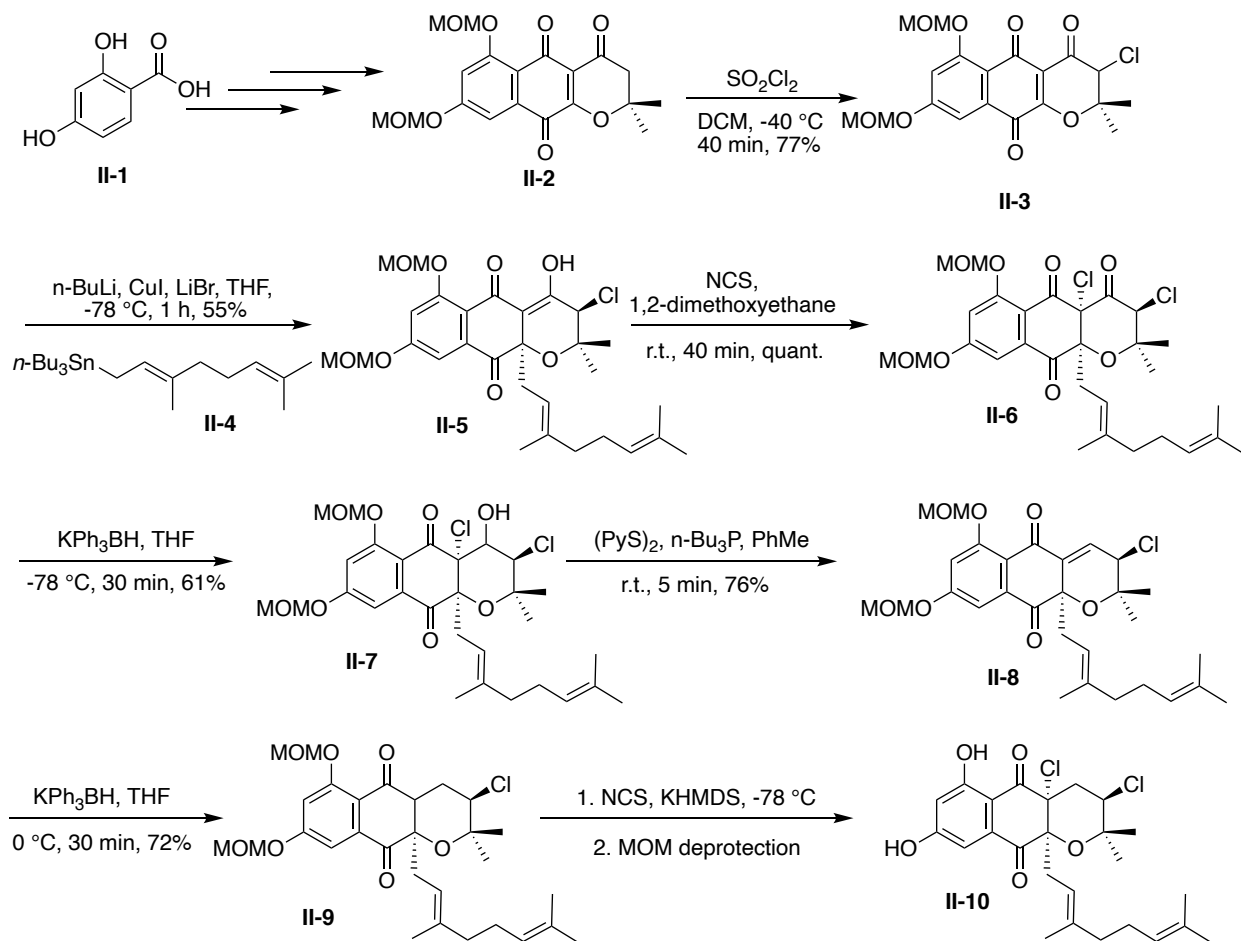


Figure II-1 The first total synthesis of (\pm)-napyradiomycin A1

total synthesis. The first chlorine atom was appended by α -chlorination of dihydropyranone using SO_2Cl_2 . The geranyl segment was added to intermediate **II-3** via Michael addition.

It is believed that the trans relative stereochemistry between the geranyl group and the chlorine atom results from the semi-axial orientation of the chlorine atom next to the geminal dimethyl groups. Chlorine was installed at the C4a position with the use of NCS as a chloronium ion source. Deprotection completes the racemic synthesis of napyradiomycin A1.

II-3 Enantioselective synthesis of napyradiomycin A1

In 2009, Snyder and coworkers report the only literature precedent for the asymmetric chemical synthesis of napyradiomycin A1.⁵⁶ Two step synthesis of flaviolin, asymmetric dichlorination of an isolated alkene, and forging the geranyl side chain at C10-a via

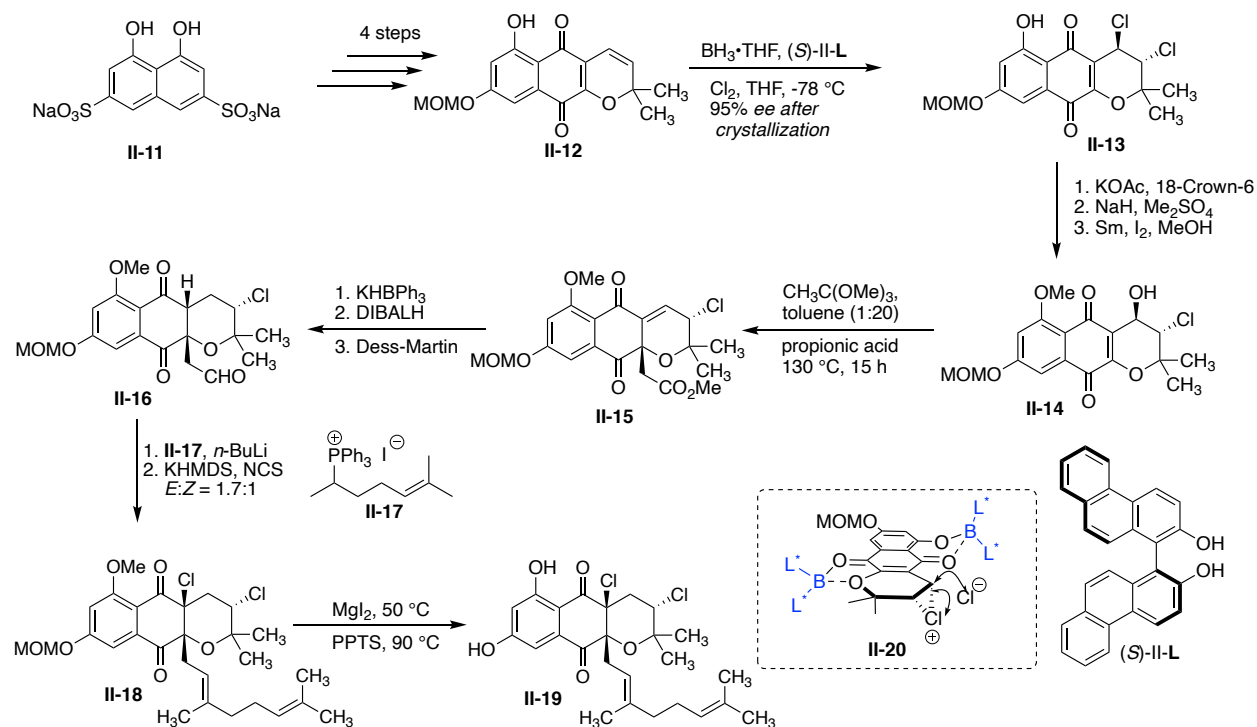


Figure II-2 Enantioselective synthesis of napyradiomycin A1.

Johnson-Claisen rearrangement were the strategic steps in the synthesis of napyradiomycin A1. They proposed a stereochemical model to rationalize the stereochemical outcome of the halogenation reaction. It was hypothesized that interaction between two equivalents of 1,1'-biphenanthryl ligand and the substrate results in the formation of the complex **II-20**. π - π interactions between one of the biphenanthryl groups and the substrate dictates the second ligand's orientation, which results in the steric block of the top face of the alkene moiety, capturing the chloronium from the bottom face. The Snyder group utilized the stereochemistry of the chlorine, adjacent to the quinone, to install the geranyl side chain with the desired stereochemistry at C10-a. This asymmetric synthesis requires a super stoichiometric amount of the chiral ligand to induce enantioselectivity in the dihalogenation reaction (Figure II-2).

II-4 Enantioselective synthesis of azamerone

Another member of this halogenated meroterpenoid family, azamerone **II-31**, was synthesized by Burns and coworkers in 2019 (Figure II-3).⁵⁹ This synthesis was the first example of a catalytic asymmetric total synthesis of a member of the napyradiomycin family. They envisioned that the synthesis of the azamerone could be achieved using three fragments: chloropyran **II-26**, tetrazine **II-30**, and chlorocyclohexane boronic hemiester **II-27**, which can be synthesized in four steps from geranyl acetate. Asymmetric chloroetherification of hydroxyquinone **II-21**, generates the benzochloropyran **II-24** intermediate, which was one of the vital steps for their synthesis. They found that the mixture of TADDOL-titanium complex and *tert*-butyl hypochlorite efficiently catalyzes the chlorocyclization of prenyl hydroxyquinone and provides the desired benzopyran product.

II-4 Divergent synthesis of napyradiomycin family

Modern synthetic chemists have evolved their capacity to create molecules of varying complexity since these naturally occurring compounds are the critical source for drug discovery. The primary consensus in reaching these complex molecular targets, entails spending ample time and energy. However, thus far, such efforts are often met with difficulty, specifically in the realm of synthesizing natural products. Modern synthetic methods fall short of sufficiently synthesizing quantities of these compounds for SAR studies. Nature utilizes common intermediates to make a large number of natural products in a divergent manner. This approach provides a robust tool to improve the efficiency of synthetic pathways in labs and enhance our ability for easier access to the abundance of natural products. Accessing numerous structural variants of natural compounds increases the possibility of discovering new medicines and drugs. One possible solution to this problem is a divergent synthesis.

The divergent synthesis was described as the synthesis of no less than two natural products in the same family from an advanced intermediate.⁶⁰ In 2011, MacMillan showed the synthesis of six natural products from a key common intermediate.⁶¹ Consequently, the opportunity of a divergent approach was expanded for the synthesis of molecules that are a subset of the family of natural products.⁶²⁻⁶⁵

To have a collection of relevant target natural products for a divergent synthesis, comprehensive features of these products must be considered. For instance, structural framework, stereochemistry, functional and substituted group. Subsequently, design of an efficient synthetic pathway to synthesize an advanced intermediate which would

eventually and easily be transferred to a set of desired natural products is essential. Some may find inspiration in structural intermediates formed during the natural biosynthetic processes which form natural products. However, due to various drawbacks in their properties, for instance solubility in organic solvents, the use of natural biosynthetic pathways in the designing a common intermediate is limited. Another aspect to consider with divergent synthesis is that more advanced intermediates often result in more efficient synthetic pathways; however, it results in fewer number of target natural products. According to well adopted approaches commonly utilized in the divergent synthesis, three categories can be considered for this approach to natural product synthesis. Firstly, natural products that share a common core structure, but they tend to differ in oxidation state and stereochemistry.⁶⁶ In a second approach, natural products that can be generated by structural reorganization of a common synthetic intermediate.⁶⁷ Lastly, natural compounds that share the same core structure but with different moieties attach to the core.⁶⁸

The napyradiomycins are a large set of unique meroterpenoids featuring a variety of halogen substitution patterns, however primarily seen with chlorine. The first member of this family was originally isolated from the actinomycete *Streptomyces ruber* by Shiomi and coworkers in 1986.⁶⁹ They share a common core structure consisting of a semi-naphthoquinone motif, a tetrahydropyran or dihydropyran ring, and a monoterpene segment attached to C-10a. The variant structure of the members of this family primarily originates from the monoterpene side chain. The members of this family of natural products are classified into three different categories: Type A (NPD-As) consisting of a

linear side chain at C-10a position (**II-32**), Type B (NPD-Bs) in which side geranyl chain goes under cyclization to generate cyclohexane ring (**II-33**), and Type C (NPD-Cs) where a 14-membered ring is formed by the connection between C7 and C10-a of naphthoquinone scaffold (**II-34**). So far, around 50 derivatives of napyradiomycins have been discovered, and the discovery of new members of this class of this natural product is ongoing.⁷⁰

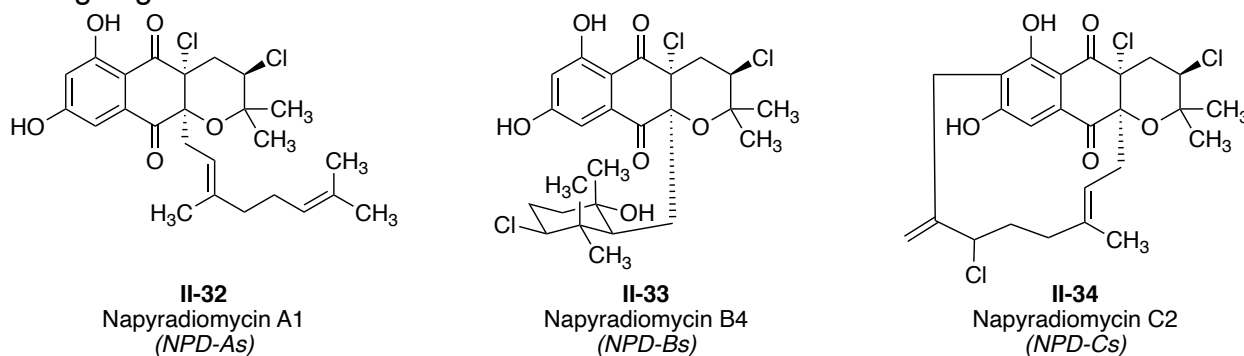


Figure II-4 Three categories of napyradiomycin family

In 2020, Reyes and coworkers reported the isolation and characterization of four new napyradiomycins (Figure II-5).⁷⁰ Of the newly discovered new napyradiomycins, they discovered the first NPD-As having a hydroxy group instead of chlorine at C3 (**II-34**). They isolated the first example of NPD-Bs in which the chlorine at the C3 position has a distinctive and different relative configuration (**II-35**). They revealed an unprecedented napyradiomycin with a 16-membered ether ring that spans ring A and B (**II-37**). This molecule can potentially be considered as a member of a new category of

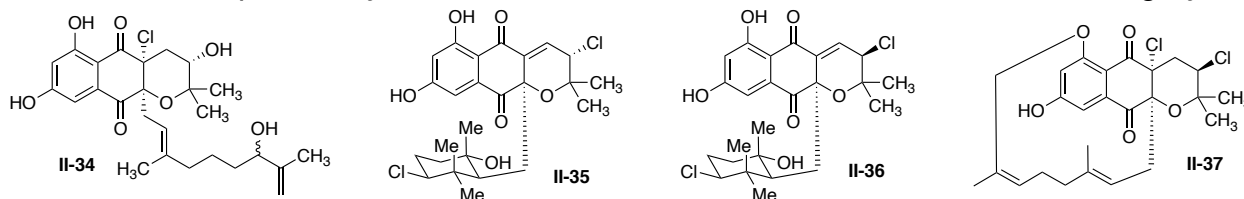


Figure II-5 Four new members of napyradiomycin family

napyradiomycins as NPD-Ds. Studies on these hybrid polyketide-terpenoid compounds have revealed a wide variety of biological activities such as cytotoxicity, antibacterial activity, promising anticancer activities, and estrogen receptor antagonization.

So far, there are no literature reports for the catalytic asymmetric synthesis of napyradiomycins. A detailed SAR study of the target molecule requires a concise and efficient synthetic route for these natural molecules along with their analogs. Unfortunately, so far, no suitable synthetic route is available to either tackle SAR studies or to permit straightforward synthesis of analogs. One major challenge in synthesizing

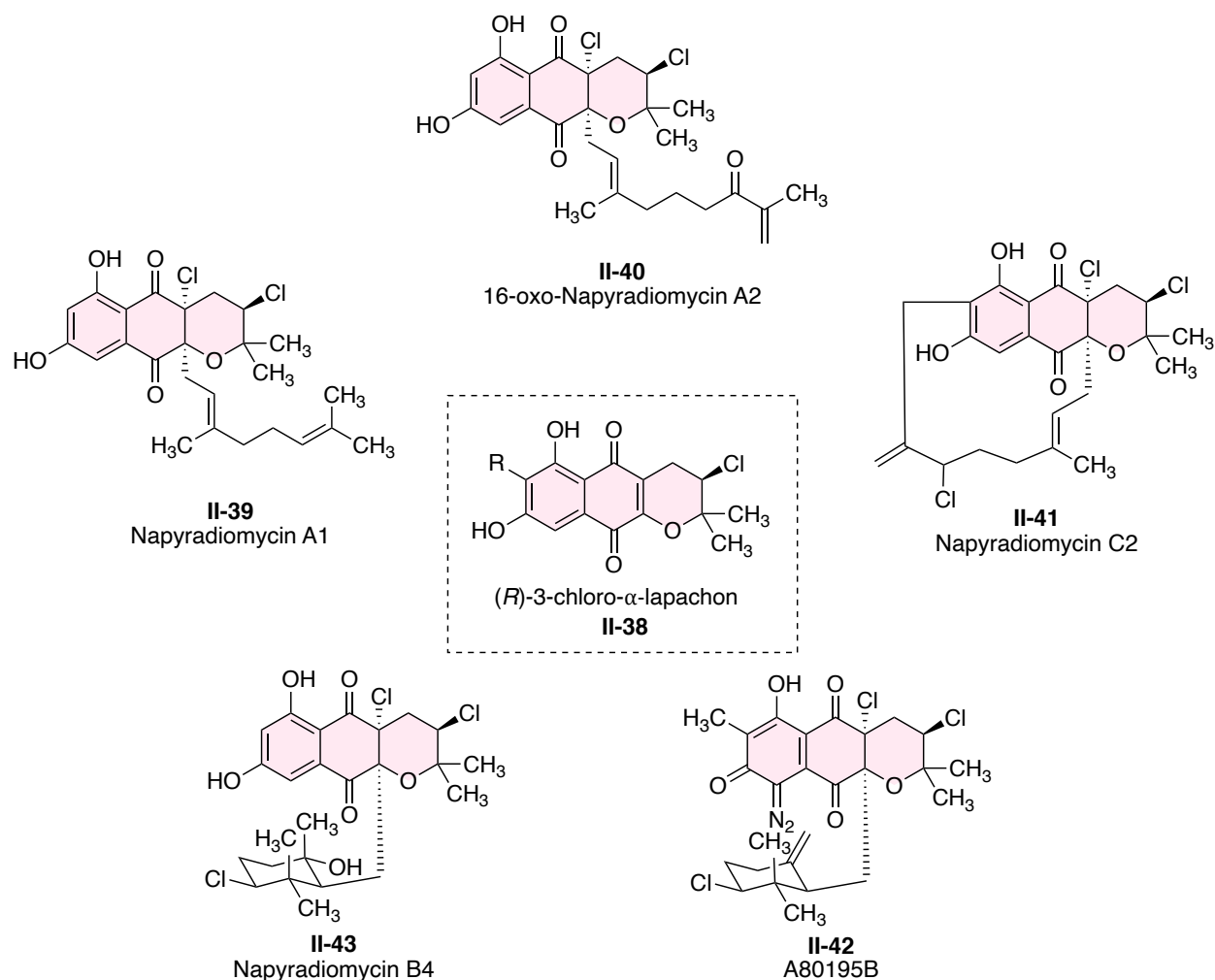


Figure II-6 α -lapachone as a common intermediate of napyradiomycin family

naypradiomycin natural products, is the lack of an efficient methodology for installing the stereogenic chlorine atom in an enantioselective fashion. Among the halogens, catalytic enantioselective haloetherification initiated by a chlorenium ion is less developed than iodo- and bromoetherification analogs. Considering the large number of natural products containing chlorine, the lack of this efficiency is highly noticeable. We address many of these issues by our proposed synthesis and employ an unprecedented enantioselective chlorocyclization of an unactivated alkene.

To propose the proper common intermediate for the convergent synthesis of the napyradiomycin family, we required familiarity with the structural features of the target natural products. Napyradiomycins share three common segments: naphthoquinone, tetrahydro- or dihydropyran, and monoterpene fragments at C10-a, which appear as a side chain or cyclohexane. A few members of the napyradiomycin family are illustrated in Figure II-6. Based on the common structural features, we envisioned the protected α -lapachone motif (**II-38**) could be a good candidate as the common intermediate for the divergent synthesis of napyradiomycins. An enantioselective chloroetherification of prenyl-containing phenol is proposed as one of the challenges for the asymmetric synthesis of the napyradiomycins. Molecular modeling was used to support the suggestion that the stereochemistry of the chlorine at the C3 position which can potentially dictate the stereochemistry of two other stereocenters at C10-a and C4. Our previous experience in asymmetric halofunctionalization of alkenes has demonstrated that a hydrogen-bonding functional group is most likely necessary to interact with the chiral ligand and helps to orient the substrate inside the chiral pocket.⁷¹⁻⁷³ Phenol was

predicted to act as a hydrogen-bonding motif; however, the distance between the hydroxyl group and the olefin in the substrate was a concern. Moreover, there were no reports for phenols as nucleophiles in halofunctionalization reactions.

Having α -lapachone as the intermediate for the divergent synthesis should provide a short, scalable, and divergent synthesis which means we would access numerous family members.⁹

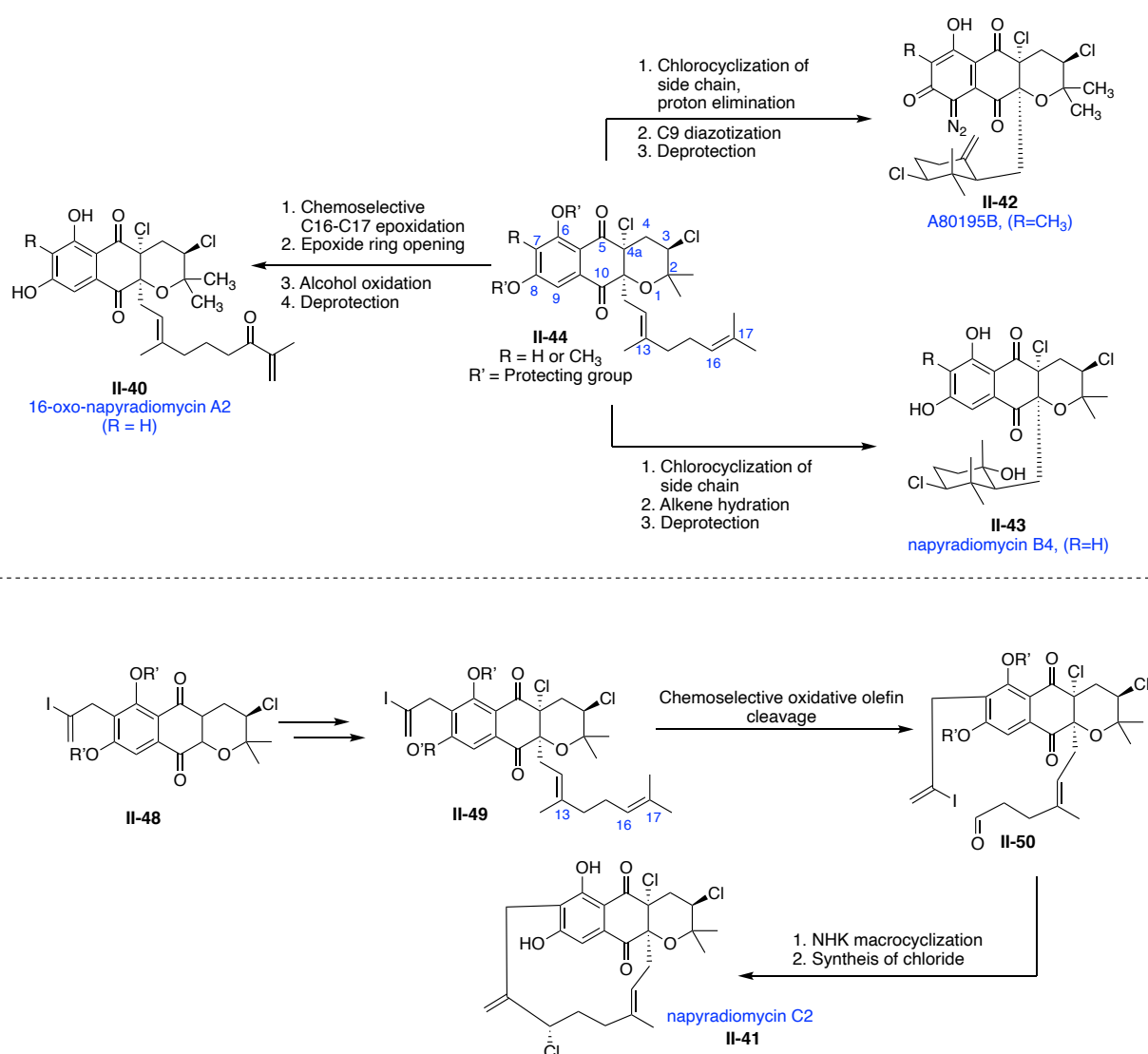


Figure II-7 Proposed divergent syntheses of napyradiomycin family

A few routine manipulations of napyradiomycin A1 or its 7-methyl derivative (**II-44**) can be used to transfer these natural products to other family members of napyradiomycin, such as 16-oxo-napyradiomycin A2 (**II-40**), napyradiomycin B4 (**II-43**), and A80195B (**II-42**) (Figure II-7).

For the synthesis of 16-oxo-napyradiomycin A2 from **II-40**, We predict chemoselective epoxidation of C16-C17 of geranyl of **II-44** would be achieved using previously reported regioselective epoxidation.^{74, 75} The reaction of the resulting epoxide with lithium diethylamine or aluminum isopropoxide results in the formation of an allylic alcohol.⁷⁶ Oxidation of the alcohol in the presence of Dess-Martin periodinane or pyridinium chlorochromate affords the C16 carbonyl. The last step of deprotection would complete the synthesis of the naturally occurring product, 16-oxo-napyradiomycin A2.

Synthesis of A80195B requires three more steps from 7-methyl napyradiomycin **II-44** (R = CH₃), including chlorocyclization, proton elimination, and C9-diazotization. This step can be accomplished by employing 2-azido-1,3-dimethylimidazolium chloride, as has been reported before.⁷⁷ Napyradiomycin B4 can be synthesized using diastereoselective chloropolyene cyclization followed by alkene hydration and deprotection.⁷⁸ Natural products that require additional functionalization at C7 or the geranyl side chain are accessible, as well. For example, precursor **II-49** can be elaborated for the synthesis of napyradiomycin C2. The requisite C7 vinyl halide motif required for the late-stage Nozaki-Hiyama-Kishi macrocyclization is easily incorporated early in the synthesis (see **II-48** in Figure II-7).⁷⁹ Well-documented NHK macrocyclization reactions in conjunction our own experience with this reaction, namely the unrelated synthesis of the Haterumalides,

provides confidence that these syntheses are reachable.⁸⁰ Due to the accessibility to several members of napyradiomycins through napyradiomycin A1, the synthesis of this molecule was selected as our first target.⁸¹

II-5 Retrosynthesis of α -lapachone II-52

As shown in Figure II-9, access to napyradiomycin A1 will pave the way for the synthesis of other family members. Here, we briefly discuss the retrosynthesis of napyradiomycin A1. This natural product can be made by C10a geranylation and C4a chlorination of α -lapachone. Our generalized retrosynthetic approach to this intermediate is illustrated in Figure II-8. We proposed that the aromatic ring in α -lapachone can be formed via Diels-Alder/aromatization reaction between Danishefsky diene **II-53** and dienophile **II-54**. It was envisioned that the enantioenriched benzo-pyran is accessible via asymmetric chloroetherification of prenyl phenol **II-55**. Intermediate **II-55** can quickly arise from commercially available 2,5-dimethoxybenzaldehyde. According to the proposed synthesis, the first goal should be to generate the common advanced-intermediate, α -lapachone **II-52**.

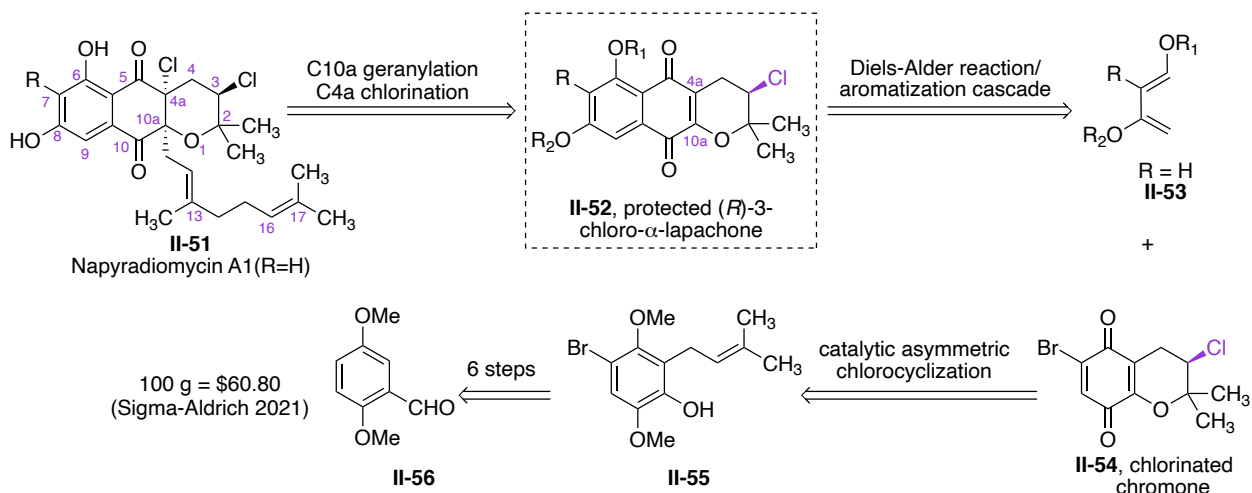


Figure II-8 Retrosynthesis analysis of napyradiomycin A1

II-6 Synthesis of α -lapachone derivative

Our synthesis commenced with the generation of aryl bromide **II-57**. The desired product was synthesized easily from commercially available 2,5-dimethoxy benzaldehyde. Regioselective bromination of **II-56** took place in the presence of a slight excess of bromine in glacial acetic acid with a moderate yield.⁸² The formation of benzo-pyran moiety required a hydroxy group on the benzene ring to act as a nucleophile in the chlorocyclization step. Baeyer-Villiger oxidation was considered to convert the aldehyde to the phenol moiety. The resulting bromo benzaldehyde from the previous step was treated with *m*-CPBA leading to the formation of the formate ester. The basic hydrolysis of the ester resulted in the formation of phenol **II-59** in good yields over two steps.⁸³

Propargylation of the hydroxyl using methyl propargyl carbonate **II-61** in conjunction with DBU and copper (II) chloride afforded the desired product **II-62** in low yield (the

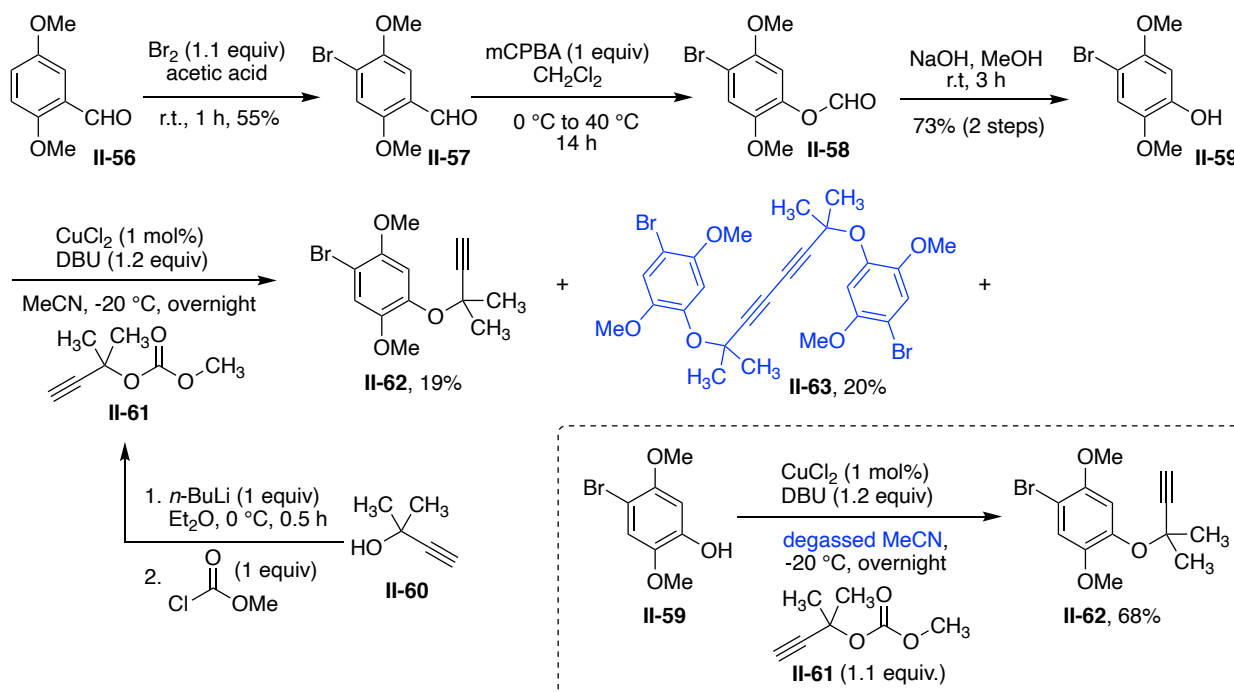


Figure II-9 Towards the synthesis of ring C

propargyl carbonate was generated using methyl chloroformate and 2-methyl-3-butyl-2-ol).⁸⁴ We decided to improve the efficiency of this step by separating and characterizing the side product of the reaction. We identified dimer **II-63** the result of Glaser coupling of terminal alkynes **II-62** which presumably is caused by the presence of oxygen and water. The mechanism of Glaser coupling, illustrated in Figure II-10, shows the involvement of oxygen as an oxidative reagent in the reaction.

A catalytic pathway for the propargylation of phenol is proposed in Figure II-10. The catalytic cycle starts with the formation of complex **II-62** between copper and the alkyne moiety. Subsequently, two steps consisting of deprotonation then protonation, promoted by the base, generates copper complex **II-63**. Elimination of acetyl moiety affords copper acetylide complex **II-63**, which is in resonance with the copper-allenylidene complex. Nucleophilic attack of the phenol to carbocation **II-64**, followed by deprotonation, provides

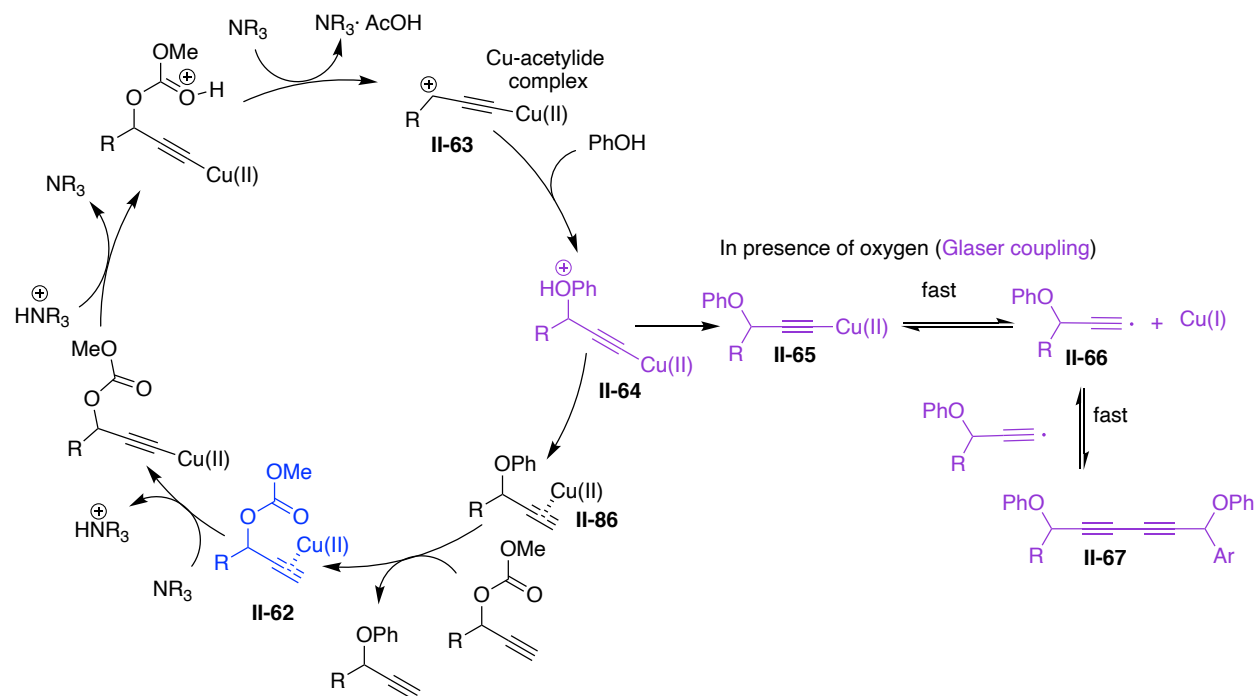


Figure II-10 Copper catalyzed propargyl substitution and Glaser coupling

the final product **II-65**. As shown in Figure II-10, copper complex **II-65** is prone to undergo homolytic cleavage in the presence of oxygen. The produced alkynyl radical dimerizes and generates compound **II-67**.⁸⁵

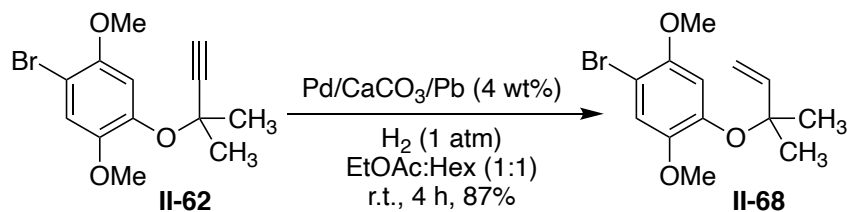


Figure II-11 Reduction of alkyne using Lindlar's catalyst

Accordingly, to prevent the formation of the undesired oxidative coupling product and stop the reaction after propargylation, the *O*-alkylation took place under an atmosphere of argon atmosphere and the solvent was degassed for 15 minutes. The desired product

Table II-1 Optimization of the Claisen rearrangement

entry	solvent	temp.	results
1	xylene	140 °C	II-69 42%
2	xylene	100 °C	II-69 40%
3	toluene	100 °C	II-68 was recovered
4	decalin	190 °C	II-69 55%
5 ^a	chloroform	100 °C	II-68 was recovered
6 ^b	THF	55 °C	II-68 was recovered

^a Eu(fod)₃ (Europium(III)-tris(1,1,1,2,2,3,3-heptafluoro-7,7-dimethyl-4,6-octanedionate) was used as a catalyst ^b zinc powder was used as catalyst. ^b These products are formed in entries 1, 2, and 4. The reported yields are for entry 1.

was attained with a significantly higher yield compared to the previous reaction (Figure II-9, dashed box).

Having alkyne **II-62** in hand, we were ready for the partial hydrogenation of alkyne using Lindlar catalyst. Treatment of the alkyne with Lindlar catalyst, quinoline in ethanol as solvent, under hydrogen atmosphere (1 atm) resulted in forming alkene **II-68** in low yields, along with the recovery of starting material.

Optimizing the reaction condition, such as increasing catalyst loading, increasing the weight percentage of catalyst, or eliminating quinoline from the reaction mixture, did not improve the yield of the corresponding alkene product. Fortunately, changing the solvent to a system compromised of 1:1 hexane:ethyl acetate afforded alkene ether **II-68** with complete conversion and high yield (Figure II-11).

Next, we turned our attention to the synthesis of *o*-prenyl phenol **II-69** using the Claisen rearrangement. We began the evaluation of the Claisen rearrangement using xylene as a solvent. Upon heating the alkene **II-68** at 140 °C for 3 hours, the Claisen product **II-69** was produced in moderate yield. Other side products were formed during the reaction, hampering the efficiency of the synthesis (Table II-1, entry 1). Allyl phenol **II-70**, benzopyran **II-71**, and dimethoxy phenol **II-72** were identified as side products. According to the structure and ratio of the side products, it appears that the ethereal C-O bond has homolytically cleaved, followed by recombination of aryl rings with the most stable quaternary carbon radical on the prenyl fragments. Further optimization was carried out in various solvents and temperatures to suppress the formation of the side products (Table II-1).

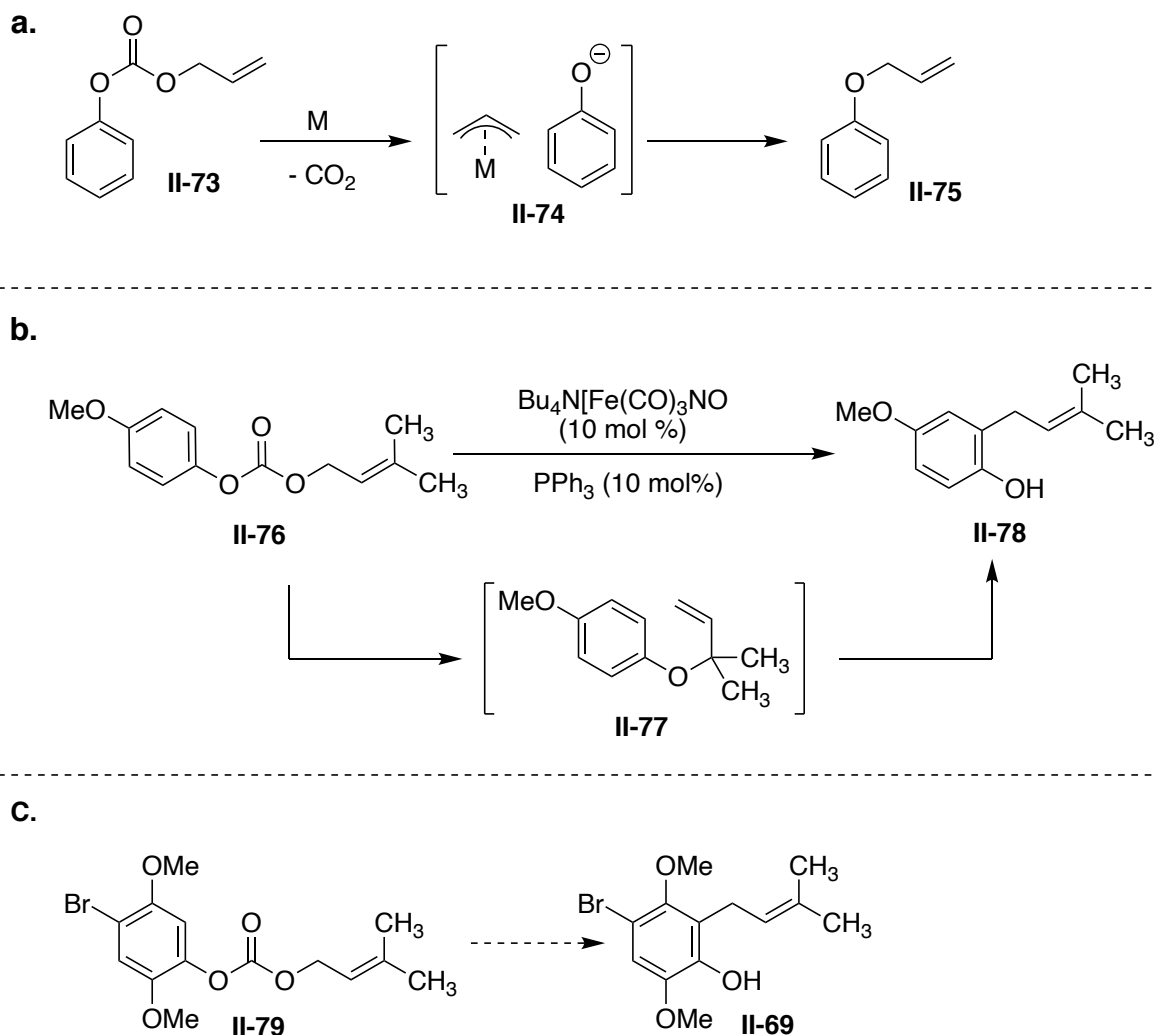


Figure II-12 a. Decarboxylative allylic etherification. b. Decarboxylative allylation/Claisen rearrangement. c. Formation of allylphenol using tandem decarboxylative allylation/Claisen

Employing xylene as a solvent at 100 °C provided the product with a similar yield (entry 2). Conducting the reaction in toluene at 100 °C resulted in the recovery of the starting material with no conversion (entry 3). Switching the solvent to decalin and raising the reaction temperature to 190 °C was slightly effective and improved the yield to 55% (entry 4). Next, we evaluated the Claisen rearrangement reported by Metz and coworkers.⁸⁶ Treatment of the prenyl ether with a catalytic amount of the europium(III)

complex in chloroform caused no conversion of starting material (entry 5). The reaction of starting material with zinc powder as the catalyst was not successful and gave rise to the recovery of starting material as well (entry 6). According to the result mentioned above, decalin as solvent was chosen as the best reaction condition for the Claisen rearrangement.

Due to the low efficiency of the Claisen rearrangement, an alternative pathway was considered to produce prenyl-containing phenol. We envisioned that a tandem decarboxylative allylic etherification/Claisen reaction could be an excellent candidate to generate product **II-69**. In 2009 Tunge et al.⁸⁷ reported the iron-catalyzed decarboxylative etherification of allylic carbonate **II-76** (Figure II-12-a). They demonstrated phenols with various substitutions develop allyl ether products in high yields in the presence of $\text{NBu}_4[\text{Fe}(\text{CO})_3(\text{NO})]$. The decarboxylative etherification of prenyl aryl ether **II-76**, an excellent biologically active precursor, was investigated (Figure II-12-b). They demonstrated the *O*-allylated product was converted to the *C*-allylated product as the reaction continues. Therefore, the iron catalyst was studied for the formation of the phenol ether **II-69**. Unfortunately, applying the same reaction condition on compound **II-79** did not provide the desired product, and the starting material was decomposed. Decarboxylative etherification transformation catalyzed by various palladium complexes was examined. Starting material **II-79** was recovered in the presence of $\text{Pd}(\text{OAc})_2$ and $\text{Pd}(\text{dba})_3$.⁸⁸ The reaction of starting material **II-79** with tetrakis(triphenylphosphine) palladium resulted in decarboxylation; however, etherification did not occur, leading to phenol **II-59** (Figure II-55).⁸⁹ Since none of the decarboxylative reactions under palladium

and iron catalysts were fruitful, we resorted to the original synthetic plan to continue our study toward the total synthesis of napyradiomycin A1. Having prenyl phenol **II-69** in hand, we were ready for catalytic asymmetric chloroetherification, enabling the construction of the chiral chromane core as a necessary step for the asymmetric synthesis of the target natural product.

Dr. Nastaran Salehi Marzijani, our former group member, previously investigated the chloroetherification of the phenol **II-80**. She was able to improve the enantioselectivity of the cyclization step with the use of EtOH to 70:30 enantiomeric ratio (Figure II-13, entry 4). To understand the poor enantio-induction outcome of the reaction, rate of the background reaction was investigated. Such a kinetic study revealed that the uncatalyzed reaction undergoes full conversion of alkenyl phenol within 2 minutes (see the graph in Figure II-13). This high rate of the background reaction could account for the moderate enantioselectivity of the reaction. To decrease the rate of background reaction, lower

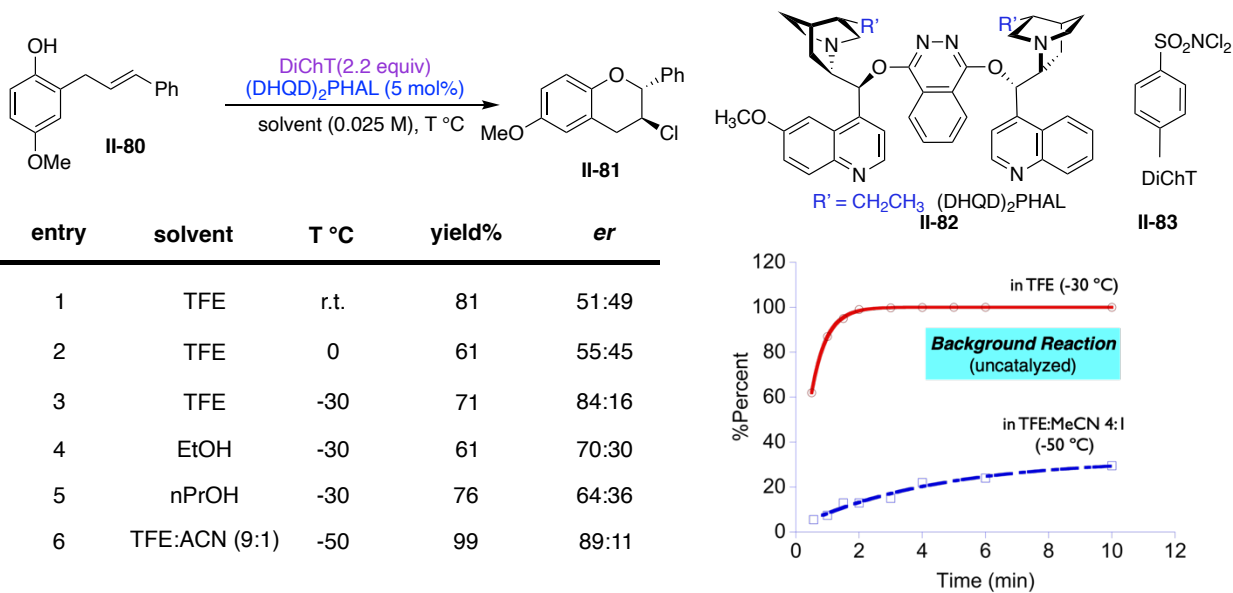
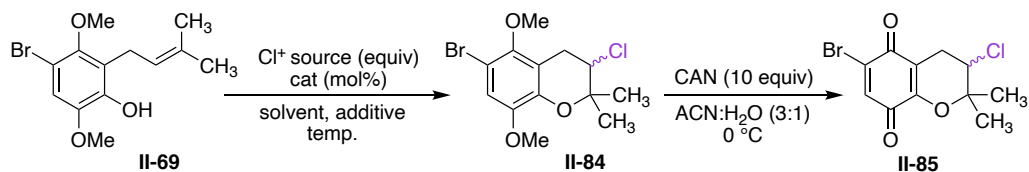


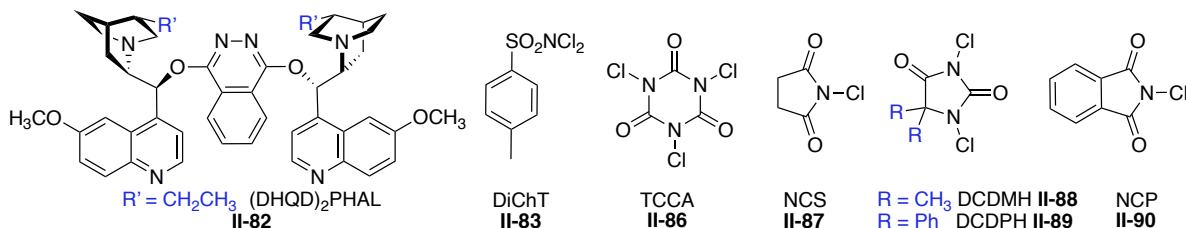
Figure II-13 improving the enantiomeric ratio via decreasing the rate of background reaction

Table II-2 Effect of solvent and chloronium ion source



entry	Cl ⁺ (equiv)	cat (mol%)	solvent	additive	temp. (°C)	yield (II-84)	er (II-85)
1	DiChT (2.2)	(DHQD) ₂ PHAL (20)	TFE/ACN (4:1)	—	-60	40	60:40
2 ^a	DiChT (2.2)	(DHQD) ₂ PHAL (20)	TFE/THF(4:1)	—	-60	—	—
3	DiChT (2.2)	(DHQD) ₂ PHAL (20)	TFE/Et ₂ O(4:1)	—	-60	45	55:45
4	DiChT (2.2)	(DHQD) ₂ PHAL (20)	ACN	—	-60	43	50:50
5	NCS (2.2)	(DHQD) ₂ PHAL (20)	TFE/ACN (4:1)	—	-60	25	50:50
6	TCCA (2.2)	(DHQD) ₂ PHAL (20)	TFE/ACN (4:1)	—	-60	—	—
7	NCP (2.2)	(DHQD) ₂ PHAL (20)	TFE/ACN (4:1)	—	-60	66	72:28
8	DCDPH (2.2)	(DHQD) ₂ PHAL (20)	TFE/ACN (4:1)	—	-60	60	84:16
9	DCDMH (2.2)	(DHQD) ₂ PHAL (20)	TFE/ACN (4:1)	—	-60	70	84:16

^aTFE incorporated product was formed

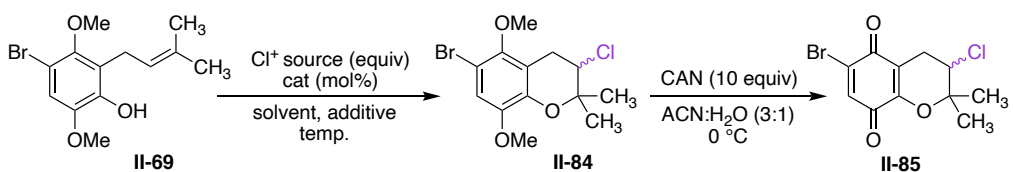


temperature and a variety of solvent combinations were examined. An enhancement of enantioselectivity (95:5 ratio) was seen when acetonitrile was used as a cosolvent at -50 °C. As a result, we decided to apply the same condition, for the chloroetherification prenyl phenol **II-69**.

Dichloramine-T **II-83** as the chloronium source, TFE:ACN (4:1) as the solvent, and (DHQD)₂PHAL **II-82** as the catalyst were chosen as a starting point to optimize the reaction conditions for the prenyl-containing phenol substrate **II-69**. It should be

mentioned that the enantiomers of benzo-pyran **II-84** were not separable using different chiral HPLC columns. Even using a chiral GC column for the separation of enantiomers was not helpful. Subsequently, the products were taken to the next step, and the quinone product was injected into HPLC, providing two separate peaks. Unfortunately, applying the optimized condition of the model substrate for phenol **II-69** was not fruitful, and resulted in the formation of the product **II-85** with poor selectivity (Table II-2, entry 1). Therefore, further optimization of the reaction on the real substrate was investigated. Beginning with the effect of the solvent on the system while keeping the other conditions the same (Table II-2, entries 2-4). Changing the solvent system to trifluoroethanol/tetrahydrofuran (4:1) did not yield the chromane product, and instead the

Table II-3 Effects of temperature and various additives



entry	Cl ⁺ (equiv)	cat (mol%)	solvent	additive (equive)	temp. (°C)	yield (II-84)	er (II-85)
10	DCDMH (2.2)	(DHQD) ₂ PHAL (20)	TFE/ACN (4:1)	—	-78	69	84:16
11	DCDMH (2.2)	(DHQD) ₂ PHAL (10)	TFE/ACN(4:1)	—	-78	68	84:16
12	DCDMH (2.2)	(DHQD) ₂ PHAL (10)	TFE/ACN(4:1)	Li ₂ CO ₃ (1)	-78	63	84:16
13	DCDMH (2.2)	(DHQD) ₂ PHAL (10)	TFE/ACN (4:1)	Li ₂ CO ₃ (5)	-78	57	81:19
14	DCDMH (2.2)	(DHQD) ₂ PHAL (10)	TFE/ACN (4:1)	Li ₂ CO ₃ (10)	-78	53	84:16
15	DCDMH (2.2)	(DHQD) ₂ PHAL (10)	TFE/ACN (4:1)	Li ₂ CO ₃ (20)	-78	56	85:15
16	DCDMH (2.2)	(DHQD) ₂ PHAL (10)	TFE/ACN (4:1)	Li ₂ CO ₃ (50)	-78	53	84:16
17	DCDPH (2.2)	(DHQD) ₂ PHAL (10)	TFE/ACN (4:1)	Na ₂ CO ₃ (1)	-78	65	84:16
18	DCDMH (2.2)	(DHQD) ₂ PHAL (10)	TFE/ACN (4:1)	benzoic acid (1)	-78	87	75:25
19	DCDMH (2.2)	(DHQD) ₂ PHAL (10)	TFE/ACN (4:1)	B(OPh) ₃ (1)	-78	80	75:25
20	DCDMH (2.2)	(DHQD) ₂ PHAL (10)	TFE/ACN (4:1)	AlCl ₃ (1)	-78	56	50:50

TFE incorporated product was formed (entry 2). Chlorocyclization in trifluoroethanol/ethyl ether and acetonitrile resulted in the formation of the product as a racemic mixture (entries 3 and 4, respectively).

Next, we turned our attention to the chlorenium source as one factor to enhance enantioselectivity (Table II-2, entries 5-9). We found that the chlorenium source has a significant effect on enantioinduction. NCS provided the product as a racemic mixture (entry 5). TCCA led to the formation of the TFE incorporated product, and NCP resulted in the formation of the product with a slight increase in enantioselectivity (72:28 enantiomeric ratio) (entries 6 and 7, respectively). DCDMH and DCDPH generated the desired product with 84:16 enantiomeric ratio (entries 8, 9), thus DCDMH was chosen as the optimum chlorenium source.

Next, we investigated the effect of the temperature and additives on the chlorocyclization of **II-69** (Table II-3). Lowering the reaction temperature to -78 °C provided the desired product with similar enantioselectivity (entry 10). Due to the straightforward preparation of the -78 °C bath, this temperature was selected as the optimal temperature. Lowering the catalyst loading to 10 mol% led to the formation of **II-84** with 84:16 selectivity and similar yield (entry 11). Because of the cost of the catalyst, we chose 10 mol% loading as the optimum condition in this investigation for further optimization studies. Next, the use of various additives was tested. The addition of Li₂CO₃ resulted in no significant improvement in enantioselectivity. Using 1 equivalent of Li₂CO₃ provided the product with 84:16 er (entry 12). The use of 5 equivalent Li₂CO₃ lowered the enantioselectivity to 81:19 (entry 13). Increasing Li₂CO₃ loading to 10, 20, and 50

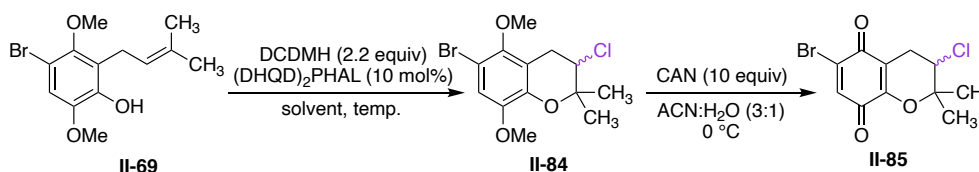
equivalents led to selectivity, comparable with the reaction's enantioselectivity without Li_2CO_3 or with 1 equivalent. (entries 14, 15, and 16). Sodium carbonate was also tested as an additive, but no noteworthy improvement was achieved (entry 17). We examined Lewis and Bronsted acidic additives such as benzoic acid, $\text{B}(\text{OPh})_3$ and AlCl_3 , all these additives resulted in either lower enantioselectivity or racemic mixtures (entries 18, 19, and 20).

Table II-4 shows the effect of a variety of solvent combinations on selectivity. Combining HFIP as cosolvent resulted in the formation of a racemate (entry 21). Ethanol, acetonitrile as a 4 to 1 mixture formed the benzo-pyran product with 72:28 selectivity (reaction temperature was increased to $-50\text{ }^\circ\text{C}$ because the solvent mixture froze at $-78\text{ }^\circ\text{C}$, entries 21 and 22). Switching from acetonitrile to the less polar solvent toluene led to a dramatic drop in selectivity and afforded the desired product in a racemic mixture (entry 23). This result revealed the importance of the polarity of acetonitrile as a cosolvent in this system. We, therefore, decided to examine the effect of the solvent with similar polarities. Combination of TFE with acetone afforded **II-84** with similar enantioselectivity as entry 11 (entry 24). Next, nitropropane was employed as a cosolvent, however, this mixture froze at $-78\text{ }^\circ\text{C}$ temperature. To address this problem, we decided to add acetone to lower the freezing point of the solution. Unfortunately, this solvent combination was ineffective as well and did not enhance the enantiomeric ratio (entry 25). We used TFE, acetone, and acetonitrile mixture to drop the reaction temperature to $-100\text{ }^\circ\text{C}$, but this condition did not affect enantiomeric induction. Replacing acetonitrile with diethyl ether led to an inferior result, and a racemic mix was obtained (entry 27). Next, changing the

ratio of TFE and acetonitrile was examined. We found that increasing or decreasing the proportion of either acetonitrile or TFE did not give us a promising result for this transformation (entries 29-30).

After optimizing several factors in the reaction, we turned our attention toward the cinchona catalyst. In an effort to improve the enantioselectivity of the reaction, we took a more detailed look into the structure enantioselectivity relationship of (DHQD)₂PHAL, which was examined by a previous labmate, Dr. Sarah Marshal. She examined the influence of various structural components of (DHQD)₂PHAL structure on the enantioselectivity of a set of chlorofunctionalization reactions (Figure II-14). She demonstrated that replacing the dimeric catalyst with a monomer drops the

Table II-4 Solvent screening for chloroetherification reaction



entry	Cl ⁺ (equiv)	cat (mol%)	solvent	additive (equive)	temp. (°C)	yield (II-84)	er (II-85)
21	DCDMH (2.2)	(DHQD) ₂ PHAL (10)	HFIP/ACN (4:1)	—	-50	75	50:50
22	DCDMH (2.2)	(DHQD) ₂ PHAL (10)	EtOH/ACN (4:1)	—	-50	52	72:28
23	DCDMH (2.2)	(DHQD) ₂ PHAL (10)	TFE/PhCH ₃ (4:1)	—	-78	63	50:50
24	DCDMH (2.2)	(DHQD) ₂ PHAL (10)	TFE/acetone (4:1)	—	-78	63	84:16
25	DCDMH (2.2)	(DHQD) ₂ PHAL (10)	TFE/actone/nitropropane (4:1:1)	—	-78	72	73:27
26	DCDMH (2.2)	(DHQD) ₂ PHAL (10)	TFE/acetone/ACN (4:1:1)	—	-100	73	82:18
27	DCDMH (2.2)	(DHQD) ₂ PHAL (10)	TFE/Et ₂ O (4:1)	—	-78	60	50:50
28	DCDMH (2.2)	(DHQD) ₂ PHAL (10)	TFE/ACN (1:4)	—	-78	45	73:27
29	DCDPH (2.2)	(DHQD) ₂ PHAL (10)	TFE/ACN (1:1)	—	-78	45	84:16
30	DCDMH (2.2)	(DHQD) ₂ PHAL (10)	TFE/ACN (2:1)	—	-78	60	84:16
31	DCDMH (2.2)	(DHQD) ₂ PHAL (10)	TFE/ACN (9:1)	—	-78	67	72:28

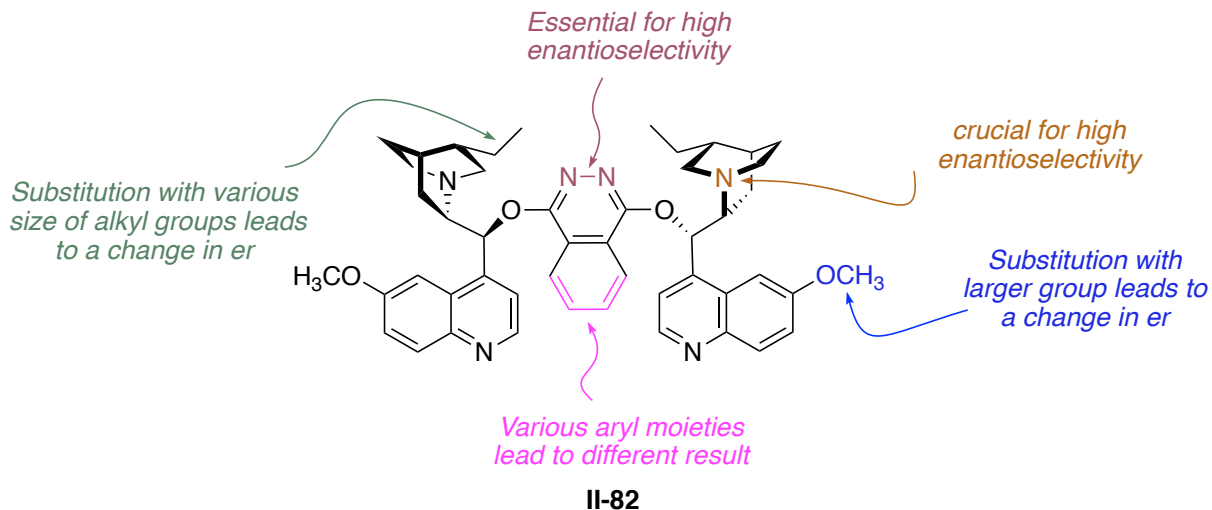


Figure II-14 Structure enantioselectivity relationship studies of (DHQD)₂PHAL on halocyclization

enantioselectivity of the reaction dramatically. (DHQD)₂PHAL contains phthalazine and dihydroquinidine. She discovered that the presence of the nitrogen atoms in pyridazine and DABCO is essential for obtaining high enantioselectivity and removing them from the linker gives the product as a racemate.

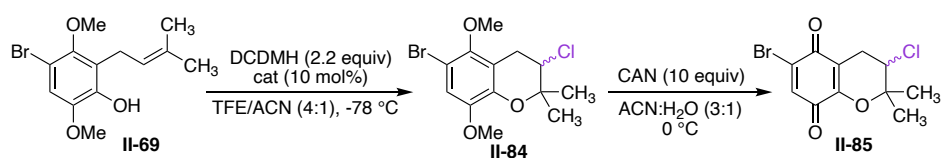
On the other hand, the substitution of phthalazine with pyridazine could drop or boost the enantiomeric ratio. The result of this substitution depends on the type of halofunctionalization. Replacing the ethyl group on DABCO with a bulkier or alkenyl group was also reaction dependent. Substitution of the methoxy with a bulky group led to a change in enantiomeric induction as well. Having a summary of her SER (structure enantioselectivity relationship) study in hand, we decided to examine the catalysts with various moieties highlighted in Figure II-14.

As shown in Table II-5 in (QD)₂PHAL (ethyl in place of ethylene of (DHQD)₂PHAL) resulted in lower selectivity (entry 32). Next, changing the core of the catalyst was

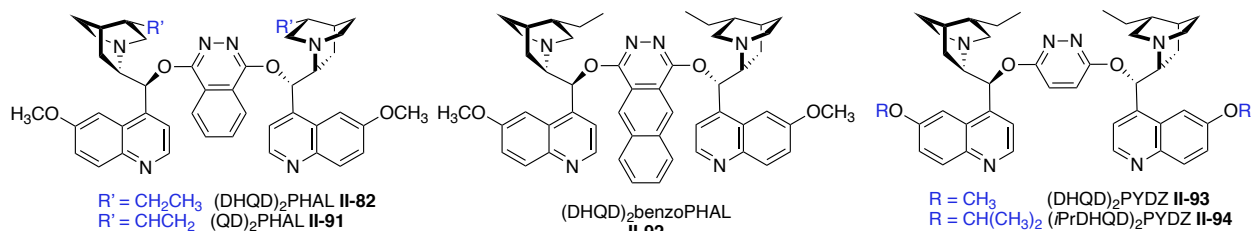
considered. Catalyst with benzo [g]phthalazine core, (DHQD)₂benzoPHAL, led to the product with similar enantioselectivity (entry 33). We were delighted to discover that employing pyridazine as a linker result in slightly higher enantioselectivity (entry 35). Switching the methoxy to isopropoxy in (iPrDHQD)₂PYDZ, did not influence the enantioselectivity. Thus (DHQD)₂PYDZ was chosen as the optimal catalyst. It should be mentioned that catalysts in this section were synthesized according to the procedure which has been reported in Dr. Marshal's thesis.

Having optimized reaction conditions for benzo-pyran formation, we explored the next step for the construction of quinone **II-85**. Oxidation of benzo-pyran in the presence of ceric ammonium nitrate gave access to the quinone as a yellow solid with good yield. We used this opportunity to explore the improvement of the enantiomeric excess via crystallography. Luckily, employing this method provides higher enantiomeric purity of

Table II-5 Asymmetric chloroetherification in the presence of cinchona alkaloids



entry	cat	yield (II-84)	er (II-85)
32	(QD) ₂ PHAL	56	78:22
33	(DHQD) ₂ benzoPHAL	60	83:17
34	(iPrDHQD) ₂ PYDZ	78	88:12
35	(DHQD) ₂ PYDZ	81	88:12



compound **II-85**. The absolute configuration of the chlorine center was confirmed using quinone's crystal structure which agreed with the stereochemistry required for the natural product (Figure II-15).

II-7 Synthesis of Ring A

We envisioned that the last ring of α -lapachone derivative **II-99/100** could be synthesized using Diels-Alder/aromatization reaction. Multiple dienes could be considered as candidates to accomplish this step. 1,3-Cyclohexadiene **II-95** was explored first. This diene was prepared from the commercially available 1,3-cyclohexanedione. Treating quinone with diene **II-95** in the presence of triethylamine resulted in the recovery of the starting material.

Interestingly, diene **II-98**, prepared from methyl acetoacetate, underwent the reaction and led to complete conversion. Reaction of diene **II-98** and dienophile **II-85** with pyridine and benzene provided a mixture of **II-99** and **II-100** in a 1:1 ratio. As highlighted in Figure

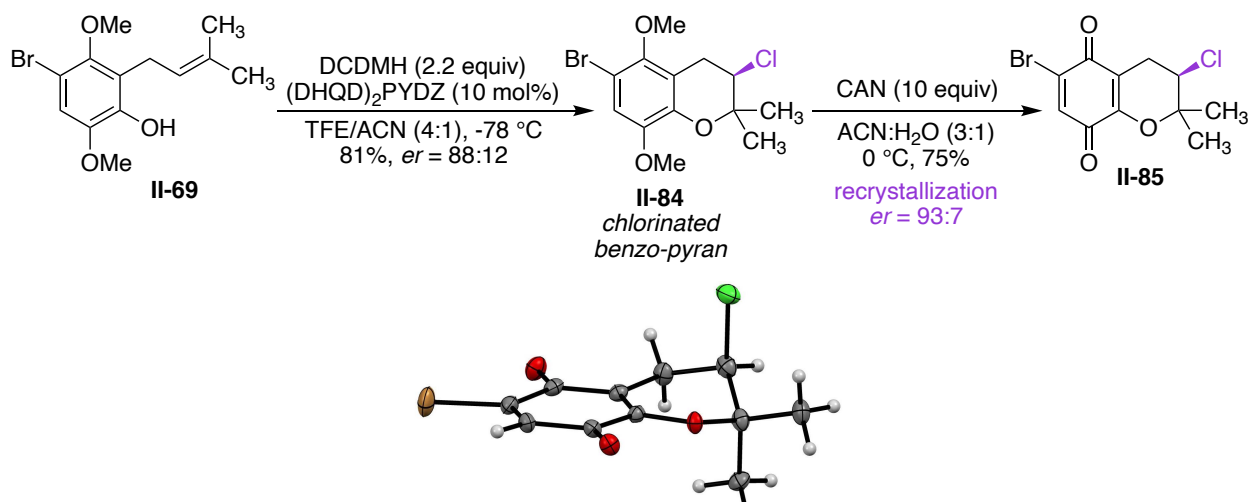


Figure II-15 Oxidation of benzene ring and improvement of enantioselectivity

II-16, the substitution on C-6 of the benzene ring differs between the two compounds. However, **II-99** contains an impurity that was not separable from the desired products.

Our approach to this issue was to explore other basic conditions such as triethylamine (entry 1) and running the reaction at lower temperatures (entries 2 and 3). NMR spectra of **II-99** presented a solution to this issue. The presence of extra peaks below and around 1 ppm, originating from a silylated product, led us to the assumption that the Diels-Alder reaction might require the presence of an acidic additive, which would remove the silicon impurity from the target molecule.⁹⁰ Fortunately, we found out using silica gel as an acidic reagent resulted in the exclusive formation of tricyclic core **II-99** in 73% yield without the appearance of any impurity (entry 4). Next, to minimize the complexity of the synthesis

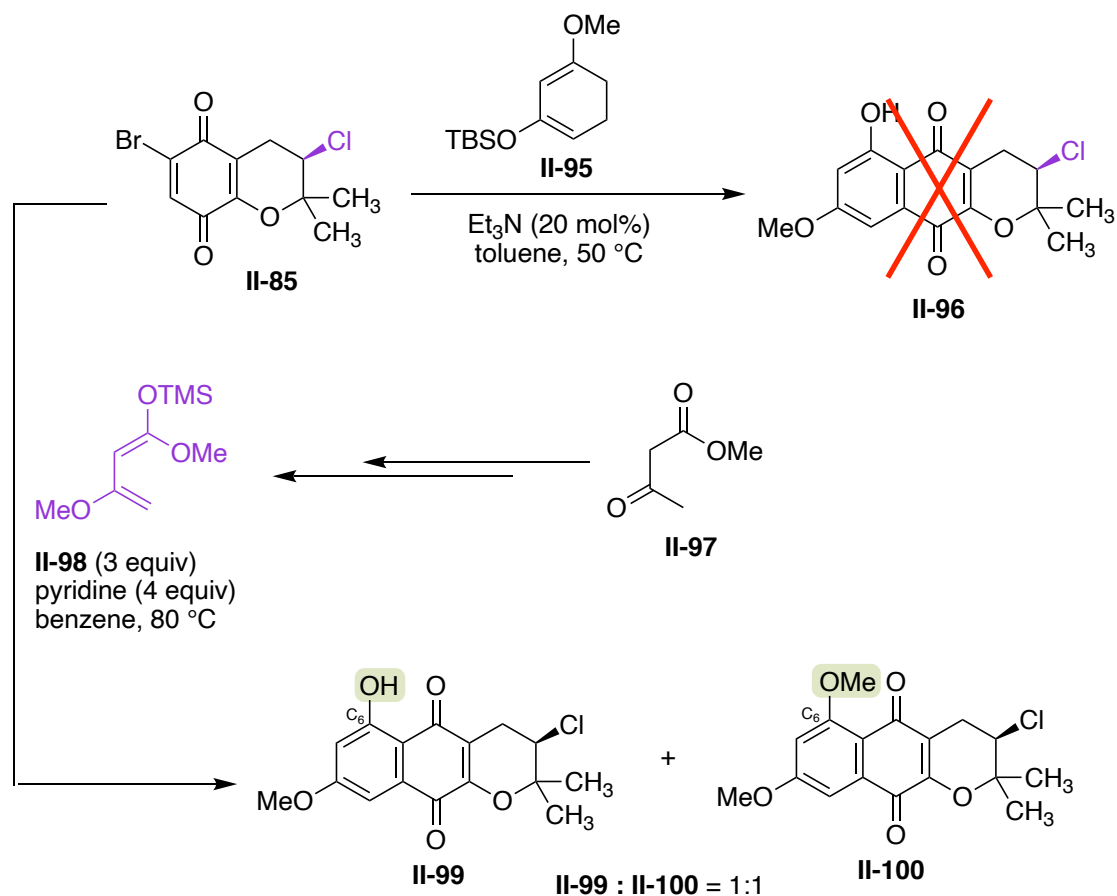
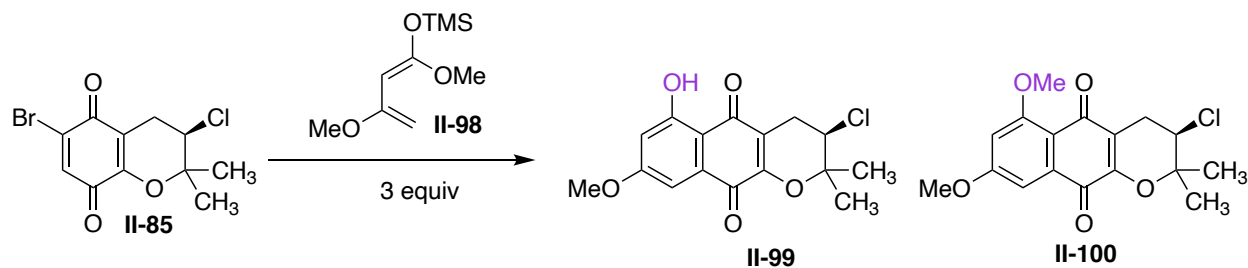


Figure II-16 Regioselective Diels-Alder reaction/aromatization cascade

Table II-6 Optimization of Diels-Alder/Aromatization

entry	solvent	condition	temp. °C	II-99 : II-100	yield ^a (%)
1	benzene	Et ₃ N (4 equiv)	80	1:1	81
2	toluene	pyridine (4 equiv)	r.t	1.5:1	90
3	toluene	pyridine (4 equiv)	0	2.2:1	83
4 ^b	CH ₂ Cl ₂	SiO ₂ (excess)	-30 to r.t	>99:1	73

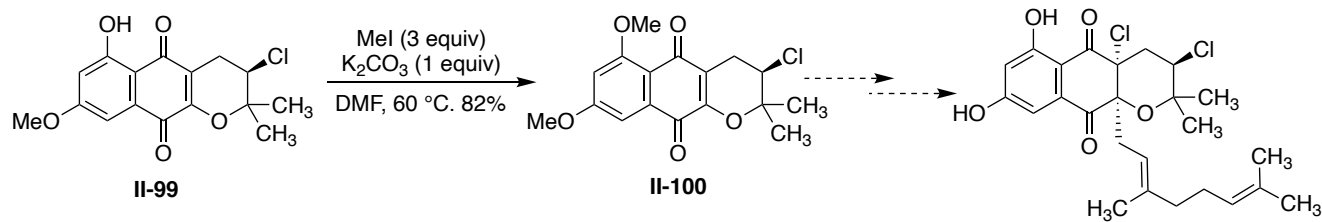
^aCombined NMR yield of the product **II-99** and **II-100** ^b only formation of compound **II-99** was observed

for the following steps, the resulting phenol from the previous step was protected as a methoxy using methyl iodide and potassium carbonate as reagents (Figure II-17).

II-8 Attachment of geranyl side chain

II-8-1 Prediction of diastereoselectivity using theoretical calculations

Our next target was the attachment of the geranyl moiety on the C10a position. Prior to pursuing this target, we utilized molecular modeling to predict the relative energy of potential diastereomers, formed from the conjugate addition of a geranyl side chain with

**Figure II-17** Synthesis of protected α -lapachone derivative **II-100**

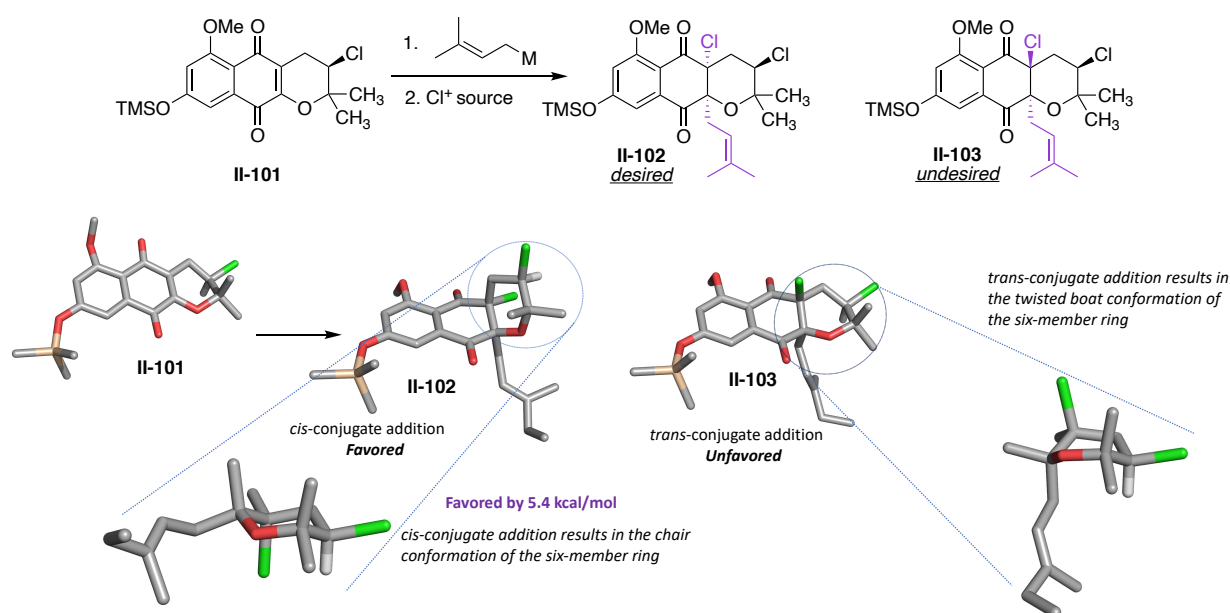


Figure II-18 Theoretical calculations to predict stereochemistry of the final product

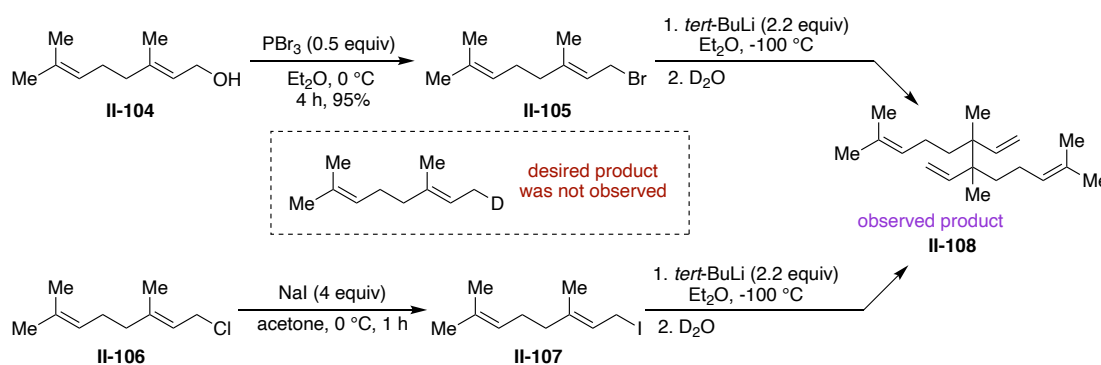
subsequent electrophilic trap with a chloronium source. To simplify the calculation, we replaced the geranyl side chain with prenyl. As depicted in Figure II-18, we predicted that the addition of a prenyl organometallic reagent and chloronium ion across the olefin of the quinone leads to the formation of two diastereomers. We predicted the face selectivity of the double bond for addition of the prenyl group would be dictated by the chlorine stereocenter. However, trapping the chloronium ion from both faces of the enolate would result in the formation of the two diastereomers. Diastereomers **II-102** and **II-103** were subjected to a conformational search followed by geometry optimization. The calculation was performed using density functional methods (DFT) and B3LYP/6-31G* as a basis set. The electronic energy of each diastereomer was extracted from the output file. Comparing the relative energy of these diastereomers indicates that the stereoisomer with cis-conjugate addition **II-102** is 5.4 kcal/mol more favored than the trans-conjugated

adduct **II-103**. Closer evaluation of the structures revealed that the putative TS of the *cis*-diastereomer proceeds through a chair conformer of the pyran ring, while the pyran ring of the *trans*-conjugated adduct adopts a twisted boat conformer. Different stability of the pyran ring conformers could be the reason for the energy difference which is observed between the two diastereomers.

II-8-2 Experiment Investigating the geranyl side-chain attachment

Having the preliminary result in hand for prediction of diastereoselectivity, an experiment investigation on the attachment of the geranyl moiety was initiated. One of our early approaches was to subject protected α -lapachone **II-100** to a direct Michael addition of geranyl cuprate. Therefore, the synthesis of geranyl lithium as a precursor for geranyl cuprate was investigated. The synthesis was initiated by transformation of geranyl alcohol **II-104** to alkyl bromide **II-105**, followed by the addition of *tert*-butyllithium. Before generation of cuprate reagent, the resulting mixture was quenched by the addition of D₂O

a. M = Li



b. M = Sn

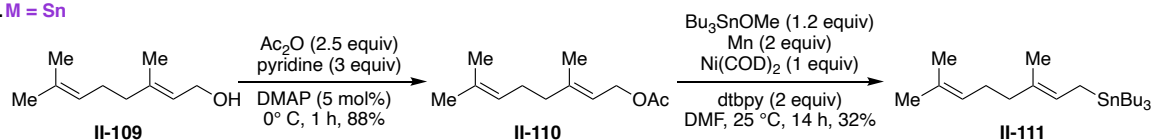


Figure II-19 a. Wurtz coupling of geranyl radical. b. Synthesis of geranyl tin species

to assure metal-halogen exchange has occurred. NMR analysis of the crude mixture revealed a formation of the complex mix of products. Therefore, we considered to look at the GC-MS analysis of the mixture. GC-MS analysis of the products revealed that the dimerization of geranyl was the major product of the reaction. We hypothesized that dimerized products are the result of Wurtz coupling of geranyl radical. To remedy this issue, we predicted that the conversion of an alkyl iodide **II-107** undergoes the metal halogen exchange faster than alkyl bromide; therefore, the synthesis of alkyl iodide followed was explored. However, the reaction of alkyl iodide **II-116** under the same reaction condition resulted in a similar complex mixture (Figure II-19-a). Since employing alkyl iodide did not solve the problem, we decided to solve the problem in a different manner. Instead of metal-halogen exchange, the lithium-metalloid exchange was studied. Consequently, geranyl tin was considered as a candidate for this purpose. Nickel catalyzed geranyl stannylation of geranyl acetate using Bu_3SnOMe in the presence of Mn powder affords the desired geranyl tin product (Figure II-19-b).^{91, 92}

II-8-3 Michael addition of allyl organocuprate to quinone

With geranyl tin **II-111** in hand, 1,4- addition of this organotin reagent for installing the carbon chain at C-10a was pursued (Figure II-20). Before investigating the possible 1,4- addition using cyclohexanone as a model reaction, the geranyl copper species was prepared from a geranyl lithium reagent and copper iodide. The reaction of the resulting cuprate reagent with cyclohexenone and TMSCl yielded **II-113** in 20% yield. We hypothesized that using the same reaction condition on a more hindered quinone **II-100** would afford the desired compound with even lower efficiency.⁹³ As a result, we turned

our attention to the less hindered organocopper reagent, which can further be transformed to the geranyl moiety. Michael addition of the allylcuprate to cyclohexenone led to the formation of **II-116** with a higher yield (70%). The latter result convinced us to go forward with allyl reagent instead of geranyl, and further, the rest of the side chain can be installed using olefin cross-metathesis.

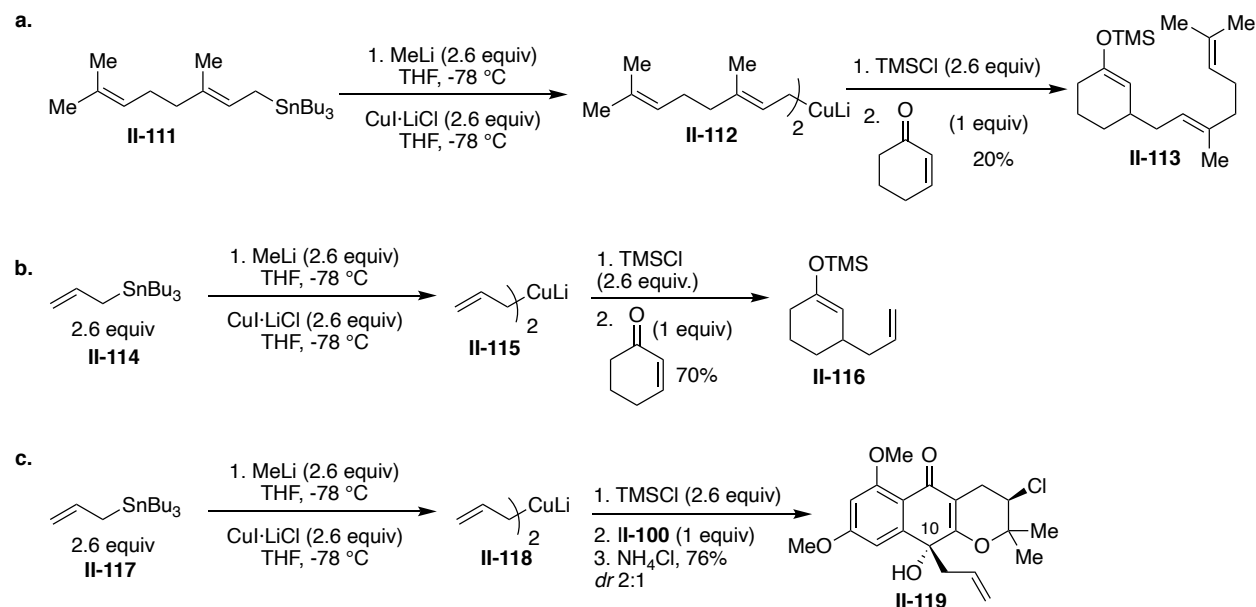


Figure II-20 a. 1,4-addition of geranylcuprate to cyclohexenone. b. 1,4-addition of allylcuprate to cyclohexenone. c. 1,2-addition of allylcuprate to **II-100**.

Unfortunately, the reaction of protected α -lapachone **II-100** with *in situ* generated allyl cuprate resulted in the formation of two diastereomers from 1,2-addition of allyl cuprate to C10 carbonyl. Other organometals such as allyl lithium and allyl Grignard were tested to solve the chemoselectivity issue of the reaction. However, neither of those reagents were effective and resulted in the recovery of starting material or undesired product.

To solve this issue another approach was pursued. We decided to manipulate the 1,2-addition product. After looking through all possible solution we realized that an acyloin

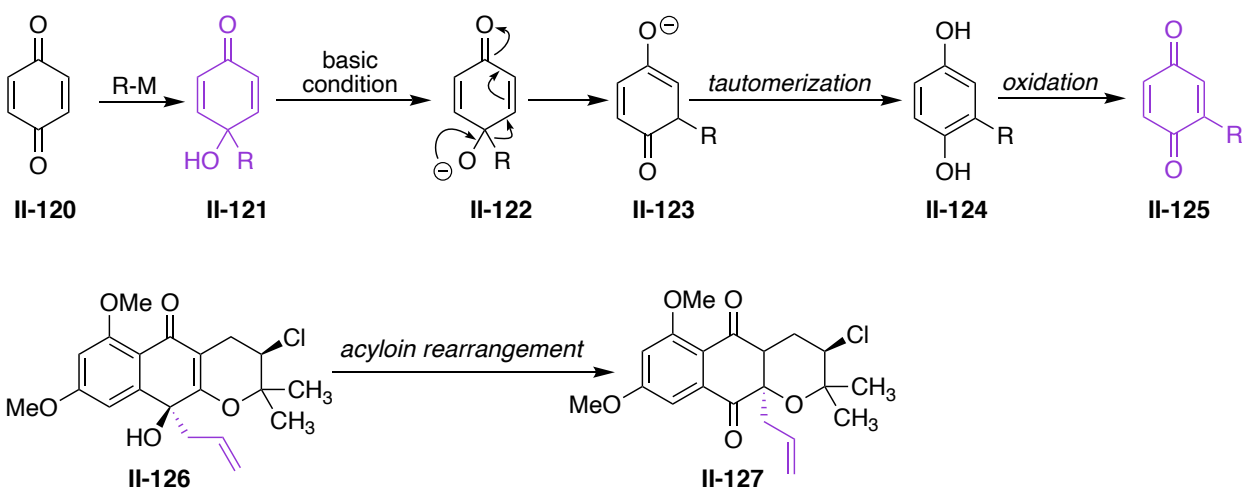
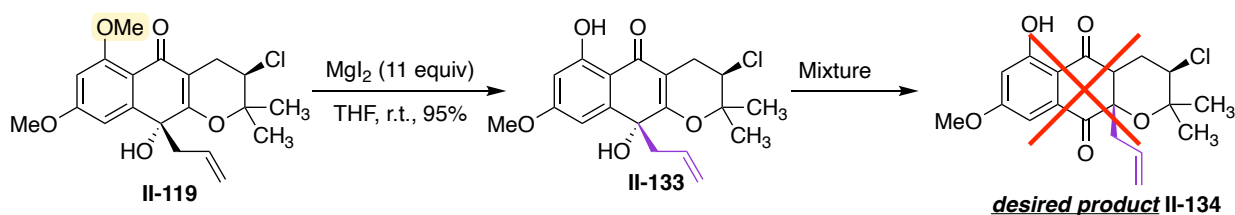


Figure II-21 Acyloin rearrangement of *p*-quinol to 2-substituted quinone

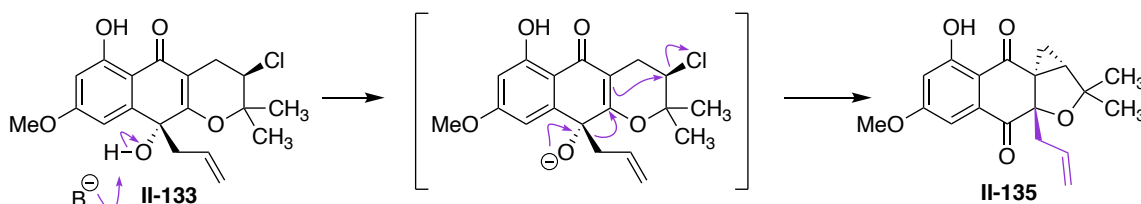
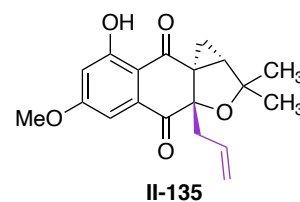
rearrangement as a new strategy for C-10a alkyl substitution could be pursued. This rearrangement entails converting the 3° alcohol to a carbonyl group via migration of the alkyl group to the vicinal sp^2 carbon center. Ketol rearrangement proceeds under both acidic and basic conditions, however the migratory aptitude of the R group is the opposite under basic or acidic conditions (methyl has a facile migration under basic conditions but difficulties under acidic conditions). As shown in Figure II-21, the product resulting from the 1,2-addition of an organometallic is prone to undergo acyloin rearrangement to afford *p*-hydroquinone **II-124** product. Further oxidation of hydroquinone would access the desired substituted quinone. The tautomerization step leads to the formation of the aromatic compound **II-124**, thermodynamically more favored than the quinone starting material. This energy difference could drive the reaction to completion. However, it should be noted that the tautomerization step in the acyloin rearrangement of **II-126** cannot enjoy aromatic stability due to the absence of a hydrogen atom on C-10a. Still, we were hopeful

Exploring the literature; we found a similar transformation as our proposed acyloin rearrangement. In 1999, Tobinaga and coworkers revealed that the dienone-phenol type rearrangement of quinol **II-129**, was not plausible before removal to the tributyl(dimethyl)silyl protecting group (see the Scheme under Table II-7) and this transformation was accessible after deprotection of phenol moiety.⁹⁵ Therefore, we decided to investigate this migration on the unprotected phenol **II-133**. Selective deprotection of phenol adjacent to carbonyl was pursued with magnesium iodide. Coordination of magnesium to the carbonyl and the adjacent methoxy would activate the desired methoxy for deprotection. As illustrated in Table II-8, treatment of **II-133** with the

Table II-8 Optimization of 1,2-allyl migration of unprotected quinol under acidic and basic conditions



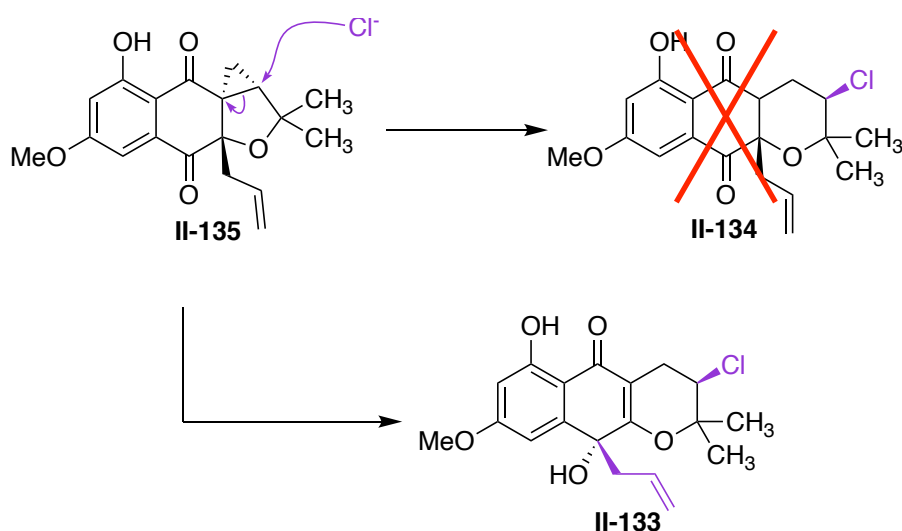
entry	Mixture	result (yield %)
1	NaOH (2N), EtOH, 140 °C	II-135 (43%)
2	KOH (2N), EtOH, 140 °C	II-135 (41%)
3	Me ₄ NOH · 5 H ₂ O (5 equiv), EtOH, 140 °C	complicated crude mixture
4	BF ₃ · Et ₂ O (1.1 equiv), THF, r.t.	complicated crude mixture
5	Al(<i>i</i> -OPr) ₃ (1.1 equiv), THF, r.t.	SM was recovered
6	H ₂ SO ₄ , EtOH, 140 °C	SM was recovered



reported condition resulted in the complete consumption of the starting material; however, it failed to give access to C-10a alkyl substituted product **II-134**, and to our surprise, exclusive formation of oxabicyclo[3.1.0]hexane **II-135** was observed (Table II-8, entry 1).

As shown in Table II-8, a variety of basic and acidic conditions were tested without any success. Employing potassium hydroxide as a basic source delivered the same bicyclo product (entry 2). Ammonium hydroxide led to a complicated mixture (entry 3). Exploring the migration using Lewis or Brønsted acids such as BF₃ etherate, aluminum isopropoxide, and sulfuric acid did not form the desired product.

Table II-9 Nucleophilic ring opening of cyclopropane with the chloride ion



entry	condition	result
1	HCl (38%), acetic acid, r.t	SM was recovered
2	HCl:H ₂ SO ₄ (1:1), r.t.	SM was recovered
3	TMSCl, NaCl, ACN, 55 °C	SM was recovered
4	TiCl ₄ , PhCH ₃ , r.t.	II-133 , 63%

As illustrated under Table II-8, we proposed that the treatment of 3° alcohol **II-133** would generate the alkoxide intermediate followed by allyl migration. Enolate developed from the migration of the allyl moiety acts as a nucleophile and displaces the chlorine atom at C-3. This overall process generates oxabicyclo[3.1.0]hexane **II-135**. As a result, the elimination of the C3 chlorine was an unavoidable occurrence associated with the allyl migration. To remedy this issue, we explored chloride-induced cyclopropyl ring-opening reactions.

As listed in Table II-9, many trials using chloride under acidic conditions failed presumably, due to the inactive cyclopropyl ring for nucleophilic addition (entries 1-3).⁹⁶ Our approach to this problem was to employ a Lewis acid with stronger binding interactions with the carbonyl functionality. We hypothesized that this interaction would generate an electrophilic carbon center with a higher positive charge. For this purpose, titanium chloride was selected as a candidate for the cyclopropyl ring-opening process.⁹⁷ Although, this led to the opening of the cyclopropane ring; the isolated product was identified as the starting material prior to the base-induced rearrangement (entry 4).

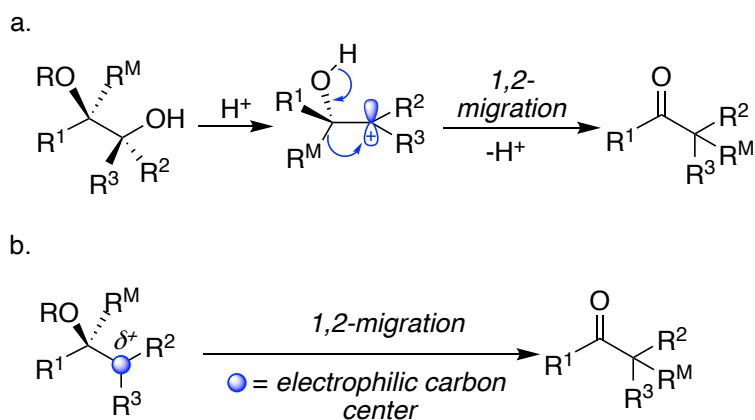


Figure II-22 a. Classical Pinacol rearrangement, b. General picture of the semipinacol rearrangement

Interestingly, the relative stereochemistry of the product matched with the original compound **II-133**, which supports this hypothesis that nucleophilic ring opening of the cyclopropane and allyl migration coincide.

II-9 Semipinacol rearrangement as a possible solution for C10a allylation

Pinacol rearrangement is a well-known transformation in which 1,2-diols convert to ketones or aldehydes by 1,2- migration of C-C or C-H bond using acidic conditions. However, due to poor control of regio- and diastereoselectivity, its application is limited (Figure II-22). The analogous, semipinacol rearrangement, has captured the interest of synthetic chemists as an efficient method for the synthesis of various natural products.⁹⁸

Mechanistically, these processes go through a common intermediate with an electrophilic carbon center next to an oxygen-carbon bond that can drive a C-C or C-H bond 1,2- migration and form a carbonyl functional group. A general description of these transformations is shown in Figure II-22.

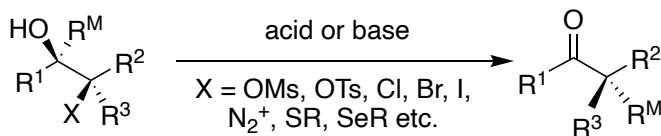
The semipinacol rearrangement has been classified into four categories based on the type of electrophilic carbon generated in the typical intermediate. With a good leaving group vicinal to the hydroxy group in type I, treatment of 2-heterosubstituted alcohols with base or acid drives the desired 1,2- migration reaction (Figure II-23-a).⁹⁹⁻¹⁰²

The carbocation center can be generated by the reaction of a C=C bond with an electrophile (type II). Relative to the employed electrophile, allylic alcohols can go under inter- or intramolecular reactions (Figure II-23-b).¹⁰³⁻¹⁰⁵

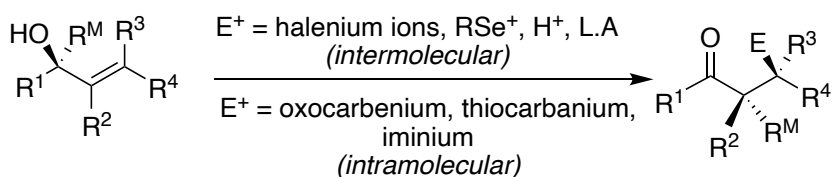
The rearrangement of 2,3-epoxy alcohols is categorized as type III semipinacol rearrangement. In this type of rearrangement, both carbons of the oxirane are considered

as electrophilic carbon for the 1,2-migration. Various kinds of migration such as 1,2-, 2,3-, or 3,2-migration can occur, depending on the substrate structure and reaction conditions

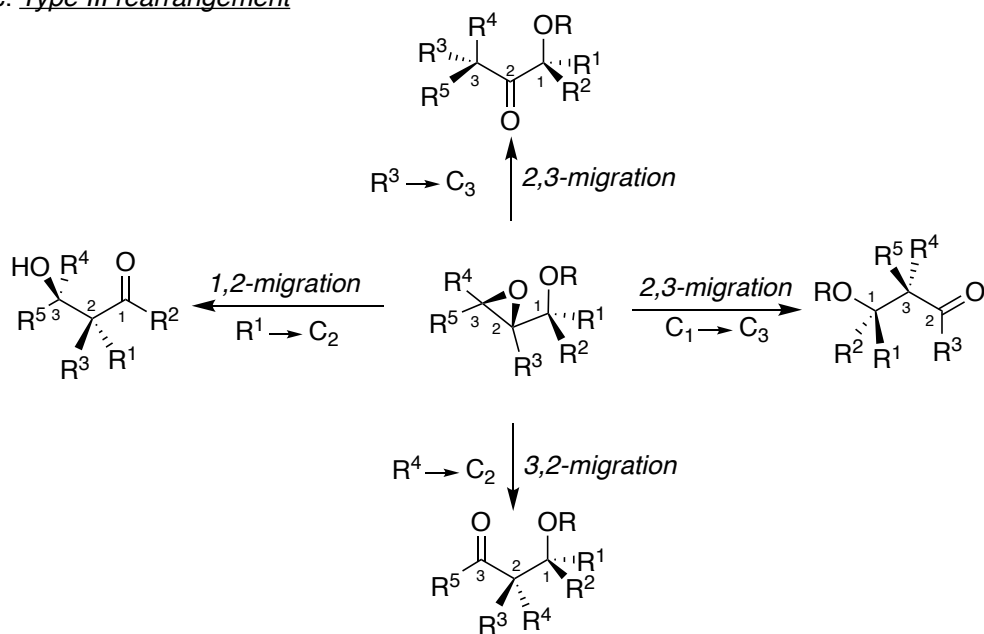
a. Type I rearrangement



b. Type II rearrangement



c. Type III rearrangement



d. Type IV rearrangement

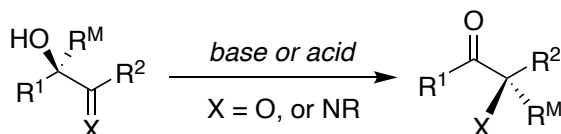


Figure II-23 A classification scheme for semipinacol rearrangement based on the electrophile carbon center

(Figure II-23-c).¹⁰⁶⁻¹⁰⁸

Finally, Type IV includes the 1,2-migration of 3° α -hydroxy ketones or imines, known as "acyloin rearrangement," (Figure II-23-d).¹⁰⁹⁻¹¹¹

There are several advantages of semipinacol rearrangement over pinacol rearrangement.

1. The substrate is not restricted to 1,2-diols.
2. The rearrangement can proceed under various reaction conditions, such as acidic, basic, and neutral conditions.
3. The site selectivity problem can be addressed in this rearrangement since several methods can be employed to generate carbocation on the desired and specific site.
4. Diastereoselectivity is not an issue in semipinacol rearrangement. The migratory group on hydroxy group must be antiperiplanar to the leaving group. Therefore, leading to the formation of quaternary stereocenter with inversion of stereochemistry at the migration terminus.

II-9-1 1,2-Rearrangement of epoxides

Semipinacol rearrangement of epoxides initiated by an oxirane ring-opening has had application in natural product syntheses. We envisioned this type of rearrangement on substrate **II-137** (3° allylic alcohol) would result in the formation of desired product **II-139** via the migration of the allylic group from C10 to C10a.

II-9-2 1,2-migration of 2,3-epoxy alcohols

From the list of possible semipinacol rearrangements of epoxide shown in Figure II-25-c, it was anticipated that 1,2-migration ($R^1 \rightarrow C_2$) would give us the desired product **II-139**. We anticipated our precursor **II-136** would favor the aforementioned 1,2-migration since the ring-opening of the oxirane could be accelerated through the participation of the THP oxygen which generates an oxocarbenium ion. This process raises the possibility for allyl group migration (Figure II-24).

Therefore, we turn our attention to the synthesis of epoxy alcohol **II-137**. Of the various methods for epoxidation, nucleophilic epoxidation was selected as the method for the epoxidation of electron deficient double bond **II-136**.¹¹²

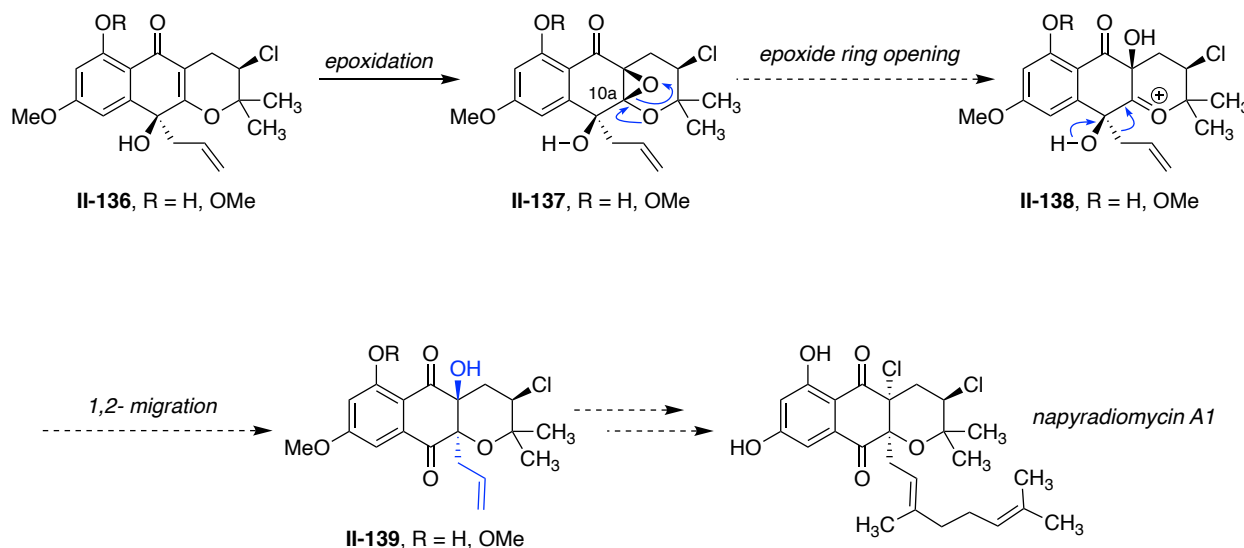


Figure II-24 Anticipated 1,2-migration of 2,3-epoxy alcohol which would lead to the desired α -hydroxy diketone

It was decided that the nucleophilic epoxidation of both enone **II-126** and **II-135** should be investigated since entirely different reactivity of these two substrates was observed for

acyloin rearrangement. The reaction of **II-135** with hydrogen peroxide resulted in the recovery of the starting material due to solubility issues. The reaction of hydrogen peroxide and sodium hydroxide with **II-126** resulted in the consumption of the starting material. The crude NMR of the reaction mixture represents the formation of a new species, which showed the presence of two carbonyl peaks around 200 ppm in the ^{13}C NMR. Surprisingly, when the crude mixture was purified with the silica gel column, a completely different compound was isolated after purification. NMR analysis was employed to characterize and establish the structure for both compounds **II-141** and **II-142** (Figure II-25). Considering possible 1,2-migration of 2,3-epoxy alcohol, we propose that spirodiketone **II-141** results from the migration of the carbonyl group from C4a to C10a. Although our wish was for a 1,2-migration ($\text{R}^1 \rightarrow \text{C}_2$) to install the allyl group at C10a, the epoxy alcohol **II-143** undergoes the undesired 3,2-migration (Figure II-26-b).

One could consider utilizing the orbital geometry and orientation of different groups around the oxirane ring to explain the outcome of the migratory manner of the epoxy

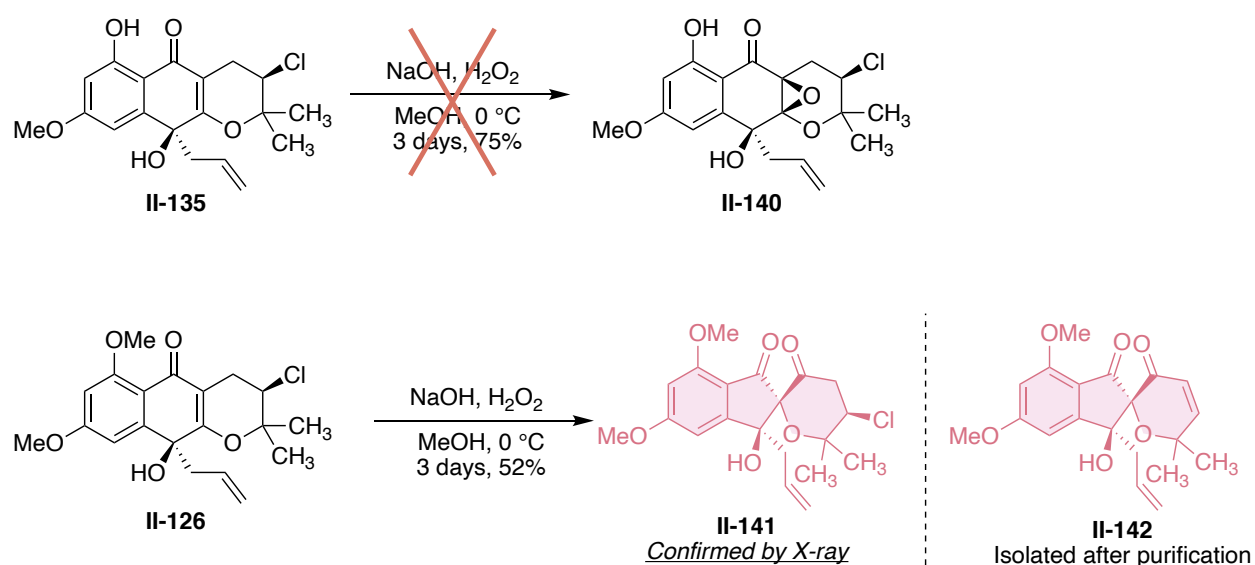


Figure II-25 Formation of the unexpected product under epoxidation condition

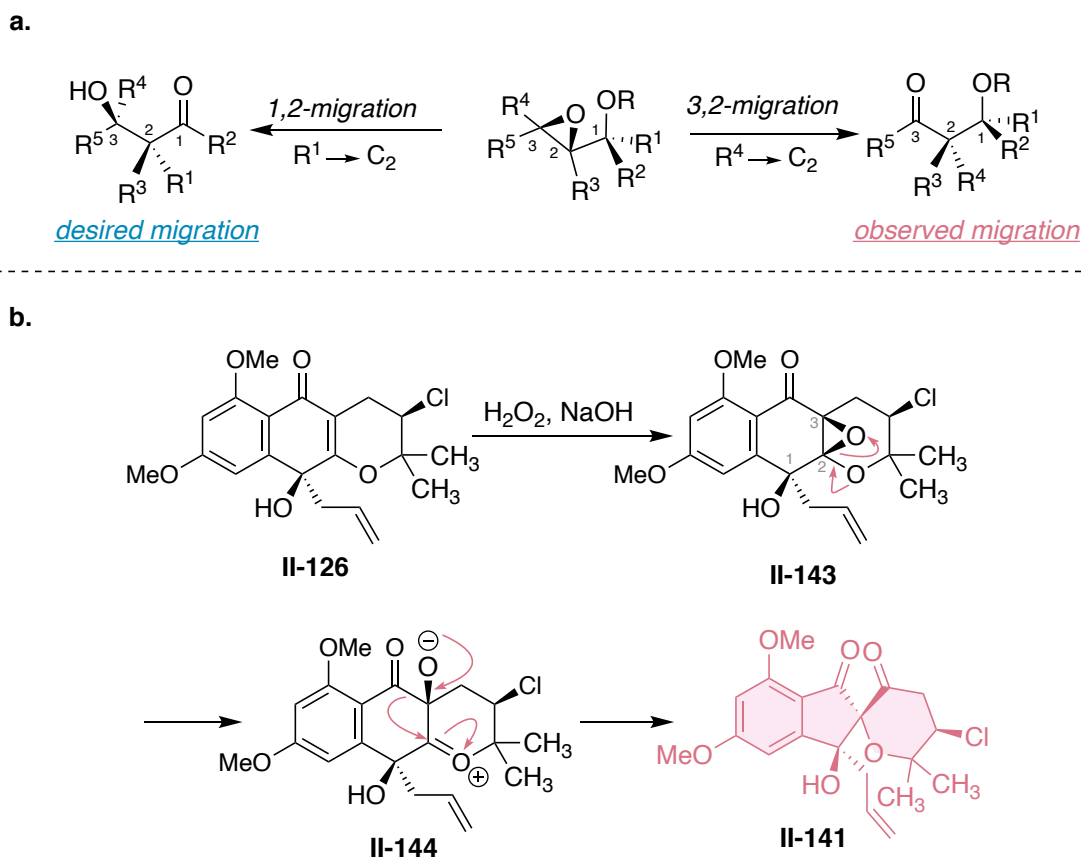


Figure II-26 Proposed mechanism for the formation of oxaspirodecene

alcohol. For desired migration to occur, the corresponding migrating group in the rearrangement should be held anti to the epoxide oxygen. As shown in Figure II-27, it was expected from intermediate **II-149**, allyl migration would dominate in rearrangement because of the antiperiplanar position of allyl moiety relative to the C-O bond of the epoxide. Interestingly, the oxocarbenium intermediate indicates the anti-alignment of the C5-C4a bond with the electrophilic carbon center. The latter intermediate leads to the migration of the carbonyl group and affords the spiro[4,5]diketone.

Several studies showed that either 1,2-, 2-3, or 3,2-migration could proceed depending on the structural features of the substrate and reaction conditions. To improve

the migratory ability of the allyl group over C5-C4a to favor the desired migration, modification of the structure of the substrate and epoxidation conditions should be considered. It should be mentioned that according to literature precedent, epoxy ethers, an analog to Rubottom oxidation intermediate, are prone to rearrangement. These moieties are not stable at room temperature for an extended period, and caution should be taken how to handle these types of compounds and temperature should be kept under 0 °C.

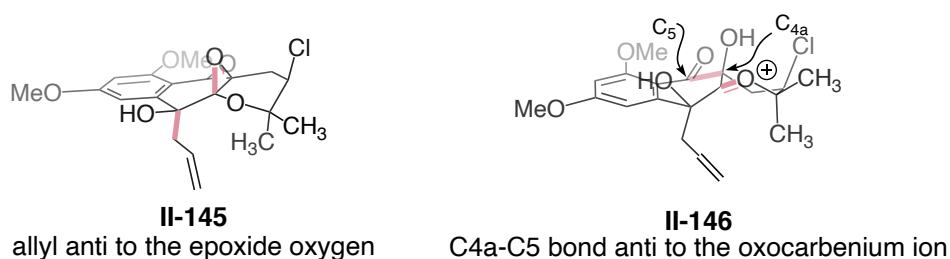


Figure II-27 Mandatory antiperiplanar alignment of the migratory group relative to the leaving group

II-10 Rearrangement of allylic alcohols induced by chloronium ion

According to all possible rearrangements illustrated in Figure II-23, in Type II rearrangement, electrophilic carbon center, a carbocation, can be generated by adding halonium ions to the alkene moiety. Halonium ions are electrophiles that can initiate the intermolecularly of the allylic rearrangement and give β -halo carbonyl species. Therefore, we turned our attention to the chloronium ion as an electrophilic candidate for our desired semipinacol rearrangement. Consequently, the treatment of tertiary alcohol **II-139** with a variety of chloronium ions was investigated. However, the reaction of the **II-139** with several chloronium sources such as NCS, DCDMH, DCDPH was unproductive and resulted in the recovery of the starting material. One of the anticipated challenges we

might face was the formation of chlorinated benzene because of the presence of the electron-rich benzene ring. However, to our surprise, we did not see any formation of the chlorinated benzene ring.

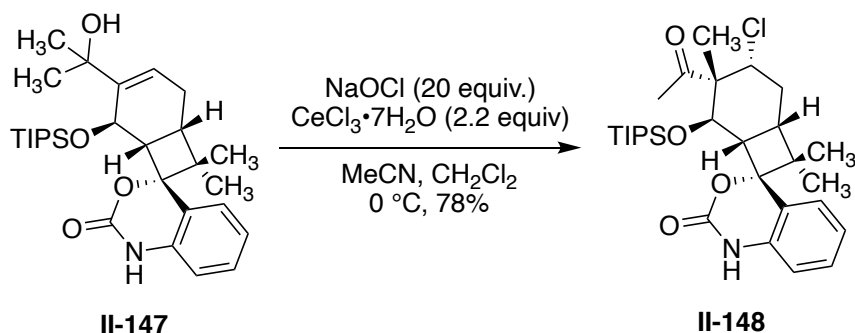


Figure II-28 Semipinacol rearrangement of the tertiary alcohol **II-147** using NaOCl as chloronium source

Looking through previously reported procedures for tertiary allylic alcohols and their derivatives, we found out that in 2008, Wood and coworkers reported treating tertiary allylic alcohol **II-147** with NaOCl as chloronium source and $\text{CeCl}_3 \cdot 7\text{H}_2\text{O}$ led to the 1,2-migration of the methyl group (Figure II-28).¹¹³ Therefore, we decided to expose tertiary alcohol **II-126** to the same condition. Nonetheless, the reaction led to the formation of two regioisomers arising from the chlorination of C7 and C9 of a benzene ring with a 1:1 ratio.

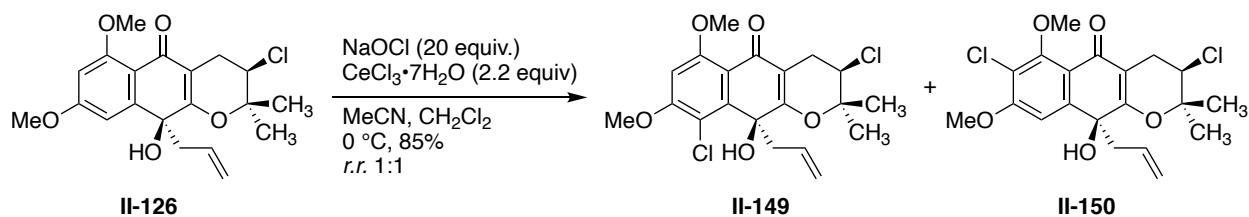


Figure II-29 Treatment of the **II-126** with chloronium ion resulted in the formation of chloro benzene product

II-11 New pathway for attachment of the geranyl chain

After several failures for semipinacol rearrangement of the allyl alcohol **II-126**, we decided to pursue another possible pathway to synthesize napyradiomycin A1. As illustrated in Figure II-30, in the new path, the installation of the geranyl group in the middle stage of the synthesis was pursued. We assumed that the geranyl side chain could be installed at C10a using the chloronium ion initiating semipinacol rearrangement on allylic alcohol **II-126**.

Alcohol **II-151** was synthesized via nucleophilic addition of allylindium sesquiodide to the carbonyl C10, resulting in the formation of the two diastereomers with a 1:1 ratio (Figure II-31-a). However, the undesired diastereomer was not stable at room temperature and decomposed into a complicated mixture. It was assumed that the allyl alcohol generated from allylic 1,2-addition is prone to undergo [3,3]-sigmatropic rearrangement. The desired diastereomer **II-151** was treated with both NCS and H₂O₂/NaOH. Still, none of the conditions was fruitful, and the starting material was undergoing the same rearrangement as the other diastereomer. The plausible reaction pathway for this rearrangement has shown in Figure II-31. 1,2-Addition of allylindium to the most electrophilic carbonyl generates the quinol **II-151** followed by [3,3]-sigmatropic

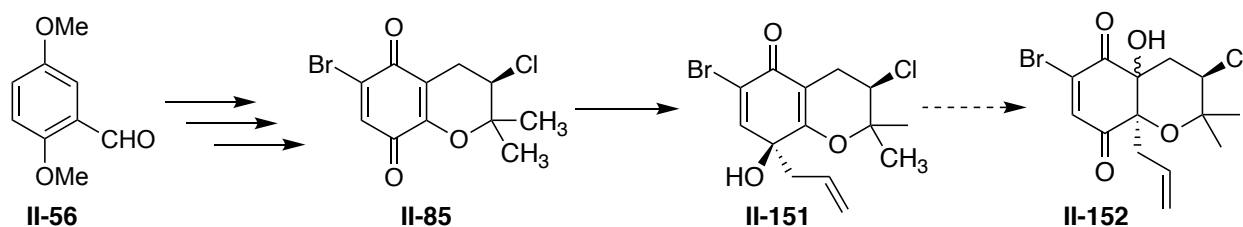
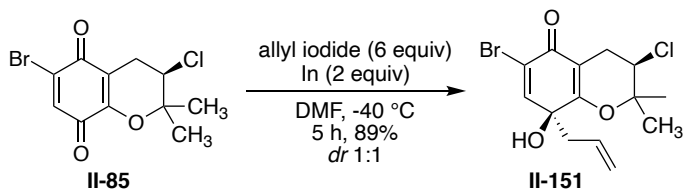


Figure II-30 New pathway for installation of the geranyl side chain

rearrangement furnishes the total addition of the allylic group to the adjacent carbon of the less electrophilic carbon.

a



b

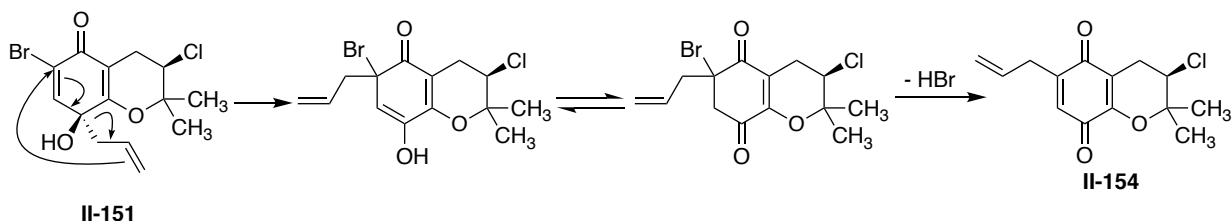


Figure II-31 a. Synthesis of allyl naphthoquinol **II-151**. b. Plausible reaction pathway for decomposition of the allyl alcohol **II-151**

II-12 Summary

The progress towards the asymmetric catalytic synthesis of napyradiomycin A1 can be divided to three goals. The first goal, which was installation of chlorine chiral center at C3, was achieved using cinchona chiral catalyst. The second goal, which was the synthesis of the α -lapachone core of napyradiomycin A1, was accomplished using Diels-Alder/aromatization cascade reaction. Unfortunately, all efforts towards the final target, attachment of the geranyl side chain and chlorine atom at C4a position, was not fruitful and resulted in the formation of undesired products. Current efforts focus on optimizing the latter transformation for attachment of the geranyl chain. Some possible solution for the last goal of the synthesis includes the protection of phenol **II-135** or reduction of carbonyl C10 before cyclopropyl ring opening, and epoxidation of α -lapachone.

Chapter III – Experimental Section

III-1 Materials and general instrumentations

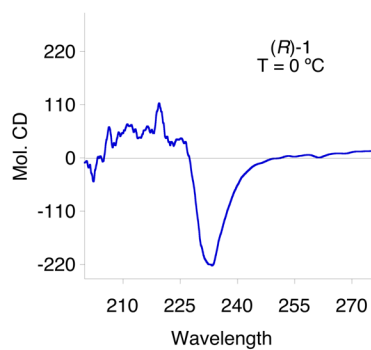
HPLC grade solvents used for CD measurements were purchased from Sigma Aldrich. All reactions were performed in dried glassware under nitrogen. Column chromatography was performed using SiliCycle silica gel (230-400 mesh). $^1\text{H-NMR}$ and $^{13}\text{C-NMR}$ spectra were obtained on Varian 500 MHz instrument and are reported in parts per million (ppm) relative to the solvent resonances (δ), with coupling constants (J) in Hertz (Hz). CD spectra were recorded on a JASCO J-810 spectropolarimeter, equipped with a temperature controller (Neslab 111) and are reported as λ [nm] ($\Delta\epsilon_{\text{max}}$ [$\text{mol}^{-1} \text{cm}^{-1}$]). Optical rotations were recorded on a Perkin Elmer 341 Polarimeter ($\lambda = 589 \text{ nm}$, 1 dm cell). HRMS analyses were performed on a Q-TOF Ultima system using electrospray ionization in positive mode.

III-2 CD measurements

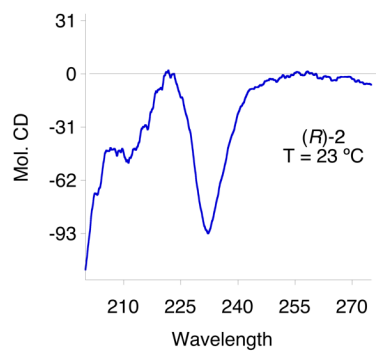
Dinaphthyl Borinic acid (1 μL of a 1 mM solution in acetonitrile) was added to acetonitrile (1 mL) in a 1.0 cm cell to obtain a 1 μM borinic acid solution. The background spectrum was then taken from 200 nm to 350 nm with a scan rate of 100 nm/min (at various temperature depending on the substrate). Chiral substrate solution (up to 5 μL of a 1 mM solution in acetonitrile) was added into the prepared dinaphthyl borinic acid solution to afford the host/guest complex. CD spectra of samples measured with 10 accumulations, was subtracted from background and normalized based on the concentration to obtain the molecular CD (Mol. CD).

III-3 CD spectra

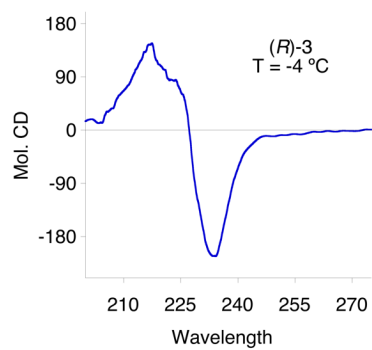
(*R*)-1-(4-bromophenyl) ethane-1,2-diol, I-41



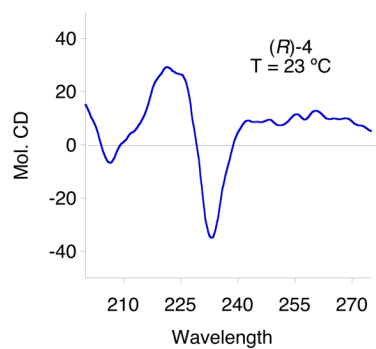
(*R*)-1-(4-(trifluoromethyl) phenyl) ethane-1,2-diol, I-42



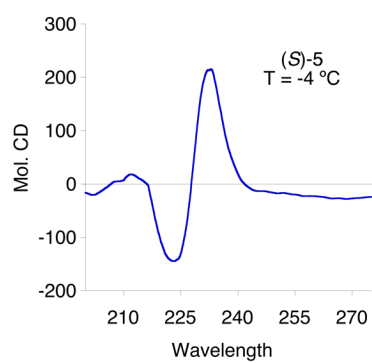
(*R*)-1-(naphthalen-2-yl) ethane-1,2-diol, I-43



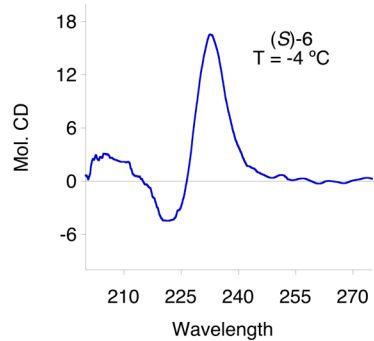
(*R*)-1-cyclohexylethane-1,2-diol, I-44



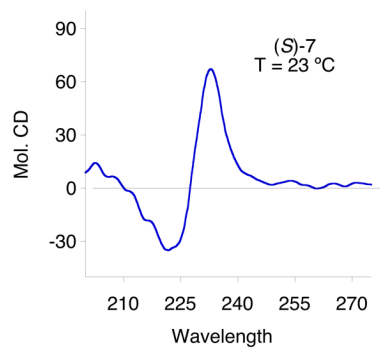
(S)- 2-phenylpropane-1,2-diol, I-45



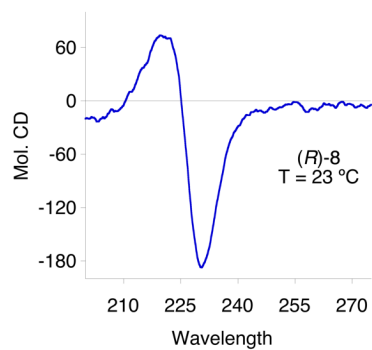
(S)-1-phenylethane-1,2-diol, I-46



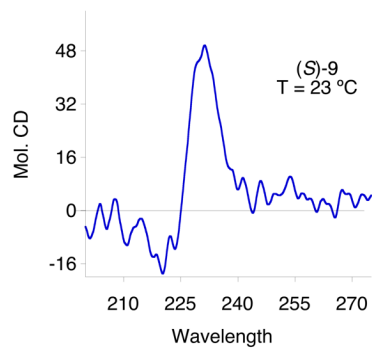
(S)-3-methylbutane-1,2-diol, I-47



(R)-mandelic acid, I-48



(S)-phenyllactic acid, I-49



III-4 Synthetic procedures

III-4-1 Di(1-naphthyl) borinic acid ¹¹⁴

Under a nitrogen atmosphere, to a dried 250 mL round bottom flask, a mixture of tributyl borate (5 mL, 18 mmol) and 1-bromonaphthalene (5 mL, 36 mmol) in dry THF (18 mL) was added to a solution of magnesium turning (954 mg, 39 mmol) and small crystal of iodine in dry THF (18 mL) at 40 °C over 30 minutes. The reaction mixture was kept at 40 °C for 2 h. After that, reaction was cool down to room temperature, followed by hydrolysis of the product by using 10 mL of 5% aqueous solution of HCl. Product was extracted by ethyl acetate (200 x 3). Organic layers were combined and dried over Na₂SO₄ following by filtration. The organics were concentrated under vacuo (7.2 mL) following by addition of 2-ethanolamine (1.6 mL, 0.75 equiv.). The mixture was allowed to stir at room temperature for 2 h before water was added to the reaction. The organic layer was separated, dried over sodium sulfate and concentrated in vacuo to afford the crude product. The crude product was recrystallized in methanol as a white solid (4 g, 34 %). The solids (144 mg, 0.44 mmol) were dissolved in 1:1:1 methanol:acetone:HCl (10%) (6 mL total volume) and stirred at room temperature for 1 h. The product was extracted by ethyl acetate and dried over sodium sulfate. The organic layer was dried over anhydrous sodium sulfate and concentrated in vacuo to provide pure di(1-naphthyl) borinic acid

Isolated weight: 110 mg, Yield: 89%.

¹H-NMR (500 MHz, CD₃SOCD₃): δ 10.9 (s, 1H), 8.29 (d, *J* = 8.3 Hz, 2H), 7.94-7.99 (m, 4H), 7.56 (dd, *J* = 1.2 Hz, 5.6 Hz, 2H), 7.42-7.51 (m, 6H).

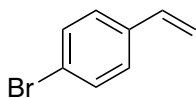
^{13}C -NMR (125 MHz, CD_3SOCD_3): 136, 133.9, 133.4, 130.2, 129, 128.9, 126.4, 126, 125.6.

^{11}B -NMR (160 MHz, CD_3SOCD_3): 47.7 ¹¹⁵

TOF MS ES^+ ($\text{C}_{20}\text{H}_{14}\text{BO}$) Calc. $[\text{MH}]^-$: 281.1490, Found $[\text{M}]^+$: 281.1181.

III-4-2 Typical procedure for synthesis of chiral diols using Sharpless asymmetric dihydroxylation (SAE)

AD-mix (1.4 g), MeSO_2NH_2 (95 mg, 1 mmol), *t*-BuOH (4.7 mL) and H_2O (4.7 mL) were mixed in a 50 mL round bottom flask and cooled to 4 °C. The orange suspension was stirred for 30 min followed by addition of olefin (1 mmol) via syringe. The resultant solution was stirred at 4 °C for 24 h, after which Na_2SO_3 (1.5 g) was added. After being stirred for further 45 min at room temperature, the clear solution was diluted by EtOAc (10 mL) and H_2O (2 mL). The aqueous layer was extracted with EtOAc (3 × 10 mL). Combined EtOAc extracts were dried over Na_2SO_4 , concentrated under reduced pressure, and purified by flash column chromatography (30% EtOAc/Hexane) to afford pure diol.

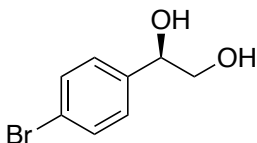


III-4-3 1-Bromo-4-vinylbenzene (I-51)

Wittig olefination of 4-Br-benzaldehyde (555 mg, 3 mmol) following procedures described below for the synthesis of 1-(trifluoromethyl)-4-vinylbenzene **I-52** afforded 4-bromo-styrene as colorless oil

Isolated weight: 450 mg, Yield: 81%.

^1H NMR (300 MHz, CDCl_3) δ 7.43 (d, $J = 8.4$ Hz, 2H) , 7.26 (d, $J = 8.4$ Hz, 2H), 6.62 (dd, $J = 17.4, 10.8$ Hz, 1H), 5.69 (dd, $J = 17.4, 0.9$ Hz, 1H), 5.24 (dd, $J = 10.8, 0.9$ Hz, 1H).¹¹⁶



III-4-4 (*R*)-1-(4-Bromophenyl) ethane-1,2-diol (I-41)

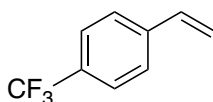
SAD of 4-bromo-styrene (183 mg, 1 mmol) with AD-mix- β following typical procedure afforded the diol as a white solid.

Isolated weight: 178, Yield: 82%

$[\alpha_D]^{20} = -46$, ($c = 0.44$, CDCl_3), lit.¹¹⁷ $[\alpha_D]^{23} = -47$, ($c = 1.02$, Chloroform).

^1H -NMR (500 MHz, CDCl_3) δ 7.46 (d, $J = 8.7$ Hz, 2H), 7.26 (d, $J = 8.7$ Hz, 2H), 4.80 (dd, $J = 8.3, 3.4$ Hz, 1H), 3.76 (d, $J = 11.3$ Hz, 1H), 3.62 (dd, $J = 11.3, 8.2$ Hz, 1H), 2.57 (s, 1H), 2.03 (s, 1H).

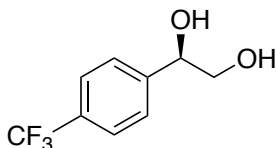
^{13}C -NMR (126 MHz, CDCl_3) δ 139.42, 131.65, 127.78, 121.87, 74.01, 67.90. ¹¹⁸



III-4-5 1-(Trifluoromethyl)-4-vinylbenzene (I-52)

To a solution of methyltriphenylphosphonium bromide (2.14 g, 6 mmol) in dry THF (20 mL) at 0 °C was added *n*-BuLi (2.5 M in hexane, 2.4 mL, 6 mmol) dropwise. The solution was stirred for 20 min followed by slow addition of 4- CF_3 -benzaldehyde (522 mg, 3 mmol) solution in dry THF (5 mL) via syringe at 0 °C. The mixture was stirred for 2.5 h and then quenched by addition of saturated NH_4Cl (10 mL) and EtOAc (30 mL). The aqueous layer

was separated and extracted with EtOAc (2 × 20 mL). Combined extracts were dried over Na₂SO₄, concentrated under reduced pressure and purified by flash chromatography (0-5% EtOAc/hexane) to afford 1-(trifluoromethyl)-4-vinylbenzene pure colorless oil (300 g, 58%). The product used without purification in the next step.



III-4-6 (R)-1-(4-(Trifluoromethyl) phenyl) ethane-1,2-diol (I-42)

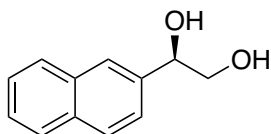
SAD of 1-(trifluoromethyl)-4-vinylbenzene (103 mg, 0.59 mmol) with AD-mix-β following typical procedure afforded the diol as a white solid.

Isolated weight: 38 mg, Yield: 31%

$[\alpha_D]^{20} = -24.5$, (c = 1.0, MeOH), lit.¹¹⁹ $[\alpha_D]^{20} = -26.5$, (c = 1.01, MeOH).

¹H NMR (500 MHz, CDCl₃) δ 7.63 (d, *J* = 8.1 Hz, 2H), 7.51 (d, *J* = 8.0 Hz, 2H), 4.91 (dd, *J* = 8.2, 3.4 Hz, 1H), 3.85 – 3.76 (m, 1H), 3.65 (dd, *J* = 11.3, 8.1 Hz, 1H), 2.70 (s, 1H), 2.07 (s, 1H).

¹³C NMR (126 MHz, CDCl₃) δ 144.38, 130.20 (d, *J* = 32.2 Hz), 126.36, 125.48 (q, *J* = 3.8 Hz), 124.04 (d, *J* = 272.2 Hz), 74.04, 67.88.⁴⁵

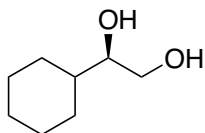


III-4-7 (R)-1-(Naphthalen-2-yl) ethane-1,2-diol (I-43)

$[\alpha_D]^{20} = -28.3$, ($c = 1.2$, EtOH), lit.⁴⁵ $[\alpha_D]^{24} = -33.7$, ($c = 1.2$, EtOH).

$^1\text{H-NMR}$ (500 MHz, CDCl_3) δ 7.88 – 7.82 (m, 4H), 7.52 – 7.45 (m, 3H), 5.01 (d, $J = 8.2$ Hz, 1 H), 3.92 – 3.82 (m, 1H), 3.77 (t, $J = 9.8$ Hz, 1H), 2.62 (s, 1H), 2.06 (s, 1H).

$^{13}\text{C-NMR}$ (126 MHz, CDCl_3) δ 137.85, 133.22, 133.14, 128.37, 127.95, 127.71, 126.32, 126.09, 125.02, 123.94, 74.77, 68.04.⁴⁵



III-4-8 (R)-1-Cyclohexylethane-1,2-diol (I-44)

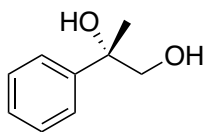
SAD of vinylcyclohexane (165 mg, 1.5 mmol) with AD-mix- β following typical procedure afforded the diol as a white solid.

Isolated weight: 208 mg, Yield: 96%.

$[\alpha_D]^{20} = +2.8$, ($c = 1.0$, EtOH), lit.¹²⁰ $[\alpha_D]^{20} = +3.58$, ($c = 1.17$, EtOH).

$^1\text{H-NMR}$ (500 MHz, CDCl_3) δ 3.71 (m, 1H), 3.53 (m, 1H), 3.45 (m, 1H), 2.02 (br, 2H), 1.87 (d, $J = 11.2$ Hz, 1H), 1.81 – 1.70 (m, 2H), 1.70 – 1.49 (m, 2H), 1.41 (m, 1H), 1.30 – 0.96 (m, 5H).

$^{13}\text{C-NMR}$ (126 MHz, CDCl_3) δ 76.49, 64.83, 28.91, 28.65, 26.36, 26.05, 25.96.¹¹⁶

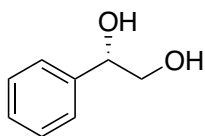


III-4-9 (S)-2-Phenylpropane-1,2-diol (I-45)

$[\alpha_D]^{20} = 10.1$, ($c = 0.4$, CHCl_3), lit. ¹²¹ $[\alpha_D]^{24} = 11.4$, ($c = 0.4$, CHCl_3).

$^1\text{H-NMR}$ (500 MHz, CDCl_3) δ 7.47 (dd, $J = 2.0, 1.4$ Hz, 1H), 7.46 (dd, $J = 2.1, 1.0$ Hz, 1H), 7.40 – 7.35 (m, 2H), 7.31 – 7.27 (m, 1H), 3.81 (d, $J = 11.1$ Hz, 1H), 3.64 (d, $J = 11.1$ Hz, 1H), 2.59 (br, 1H), 1.81 (br, 1H).

$^{13}\text{C-NMR}$ (126 MHz, CDCl_3) δ 144.92, 128.46, 127.22, 125.06, 74.83, 71.12, 26.04.¹²¹



III-4-10 (S)-1-Phenylethane-1,2-diol (I-46)

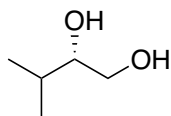
SAD of styrene (624 mg, 6 mmol) with AD-mix- β following typical procedure afforded the diol as a white solid.

Isolated weight: 720 mg, Yield: 87%.

$[\alpha_D]^{20} = -36.7$, ($c = 1.0$, EtOH), lit. ¹²² $[\alpha_D]^{20} = -37.3$, ($c = 4.33$, EtOH).

$^1\text{H-NMR}$ (500 MHz, CDCl_3) δ 7.41 – 7.35 (m, 4H), 7.31 (m, 1H), 4.84 (dd, $J = 8.2, 3.5$ Hz, 1H), 3.78 (dd, $J = 11.3, 3.5$ Hz, 1H), 3.68 (dd, $J = 11.3, 8.2$ Hz, 1H), 2.53 (s, 1H), 2.08 (s, 1H).

$^{13}\text{C-NMR}$ (126 MHz, CDCl_3) δ 140.45, 128.57, 128.06, 126.06, 74.68, 68.10. ¹²³

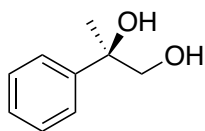


III-4-11 (S)-3-Methylbutane-1,2-diol (I-47)

$[\alpha_D]^{20} = +9.2$, ($c = 0.9$, EtOH), lit. ¹²⁴ $[\alpha_D]^{26} = +9.2$, ($c = 0.9$, EtOH).

¹H-NMR (500 MHz, CDCl₃) δ 3.69 (dd, $J = 11.1, 2.8$ Hz, 1H), 3.49 (dd, $J = 11.1, 8.2$ Hz, 1H), 3.41 (ddd, $J = 8.2, 6.5, 2.8$ Hz, 1H), 2.62 – 2.47 (m, 2H), 1.76 – 1.61 (m, $J = 6.8$ Hz, 1H), 0.96 (d, $J = 6.8$ Hz, 3H), 0.91 (d, $J = 6.8$ Hz, 3H).

¹³C-NMR (126 MHz, CDCl₃) δ 77.95, 64.89, 30.90, 18.70, 18.21. ¹²⁴



III-4-12 (R)-2-Phenylpropane-1,2-diol (I-53)

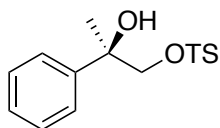
SAD of α -methyl styrene (590 mg, 5.0 mmol) with AD-mix- β following typical procedure afforded the diol as a white solid.

Isolated weight: 620 mg, Yield: 82%.

$[\alpha_D]^{20} = -5.1$, ($c = 1.0$, EtOH), lit. ¹²⁵ $[\alpha_D]^{24} = -4.89$, ($c = 3.9$, EtOH).

¹H-NMR (500 MHz, CDCl₃) δ 7.47 (dd, $J = 2.0, 1.4$ Hz, 1H), 7.46 (dd, $J = 2.1, 1.0$ Hz, 1H), 7.40 – 7.35 (m, 2H), 7.31 – 7.27 (m, 1H), 3.81 (d, $J = 11.1$ Hz, 1H), 3.64 (d, $J = 11.1$ Hz, 1H), 2.59 (br, 1H), 1.81 (br, 1H).

¹³C-NMR (126 MHz, CDCl₃) δ 144.92, 128.46, 127.22, 125.06, 74.83, 71.12, 26.04. ¹²⁵



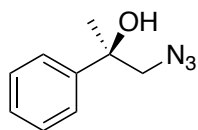
III-4-13 (*R*)-2-Hydroxy-2-phenylpropyl 4-methylbenzenesulfonate (I-54)

To a solution of (*R*)-2-phenylpropane-1,2-diol (620 mg, 4.08 mmol) in dry pyridine (30 mL) at 0 °C was added tosyl chloride (860 mg, 4.5 mmol). The solution was stirred for 6 h and then was quenched by addition of dilute HCl (1 M, 20 mL) and CH₂Cl₂ (60 mL). The organic layer was separated and washed with dilute HCl (1 M, 30 mL) and brine. The organic phase was dried over Na₂SO₄, concentrated under reduced pressure, and purified by flash chromatography to afford product as light brown solid.

Isolated weight: 1.04 g, Yield: 87%.

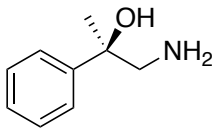
¹H-NMR (300 MHz, CDCl₃) δ 7.67 (d, 2H, *J* = 8.4 Hz), 7.30 (m, 7H), 4.07 (s, 2H), 2.55 (br, 1H), 2.42 (s, 3H).

¹³C-NMR (75 MHz, CDCl₃) δ 144.9, 142.8, 132.3, 129.8, 128.3, 127.8, 127.5, 124.9, 76.7, 73.1, 26.0, 21.6.¹²⁶



III-4-14 (*R*)-1-Azido-2-phenylpropan-2-ol (I-55)

To a solution of (*R*)-2-hydroxy-2-phenylpropyl 4-methylbenzenesulfonate (500 mg, 1.63 mmol) in dry DMF (40 mL) was added sodium azide (531 mg, 8.17 mmol). The solution was stirred for 24 h at 60 °C and then quenched by addition of H₂O (60 mL). The aqueous layer was separated and extracted with CH₂Cl₂ (4 ×60 mL). Combined organic extracts were dried over Na₂SO₄, concentrated under reduced pressure to afford the crude azide as an oil, which was used directly for next step.



III-4-15 (*R*)-1-Amino-2-phenylpropan-2-ol (I-50)

To a solution of (*R*)-1-azido-2-phenylpropan-2-ol (108 mg, 0.61 mmol) in EtOAc (10 mL) was added 10 wt% Pd/C (65.2 mg, 0.06 mmol of Pd, 0.1 equiv.). The mixture was stirred overnight under hydrogen atmosphere and filtered through celite. The organic phase was concentrated under reduced pressure and purified by flash chromatography to afford pure amino alcohol product as light yellow oil.

Isolated weight: 91 mg, Yield: 99%.

$[\alpha]_D^{20} = -12$, ($c = 0.28$, EtOH).

$^1\text{H-NMR}$ (500 MHz, CDCl_3) δ 7.52 – 7.41 (m, 2H), 7.36 (t, $J = 7.7$ Hz, 2H), 7.29 – 7.22 (m, 1H), 3.10 (d, $J = 12.4$ Hz, 1H), 2.82 (d, $J = 12.4$ Hz, 1H), 2.10 (d, $J = 40.6$ Hz, 3H), 1.50 (s, 3H).

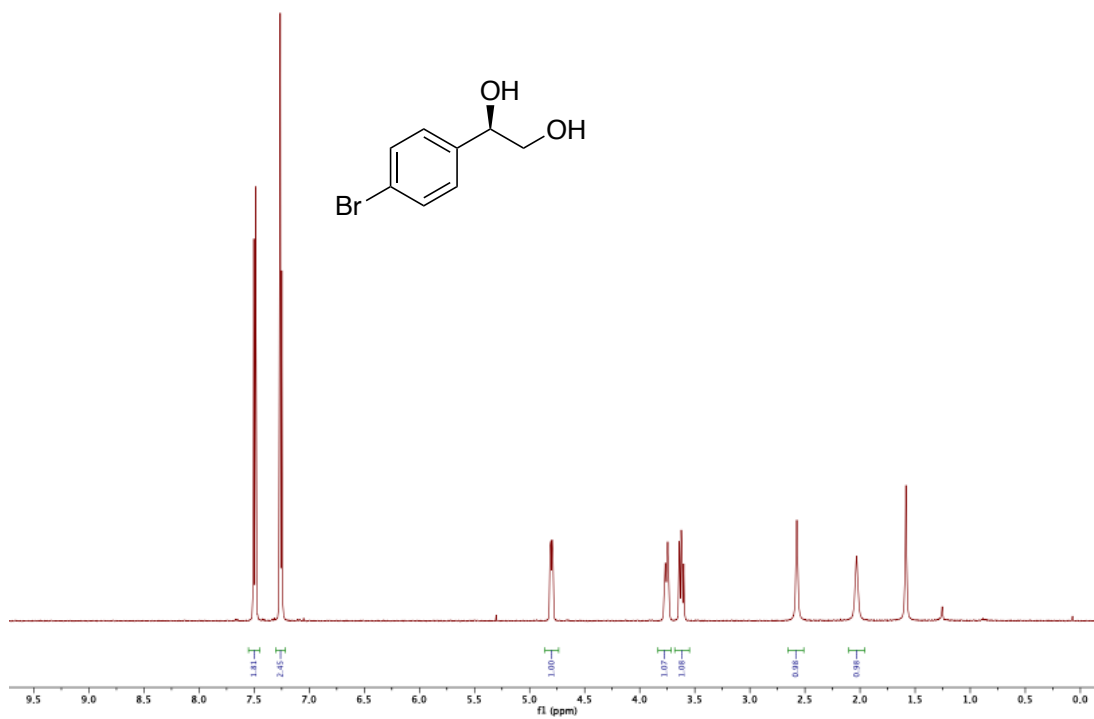
$^{13}\text{C-NMR}$ (126 MHz, CDCl_3) δ 146.41, 128.25, 126.66, 125.09, 73.38, 52.65, 27.77. ¹²⁷

II-5 Extinction coefficient measurement

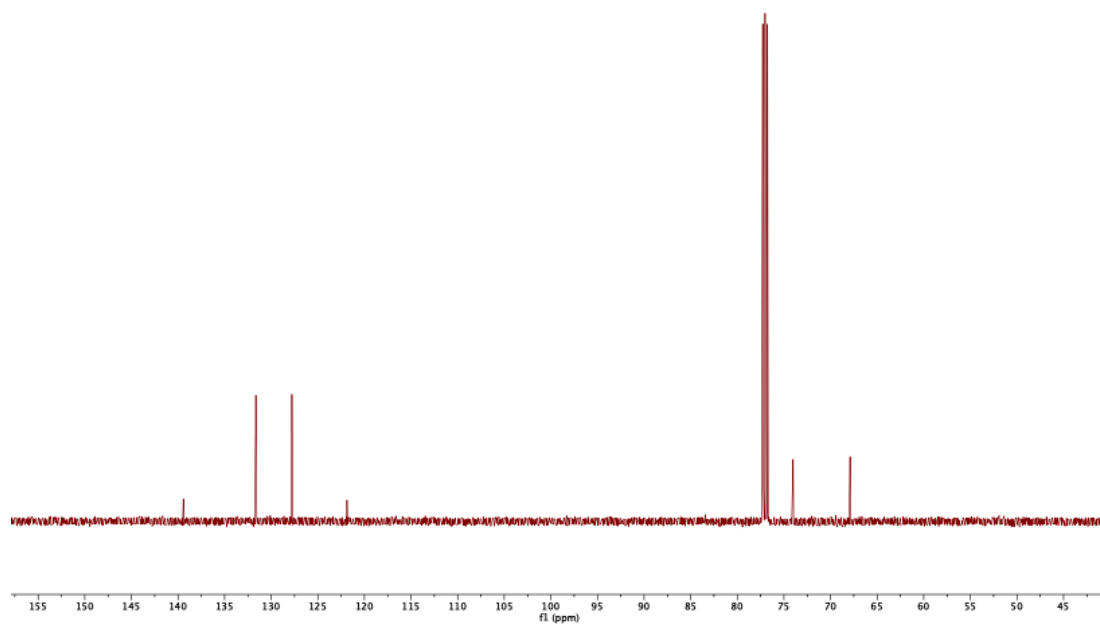
A 0.01 mM solution of triphenylmethane in acetonitrile was used as internal standard to accurately measure the concentration of the **DBA** solution for UV analysis. An exact volume of a solution of **DBA** in acetonitrile was added to the Ph_3CH solution. The solvent was evaporated, and the resultant residue was dissolved in CDCl_3 (1 mL) and the NMR

of the mixture was obtained (long relaxation delay was used to ensure accurate integration values). The integrated ratio of the CH of Ph₃CH and the H of Ar₂B-OH in DBA was used to calculate the concentration of **DBA** solution. The same **DBA** solution was used to measure its UV spectrum. The absorbance at 220 nm (λ_{max}) and the calculated concentration from NMR, along with Beer's law equation was used to calculate the extinction coefficient for DBA ($\epsilon = 153,500 \text{ M}^{-1}\text{cm}^{-1}$).

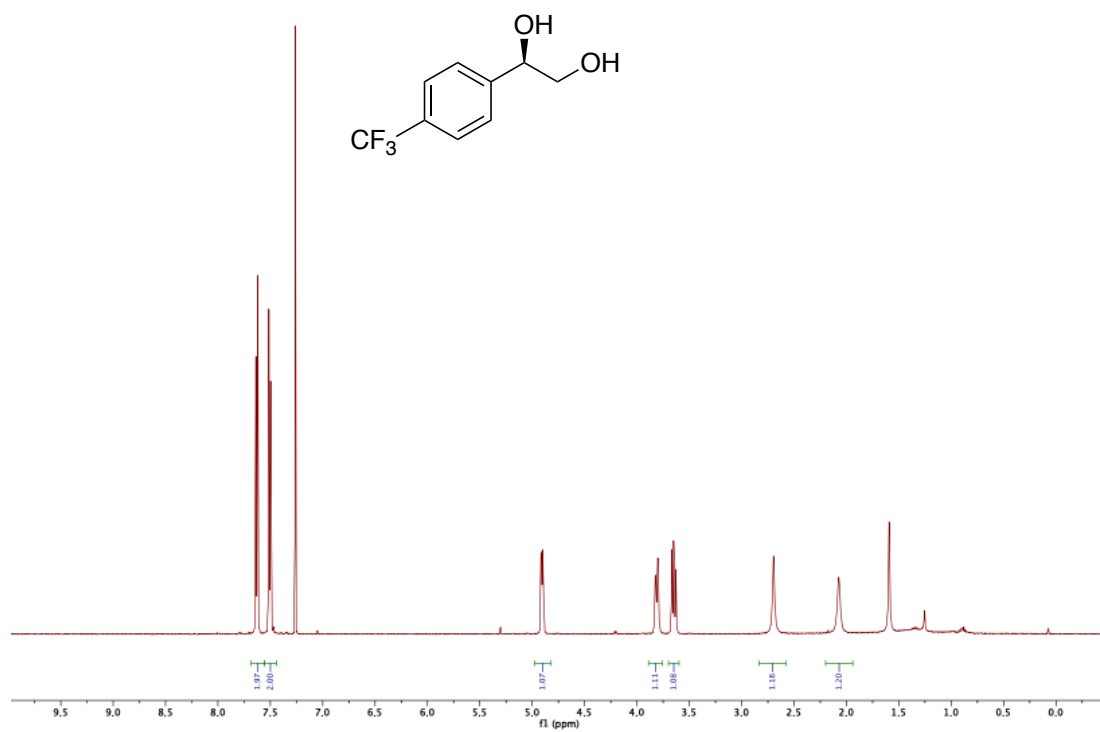
ST-CD-02_PROTON_01



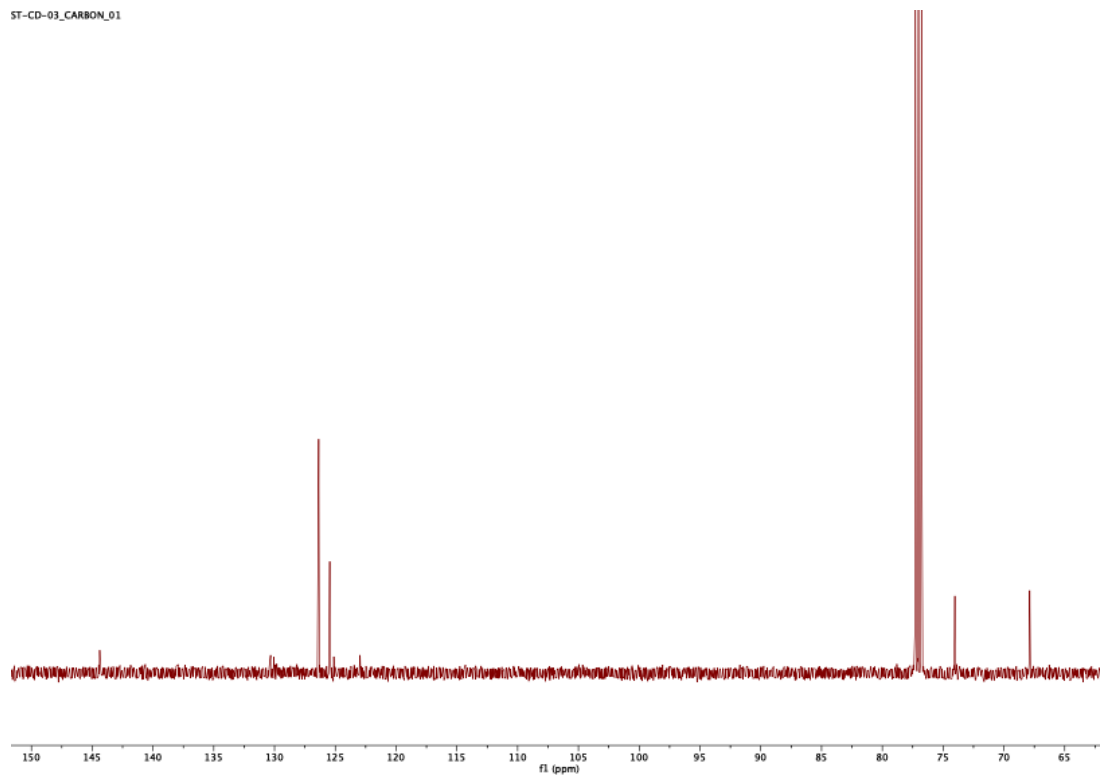
ST-CD-02_CARBON_01



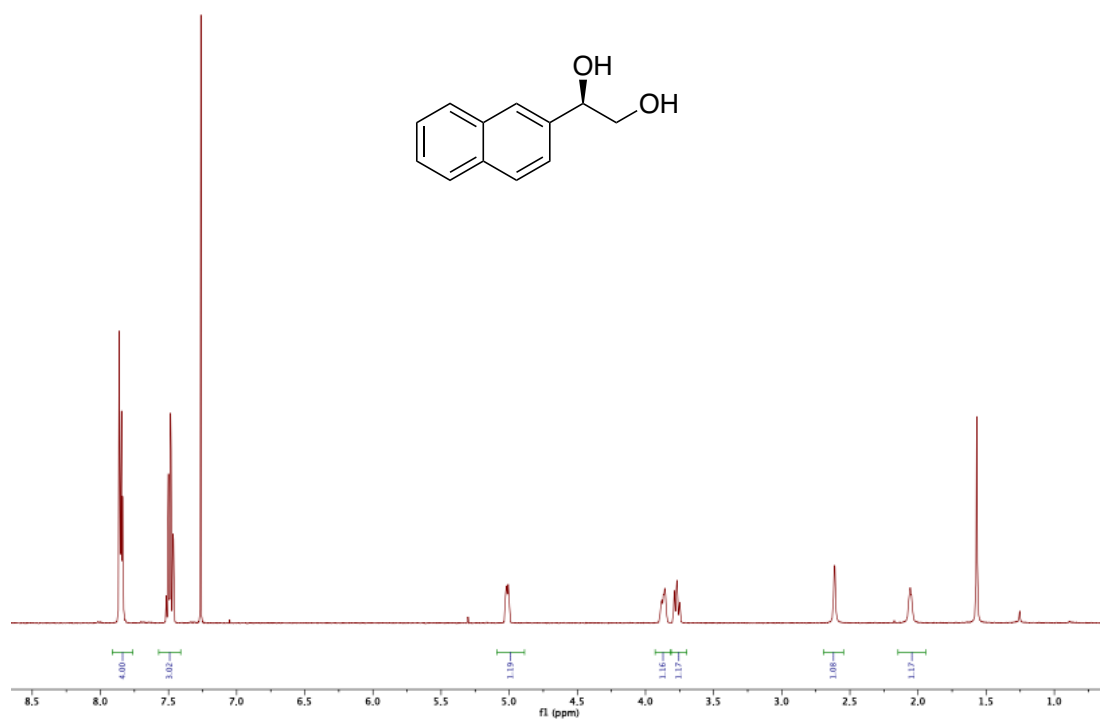
ST-CD-03_PROTON_01



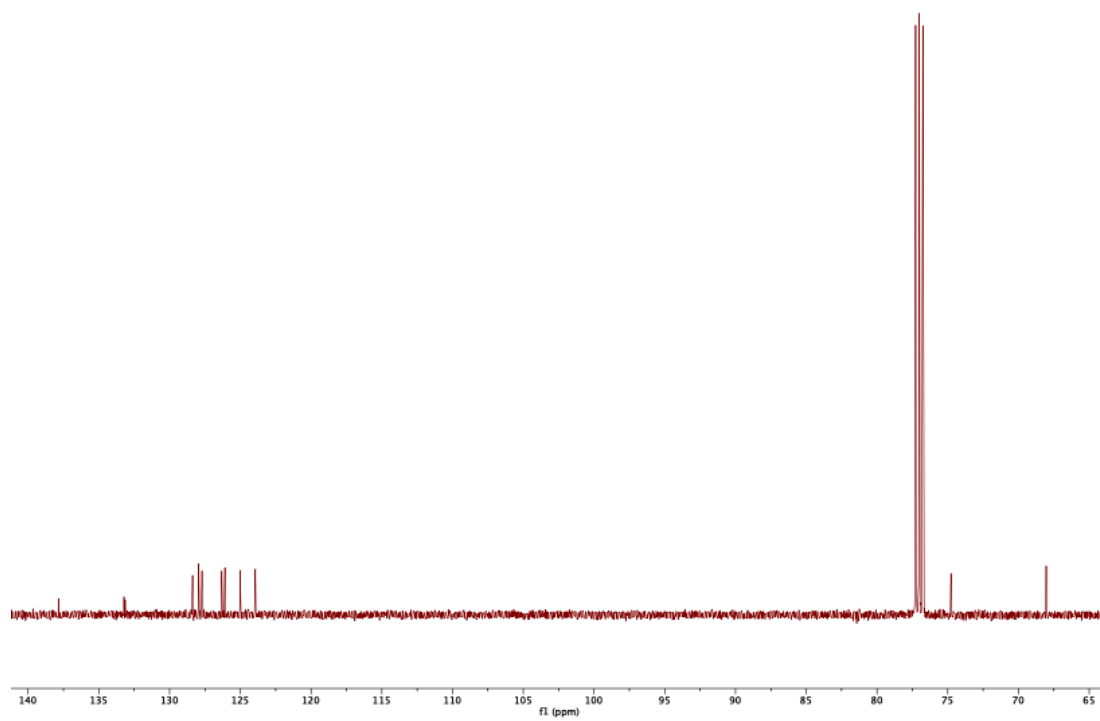
ST-CD-03_CARBON_01



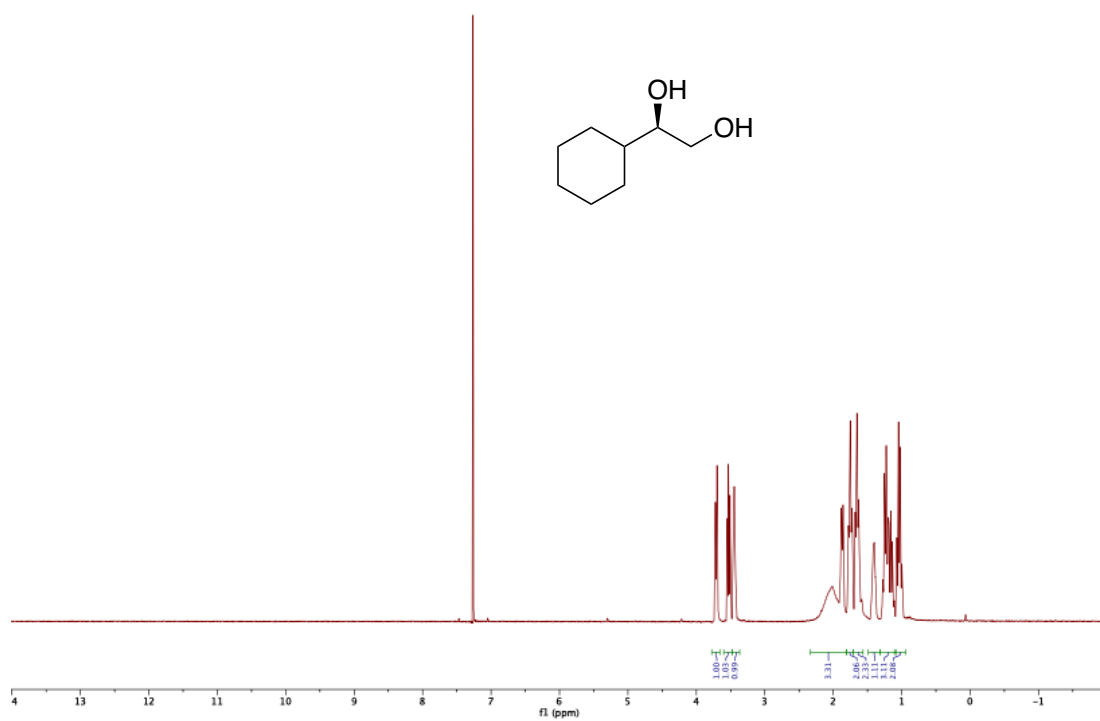
ST-CD-08_PROTON_01



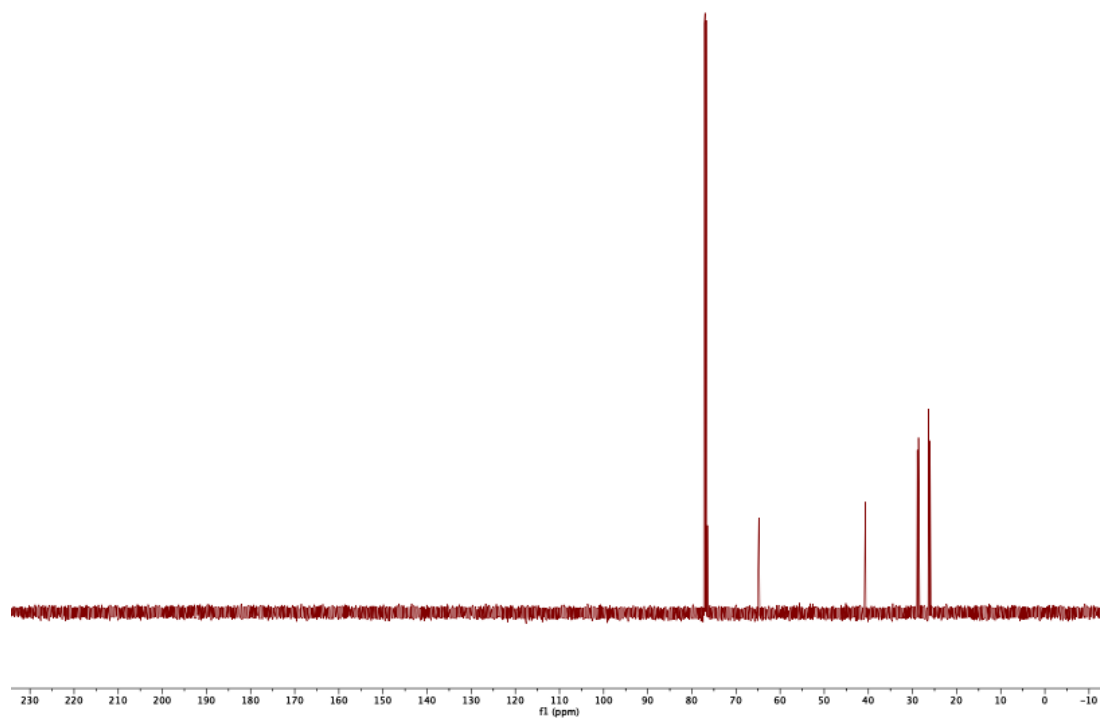
ST-CD-08_CARBON_01



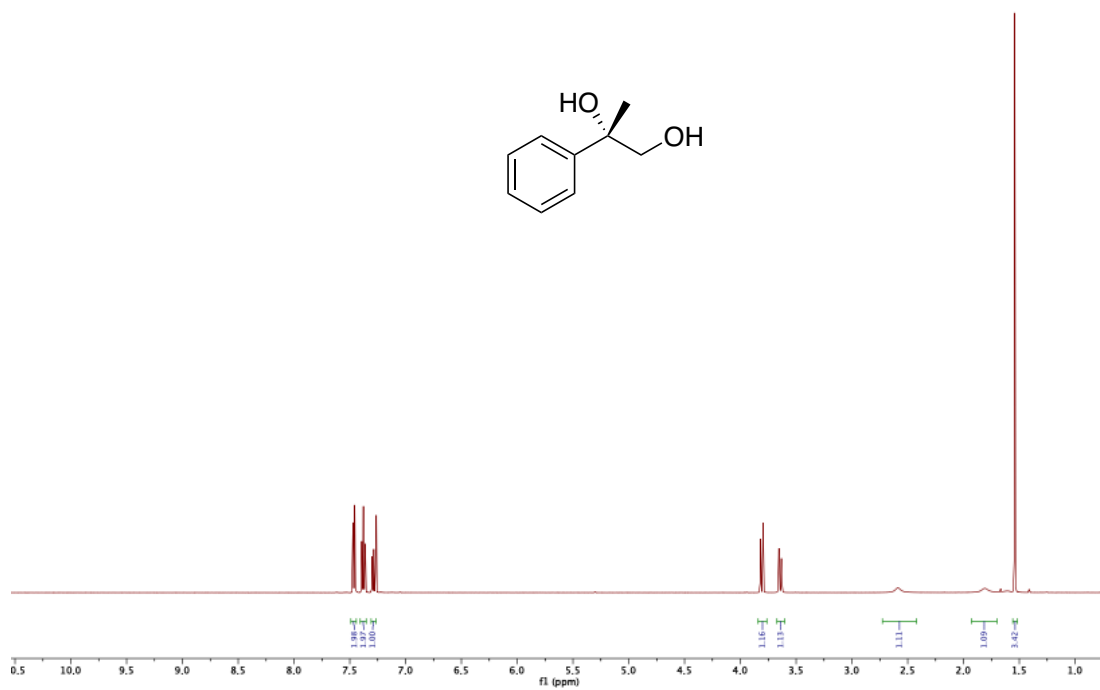
ST-CD-04_PROTON_01



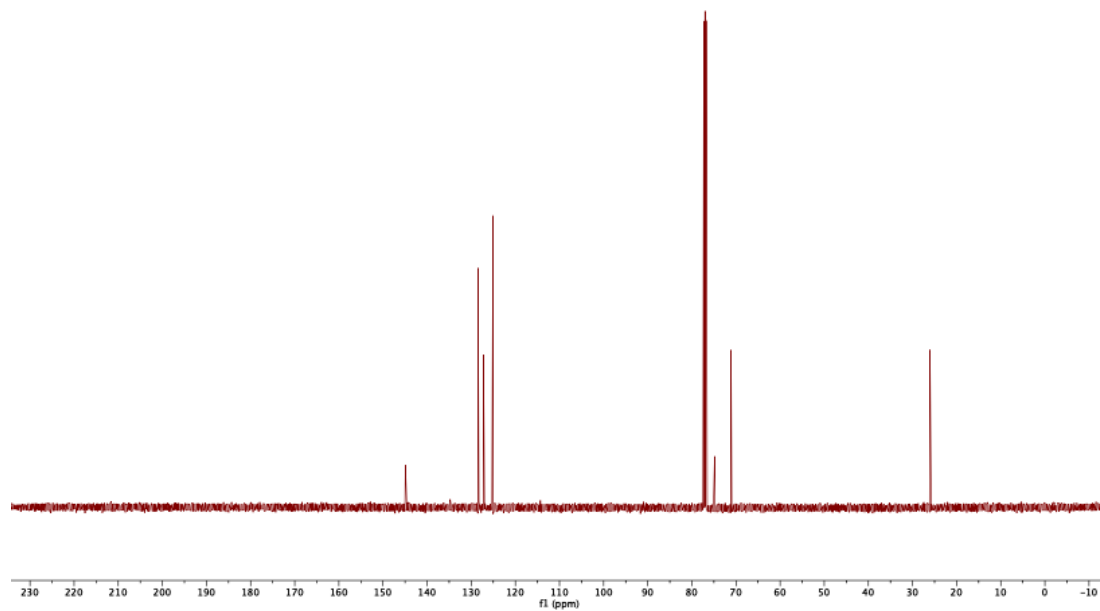
ST-CD-04_CARBON_01



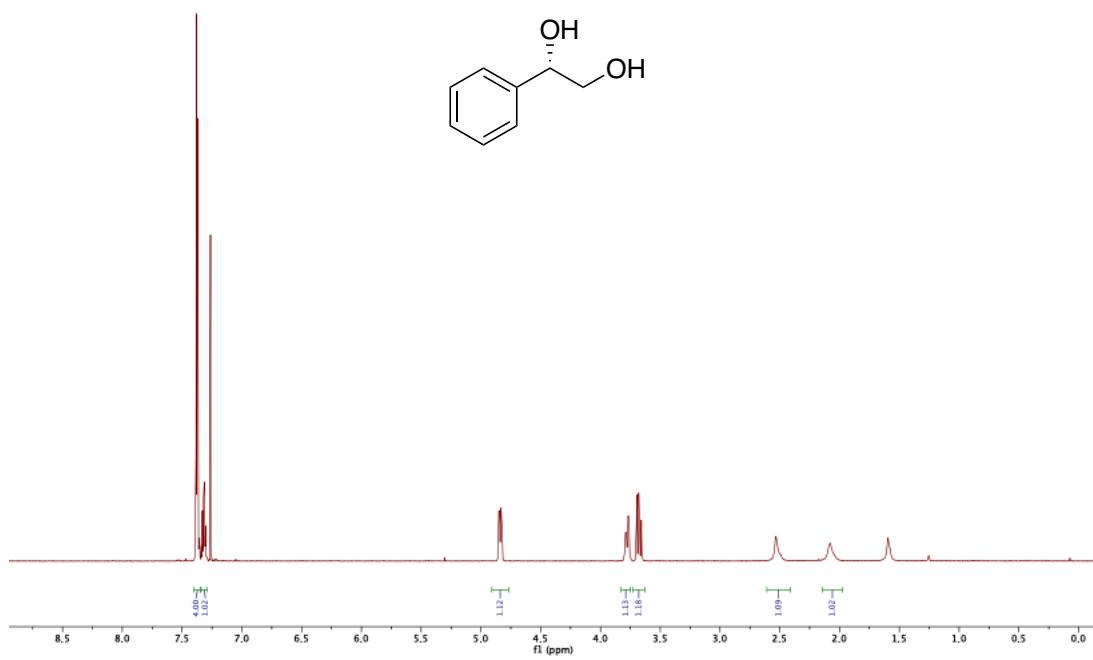
ST-CD-01_PROTON_01



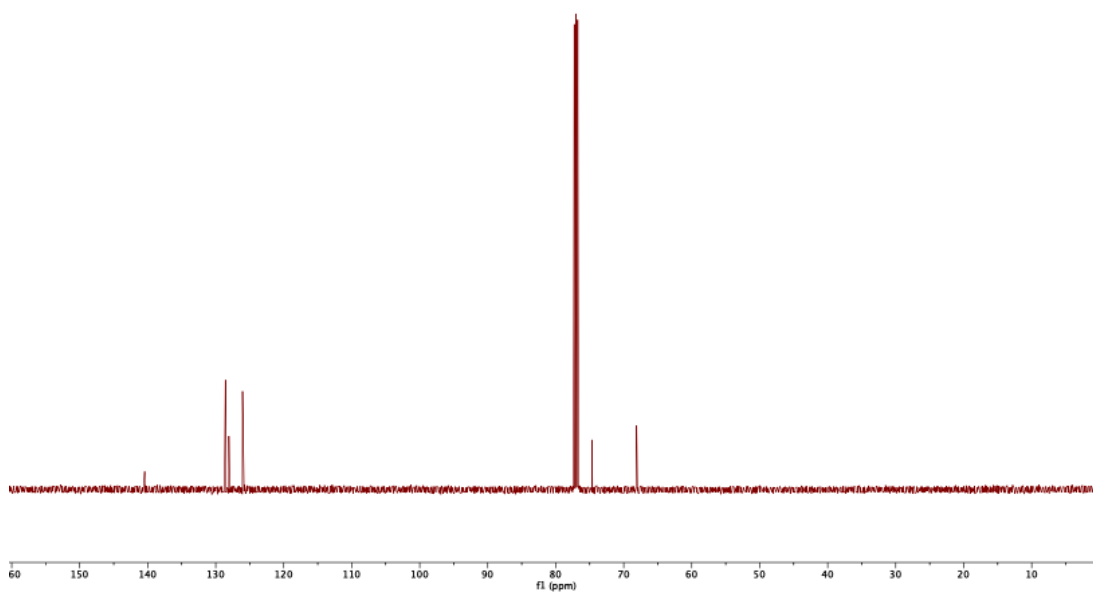
ST-CD-01_CARBON_01



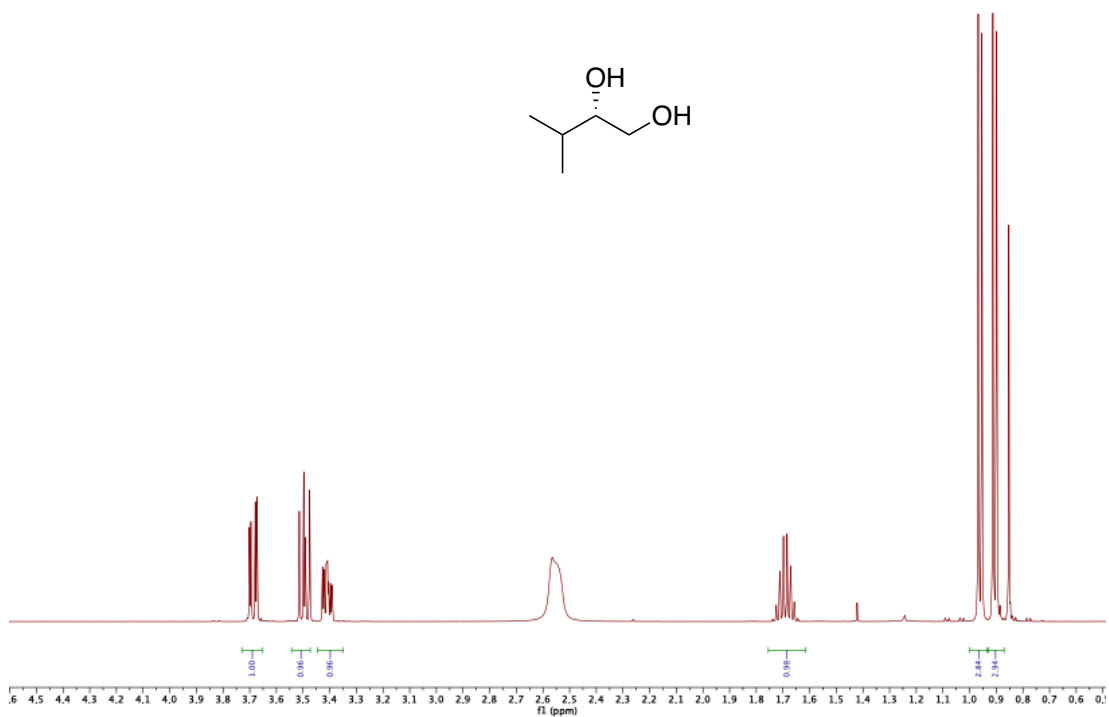
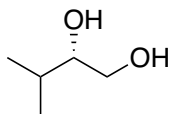
ST-CD-06_PROTON_01



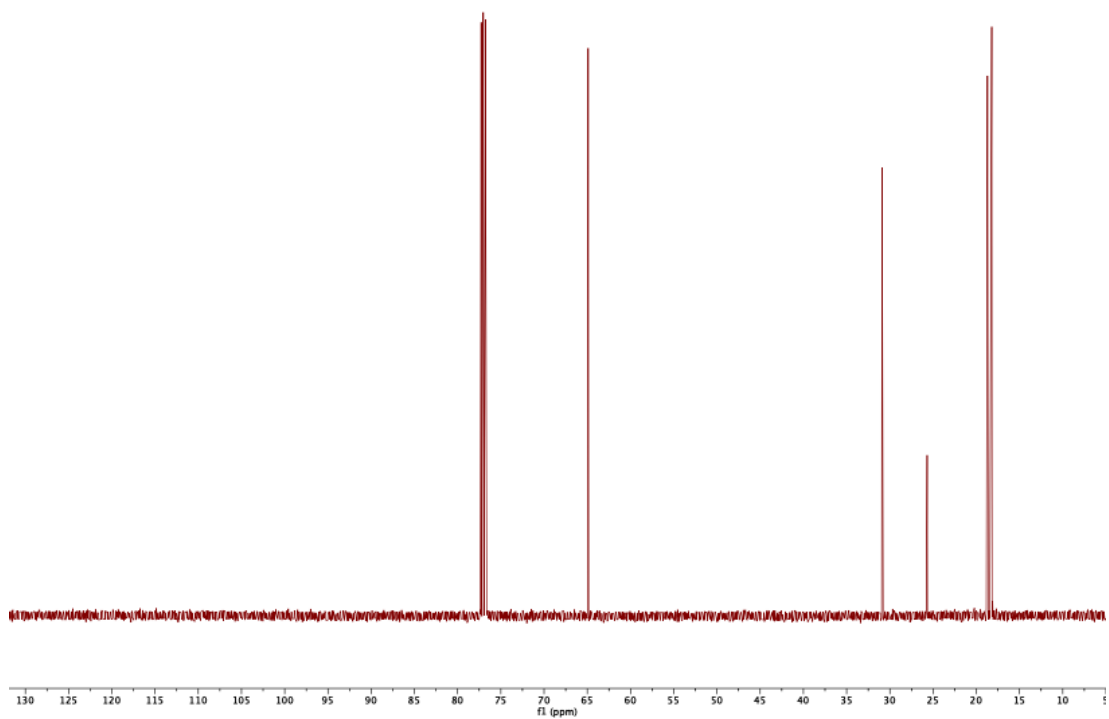
ST-CD-06_CARBON_01



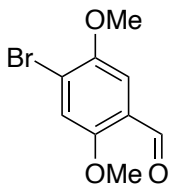
ST-CD-07_PROTON_01



ST-CD-07_CARBOON_01



III-6 Napyradiomycin experimental section



III-6-1 6,4-Bromo-2,5-dimethoxybenzaldehyde (II-57)

To a solution of 2,5-dimethoxybenzaldehyde (12.0 g, 72.2 mmol, 1.0 equiv.) in glacial acetic acid (180 mL) at 0 °C was added a solution of bromine (4.0 mL, 79 mmol, 1.1 equiv.) in acetic acid (72.0 mL) dropwise. After the addition of bromine was complete, the reaction was warmed up to room temperature and allowed to stir at this temperature overnight. The reaction mixture was poured into distilled water, and the pale-yellow precipitate was collected by filtration. This crude mixture was dissolved in DCM and was washed with water and saturated $\text{Na}_2\text{S}_2\text{O}_3$ solution. The organic layer was separated and dried by Na_2SO_4 following by filtration and concentration under a low-pressure vacuum. Finally, the mono-brominated product was obtained by recrystallization with DCM and Hexane.

Isolated weight: 9.7 g, Yield: 55%.

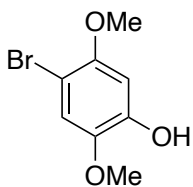
^1H NMR (500 MHz, CDCl_3) δ 10.41 (s, 1H), 7.35 (s, 1H), 7.26 (s, 1H), 3.92 (s, 3H), 3.91 (s, 3H).

^{13}C NMR (126 MHz, CDCl_3) δ 188.78, 156.20, 150.41, 124.13, 120.31, 117.64, 109.59, 56.74, 56.38.

FTIR (neat), cm^{-1} : 3073, 1678, 1250, 1015.

TOF MS ES⁺ (C₉H₁₀BrO₃): Calc. [M+H]⁺: 244.9816, Found [M+H]⁺ 244.9809.

Melting Point: 130 °C



III-6-2 4-Bromo-2,5-dimethoxyphenol (II-59)

To a solution of *m*-CPBA (16.2 g (77% *m*CPBA), 72.2 mmol, 1.0) in DCM (24.0 mL) at 0 °C was added a solution of compound **II-57** (18.0 g, 72.2 mmol, 1.0 equiv.) in DCM (72.0 mL). After completion, the reaction was warmed up to room temperature and then refluxed for 14 h. The reaction was cooled down to room temperature and quenched by the addition of saturated NaHCO₃ aqueous solution and saturated Na₂S₂O₃ solution. The organic layer was separated and dried over Na₂SO₄, filtered, and concentrated under reduced pressure. The resulting residue was dissolved in methanol (200 mL), and then 10% NaOH solution (200 mL) was added for saponification. The reaction mixture was stirred for 3 h. After completion of the reaction, the resulting mixture was acidified to pH = 1 using HCl (2.0 *M*). The crude product was extracted using DCM, dried over Na₂SO₄, filtered, and concentrated under reduced pressure. The product was purified using column chromatography (10% EtOAc/Hex).

Isolated weight: 12.3 g, Yield: 73%.

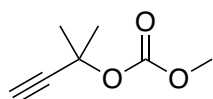
¹H NMR (500 MHz, CDCl₃) δ 7.03 (s, 1H), 6.62 (s, 1H), 5.61 (s, 1H), 3.85 (s, 3H), 3.83 (s, 3H).

^{13}C NMR (126 MHz, CDCl_3) δ 150.65, 145.69, 140.90, 115.73, 100.43, 99.78, 56.77, 56.73.

FTIR (neat), cm^{-1} : 3498, 3369, 3078, 1301, 1264, 1076.

TOF MS ES^+ ($\text{C}_8\text{H}_9\text{BrO}_3$) Calc. $[\text{M}]^+$: 231.9735, Found $[\text{M}]^+$ 231.9735.

Melting Point: 137 °C



III-6-3 1,1-Dimethyl-prop-2-ynyl methyl carbonate (II-61)

To a solution of commercially available 2-methyl-but-3-yn-2-ol (3.5 mL, 35.7 mmol, 1.0 equiv.) in diethyl ether (38.0 mL) under argon at 0 °C was added *n*-BuLi (2.5 M in hexanes, 14.3 mL, 35.7 mmol, 1.0 equiv.) dropwise. After addition was completed, the reaction mixture was allowed to stir for 30 min at 0 °C. Methyl chloroformate (2.8 mL, 35.7 mmol, 1.0 equiv.) was added dropwise, and the mixture was allowed to warm up to room temperature and stirred for 2 h. The reaction was partitioned between diethyl ether and water. The water layer was extracted once more with ether, and the combined organic layers were dried with Na_2SO_4 , filtered, and concentrated, resulting in the pure carbonate.

Notes:

1. It should be mentioned that carbonate **II-61** is a volatile compound and should not be kept under low pressure for evaporation of the solvent.
2. Due to the sensitivity of the reaction toward the water and air, the round bottom flask was flame dried before running the reaction.

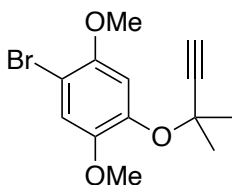
Isolated weight: 4.1 g, Yield: 82%.

^1H NMR (500 MHz, CDCl_3) δ 3.78 (s, 3H), 2.57 (s, 1H), 1.72 (s, 6H).

^{13}C NMR (126 MHz, CDCl_3) δ 153.53, 84.00, 73.78, 72.81, 54.35, 28.71.

FTIR (neat), cm^{-1} : 3288, 2958, 1749, 1472, 1266.

TOF MS EI^+ ($\text{C}_6\text{H}_7\text{O}_3$) Calc. $[\text{M}]^+$: 127.0395, Found $[\text{M}-\text{CH}_3]^+$: 127.0373.



III-6-4 1-Bromo-2,5-dimethoxy-4-((2-methylbut-3-yn-2-yl)oxy)benzene (II-62)

A flame-dried round bottom flask was charged with a solution of phenol **II-59** (7.12 g, 30.5 mmol, 1.0 equiv.) and acetonitrile (47.0 mL) under an argon atmosphere. The resulting mixture was cooled to $-20\text{ }^\circ\text{C}$, and the reaction was kept under an argon atmosphere. To this solution was added CuCl_2 (40.3 mg, 0.3 mmol, 1 mol%) and DBU (5.5 mL, 36.6 mmol, 1.2 equiv.), followed by a solution of carbonate **II-61** (5.5 g, 36.6 mmol, 1.2 equiv.) in acetonitrile (5.0 mL). The reaction was allowed to stir at this temperature overnight and quenched by the addition of water. The organic layer was washed with 300 mL of 1 M HCl, and 2 N NaOH and brine. The organic layer was dried over Na_2SO_4 , filtered, and concentrated under reduced pressure. The product was purified using column chromatography (10% EtOAc/Hex).

Note: Solvent was degassed for 30 min before the reaction. Using solvent without degassing leads to the formation of dimer **II-63**.

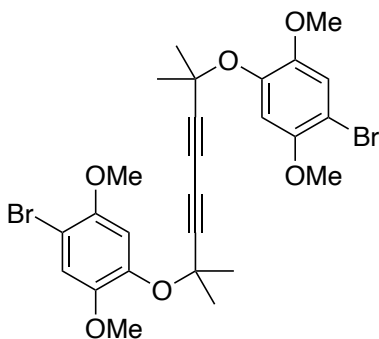
Isolated weight: 6.2 g, Yield: 68%.

^1H NMR (500 MHz, CDCl_3) δ 7.18 (s, 1H), 7.09 (s, 1H), 3.84 (s, 3H), 3.78 (s, 3H), 2.58 (s, 1H), 1.65 (s, 6H).

^{13}C NMR (126 MHz, CDCl_3) δ 149.62, 147.59, 144.38, 117.14, 109.17, 104.87, 86.37, 74.62, 73.75, 56.77, 56.58, 29.21.

FTIR (neat), cm^{-1} : 3284, 2990, 2837, 1493, 1209, 1125.

TOF MS ES^+ ($\text{C}_{13}\text{H}_{16}\text{BrO}_3$) Calc. $[\text{M}+\text{H}]^+$: 299.0283, Found $[\text{M}+\text{H}]^+$: 299.0273.



III-6-5 5,5'-((6-Methylhepta-2,4-diyne-1,6-diyl)bis(oxy))bis(2-bromo-1,4-dimethoxybenzene) (II-63)

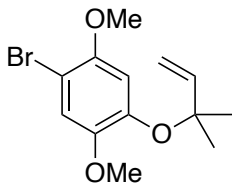
^1H NMR (500 MHz, CDCl_3) δ 7.09 (s, 2H), 7.01 (s, 2H), 3.78 (d, $J = 18.5$ Hz, 12H), 1.62 (s, 12H).

^{13}C NMR (126 MHz, CDCl_3) δ 149.57, 147.69, 143.82, 117.18, 109.53, 105.49, 82.40, 75.41, 69.71, 56.65, 56.51, 28.89.

FTIR (neat), cm^{-1} : 2930, 2840, 1755, 1497, 1440, 1378, 1201, 1126.

TOF MS ES^+ ($\text{C}_{26}\text{H}_{29}\text{Br}_2\text{O}_6$) Calc. $[\text{M}+\text{H}]^+$: 595.0331, Found $[\text{M}+\text{H}]^+$: 595.0337.

Melting point: 71°C



III-6-6 1-Bromo-2,5-dimethoxy-4-((2-methylbut-3-en-2-yl)oxy)benzene (II-68)

Bromo alkyne **II-81** (4.0 g, 13.4 mmol, 1.0 equiv.) was dissolved in hexane (67.0 mL) and ethyl acetate (67.0 mL), followed by the addition of Lindlar catalyst (320 mg, 8% w/w). The reaction atmosphere was evacuated and purged with hydrogen three times and kept under a hydrogen atmosphere for 2 h. The reaction mixture was passed through a silica pad followed by evaporation of the solvent under reduced pressure. The pure product was obtained using column chromatography (5% EtOAc/Hex)

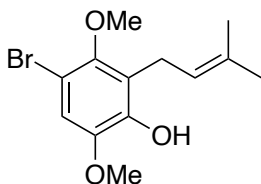
Isolated weight: 3.4 g, Yield: 87%.

$^1\text{H NMR}$ (500 MHz, CDCl_3) δ 7.06 (s, 1H), 6.71 (s, 1H), 6.17 (dd, $J = 17.6, 10.9$ Hz, 1H), 5.20 – 5.10 (m, 2H), 3.79 (s, 3H), 3.78 (s, 3H), 1.46 (s, 6H).

$^{13}\text{C NMR}$ (126 MHz, CDCl_3) δ 149.48, 147.70, 144.88, 144.00, 117.18, 113.63, 109.20, 103.98, 81.37, 56.80, 56.60, 26.36.

FTIR (neat), cm^{-1} : 3087, 2980, 2840, 1574, 1415, 1205, 1118.

TOF MS ES^+ ($\text{C}_{13}\text{H}_{18}\text{BrO}_3$) Calc. $[\text{M}+\text{H}]^+$: 300.0361, Found $[\text{M}+\text{H}]^+$ 300.0356.



III-6-7 4-Bromo-3,6-dimethoxy-2-(3-methylbut-2-en-1-yl)phenol (II-69)

In a flame-dried round bottom flask and under argon atmosphere, a solution of bromo alkene **II-68** (1.6 g, 5.3 mmol) in decalin (88.0 mL) was refluxed at 190 °C for 3 h. After completion of the reaction, the solvent was removed using short path distillation under reduced pressure. The product was purified using column chromatography (5% EtOAc/Hex).

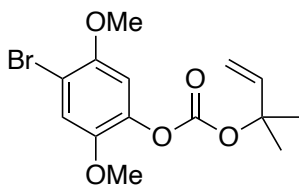
Isolated weight: 880 mg, Yield: 55%.

^1H NMR (500 MHz, CDCl_3) δ 6.88 (s, 1H), 5.66 (s, 1H), 5.22 (t, $J = 6.6$, Hz, 1H), 3.85 (s, 3H), 3.77 (s, Hz, 3H), 3.43 – 3.38 (d, $J = 6.82$ H), 1.78 (s, 3H), 1.68 (s, 3H).

^{13}C NMR (126 MHz, CDCl_3) δ 149.63, 143.64, 143.55, 132.26, 123.00, 122.04, 112.24, 105.59, 61.19, 56.34, 25.75, 23.95.

FTIR (neat), cm^{-1} : 3511, 2962, 2931, 1474, 1284, 1231, 1049.

TOF MS ES^+ ($\text{C}_{13}\text{H}_{18}\text{BrO}_3$) Calc. $[\text{M}+\text{H}]^+$: 300.0361, Found $[\text{M}+\text{H}]^+$: 300.0346.



III-6-8 4-Bromo-2,5-dimethoxyphenyl (2-methylbut-3-en-2-yl) carbonate (II-76)

To a solution of the phenol **II-59** (233 mg, 1.0 mmol, 1.0 equiv) and triphosgene (119 mg, 0.4 mmol, 0.4 equiv.) in DCM (3.0 mL) was added pyridine (81 μL , 1.0 mmol, 1.0 equiv.) dropwise at room temperature. The resulting mixture was stirred for 30 min. Allylic alcohol (105 μL , 1.0 mmol, 1.0 equiv.) was added followed by addition of pyridine (81 μL ,

1.0 mmol, 1.0 equiv.). After completion of the reaction, solvent was evaporated, and the residue was subjected to the column chromatography. Product **II-76** was purified by 5% EtOAc/Hex along with allyl ether (**II-155**).

Isolated weight: 162 mg, Yield: 47%

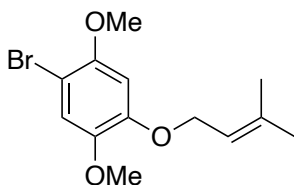
^1H NMR (500 MHz, CDCl_3) δ 7.17 (s, 1H), 6.76 (s, 1H), 6.14 (dd, $J = 17.5$ Hz, 10.9 Hz, 1H), 5.29 (dd, $J = 17.5$, 0.7 Hz, 1H), 5.18 (dd, $J = 10.9$, 0.7 Hz, 1H), 1.63 (s, 6H).

^{13}C NMR (126 MHz, CDCl_3) δ 153.06, 150.87, 149.94, 140.93, 140.79, 117.78, 114.20, 107.53, 83.92, 60.41, 56.85, 56, 75, 26.04.

FTIR (neat), cm^{-1} : 3089, 2970, 2935, 1757, 1501, 1384, 1206, 1113, 1023

TOF MS ES^+ ($\text{C}_{14}\text{H}_{18}\text{BrO}_5$) Calc. $[\text{M}+\text{H}]^+$: 345.0338, Found $[\text{M}+\text{H}]^+$

Melting point: 54 °C



III-6-9 1-Bromo-2,5-dimethoxy-4-((3-methylbut-2-en-1-yl)oxy)benzene (II-155)

Isolated weight: 29 mg, Yield: 24%

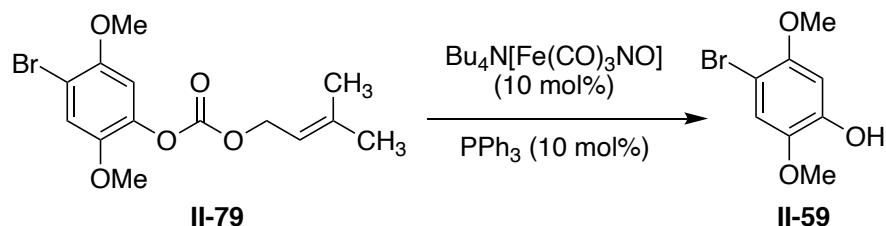
^1H NMR (500 MHz, CDCl_3) δ 7.03 (s, 1H), 6.58 (s, 1H), 5.49 (t, $J = 6.6$ Hz, 1H), 4.58 (d, $J = 6.8$ Hz, 2H), 3.84 (s, 3H), 3.81 (s, 3H), 1.78 (s, 3H), 1.74 (s, 3H).

^{13}C NMR (126 MHz, CDCl_3) δ 150.07, 148.23, 144.34, 138.16, 119.59, 116.58, 101.18, 100.78, 66.28, 57.10, 56.64, 25.86, 18.27.

FTIR (neat), cm^{-1} : 2915, 1506, 1440, 1206, 1168, 1005, 800.

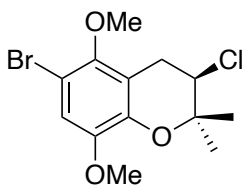
TOF MS ES^+ ($\text{C}_{13}\text{H}_{18}\text{BrO}_3$) Calc. $[\text{M}+\text{H}]^+$: 301.0439, Found $[\text{M}+\text{H}]^+$: 301.0412.

Melting point: 58 °C



III-6-10 Decarboxylative allylic etherification and tandem aromatic Claisen of **II-76** carbonate

A solution of triphenylphosphine (11.1 mg, 0.04 mmol, 10 mol%) and $\text{Bu}_4\text{N}[\text{Fe}(\text{CO})_3(\text{NO})]$ (17.4 mg, 0.04 mmol, 10 mol%) in dry toluene (2 mL) was stirred at 80 °C for 30 min in a sealed tube. The reaction was cooled down to room temperature, and carbonate **II-101** (138 mg, 0.4 mmol, 1 equiv.) was added to the mixture. The vial was heated at 110 °C until complete consumption of starting material. The solvent was removed under reduced pressure and the crude product was subjected to column chromatography. Phenol **II-78** was separated as the exclusive product.



III-6-11 6-Bromo-3-chloro-5,8-dimethoxy-2,2-dimethylchromane (**II-84**)

A solution of alkenyl phenol **II-69** (30.0 mg, 0.1 mmol, 1.0 equiv.) in TFE (3.2 mL) and acetonitrile (0.8 mL) was cooled to -78 °C. In a separate vessel, DCDMH (83.5 mg, 0.22 mmol, 2.2 equiv.), and $(\text{DHQD})_2\text{PYDZ}$ (7.3 mg, 0.01 mmol, 10 mol%) were dissolved in

the same amount of TFE and acetonitrile and cooled to -78 °C as well. After cooling both solutions for 5 min, the latter solution was added to the solution of the starting material. The completion of the reaction was followed using thin layer chromatography and quenched by the addition of a saturated Na₂S₂O₃ aqueous solution. The organic layer was extracted with DCM, and the aqueous layer was washed with DCM several times. Organic layers were combined and dried over sodium sulfate, filtered, and concentrated under reduced pressure. The desired product was purified using column chromatography (5% EtOAc/Hex).

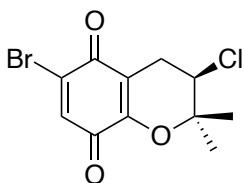
Yield: 81% (Yield was determined by NMR using triphenylmethane as standard).

¹H NMR (500 MHz, CDCl₃) δ 6.90 (s, 1H), 4.11 (dd, *J* = 8.4, 5.5 Hz, 1H), 3.82 (s, 3H), 3.80 (s, 3H), 3.32 (dd, *J* = 17.5, 5.6 Hz, 1H), 3.02 (dd, *J* = 17.5, 8.4 Hz, 1H), 1.56 (s, 3H), 1.54 (s, 3H).

¹³C NMR (126 MHz, CDCl₃) δ 148.20, 145.91, 142.05, 115.53, 113.77, 105.86, 77.18, 60.47, 59.22, 56.39, 29.12, 26.12, 20.90.

FTIR (neat), cm⁻¹: 2924, 1476, 1440, 1099, 1216, 1057.

TOF MS ES⁺ (C₁₃H₁₆BrClO₃) Calc. [M+H]⁺: 335.0050, Found [M+H]⁺: 335.0064.



III-6-12 (*R*)-6-Bromo-3-chloro-2,2-dimethyl-3,4-dihydro-2*H*-chromene-5,8-dione (II-85)

A solution of benzo-pyran **II-84** (1.0 g, 2.8 mmol, 1.0 equiv.) in acetonitrile (44.0 mL) was cooled to 0 °C followed by dropwise addition of an aqueous solution of CAN (16.4 g, 29.9 mmol, 10 equiv.) in water (5.5 mL). The desired compound was extracted using dichloromethane after allowing the reaction to stir at 0 °C for 0.5 h. The water layer was washed several times with dichloromethane. Combined organic layers were dried over Na₂SO₄, filtered, and concentrated under reduced pressure. The pure product was obtained via column chromatography (20% EtOAc/Hex).

Isolated weight: 641.6 mg, Yield: 75%.

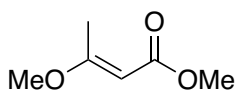
¹H NMR (500 MHz, CDCl₃) δ 7.21 (s, 1H), 4.06 (dd, J = 6.5, 5.3 Hz, 1H), 3.04 (dd, J = 18.9, 5.3 Hz, 1H), 2.84 (dd, J = 18.9, 6.4 Hz, 1H), 1.51 (s, 6H).

¹³C NMR (126 MHz, CDCl₃) δ 178.64, 178.30, 151.73, 138.47, 135.62, 115.12, 80.73, 57.36, 27.67, 25.41, 22.53.

Resolution of enantiomers: DAICEL Chiralcel AD-H, 10% *i*-PrOH/Hexanes, 1.0 mL/min, 290 nm, RT₁ = 8.6 min, RT₂ = 10.1 min. *er* (after recrystallization) = 93:7

FTIR (neat), cm⁻¹: 2924, 1633, 1588, 1178, 1132.

TOF MS ES⁺ (C₁₁H₁₁BrClO₃) Calc. [M+H]⁺: 304.9580, Found [M+H]⁺: 304.9578.



III-6-13 Methyl (*E*)-3-methoxybut-2-enoate (II-156)

A round bottom flask was charged with methyl acetoacetate (18.6 mL, 172.3 mmol, 1 equiv.) and trimethyl orthoformate (19.2 mL, 175.5 mmol, 1.0 equiv.) and concentrated H₂SO₄ (6 drops). The resulting mixture was stirred at room temperature for 24 h—distillation under reduced pressure afforded the desired product.

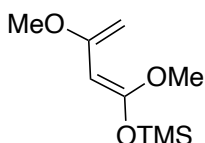
Isolated weight: 21 g, Yield: 93%

¹H NMR (500 MHz, CDCl₃) δ 5.03 (s, 1H), 3.66 (s, 3H), 3.61 (s, 3H), 2.28 (s, 3H).

¹³C NMR (126 MHz, CDCl₃) δ 173.39, 168.44, 90.59, 55.52, 50.87, 19.01.

FTIR (neat), cm⁻¹: 3012, 2979, 1711, 1620, 1274, 1135, 1049, 813.

TOF MS EI⁺ (C₆H₁₀O₃) Calc. [M]⁺: 130.0630, Found [M]⁺: 130.0635



III-6-14 (*E*)-((1,3-Dimethoxybuta-1,3-dien-1-yl)oxy)trimethylsilane (II-98)

To a solution of *i*-Pr₂NH (3.2 mL, 23 mmol, 1.2 equiv.) in THF (13.0 mL) at -78 °C was added *n*-BuLi (2.5 M in hexanes, 9.2 mL, 23.1 mmol, 1.2 equiv.) and the resulting mixture was stirred at this temperature for 15 min. To this solution was added enol ether **II-156** (2.5 g, 19.2 mmol, 1.0 equiv.). The resulting mixture was stirred for an additional hour followed by addition of TMSCl (3.0 mL, 23.5 mmol, 1.2 equiv.) to the reaction. The solution was warmed up to room temperature and kept at ambient temperature for 1 h. The solvent was removed, and the residue was dissolved in hexane resulting in the precipitation of

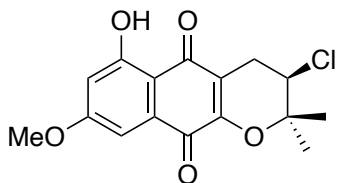
impurities. The precipitate was filtered and washed with hexane several times. Removal of the organic solvent under reduced pressure resulted in the pure product, and the desired diene was used in the next step without further purification.

^1H NMR (500 MHz, CDCl_3) δ 4.34 (d, $J = 1.9$ Hz, 1H), 4.03 (d, $J = 1.5$ Hz, 1H), 3.98 (t, $J = 1.7$ Hz, 1H), 3.57 (s, 3H), 3.56 (s, 3H), 0.26 (s, 9H).

^{13}C NMR (126 MHz, CDCl_3) δ 158.9, 158.89, 78.78, 75.70, 55.19, 54.26, 0.52.

FTIR (neat), cm^{-1} : 2954, 1658, 1254, 1095, 840.

TOF MS EI^+ ($\text{C}_9\text{H}_{18}\text{O}_3\text{Si}$) Calc. $[\text{M-TMS}]^+$: 129.0551, Found $[\text{M-TMS}]^+$: 129.0551.



III-6-15 (*R*)-3-Chloro-6-hydroxy-8-methoxy-2,2-dimethyl-3,4-dihydro-2benzo[*g*]chromene-5,10-dione (II-99)

To a solution of naphthoquinone **II-85** (2.9 g, 9.5 mmol, 1.0 equiv.) in dichloromethane (95.0 mL) cooled to -30 °C was added dropwise a solution of diene **II-98** (5.6 g, 28.6 mmol, 3.0 equiv.) in dichloromethane (38.0 mL). The reaction was gradually warmed up to room temperature over 25 min and was stirred at this temperature for 45 min. Afterward, a large excess of silica gel (10.0 g) was added, and the resulting mixture was stirred for another hour. The mixture was filtered and washed several times with dichloromethane. The filtrate was concentrated, and the resulting residue was recrystallized from chloroform.

Isolated weight: 236 mg, Yield: 73%.

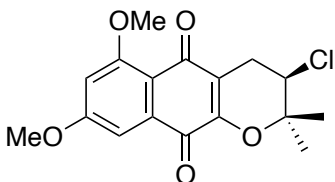
^1H NMR (500 MHz, CDCl_3) δ 12.38 (s, 1H), 7.20 (d, $J = 2.5$ Hz, 1H), 6.63 (d, $J = 2.5$ Hz, 1H), 4.10 (dd, $J = 6.8, 5.3$ Hz, 1H), 3.90 (s, 3H), 3.11 (dd, $J = 19.0, 5.4$ Hz, 1H), 2.88 (dd, $J = 19.0, 6.8$ Hz, 1H), 1.55 (s, 3H), 1.53 (s, 3H).

^{13}C NMR (126 MHz, CDCl_3): δ 187.89, 178.47, 165.28, 163.66, 153.56, 132.45, 117.52, 108.39, 108.13, 106.68, 80.39, 57.69, 56.02, 26.95, 25.58, 22.29.

FTIR (neat), cm^{-1} : 2926, 1629, 1612, 1283.

TOF MS ES^+ ($\text{C}_{16}\text{H}_{16}\text{ClO}_5$) Calc. $[\text{M}+\text{H}]^+$: 323.0686, Found $[\text{M}+\text{H}]^+$: 323.0686.

Melting Point: 183 °C



III-6-16 (*R*)-3-Chloro-6,8-dimethoxy-2,2-dimethyl-3,4-dihydro-2*H*-benzo[*g*]chromene-5,10-dione (II-100)

A flame-dried round bottom flask was charged with phenol **II-99** (712.0 mg, 2.2 mmol, 1 equiv.) and anhydrous DMF (40.0 mL). Methyl iodide (1.4 mL, 22.5 mmol, 10 equiv.) and K_2CO_3 (610 mg, 4.4 mmol, 2 equiv.) were added to this solution, and the resulting mixture was stirred at 85 °C for 24 h. The addition of water quenched the reaction, and the product was extracted using diethyl ether. The aqueous layer was washed with diethyl ether several times. Organic layers were combined, dried over Na_2SO_4 , filtered, concentrated, and the product was purified by column chromatography (20% EtOAc/Hex).

Isolated weight: 607 mg, Yield: 82%.

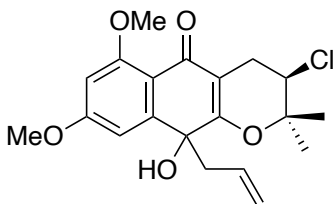
^1H NMR (500 MHz, CDCl_3) δ 7.27 (d, $J = 2.4$ Hz, 1H), 6.72 (d, $J = 2.5$ Hz, 1H), 4.06 (dd, $J = 7.1, 5.4$ Hz, 1H), 3.95 (s, 3H), 3.94 (s, 3H), 3.10 (dd, $J = 19.2, 5.4$ Hz, 1H), 2.84 (dd, $J = 19.2, 7.1$ Hz, 1H), 1.52 (s, 3H), 1.48 (s, 3H).

^{13}C NMR (126 MHz, CDCl_3) δ 182.35, 179.42, 164.15, 161.50, 151.26, 134.93, 119.63, 113.63, 104.53, 103.53, 79.57, 58.31, 56.43, 55.97, 27.67, 25.56, 21.94.

FTIR (neat), cm^{-1} : 2924, 1631, 1596, 994, 795.

TOF MS ES^+ ($\text{C}_{17}\text{H}_{18}\text{ClO}_5$) Calc. $[\text{M}+\text{H}]^+$: 337.0843, Found $[\text{M}+\text{H}]^+$: 337.0838.

Melting point: 218 °C

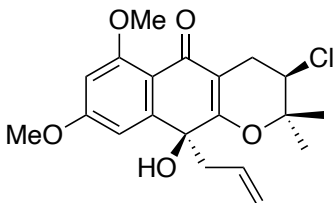


III-6-17 (3*R*)-10-Allyl-3-chloro-10-hydroxy-6,8-dimethoxy-2,2-dimethyl-2,3,4,10-tetrahydro 5*H*-benzo[*g*]chromen-5-one (II-119/126)

Preparing allyl indium solution: To a suspension of indium powder (206 mg, 1.8 mmol, 2.0 equiv.) in DMF (0.9 mL) at room temperature was added allyl iodide (0.5 mL, 5.3 mmol, 6.0 equiv.), resulting in an exothermic reaction. The mixture was stirred at room temperature until the complete consumption of Indium powder that resulted in a clear solution of the allylic indium sesquiodide.

A solution of benzoquinone **II-100** (300 mg, 0.9 mmol, 1.0 equiv.) in DMF (3.6 mL) was added to the prepared solution of allyl indium at -40 °C, and the resulting solution

was stirred for 5 h. Water was added to quench the reaction, and the product was extracted with ether. The water layer was washed with ether three more times, and the combined organic layers were combined, dried, filtered, and removed at low pressure. The pure product was isolated by column chromatography (50% EtOAc/Hex).
Isolated weight: 265 mg, Combined yield: 70% (1.5:1 *dr*, undesired diastereomer was separated as the major product. The structure of the diastereomers were assigned via 2D-NOESY NMR).



II-126

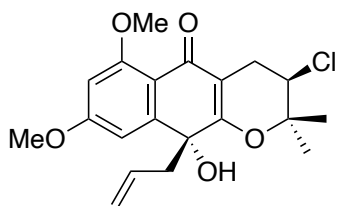
^1H NMR (500 MHz, CD_3CN) δ 6.78 (d, $J = 2.4$ Hz, 1H), 6.45 (d, $J = 2.4$ Hz, 1H), 5.19 (ddt, $J = 17.1, 10.3, 7.3$ Hz, 1H), 4.82 (m, 2H), 4.03 (dd, $J = 9.3, 5.6$ Hz, 1H), 3.92 (s, 1H), 3.89 (s, 3H), 2.99 (dd, $J = 17.5, 5.5$ Hz, 1H), 2.89 (dd, $J = 13.2, 7.7$, 1H), 2.70 (dd, $J = 13.0, 7.0$, 1H), 2.62 (dd, $J = 17.5, 7.1$ Hz, 1H), 1.48 (s, 3H), 1.44 (s, 3H).

^{13}C NMR (126 MHz, CDCl_3) δ 182.46, 163.49, 162.18, 161.28, 147.82, 131.05, 119.71, 113.25, 108.55, 102.00, 98.52, 79.30, 71.91, 59.17, 56.05, 55.54, 49.40, 26.82, 25.29, 23.41.

FTIR (neat), cm^{-1} : 2961, 1631, 1596, 934, 795.

TOF MS ES^+ ($\text{C}_{20}\text{H}_{24}\text{ClO}_5$) Calc. $[\text{M}+\text{H}]^+$: 379.1312, Found $[\text{M}+\text{H}]^+$: 379.1329.

Melting point: 67 °C



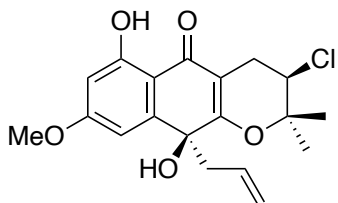
II-119

^1H NMR (500 MHz, CD_3CN) δ 6.87 (d, $J = 2.4$ Hz, 1H), 6.55 (d, $J = 2.4$ Hz, 1H), 5.36 (dddd, $J = 17.3, 10.3, 7.7, 6.9$ Hz, 1H), 4.83 (m, 2H), 4.31 (t, $J = 5.0$ Hz, 1H), 3.98 (s, 1H), 3.84 (s, 3H), 2.88 (dd, $J = 13.0, 7.0$ Hz, 1H), 2.80 (d, $J = 5.0$ Hz, 3H), 2.63 (ddt, $J = 13.0, 6.8$ Hz, 1H), 1.50 (s, 3H), 1.42 (s, 3H).

^{13}C NMR (126 MHz, CDCl_3) δ 182.45, 163.43, 162.41, 161.19, 148.05, 131.08, 119.54, 113.19, 108.54, 102.14, 98.39, 79.19, 71.82, 59.18, 55.98, 55.49, 49.09, 26.81, 25.30, 23.22.

FTIR (neat), cm^{-1} : 2958, 163, 1594, 931, 791.

TOF MS ES^+ ($\text{C}_{20}\text{H}_{24}\text{ClO}_5$) Calc. $[\text{M}+\text{H}]^+$: 379.1312, Found $[\text{M}+\text{H}]^+$: 379.1320.



III-6-18 (3*R*,10*R*)-10-Allyl-3-chloro-6,10-dihydroxy-8-methoxy-2,2-dimethyl-2,3,4,10-tetrahydro-5*H*-benzo[*g*]chromen-5-one (II-133)

Freshly prepared MgI₂ [generated by adding solid magnesium (48 mg, 1.9 mmol, 2.0 equiv.) to a solution of I₂ (254 mg, 1.0 mmol, 1.0 equiv.) in anhydrous ether (5.0 mL) at 25 °C and stirring until colorless (~ 2 h)] was added to a solution of **II-126** (379.0 mg, 1.0 mmol, 1.0 equiv.) in THF (1.3 mL) at room temperature and the mixture was stirred for 4 h. The reaction was quenched by addition of saturated aqueous NH₄Cl, poured into water and extracted with ethyl acetate. The organic layer was washed with Na₂SO₃ solution, water, brine, dried over Na₂SO₄, concentrated under reduced pressure to afford the crude mixture of the product. The pure product was obtained by column chromatography (20% to 30% EtOAc/Hex).

Isolated weight: 363 mg, Yield: 95%.

¹H NMR (500 MHz, CDCl₃) δ 12.94 (d, *J* = 1.1 Hz, 1H), 6.73 (d, *J* = 2.4 Hz, 1H), 6.36 (d, *J* = 2.5 Hz, 1H), 5.2 (dddd, *J* = 16.3, 10.3, 8.6, 6.0 Hz, 1H), 4.91 (m, 2H), 3.96 (dd, *J* = 8.3, 5.4 Hz, 1H), 3.84 (s, 3H), 3.03 (dd, *J* = 17.3, 5.3 Hz, 1H), 2.79 (dd, *J* = 12.9, 8.6 Hz, 1H), 2.64 (m, 2H), 1.53 (s, 3H), 1.44 (s, 3H).

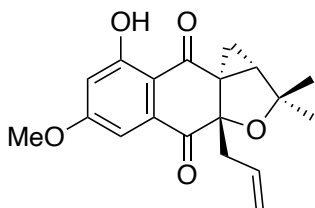
¹³C NMR (126 MHz, CDCl₃) δ 187.46, 166.00, 164.96, 163.59, 145.56, 131.01, 119.46, 107.94, 107.31, 104.83, 100.45, 80.62, 71.95, 58.69, 55.55, 49.12, 26.27, 26.20, 22.65.

TOF MS ES⁺ (C₁₉H₂₂ClO₅) Calc. [M+H]⁺: 365.1156, Found [M+H]⁺: 365.1142.

Melting point: 154 °C

FTIR (neat), cm⁻¹: 3358, 3085, 2937, 1627, 1594.

III-6-19 (10-Allyl-3-chloro-6,10-dihydroxy-8-methoxy-2,2-dimethyl-2,3,4,10-tetrahydro-5*H*-benzo[*g*]chromen-5-one (II-135)



III-6-20 3a-Allyl-8-hydroxy-6-methoxy-2,2-dimethyl-1a,2-dihydro-1*H*,9*H*-cyclopropa[*c*]naph -tho[2,3-*b*]furan-4,9(3a*H*)-dione (II-135)

Solution of the diastereomer of **II-133** (73 mg, 0.2 mmol, 1 equiv.) in EtOH (2.6 mL) and aqueous NaOH (2N, 5.2 mL) was heated at 180 °C in a sealed tube for 15 min. The mixture was removed from the oil bath and allowed to cool down to room temperature. The reaction mixture was poured into ice-water, acidified with dilute HCl, and extracted with CHCl₃. The organic layer was washed with H₂O, dried, filtered, concentrated, and the residue was subjected to column chromatography (10% EtOAc/Hex).

Note: The yield of the product depends on the reaction time. The reaction mixture should be removed from the oil bath after completion of the reaction. Keeping the reaction at high temperature for more extended time leads to the decomposition of the product and reducing the yield of the reaction.

Isolated weight: 65 mg, Yield: 82%.

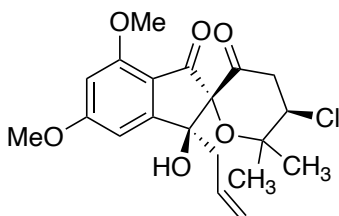
¹H NMR (500 MHz, CDCl₃) δ 12.64 (s, 1H), 7.16 (d, *J* = 2.4 Hz, 1H), 6.69 (d, *J* = 2.4 Hz, 1H), 5.53 (dddd, *J* = 17.1, 10.1, 8.0, 7.0 Hz, 1H), 4.96 (m, 2H), 3.91 (s, 3H), 2.58 (dd, *J* =

13.6, 7.0 Hz, 1H), 2.41 (dd, $J = 13.6, 8.1$ Hz, 1H), 2.12 (m, 2H), 1.35 – 1.28 (m, 4H), 1.18 (s, 3H).

^{13}C NMR (126 MHz, CDCl_3) δ 198.04, 196.67, 166.25, 164.03, 136.08, 131.02, 119.67, 112.80, 107.02, 105.97, 86.75, 81.97, 56.02, 45.44, 41.82, 41.74, 28.71, 24.70, 13.06.

FTIR (neat), cm^{-1} : 3083, 3016, 2983, 1625, 1600, 1431, 1376, 1285.

TOF MS ES^+ ($\text{C}_{19}\text{H}_{21}\text{O}_5$) Calc. $[\text{M}+\text{H}]^+$: 329.1389, Found $[\text{M}+\text{H}]^+$: 329.1426



III-6-21 1-Allyl-5'-chloro-1-hydroxy-4,6-dimethoxy-6',6'-dimethyl-5',6'-dihydrospiro[indene-2,2'-pyran]-3,3'(1H,4'H)-dione (II-141)

To a solution of enone **II-126** (88.5 mg, 0.24 mmol, 1 equiv.) in methanol (4.5 mL) and hydrogen peroxide (30% in H_2O , 0.23 mL, 8.3 equiv.) at 0 °C was added a solution of sodium hydroxide (10% in H_2O , 96.5 μL). The reaction was gradually warmed up to room temperature. After 2 days, the reaction was quenched by addition of saturated NaHCO_3 . The product was extracted using ethyl acetate. Organic layer was dried with Na_2SO_4 , filtered, concentrated under reduced pressure. The crude mixture was subjected to column chromatography and afford the pure product **II-141** (50% EtOAc/Hex).

Note: For running the column, triethylamine was added to the eluent (2 drops Et_3N per 10 mL of eluent solution).

Isolated weight: 49 mg, Yield: 52%.

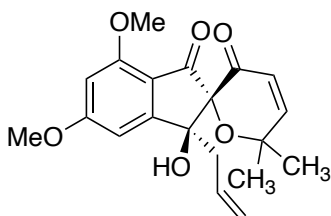
^1H NMR (500 MHz, CDCl_3) δ 6.66 (d, $J = 1.9$ Hz, 1H), 6.33 (d, $J = 1.9$ Hz, 1H), 5.70 (dddd, $J = 17.1, 10.2, 7.8, 6.9$ Hz, 1H), 5.02 (m, 2H), 4.25 (dd, $J = 10.8, 6.6$ Hz, 1H), 3.90 (s, 3H), 3.89 (s, 3H), 3.03 (dd, $J = 18.5, 6.6$ Hz, 1H), 2.82 (m, 1H), 2.62 (dd, $J = 13.8, 7.8$, 1H), 2.46 (dd, $J = 13.7, 7.2$ Hz, 1H), 1.57 (s, 3H), 1.56 (s, 3H).

^{13}C NMR (126 MHz, CDCl_3) δ 205.05, 189.76, 168.17, 160.11, 159.21, 132.20, 119.23, 114.55, 99.29, 98.98, 98.38, 81.17, 77.18, 57.15, 56.06, 55.97, 43.87, 43.80, 27.48, 20.37.

FTIR (neat), cm^{-1} : 3541, 2919, 1693, 1601, 1581, 1144, 798.

TOF MS ES^+ ($\text{C}_{20}\text{H}_{24}\text{ClO}_6$) Calc. $[\text{M}+\text{H}]^+$: 395.1261, Found $[\text{M}+\text{H}]^+$: 395.1287.

Melting Point: 134 °C



III-6-22 1-Allyl-1-hydroxy-4,6-dimethoxy-6',6'-dimethylspiro[indene-2,2'-pyran]-3,3'(1H,6'H)-dione (II-142)

II-142 was prepared from the corresponding alcohol according to the procedure described above. However, during the purification no triethylamine was used.

Yield is not reported because the yield was different from one reaction to another. (50 - 20%)

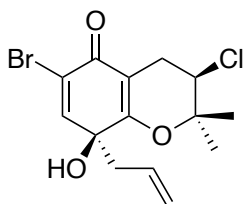
^1H NMR (500 MHz, CDCl_3) δ 7.04 (d, $J = 10.5$ Hz, 1H), 6.68 (d, $J = 1.9$ Hz, 1H), 6.34 (d, $J = 1.9$ Hz, 1H), 6.00 (d, $J = 10.6$, 1H), 5.64 (ddt, $J = 17.4, 10.1, 7.3$ Hz, 1H), 4.89 (m, 2H), 3.93 (s, 3H), 3.87 (s, 3H), 2.60 (m, 2H), 1.80 (s, 3H), 1.56 (s, 3H).

^{13}C NMR (126 MHz, CDCl_3) δ 205.05, 189.76, 168.17, 160.11, 159.21, 132.20, 119.23, 114.55, 99.29, 98.98, 98.38, 81.17, 77.18, 57.15, 56.06, 55.97, 43.87, 43.80, 27.48, 20.37.

FTIR (neat), cm^{-1} : 3468, 2919, 1709, 1667, 1585, 1156, 804.

TOF MS ES^+ ($\text{C}_{20}\text{H}_{23}\text{O}_6$) Calc. $[\text{M}+\text{H}]^+$: 359.1495, Found $[\text{M}+\text{H}]^+$: 359.1511.

Melting point: 154 $^\circ\text{C}$



III-6-23 8-Allyl-6-bromo-3-chloro-8-hydroxy-2,2-dimethyl-2,3,4,8-tetrahydro-5H-chromen-5-one (II-151)

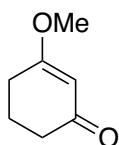
II-153 was prepared from the corresponding quinone (**II-85**, 364.5 mg, 1.2 mmol) according to the procedure described for the synthesis of **II-119/126**.

Isolated weight: 174 mg, Yield: 42%.

^1H NMR (500 MHz, CDCl_3) δ 7.09 (s, 1H), 5.54 (ddt, $J = 18.4, 9.1, 7.4$ Hz, 1H), 5.12 (m, 2H), 3.96 (dd, $J = 7.7, 5.3$ Hz, 1H), 2.95 (dd, $J = 17.6, 5.4$ Hz, 1H), 2.64 (dd, $J = 14.7, 7.6$ Hz, 3H), 1.49 (s, 3H), 1.44 (s, 3H).

^{13}C NMR (126 MHz, CDCl_3) δ 178.15, 165.64, 145.26, 130.11, 124.30, 120.56, 107.21, 80.43, 72.16, 58.40, 43.85, 27.01, 26.00, 21.64.

TOF MS ES^+ ($\text{C}_{14}\text{H}_{17}\text{BrClO}_3$) Calc. $[\text{M}+\text{H}]^+$: 347.0050, Found $[\text{M}+\text{H}]^+$: 347.0022



III-6-24 3-Methoxycyclohex-2-en-1-one (II-160)

TiCl_4 solution in dichloromethane (50 μL , 1.0 M, 0.05, 10 mol%) was added to a solution of the 1,3-cyclohexanedione (0.5 mL, 5.0 mmol, 1.0 equiv.) in methanol (10.0 mL) at room temperature. After 10 min, trimethylamine (83 μL , 0.6 mmol) was added to the resulting solution, which was stirred for an additional 45 min before the addition of water. The reaction mixture was extracted with ethyl acetate several times and the combined organic layers were dried over Na_2SO_4 , filtered, and evaporated under reduced pressure. Product was purified using column chromatography (5% EtOAc/Hex).

Isolated weight: 587 mg, Yield: 93%.

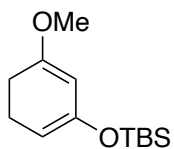
^1H NMR (500 MHz, CDCl_3) δ 5.36 (s, 1H), 3.68 (s, 3H), 2.33 (t, J = 6.3 Hz, 2H), 2.26 (t, J = 6.3, 2H), 1.90 (p, J = 6.4 Hz, 2H).

^{13}C NMR (126 MHz, CDCl_3) δ 199.83, 178.85, 102.19, 55.57, 36.62, 28.75, 21.14.

FTIR (neat), cm^{-1} : 3014, 2944, 1643, 1594, 1375, 1224, 1175, 1133.

TOF MS EI^+ ($\text{C}_7\text{H}_{11}\text{O}_2$) Calc. $[\text{M}]^+$: 127.0759, Found $[\text{M}]^+$: 127.0717.

Melting point: 35 $^\circ\text{C}$

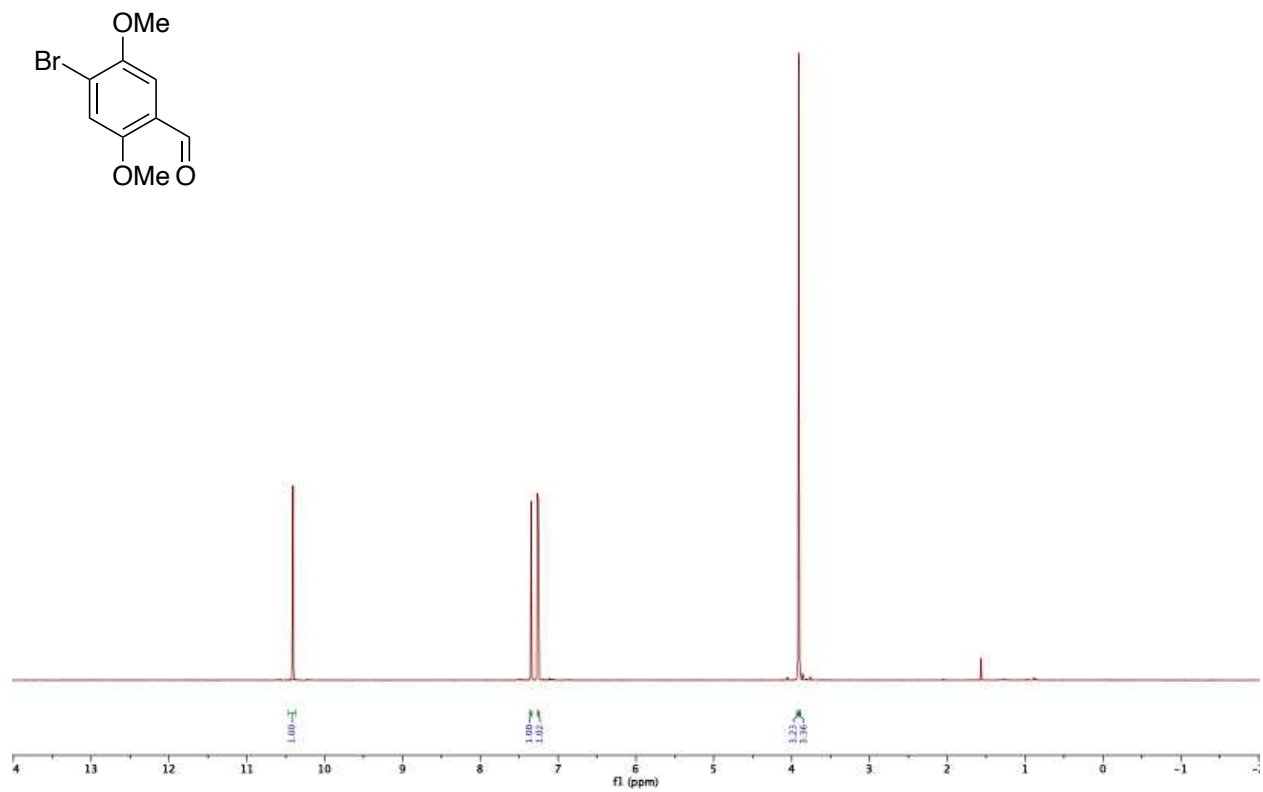


III-6-25 Tert-butyl((5-methoxycyclohexa-1,5-dien-1-yl)oxy)dimethylsilane (II-161)

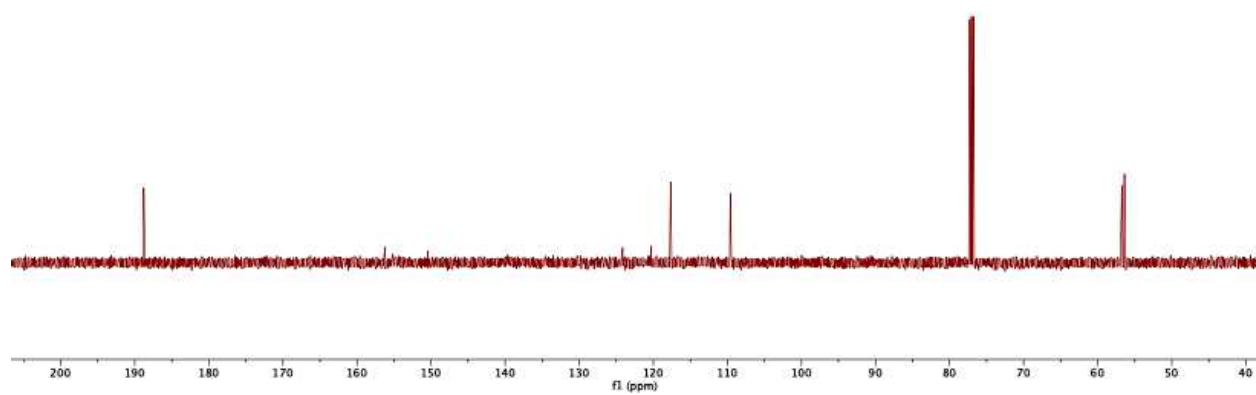
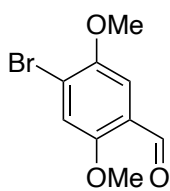
To NaHMDS (2.7 mL, 2.7 mmol, 1.0 equiv., 1.0 M in THF) at -78 °C was added a solution of enol ether **II-154** in THF (1.4 mL) over 30 min. TBSCl (428 mg, 2.8 mmol, 1.05 equiv.) in THF (1.4 mL) was added to the mixture. After stirring at -78 °C for 30 min, the solution was allowed to warm to room temperature over 1 h. The solvent was evaporated, and the crude diene was used in next step without purification.

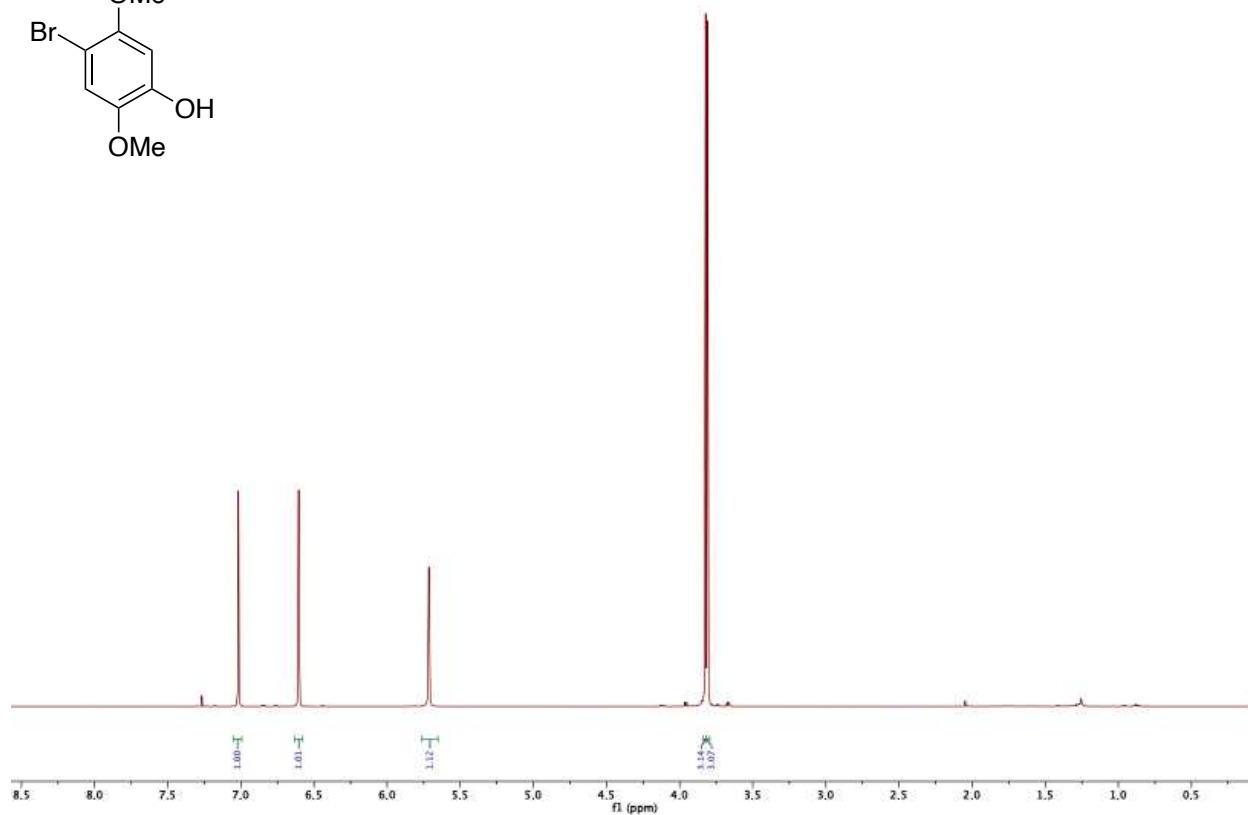
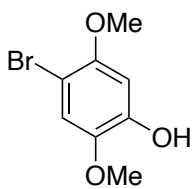
III-7 NMR spectra

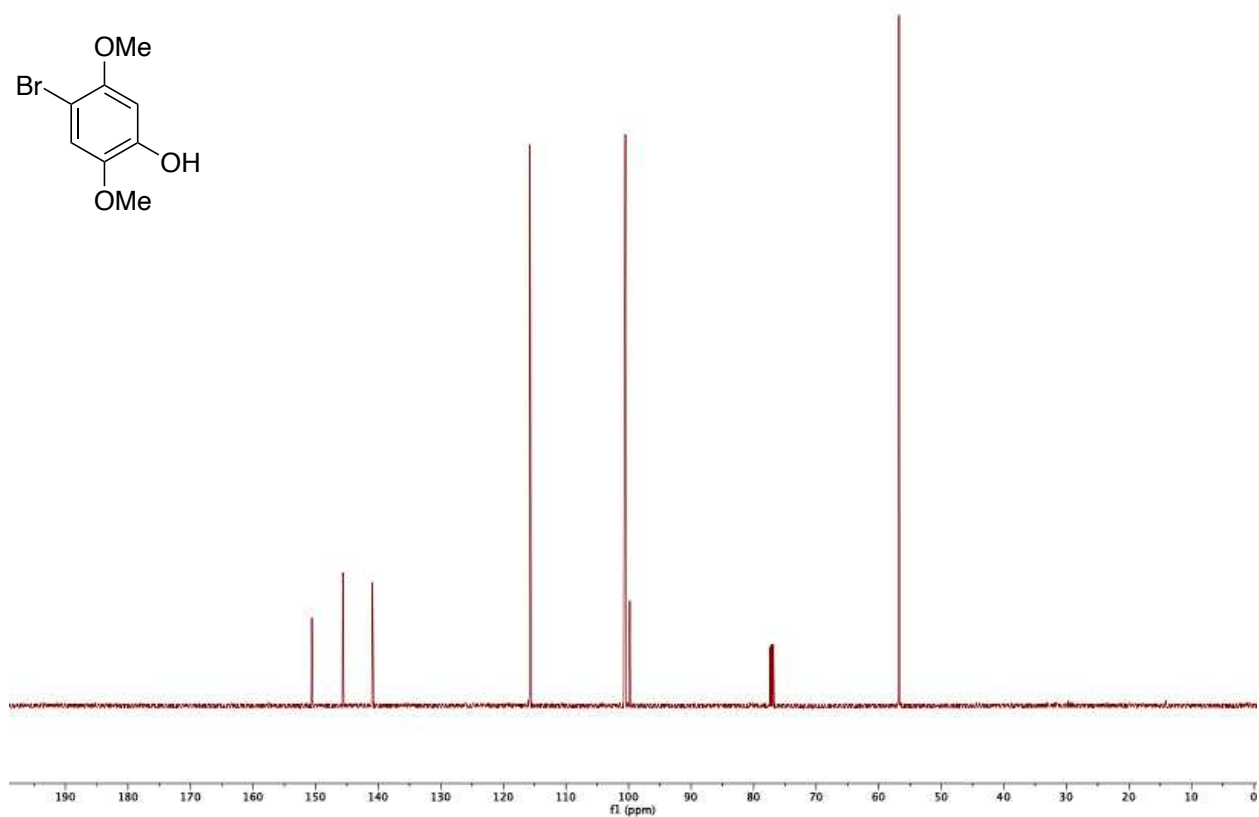
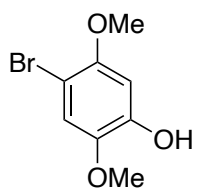
GV-01-11-P2_PROTON_01

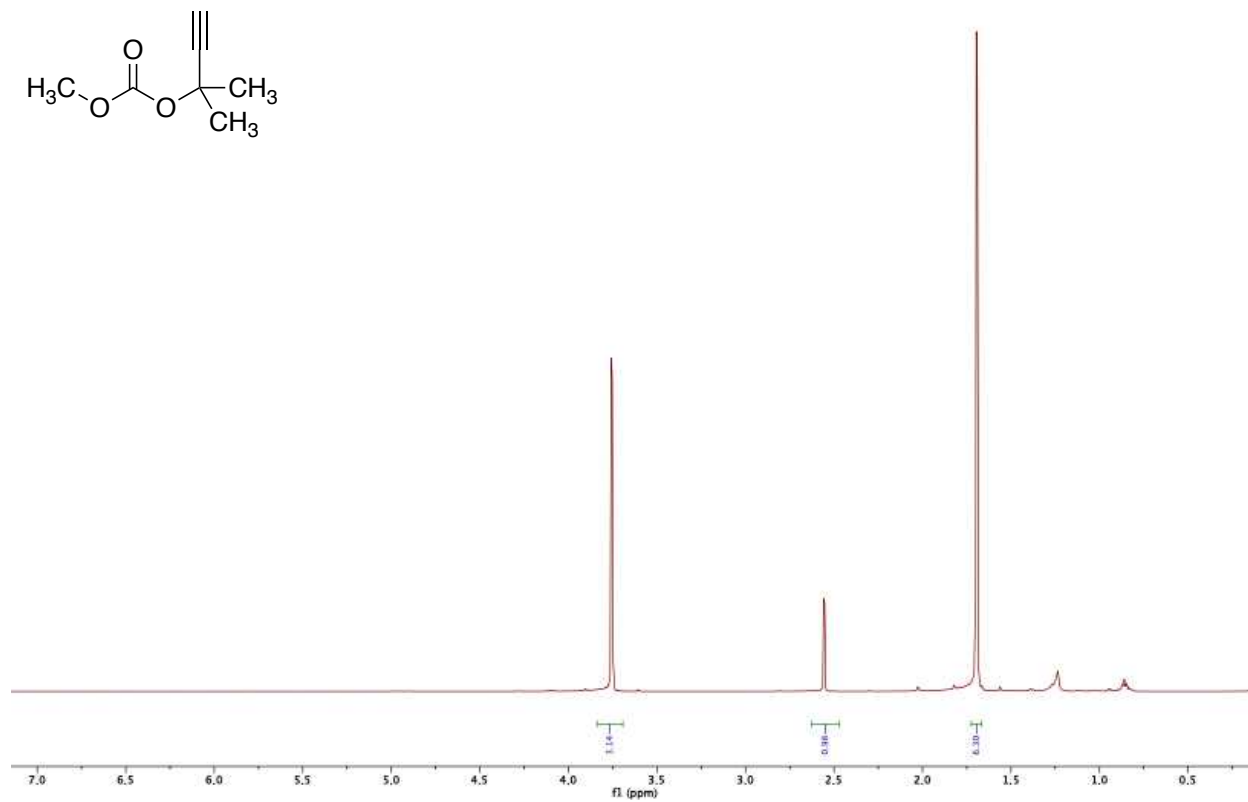


CV-01-11-P2C_CARBON_01

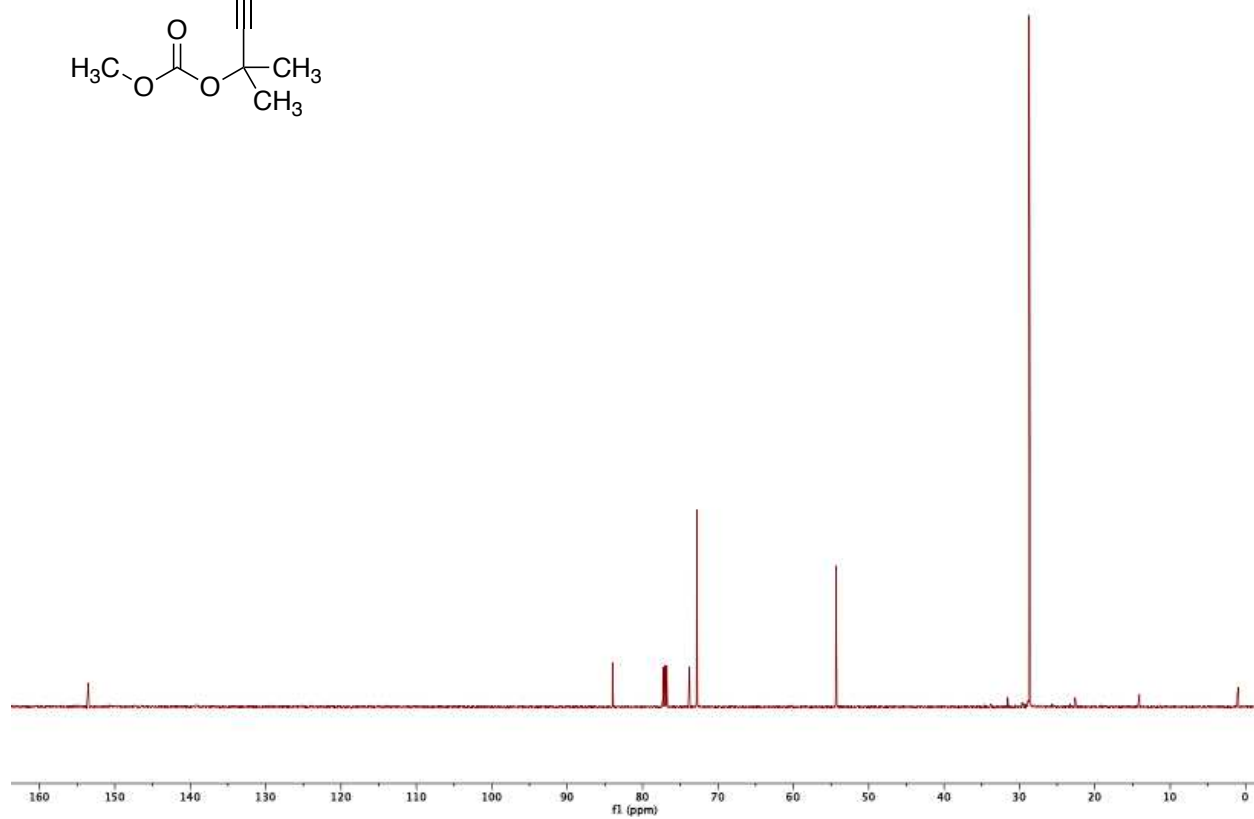
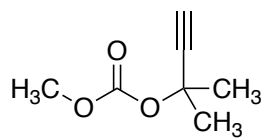


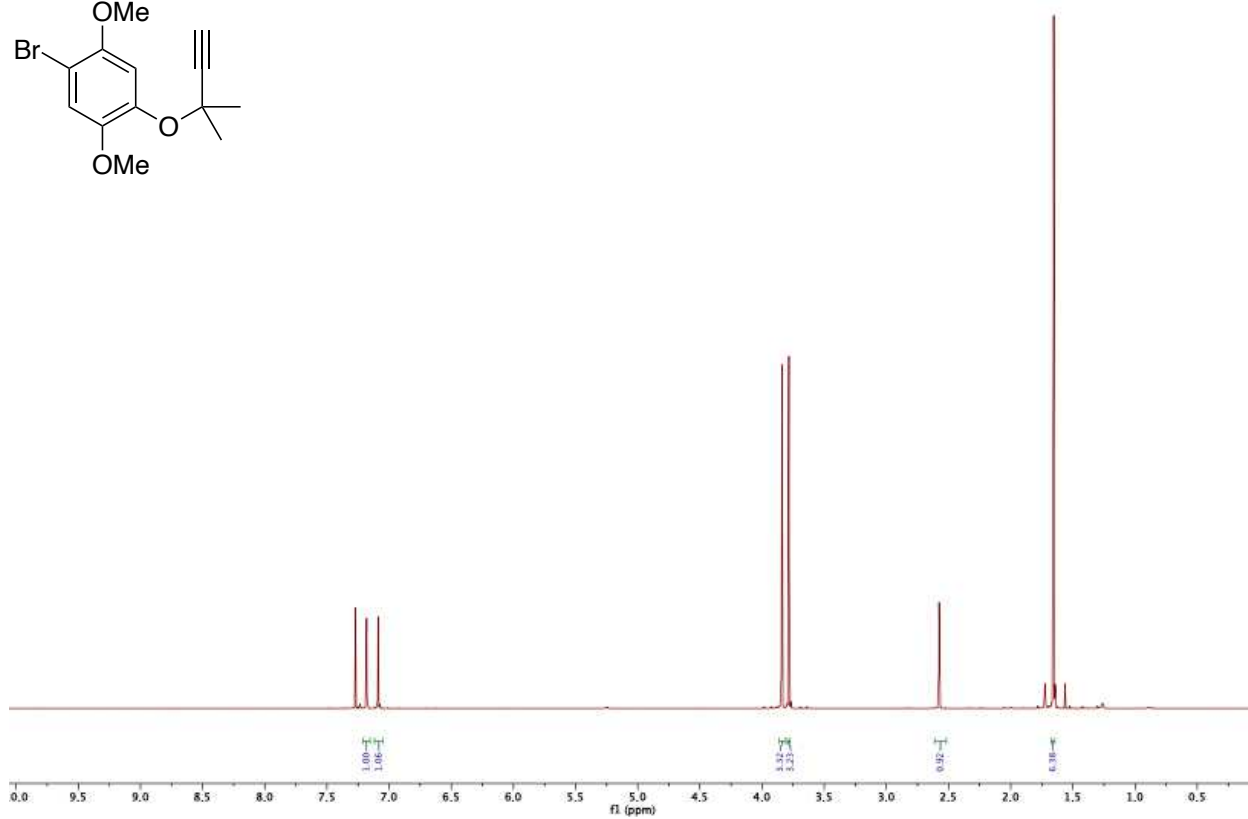
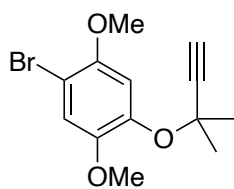




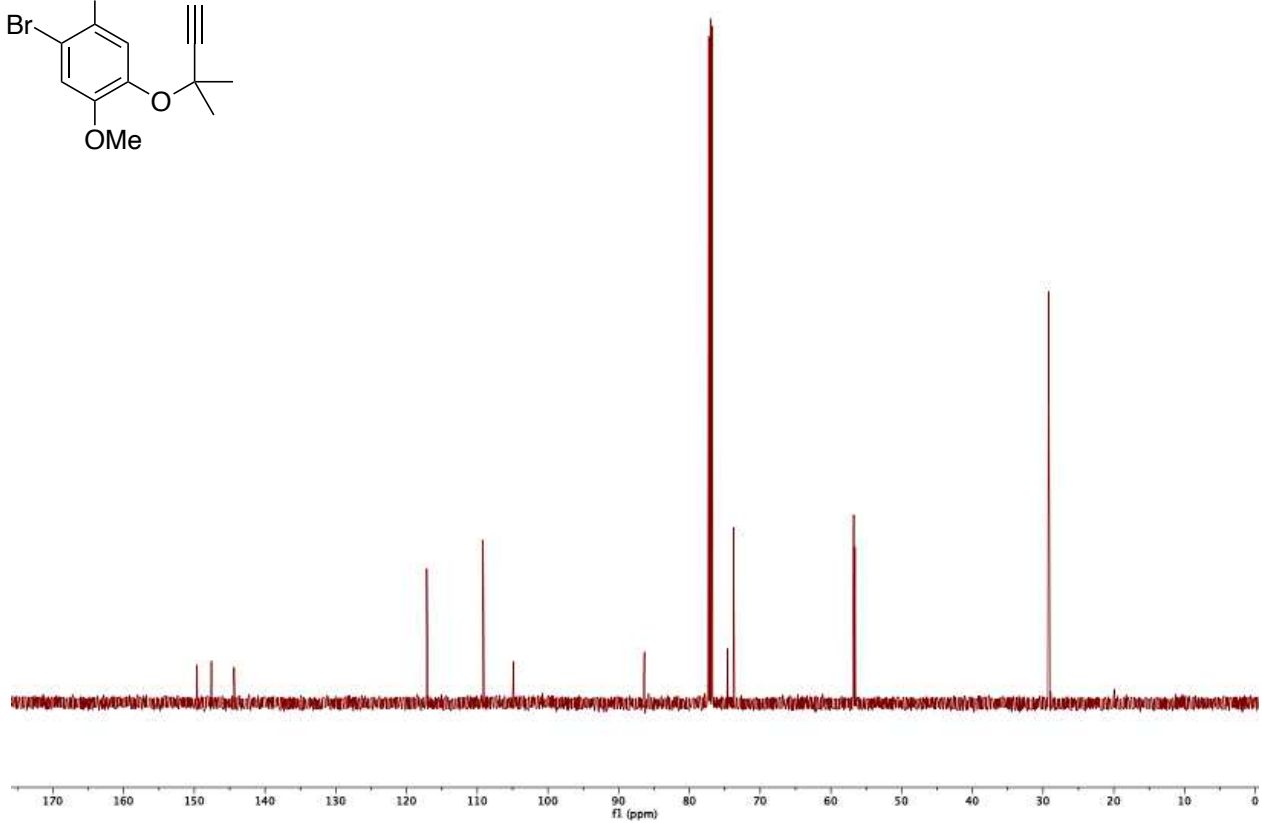
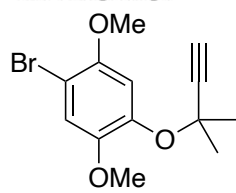


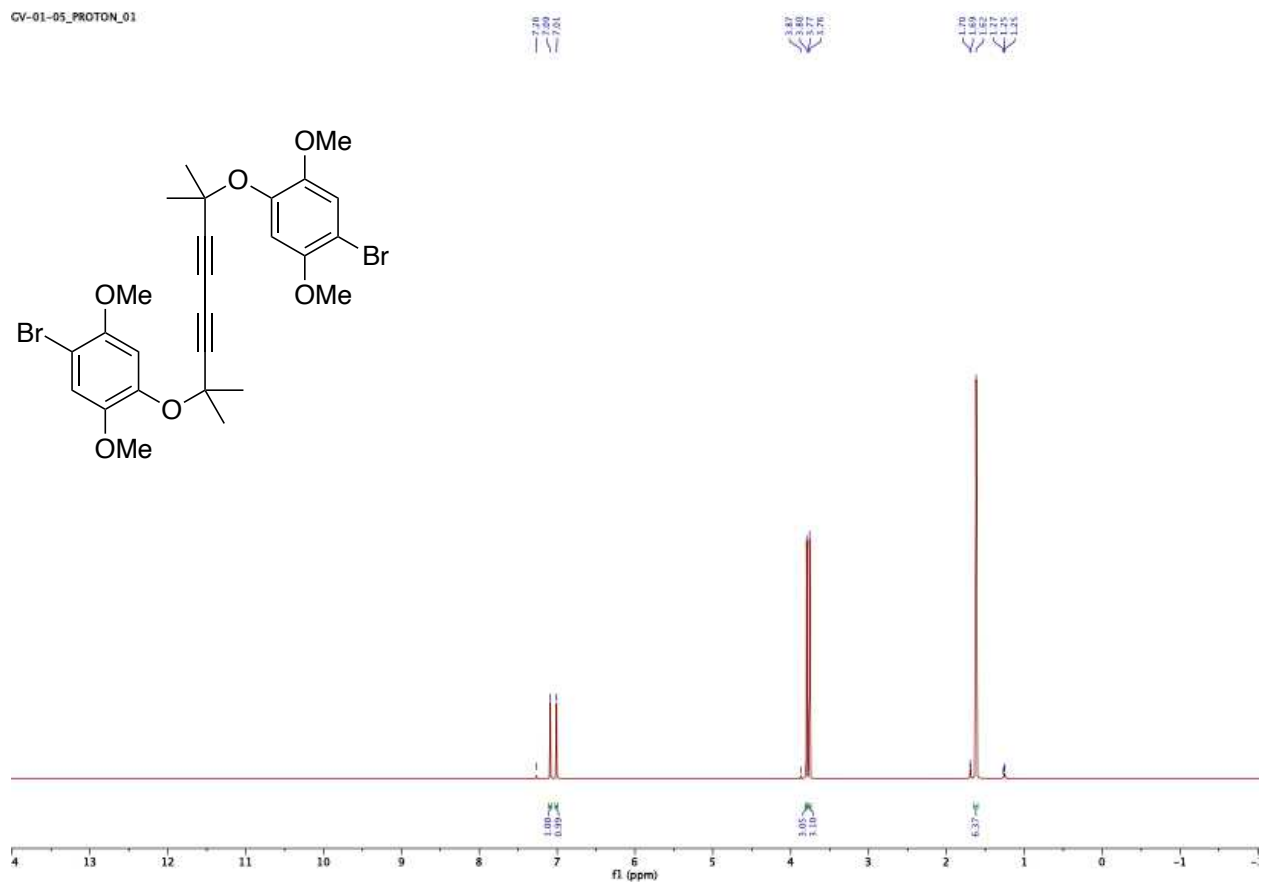
ST-03-86-Pure_CARBON_01

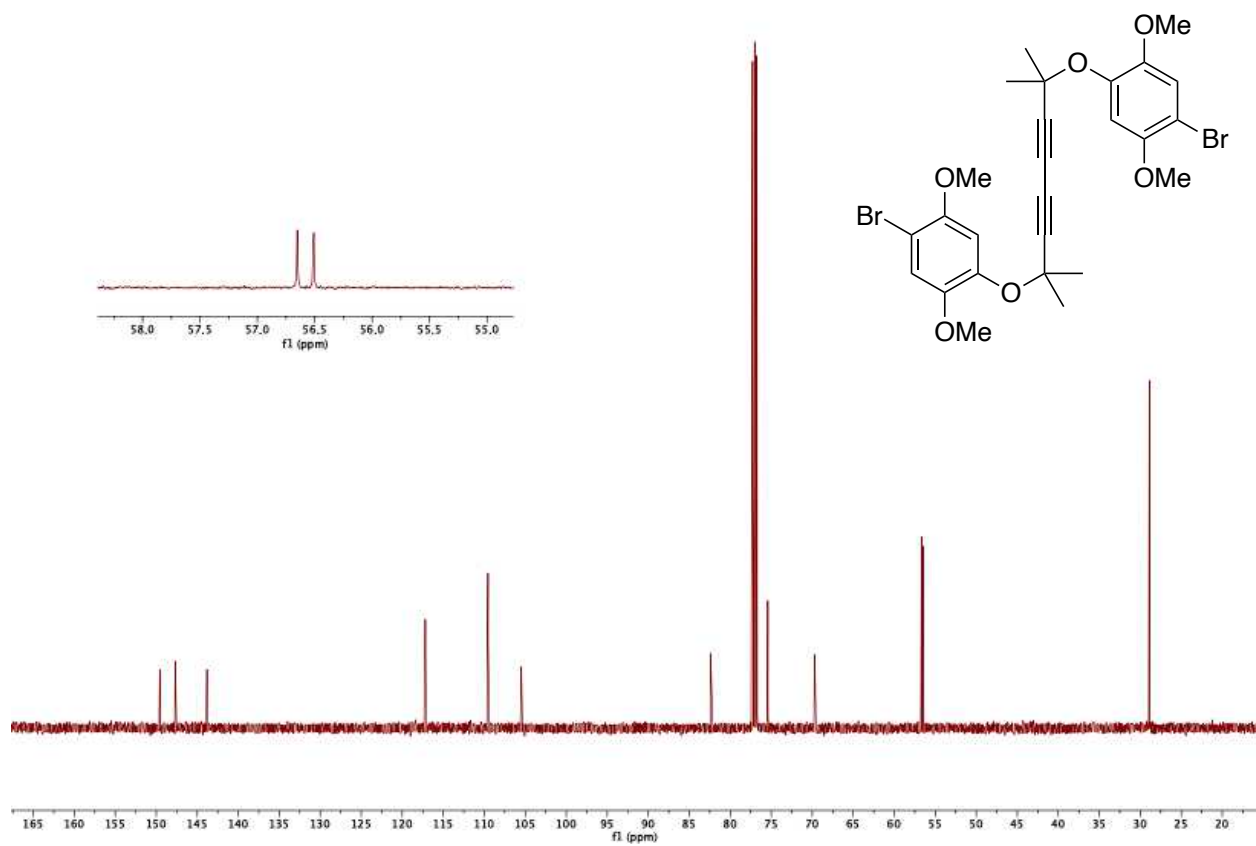




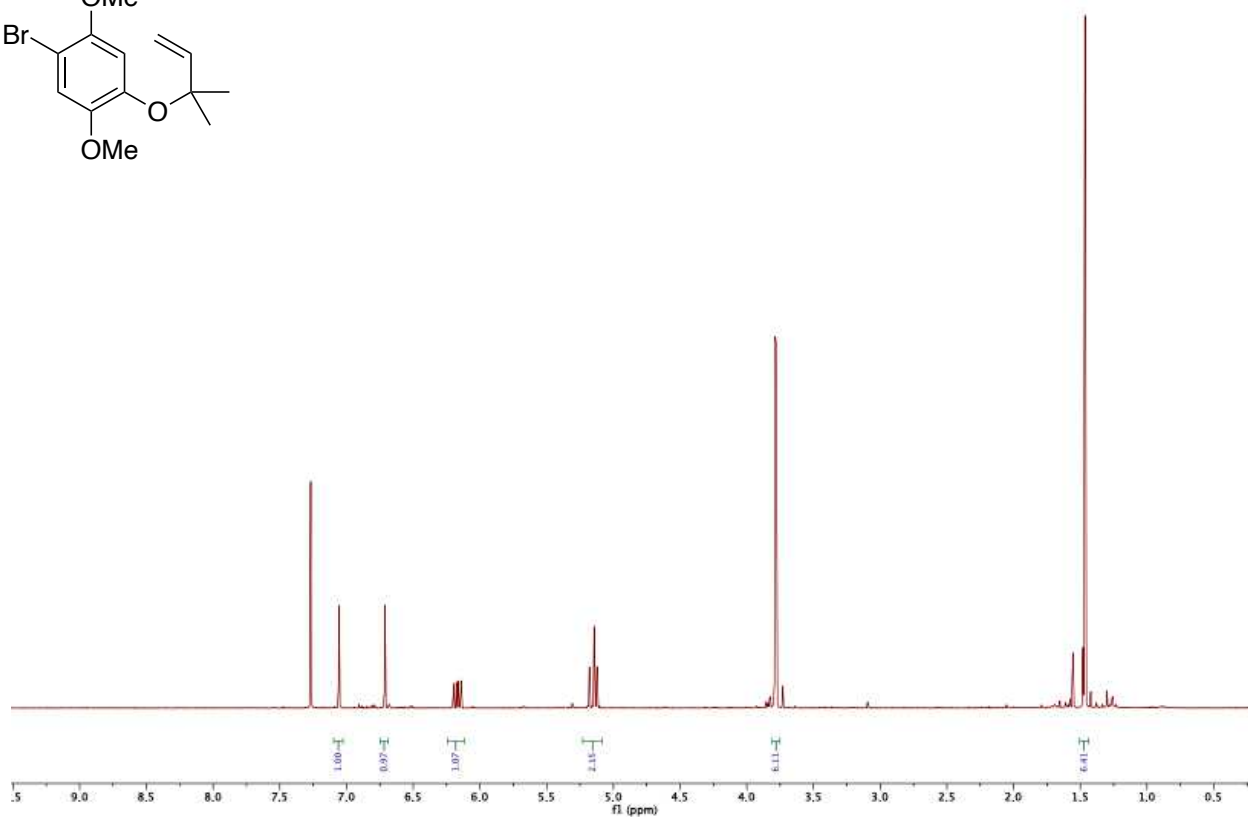
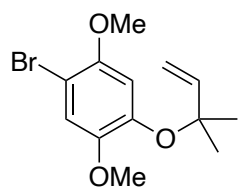
CV-01-10-Pure_CARBON_01



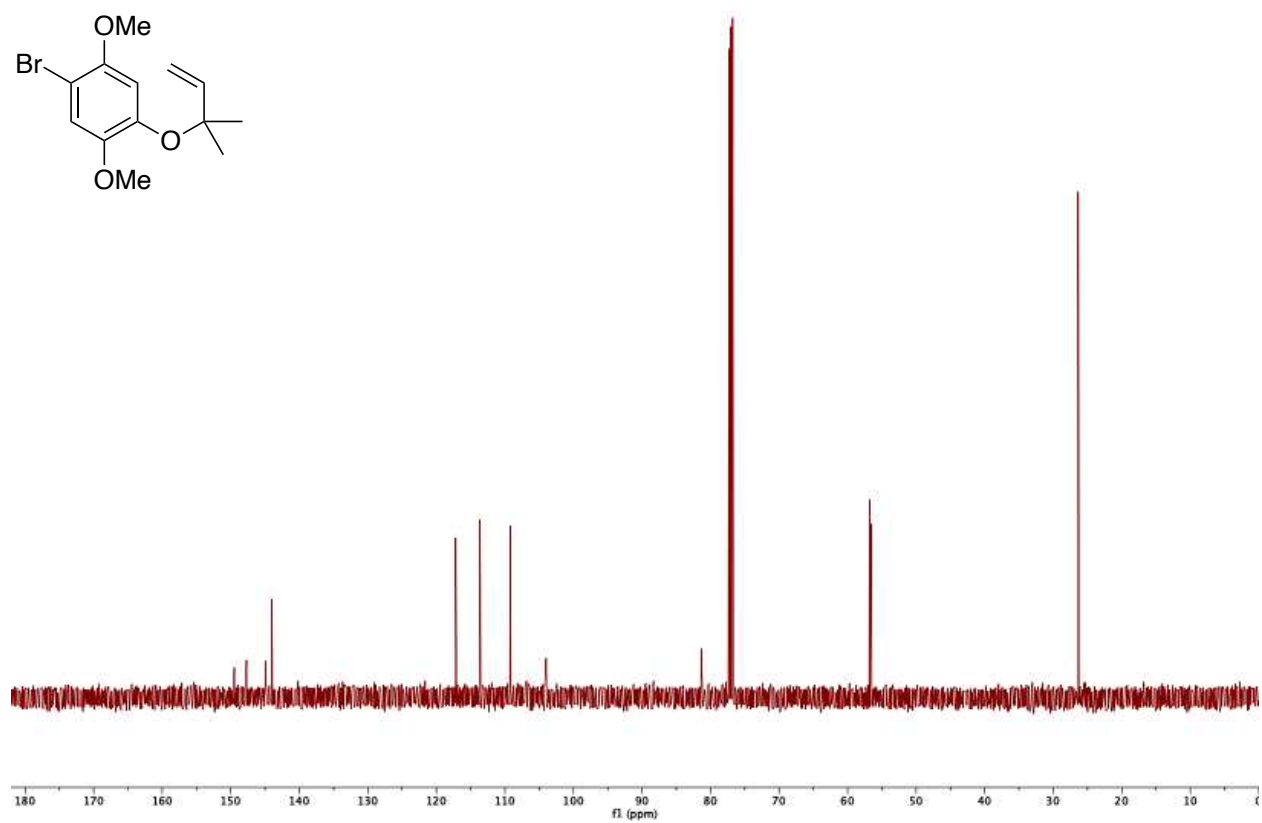
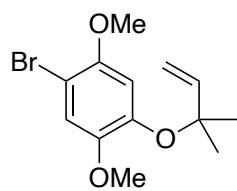




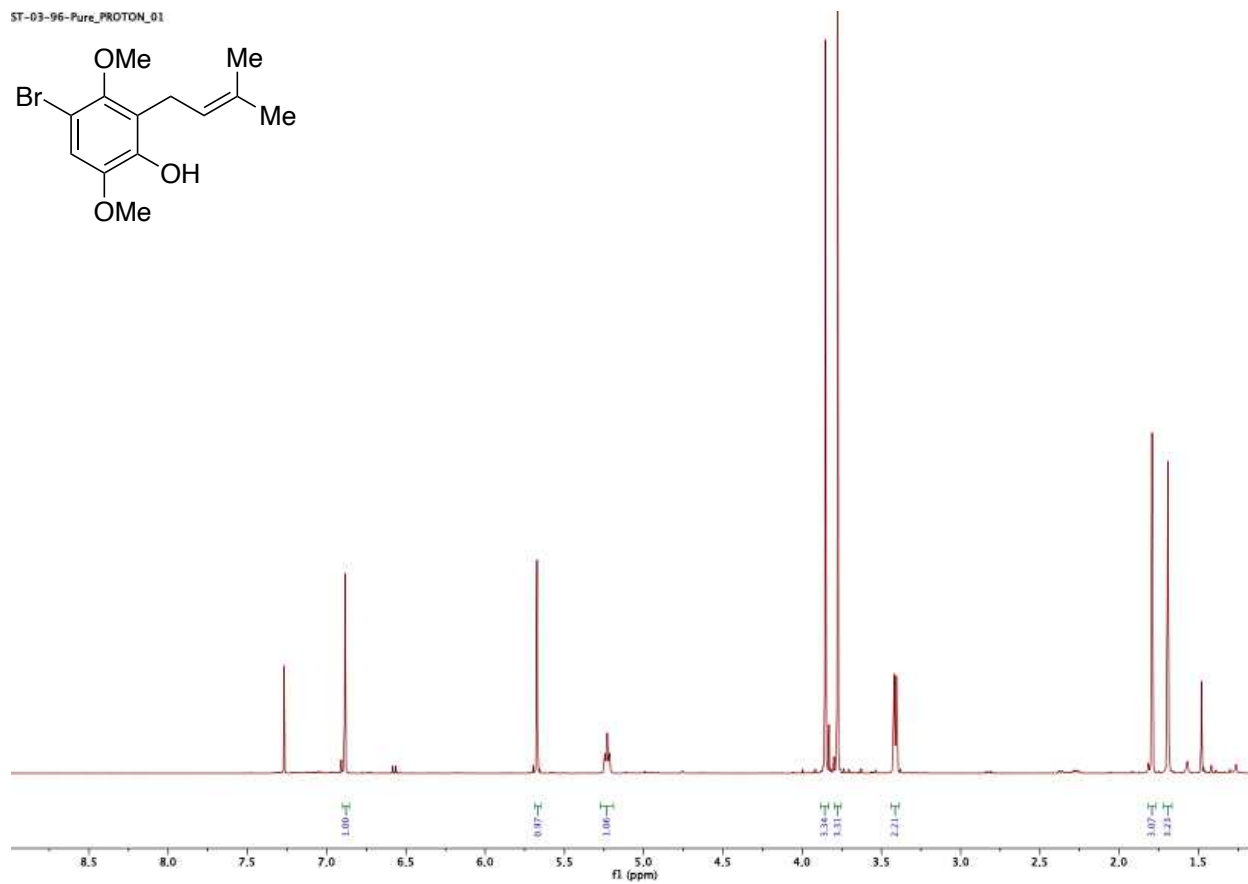
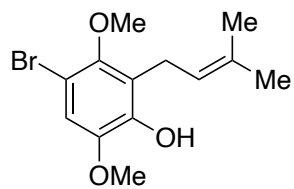
ST-03-95_PROTON_01



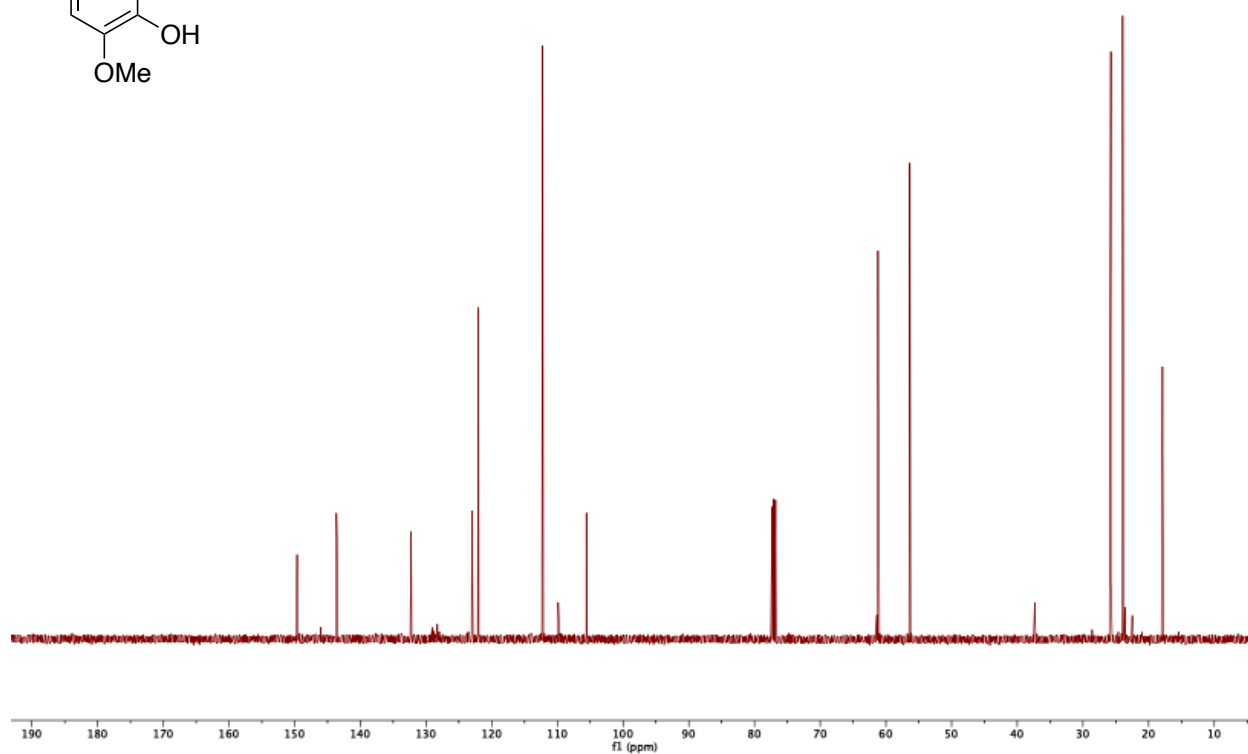
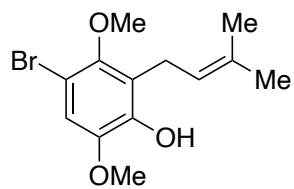
ST-03-95-Pure_CARBON_01



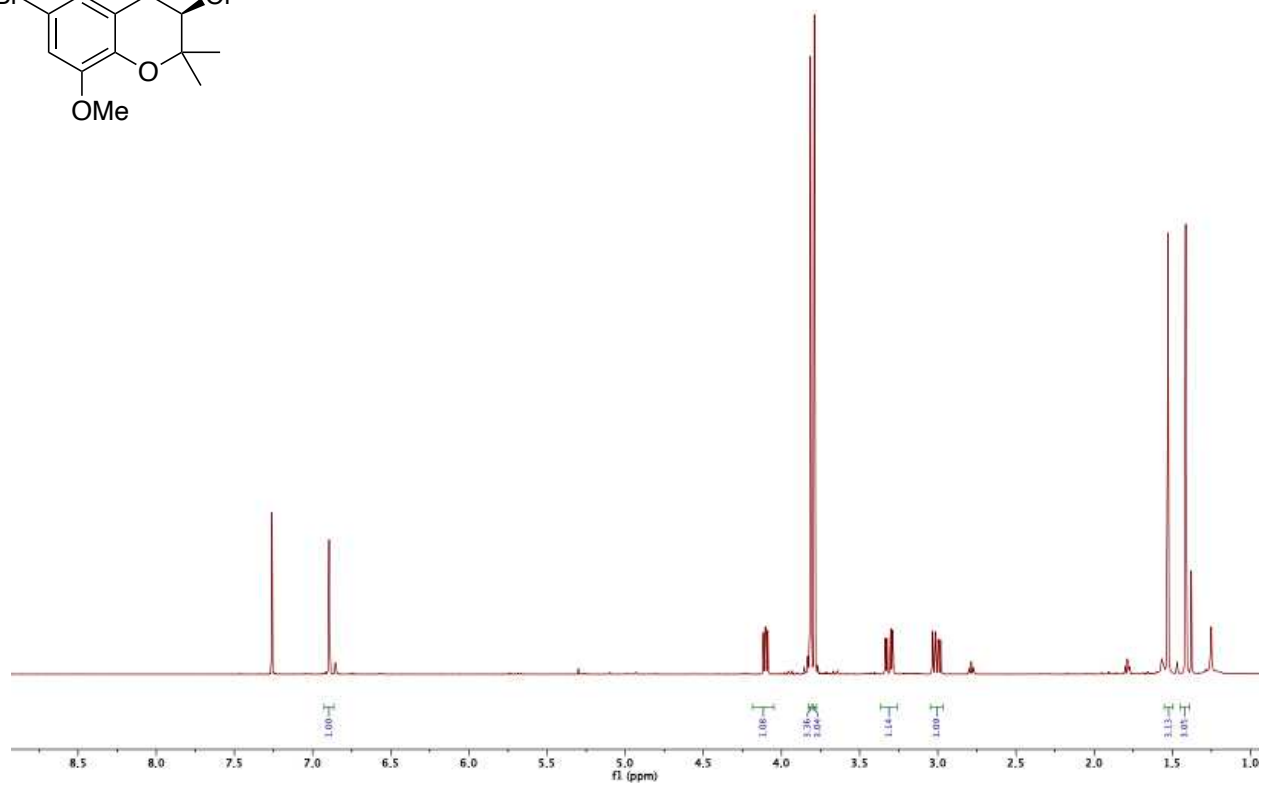
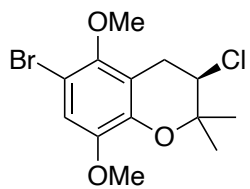
ST-03-96-Pure_PROTON_01



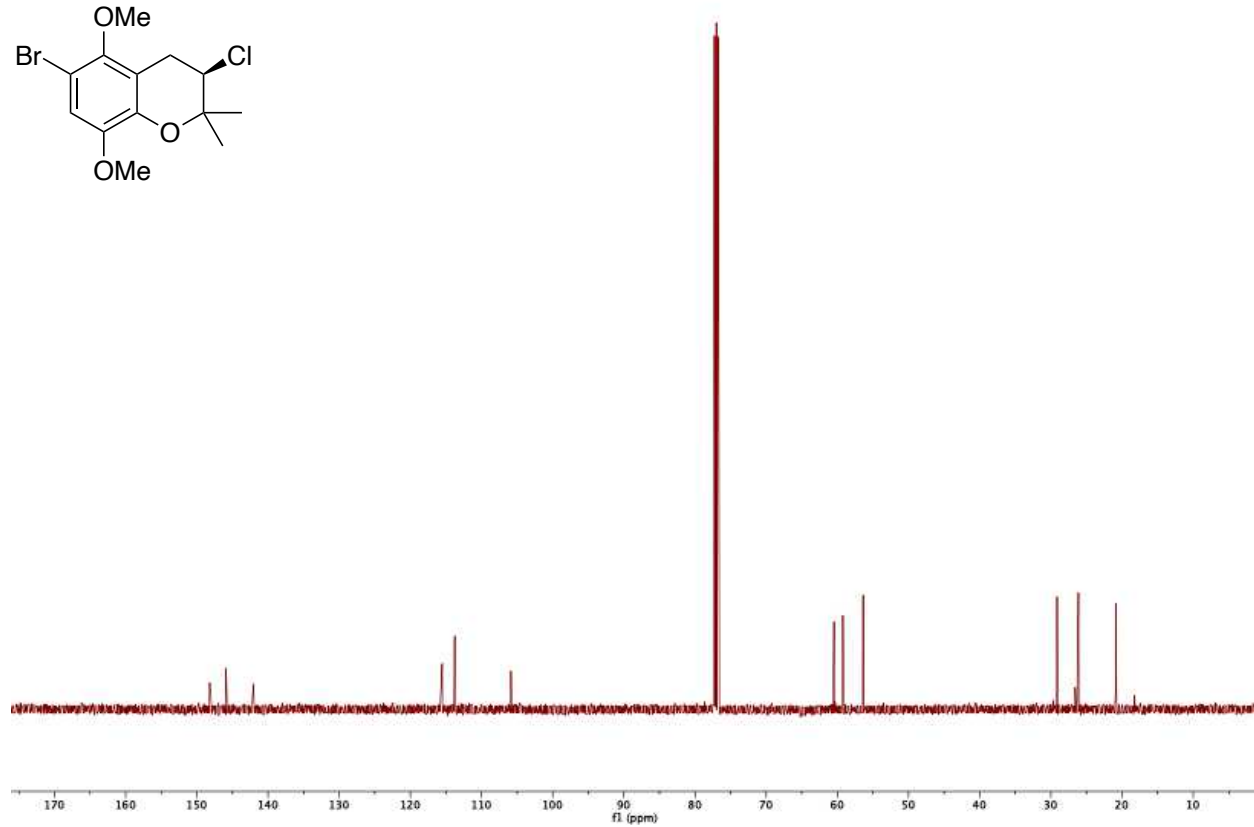
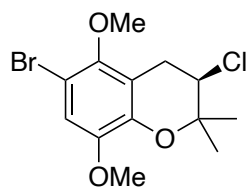
ST-03-96-Decomposed_CARBON_01



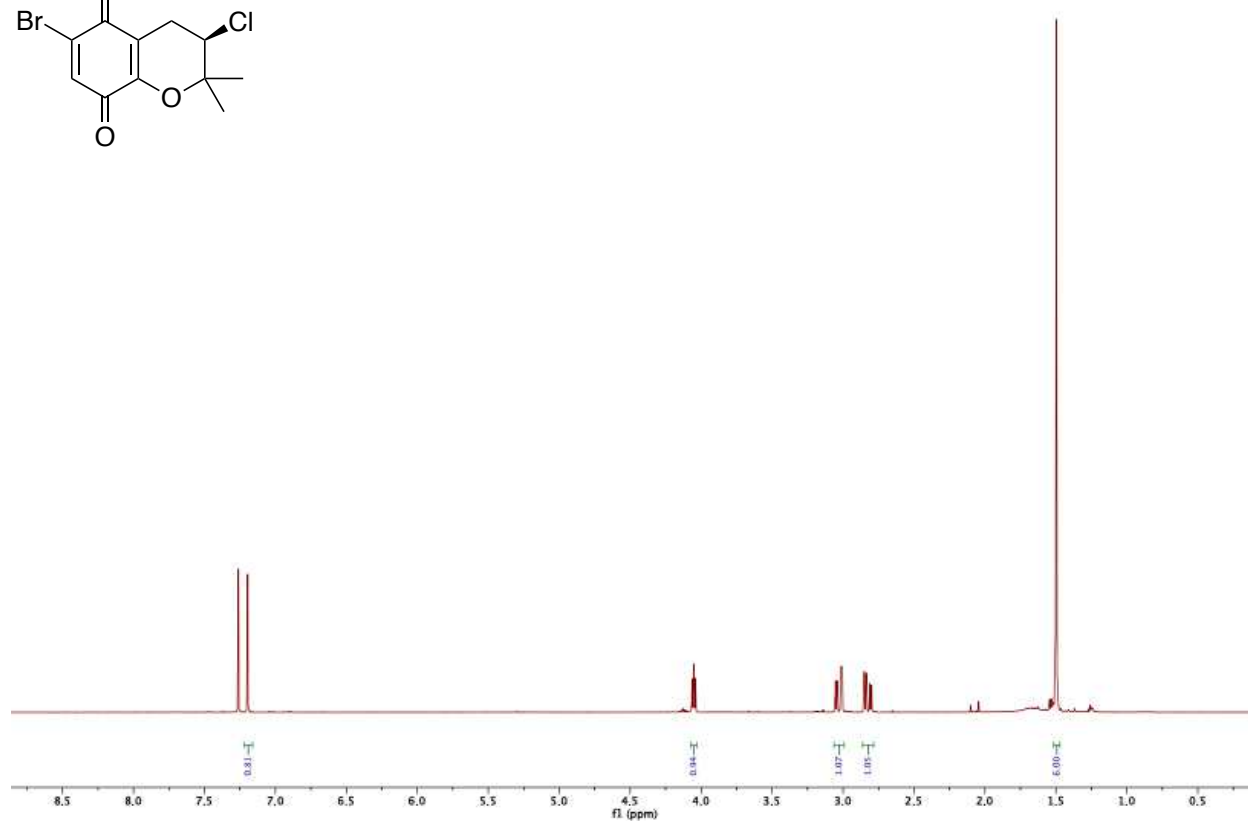
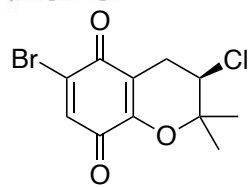
ST-05-12-Pure_PROTON_01



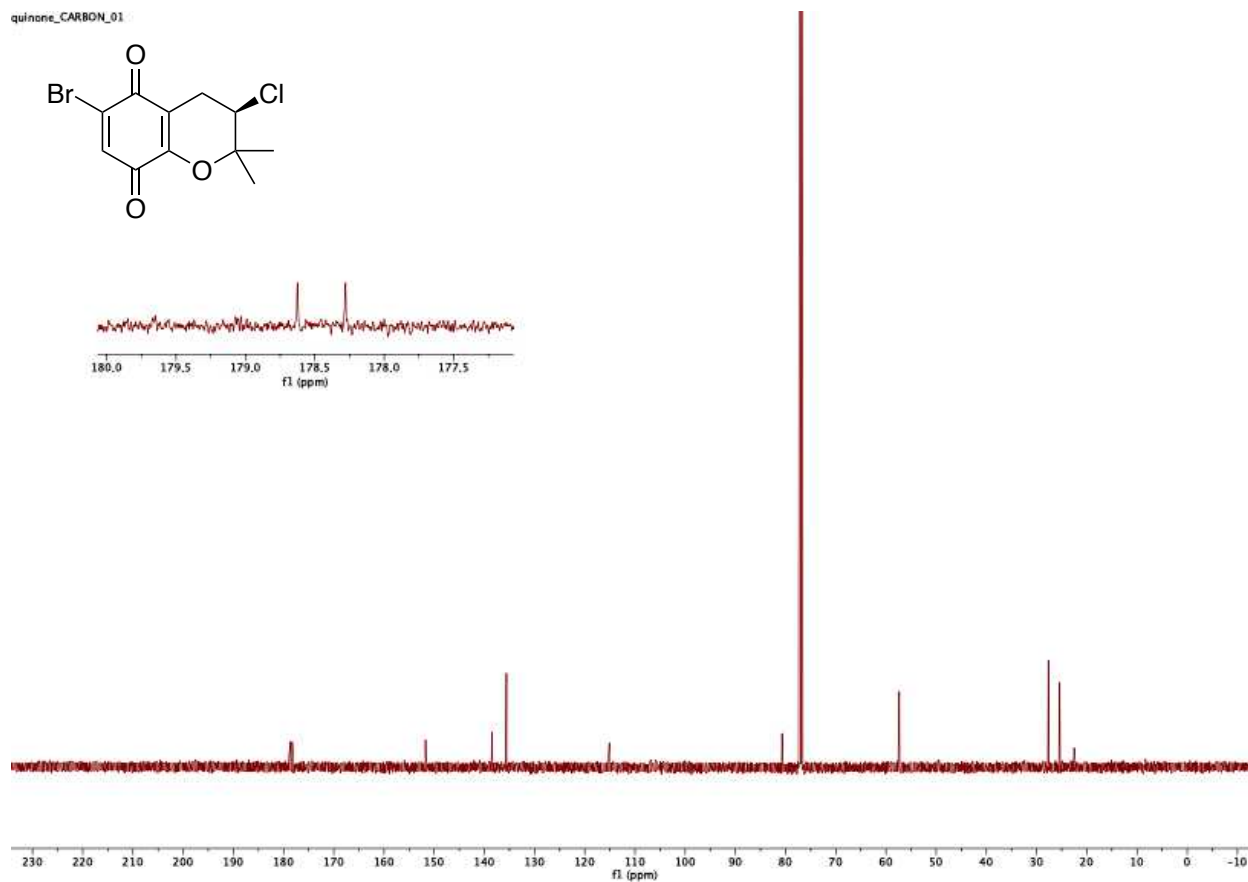
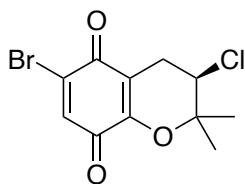
ST-05-12-Pure_CARBON_01

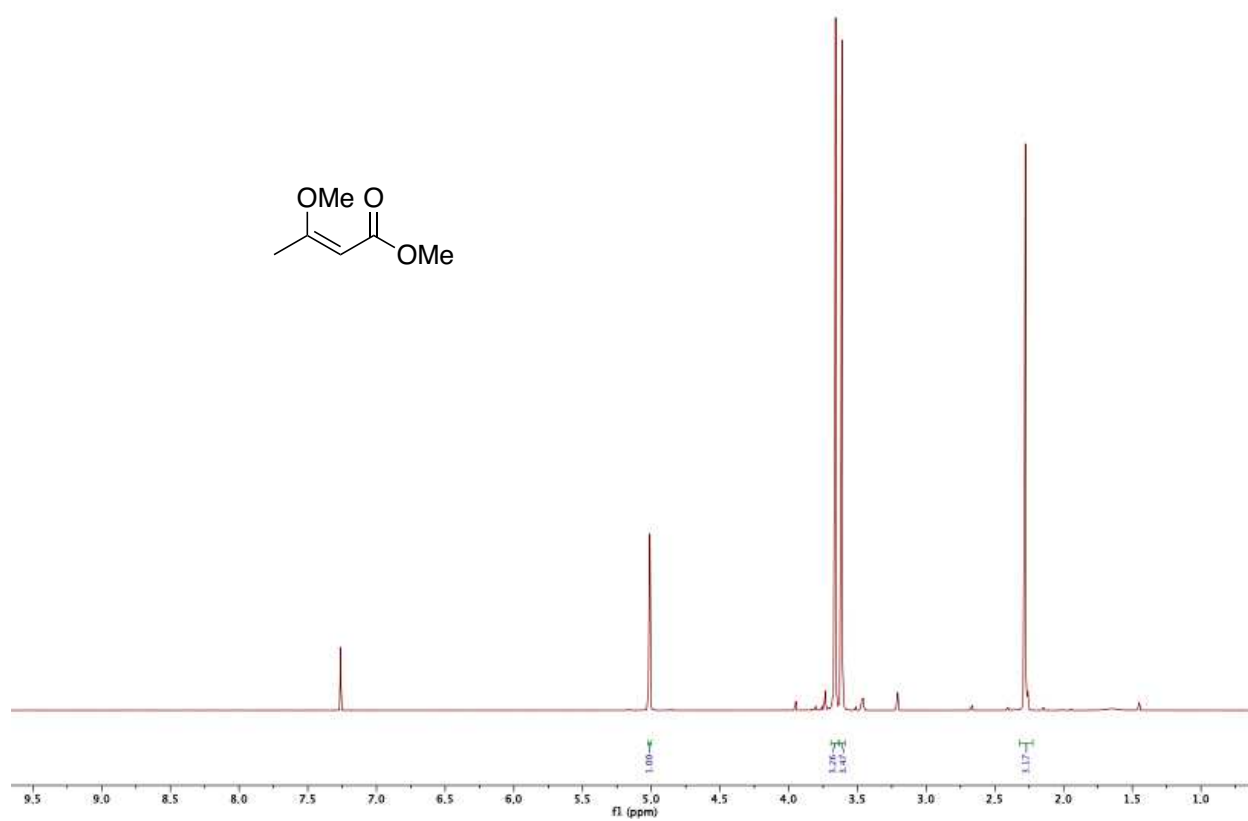


quinone_PROTON_01

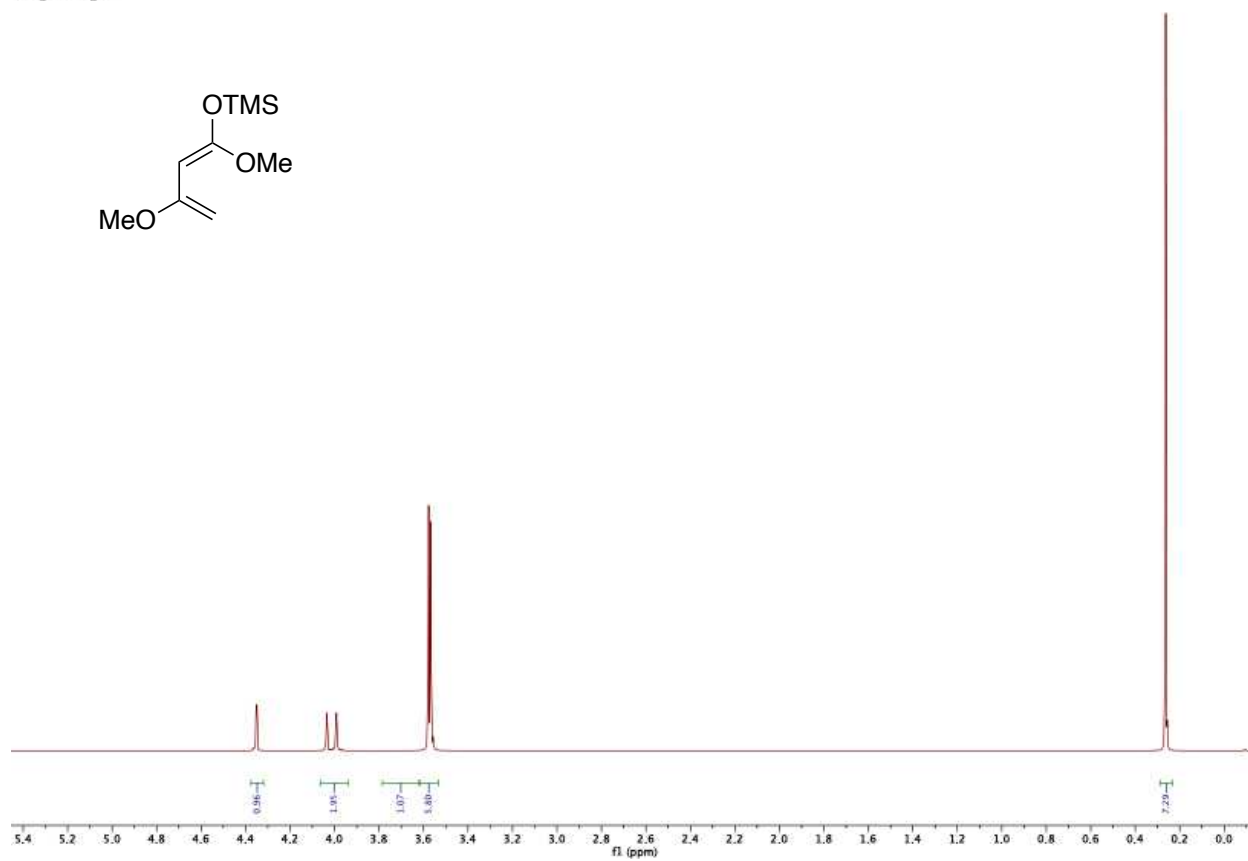
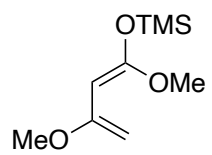


quinone_CARBON_01

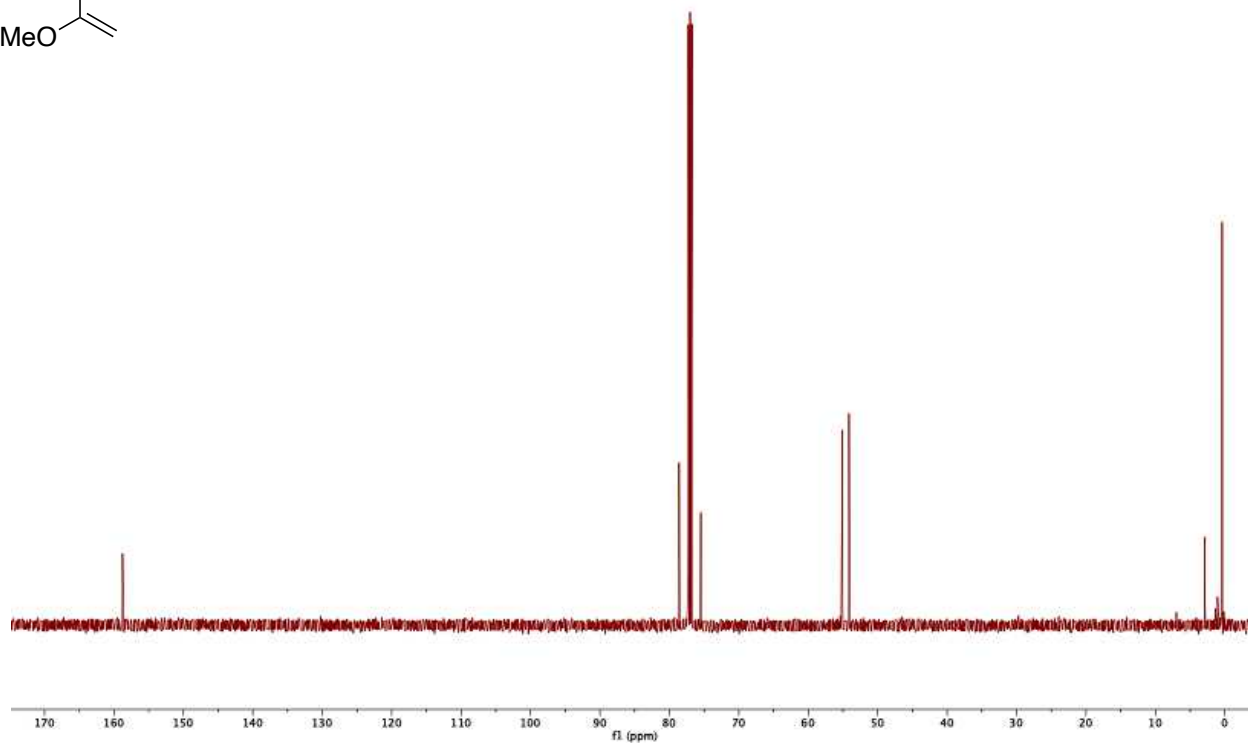
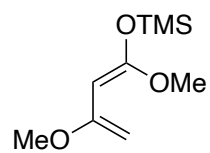




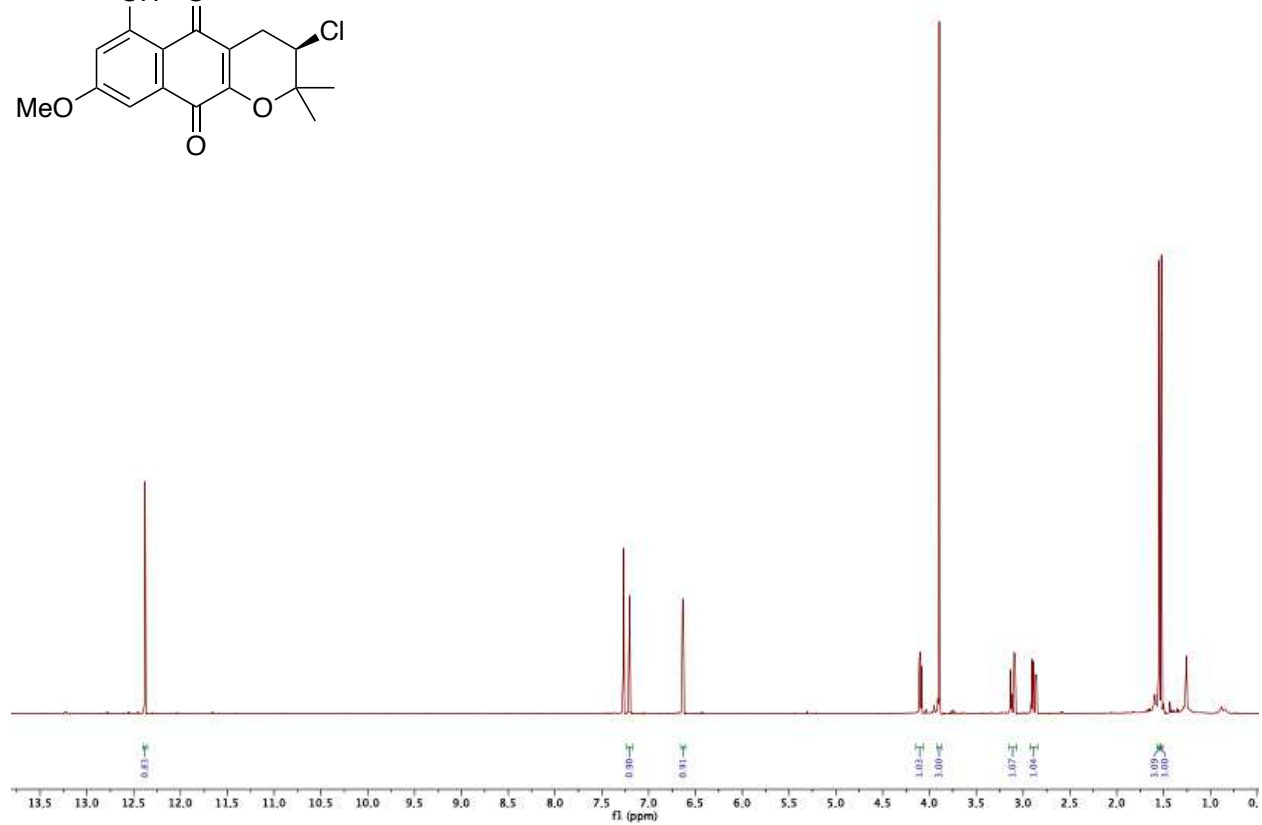
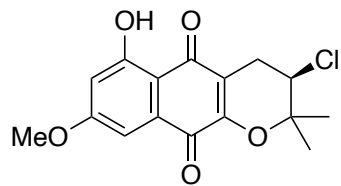
diene_PROTON_01



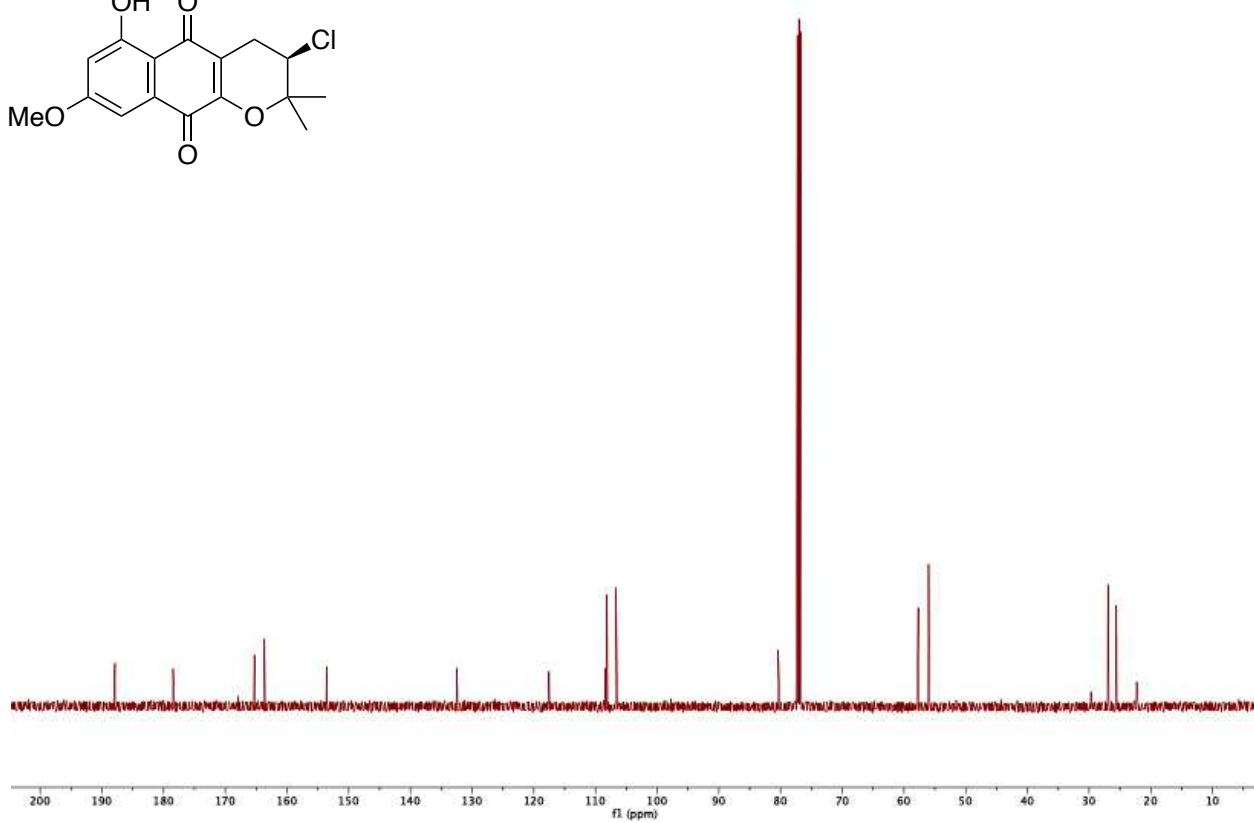
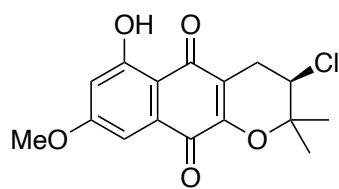
BM-03-I-020_CARBON_01



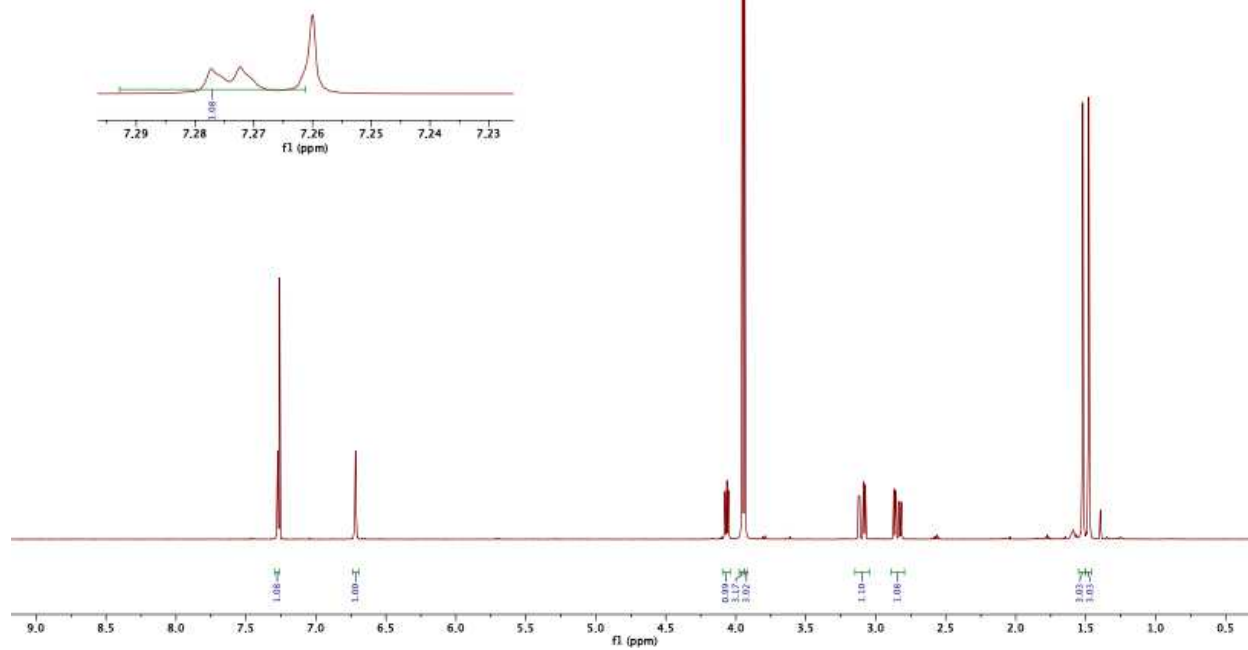
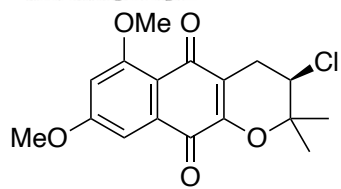
ST-05-84_PROTON_01



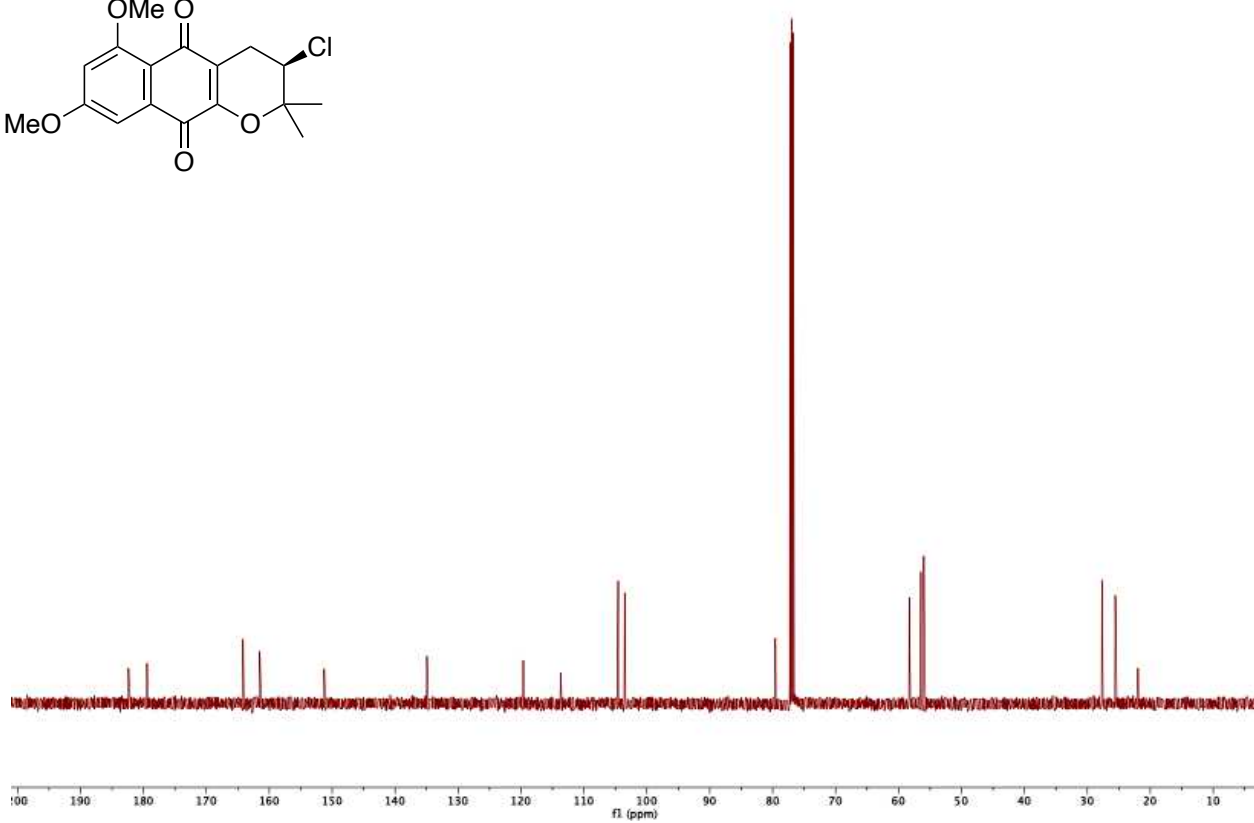
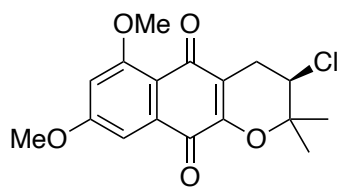
ST-05-84_CARBON_01

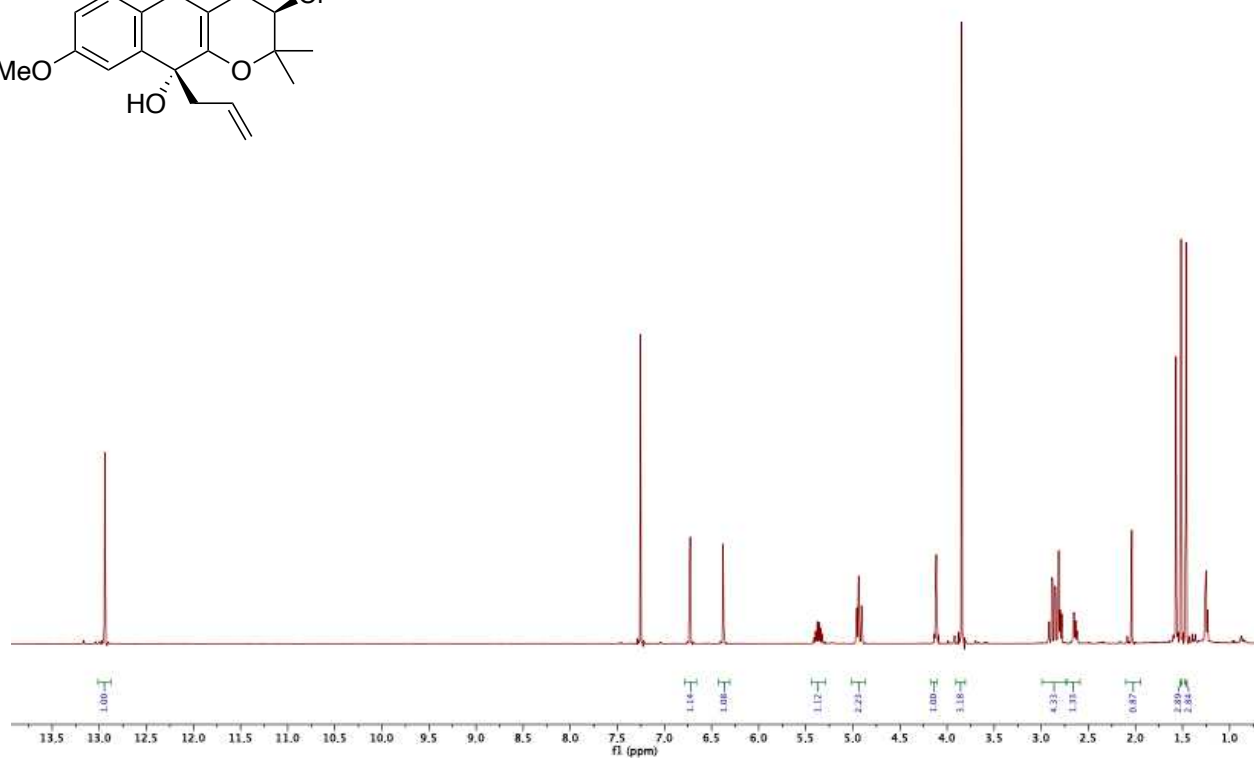


ST-04-132-Pure_PROTON_01

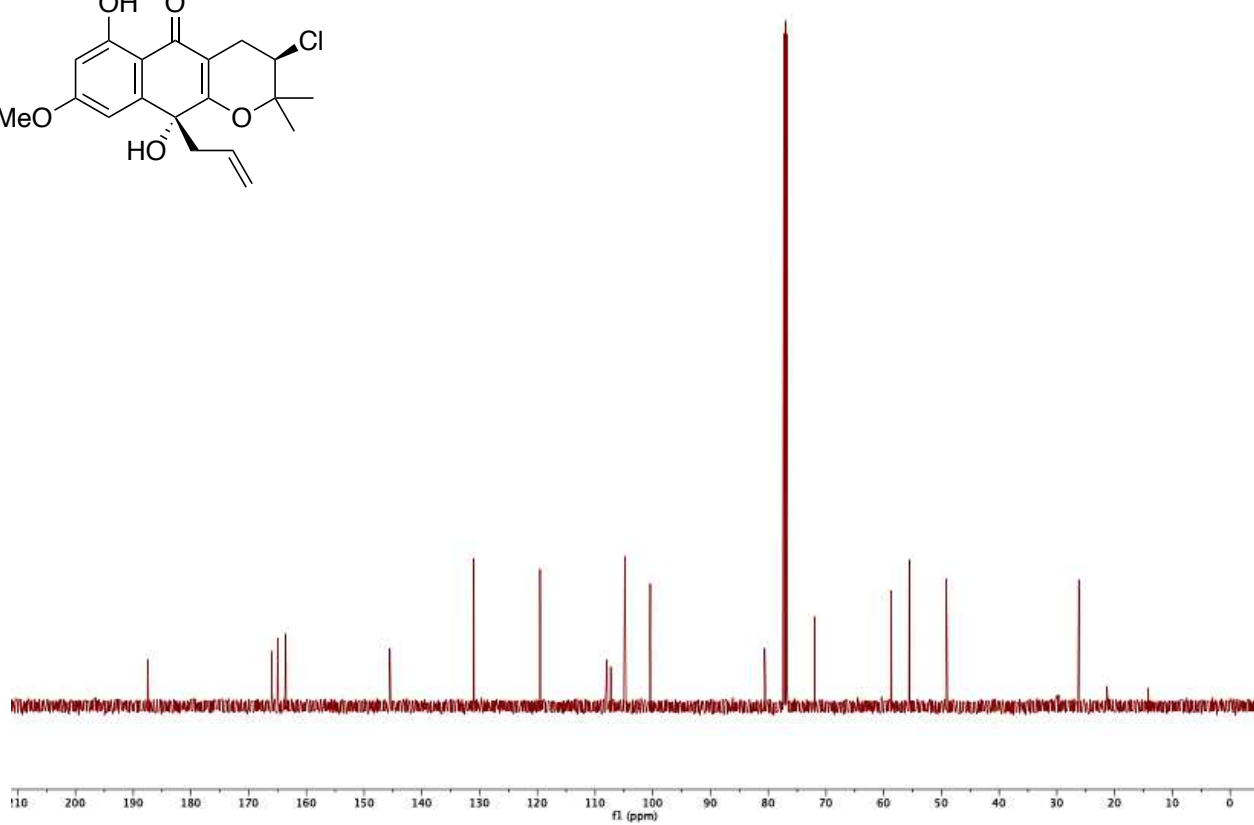
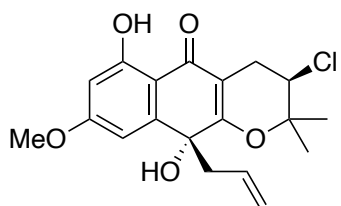


ST-04-132-Pure_CARSON_01

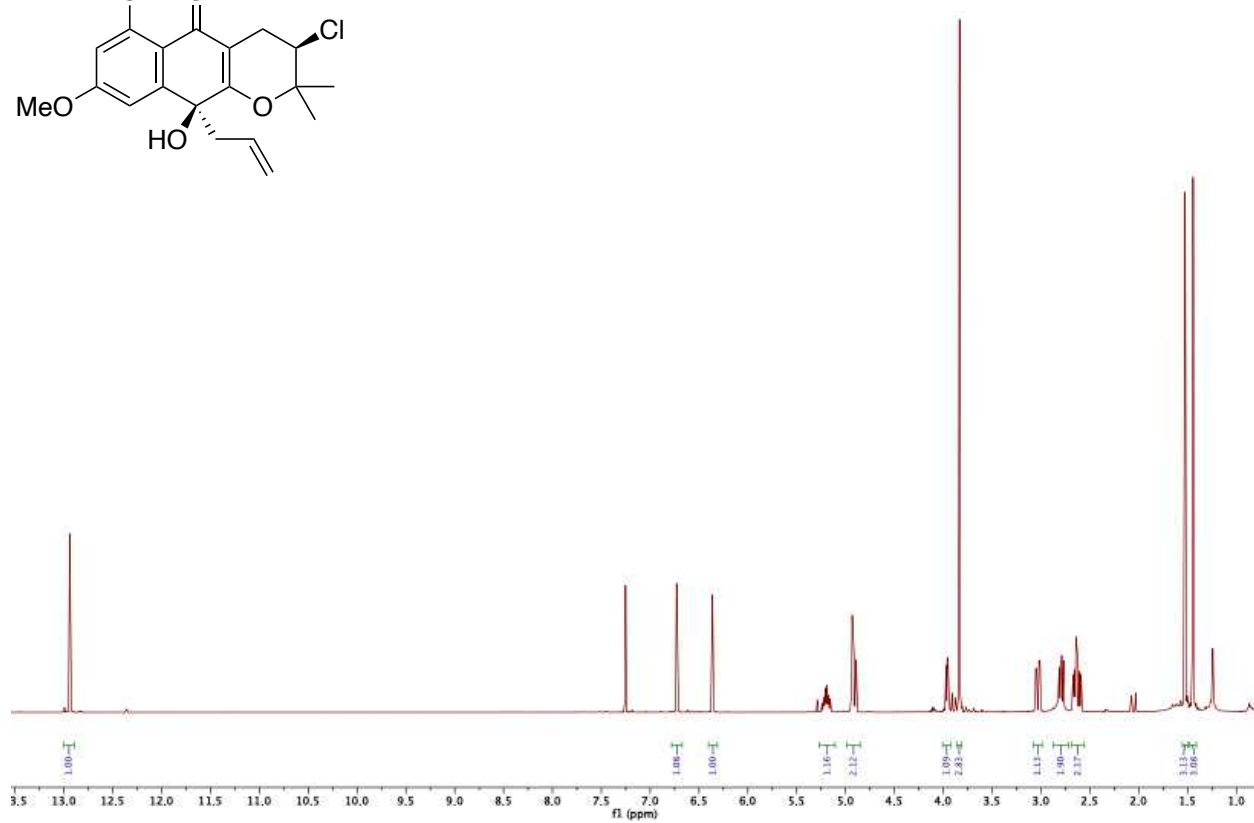
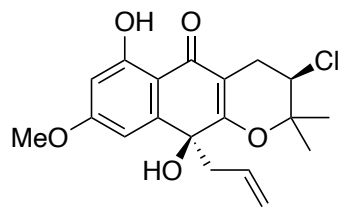




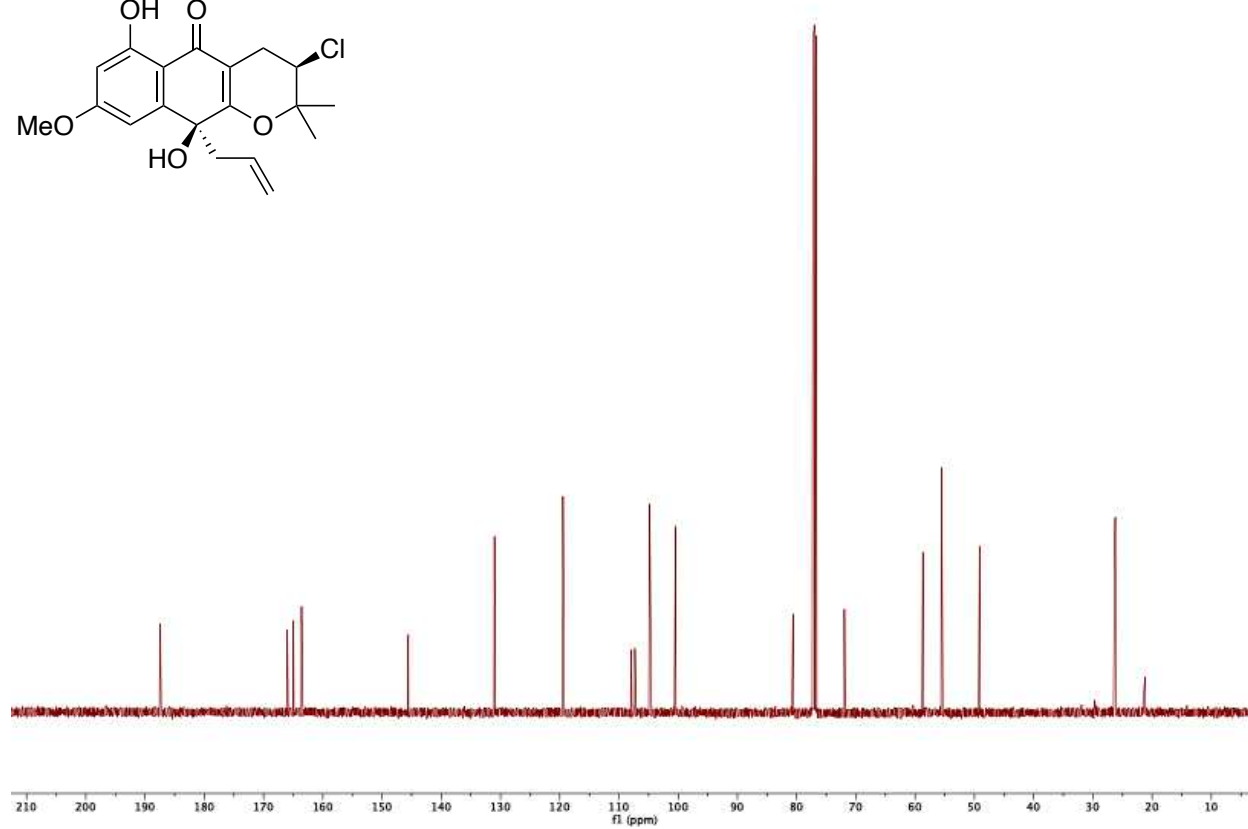
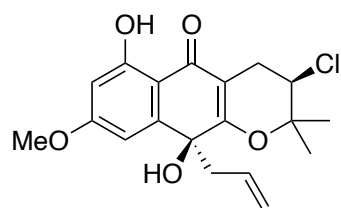
ST-05-20-Pure_CARBON_01



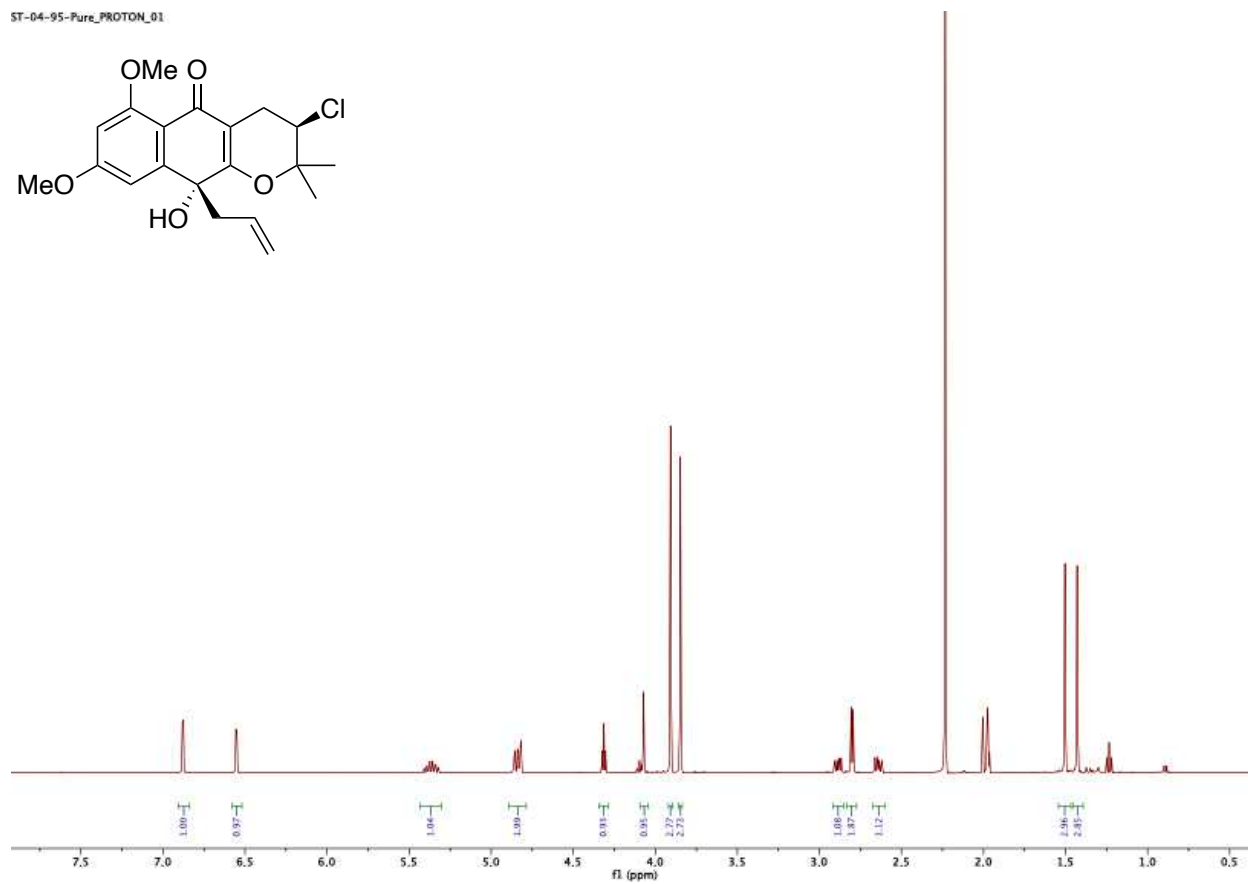
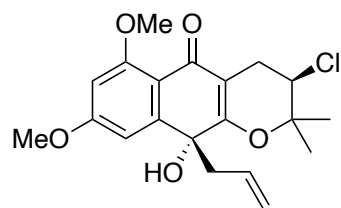
ST-04-151-H_PROTON_01



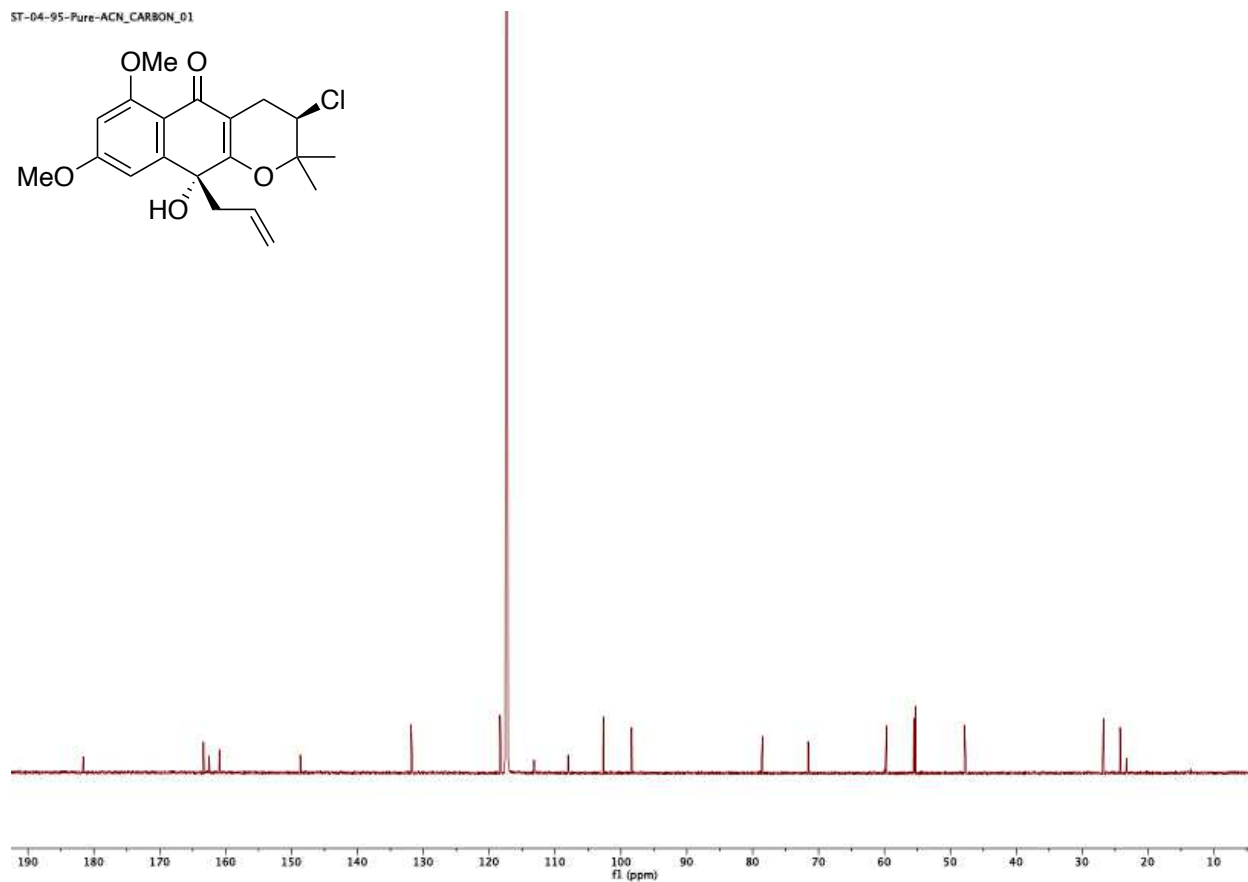
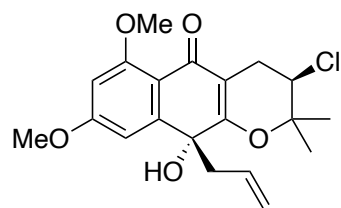
ST-04-151-II_CARBON_01

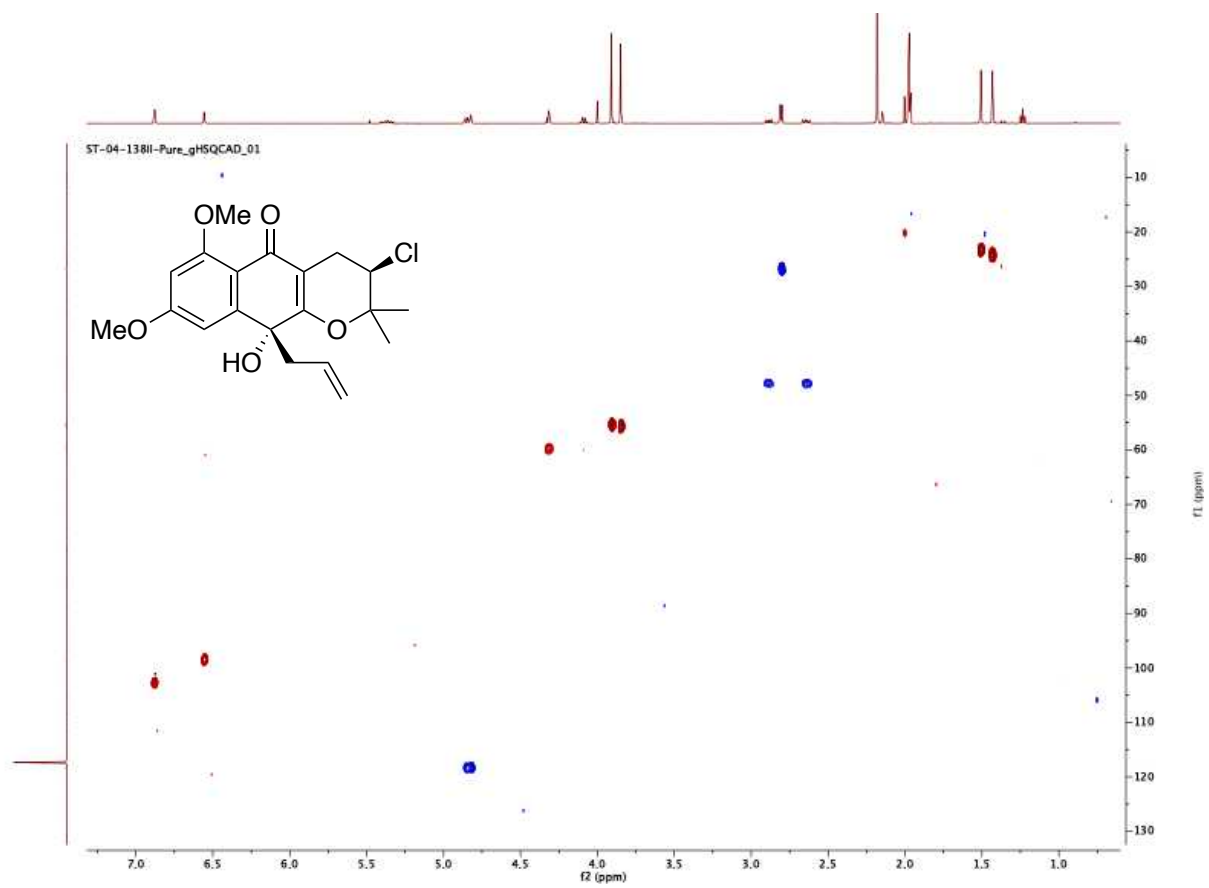


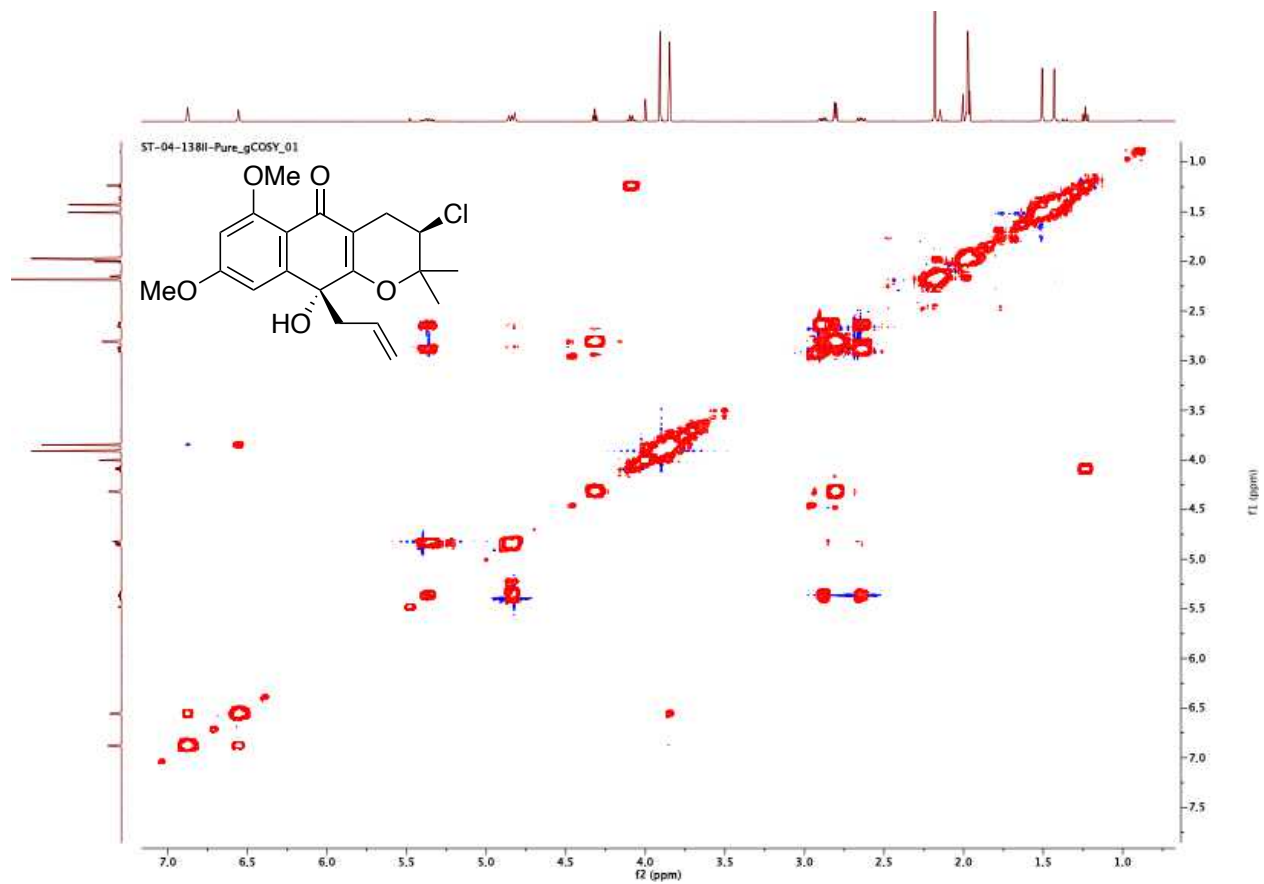
ST-04-95-Pure_PROTON_01

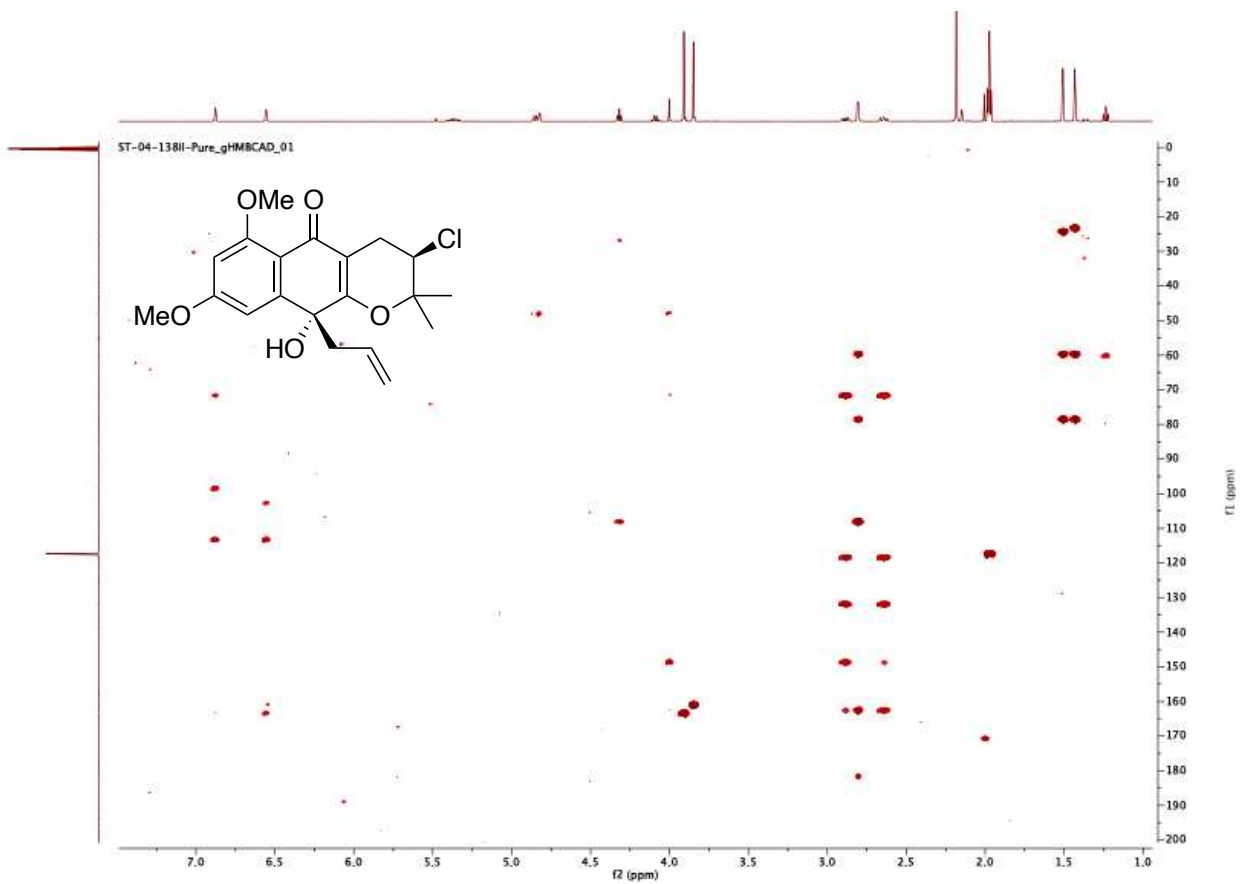


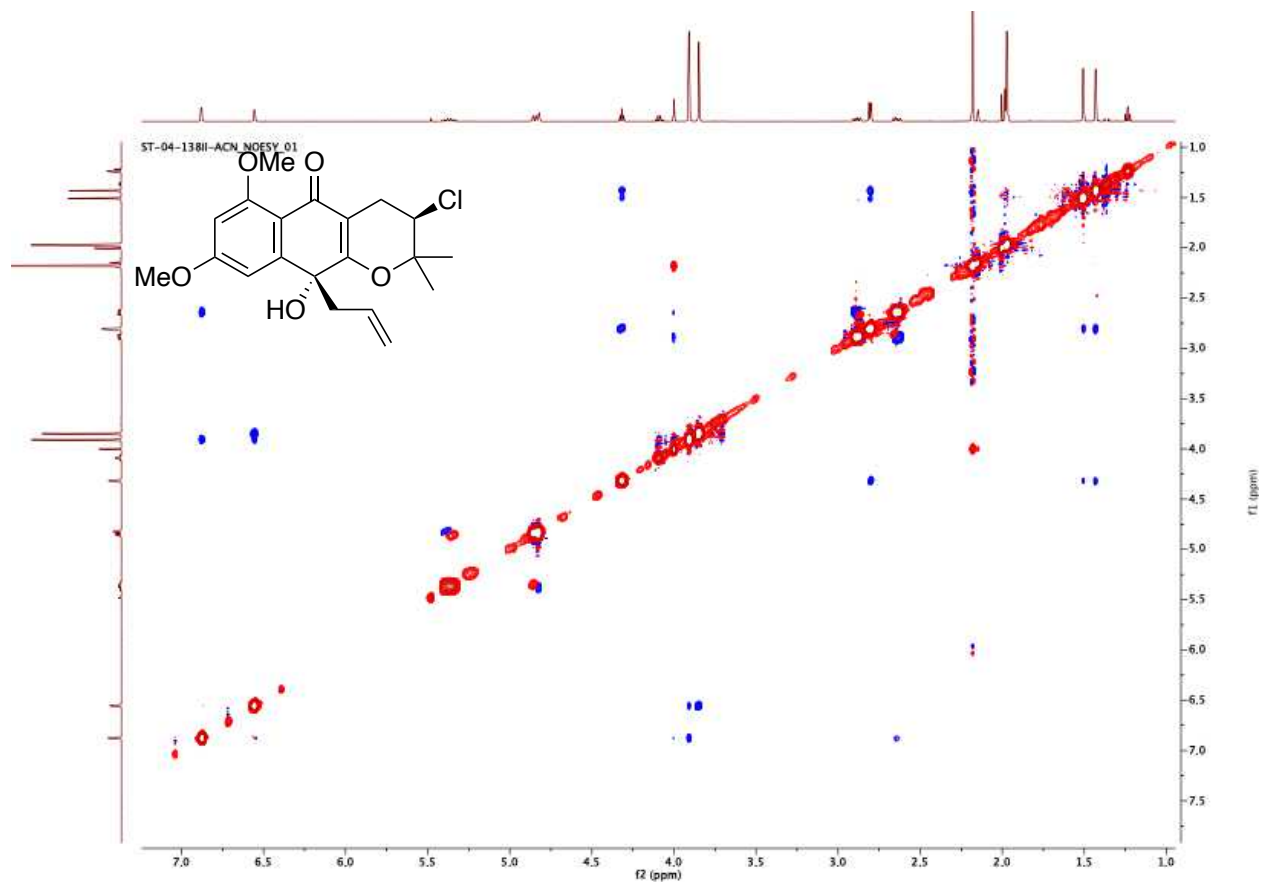
ST-04-95-Pure-ACN_CARBN_01



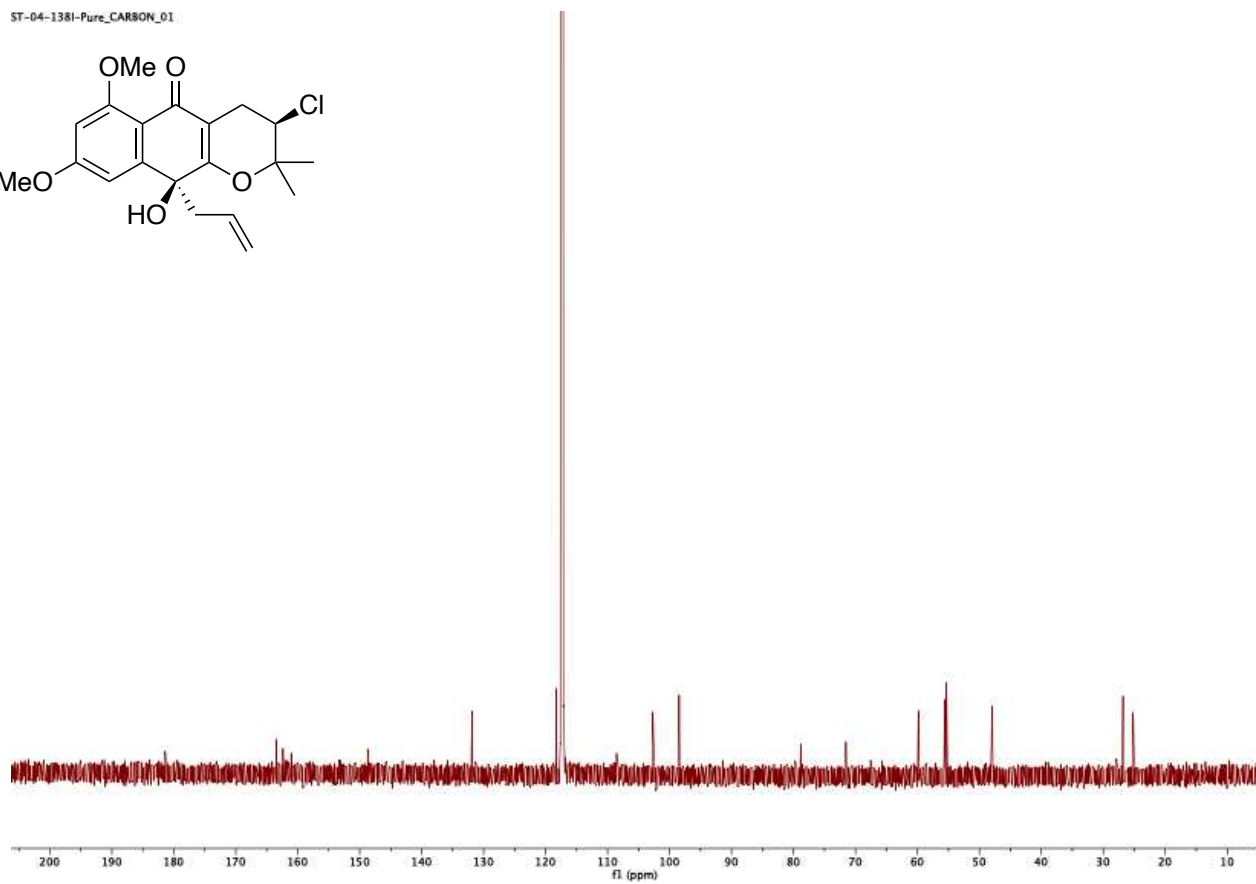
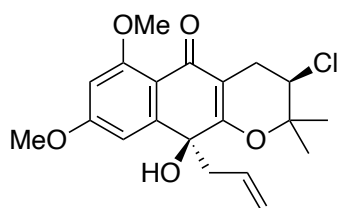


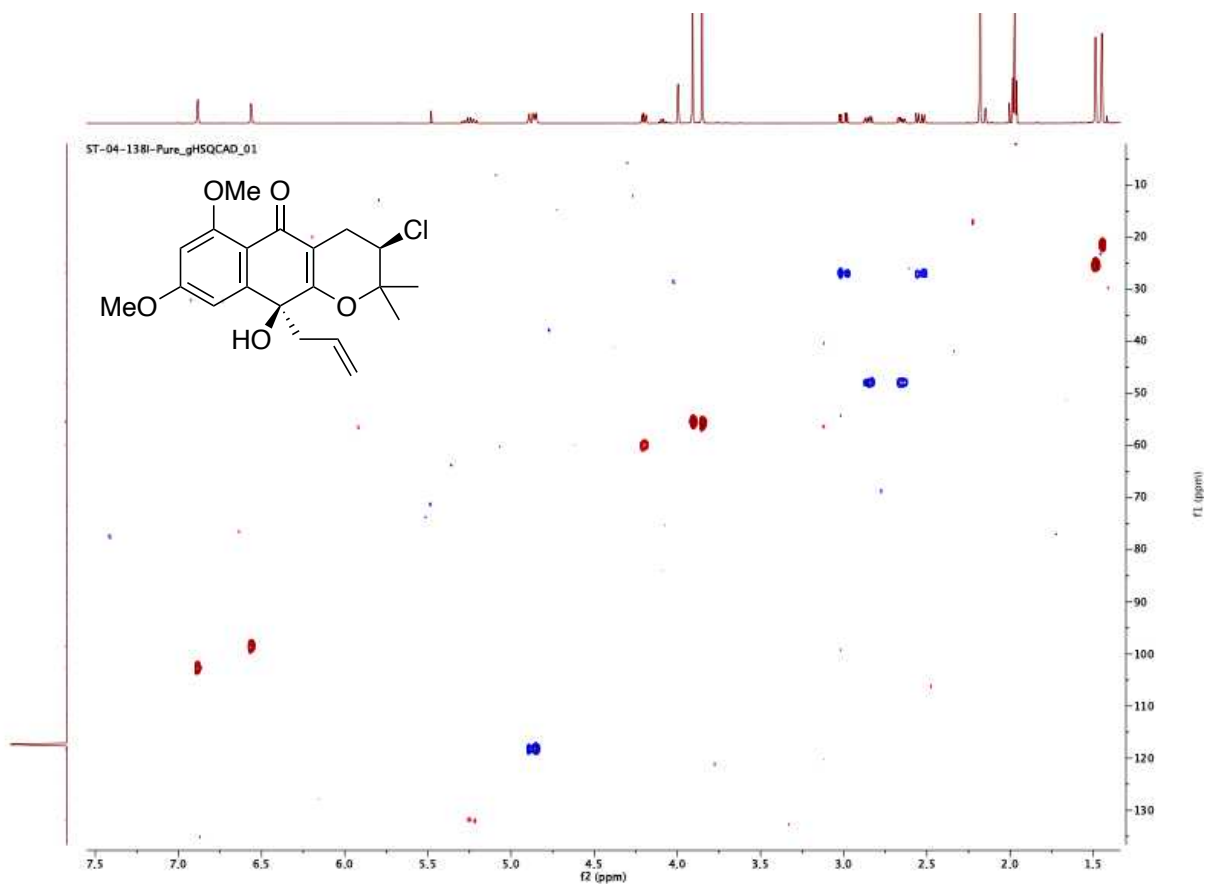


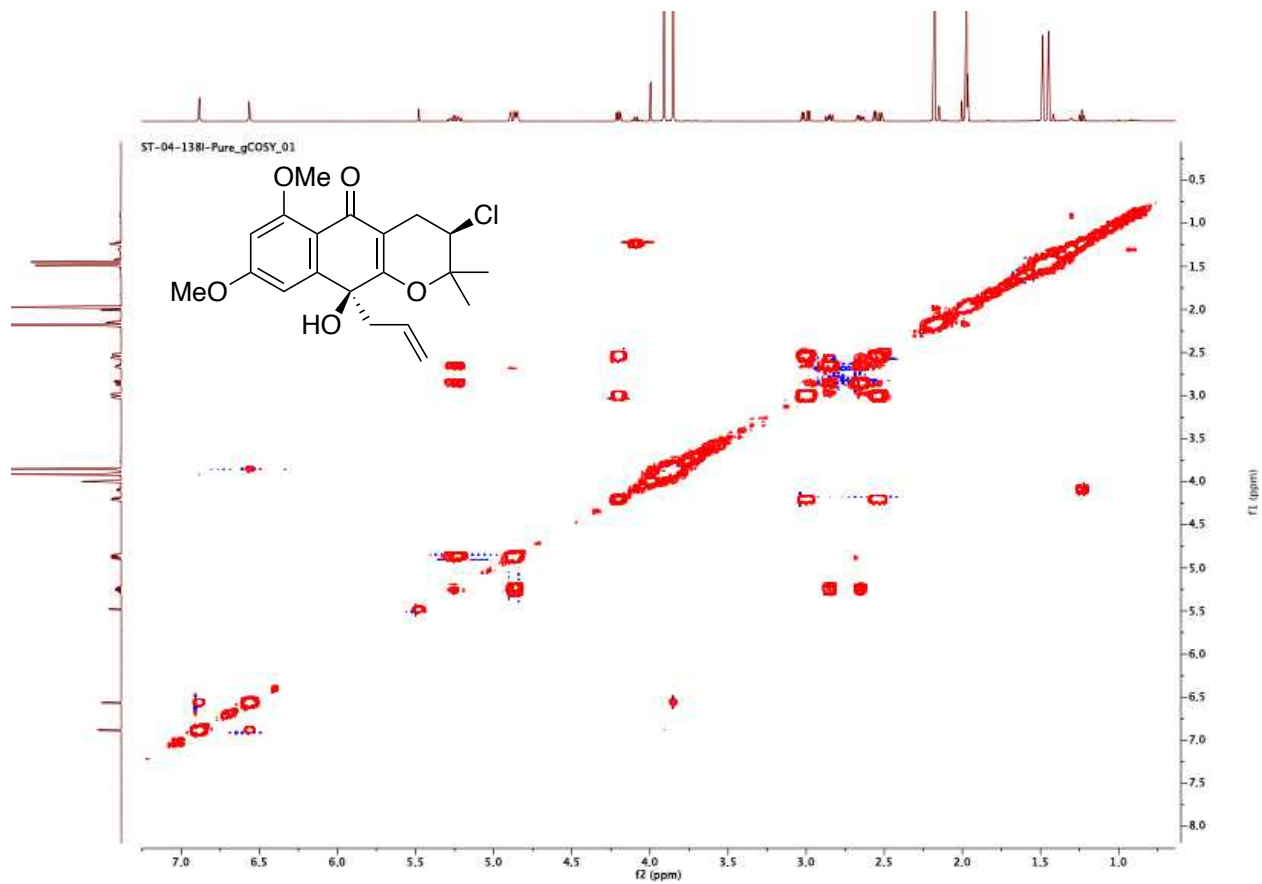


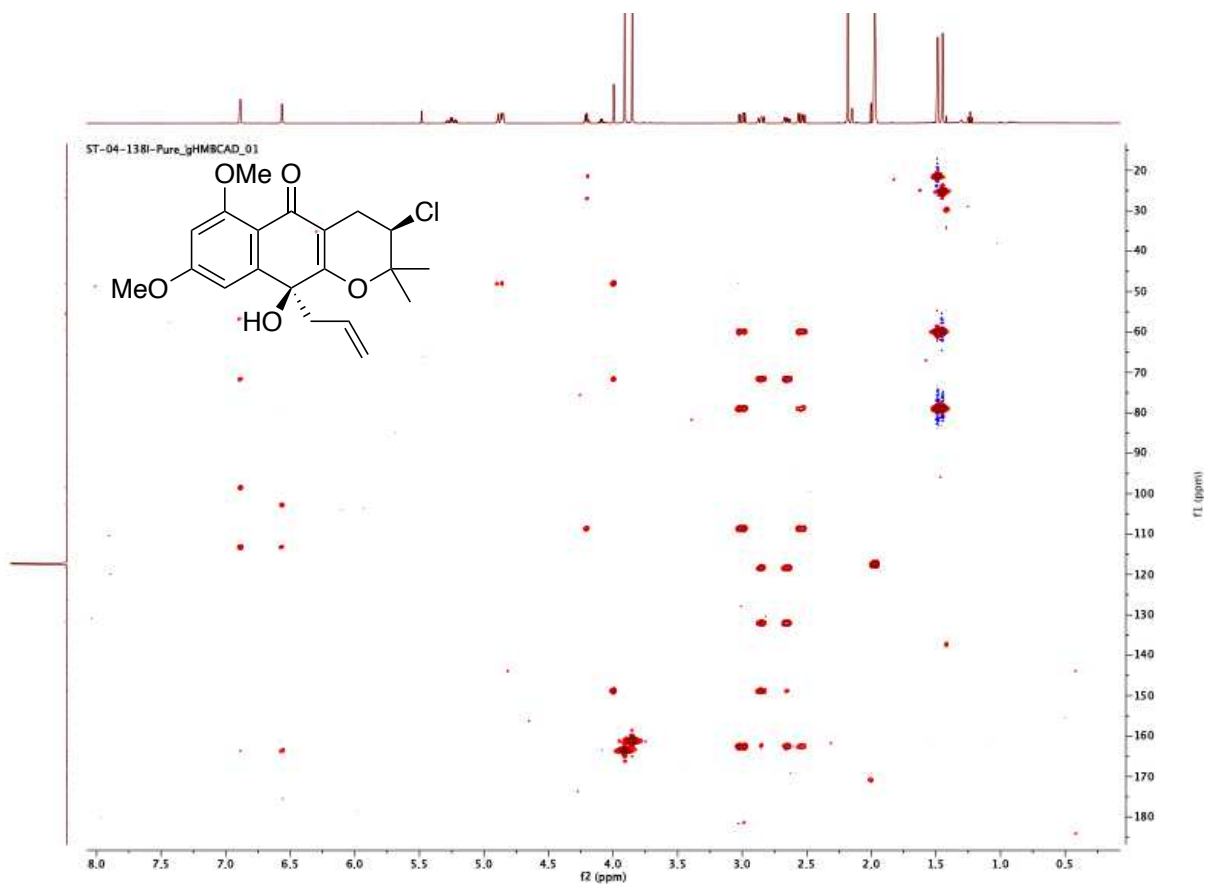


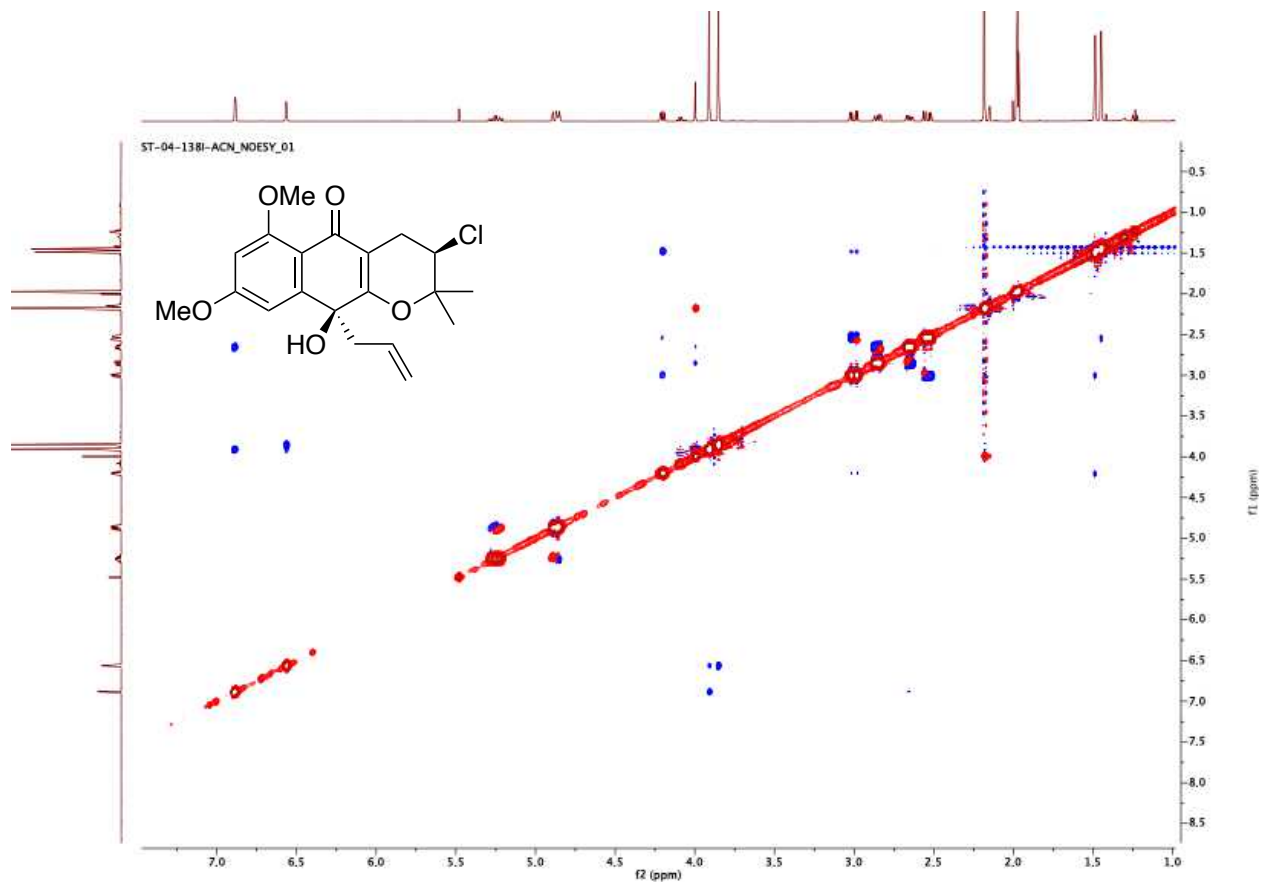
ST-04-1381-Pure_CARBOXON_O1

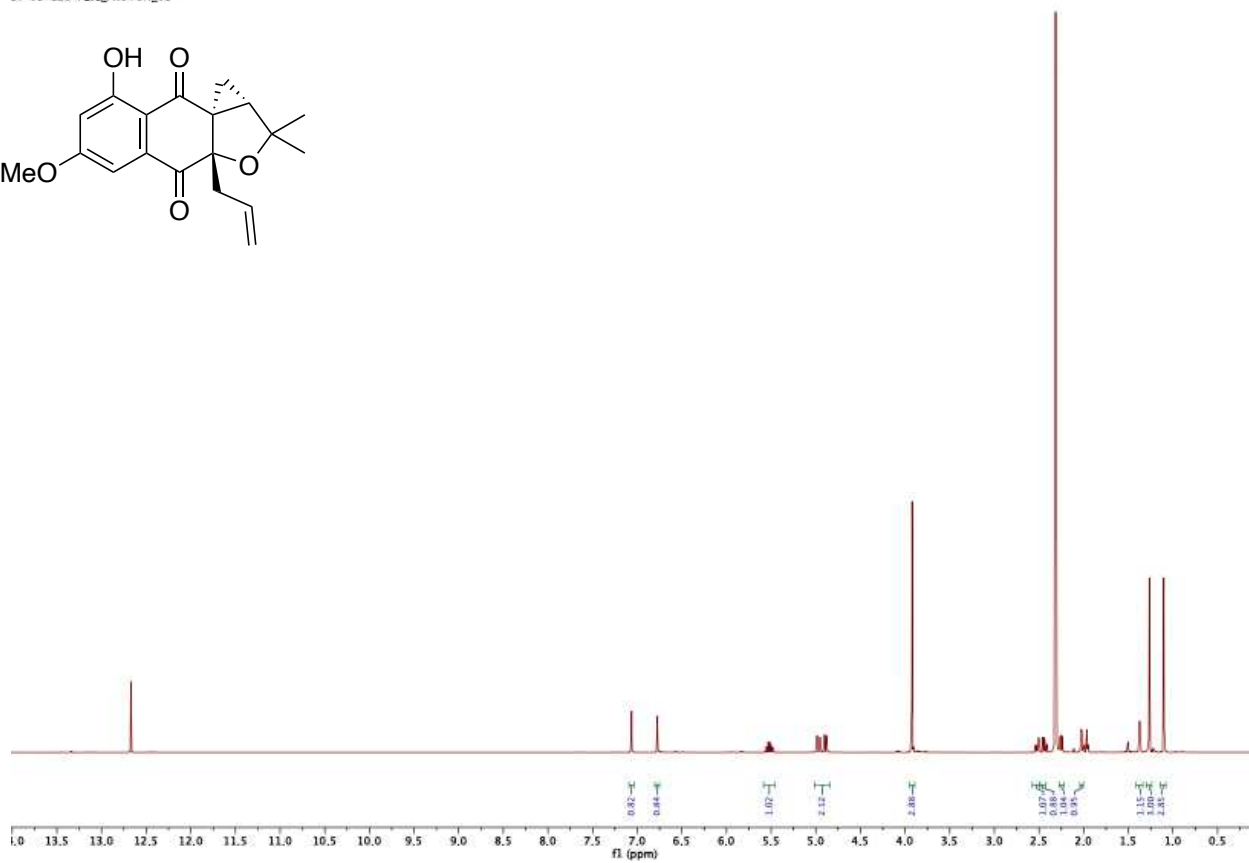
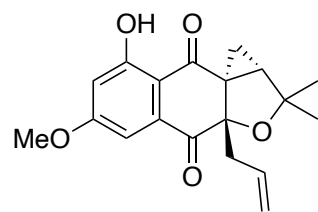




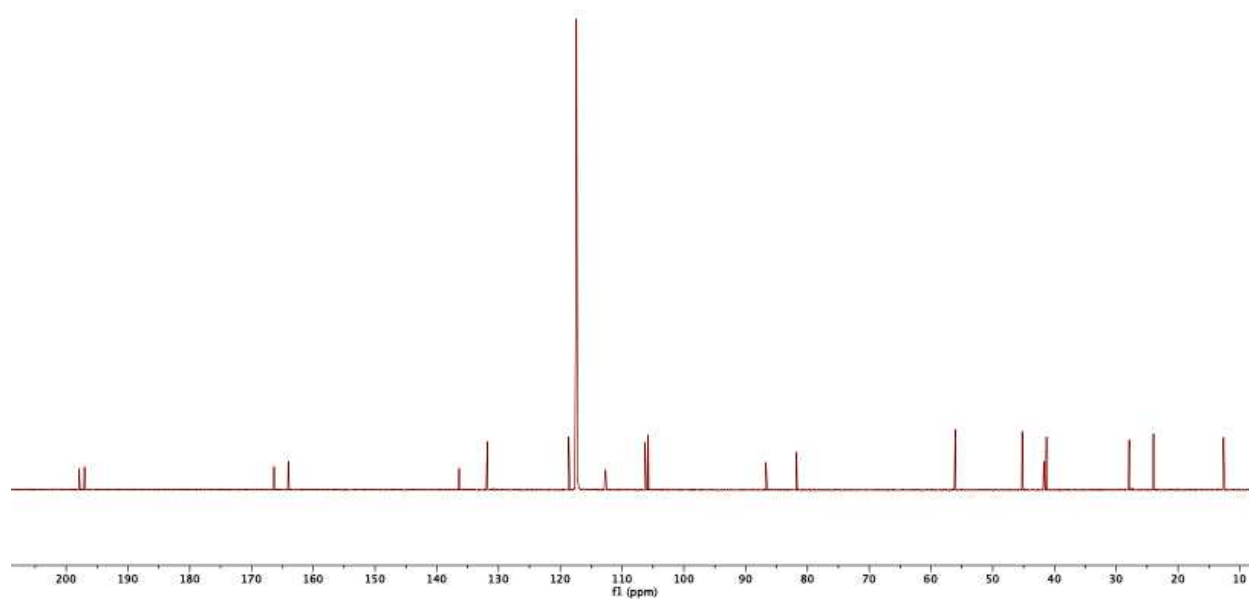
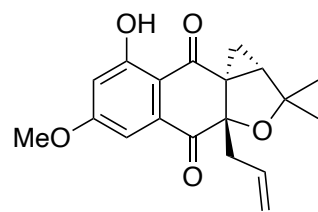


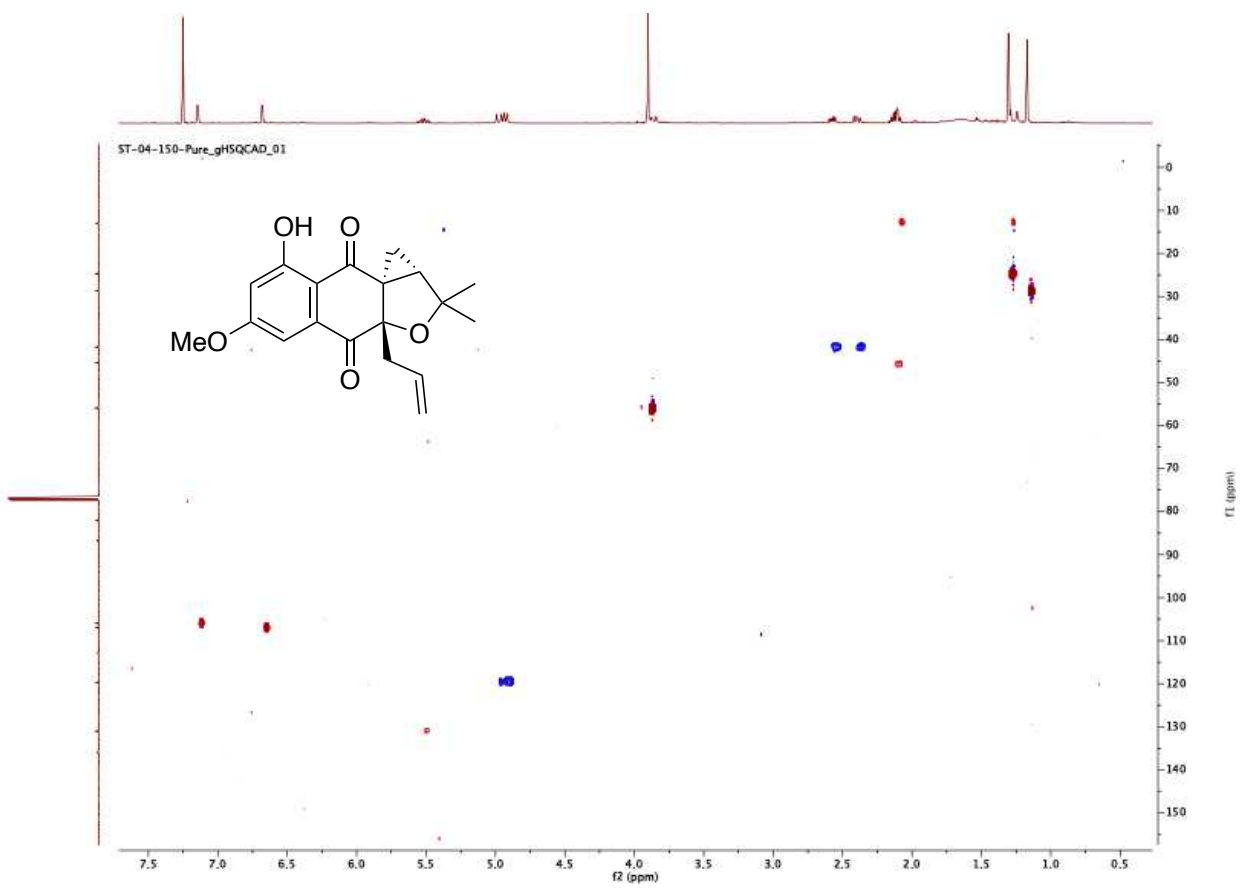


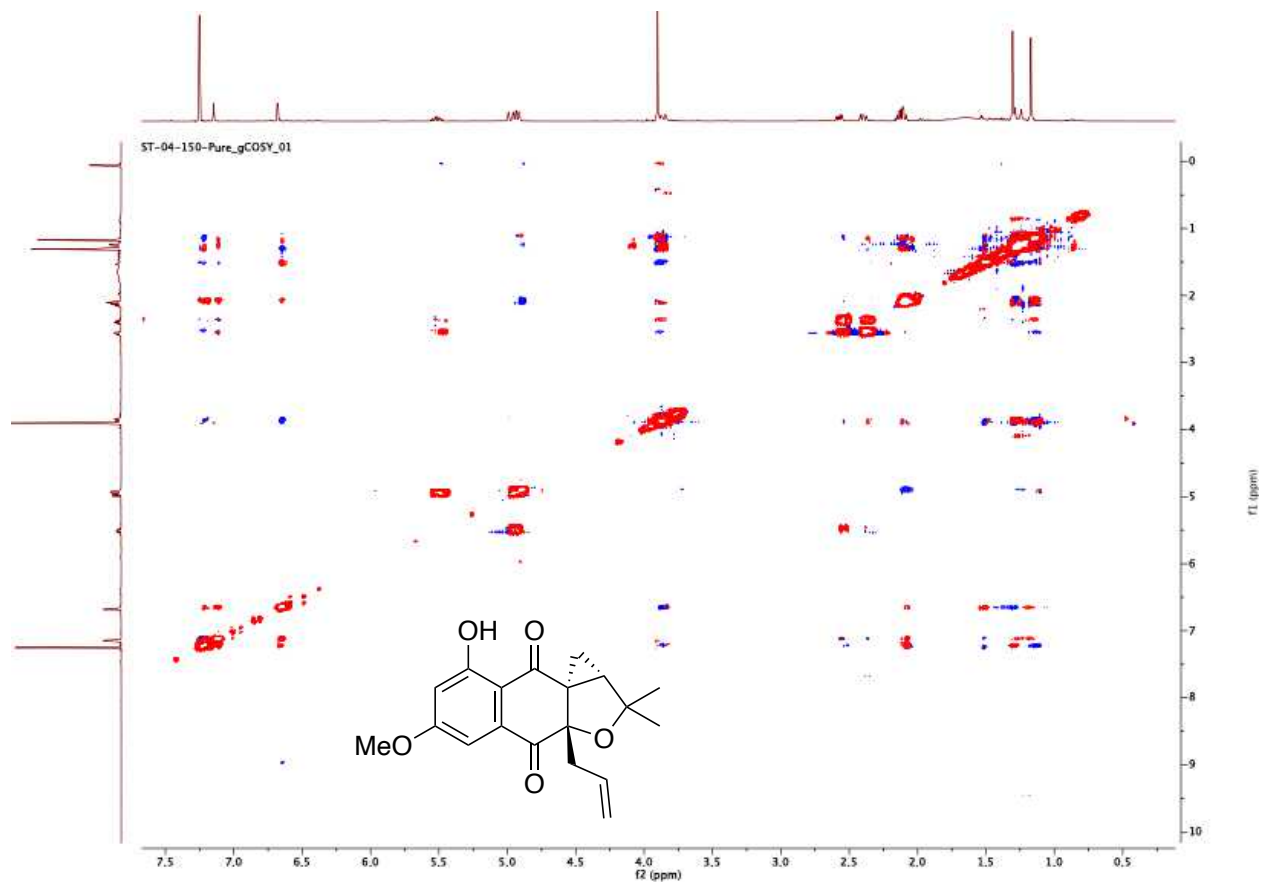


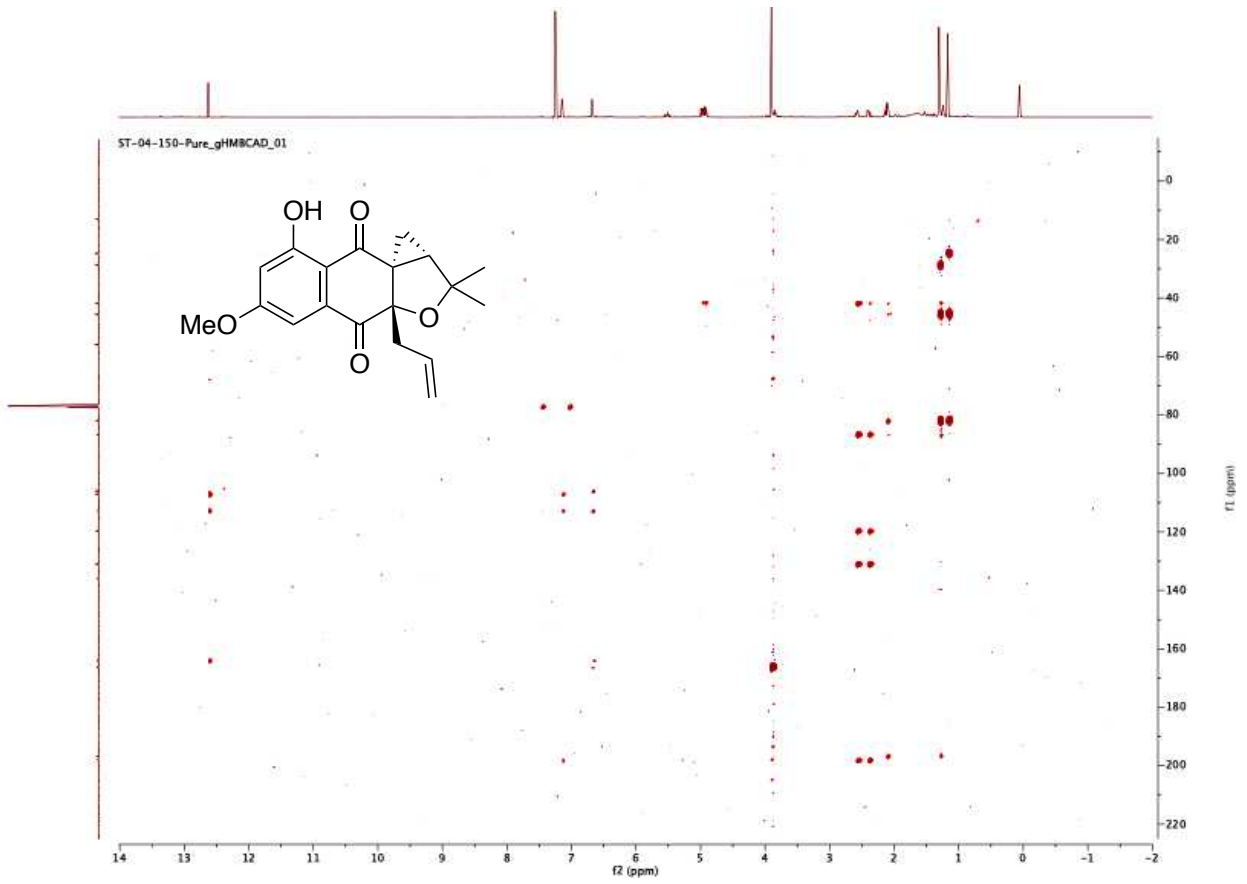


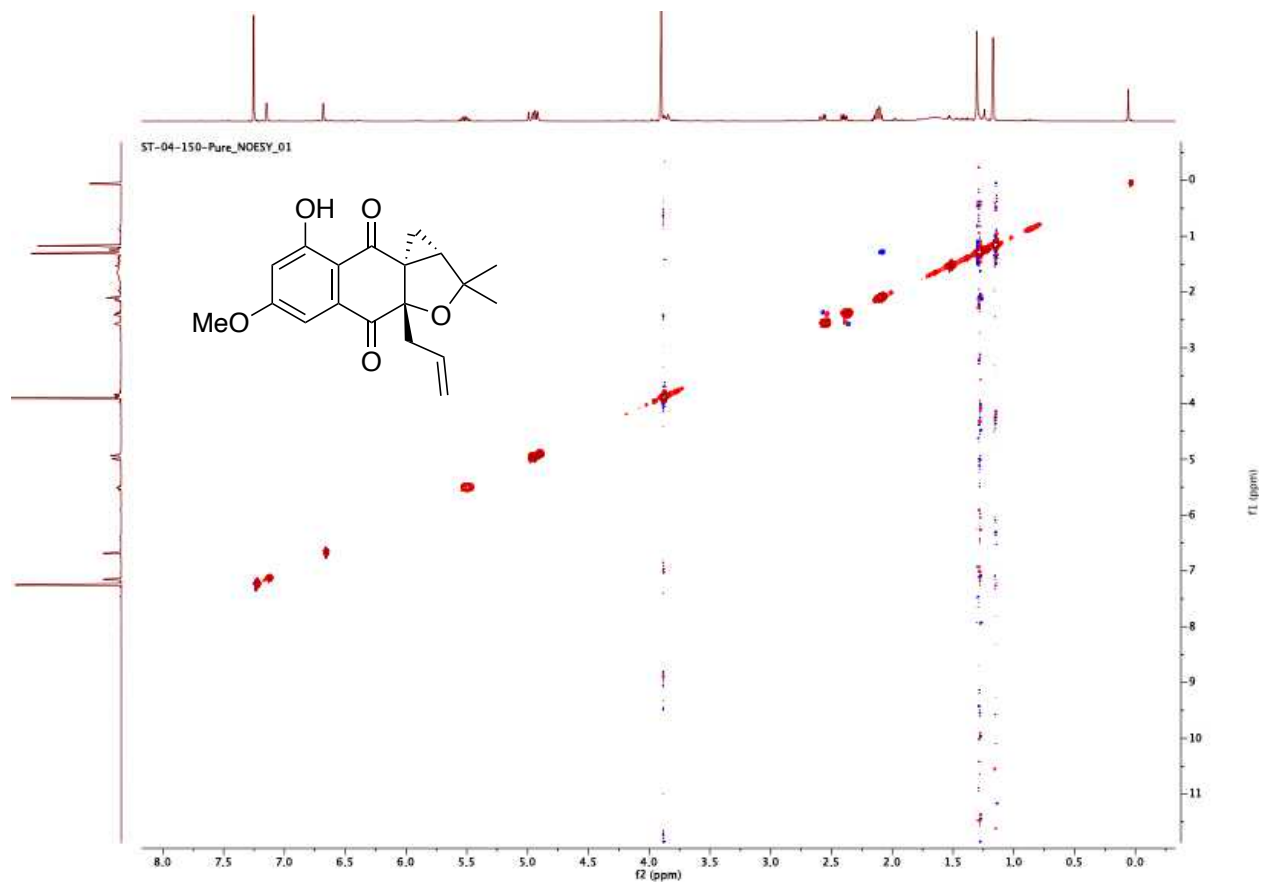
ST-05-126-Pure_CARSON_01

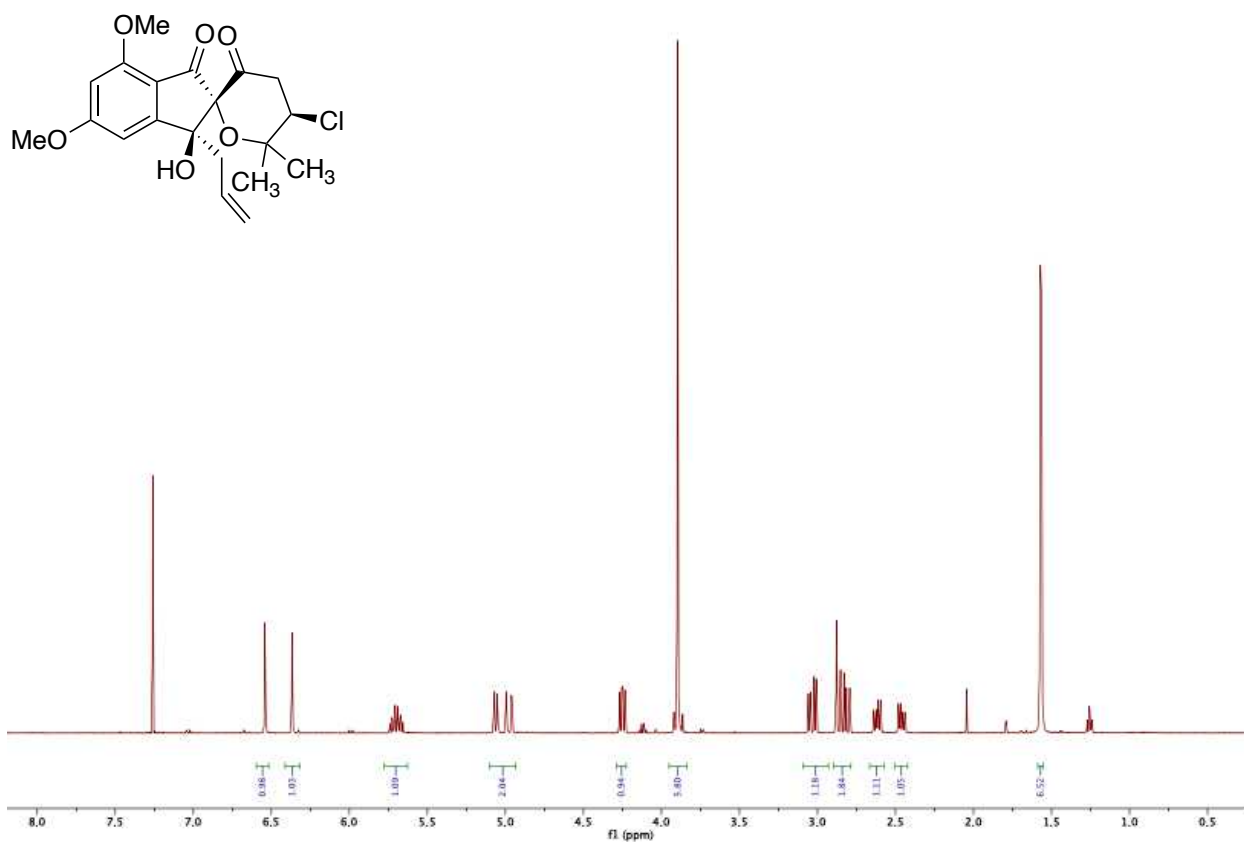


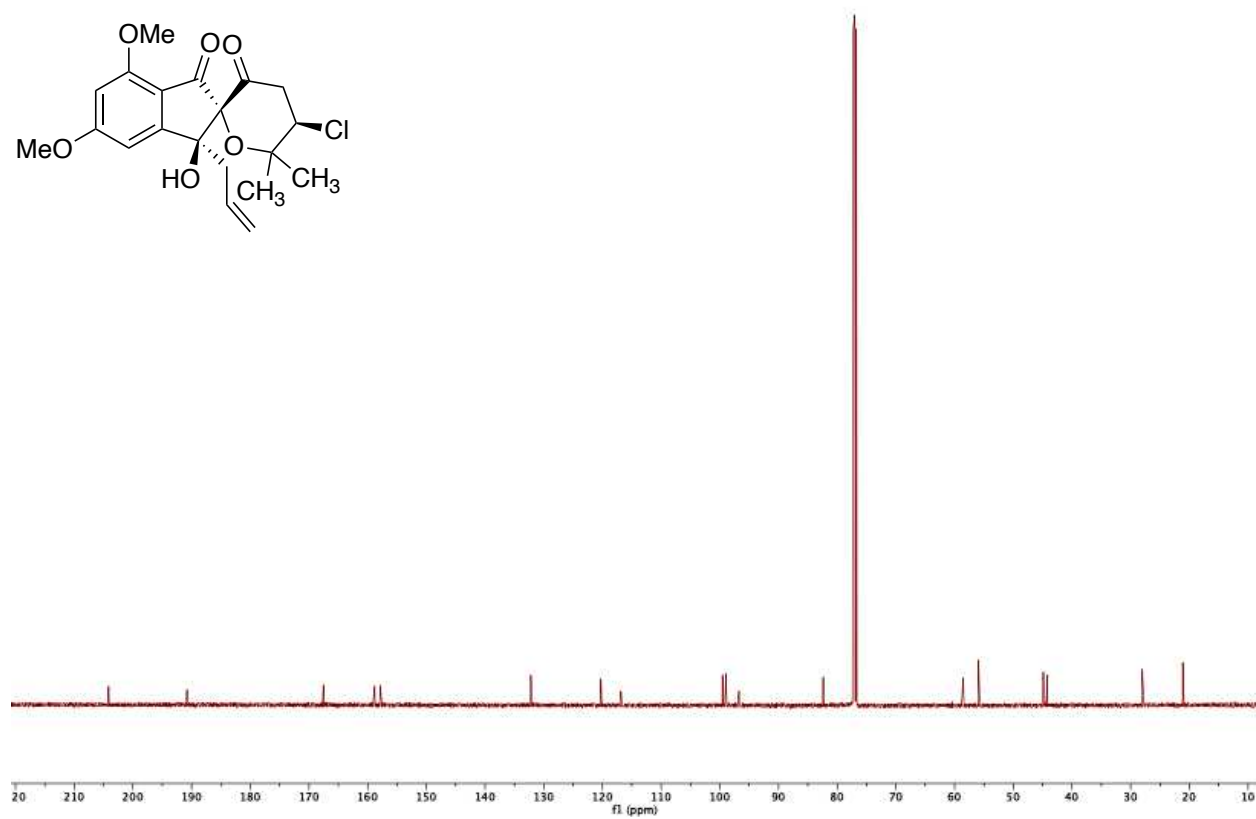
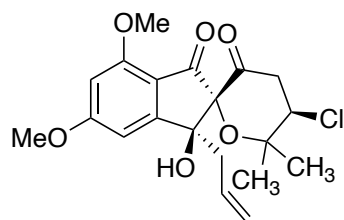


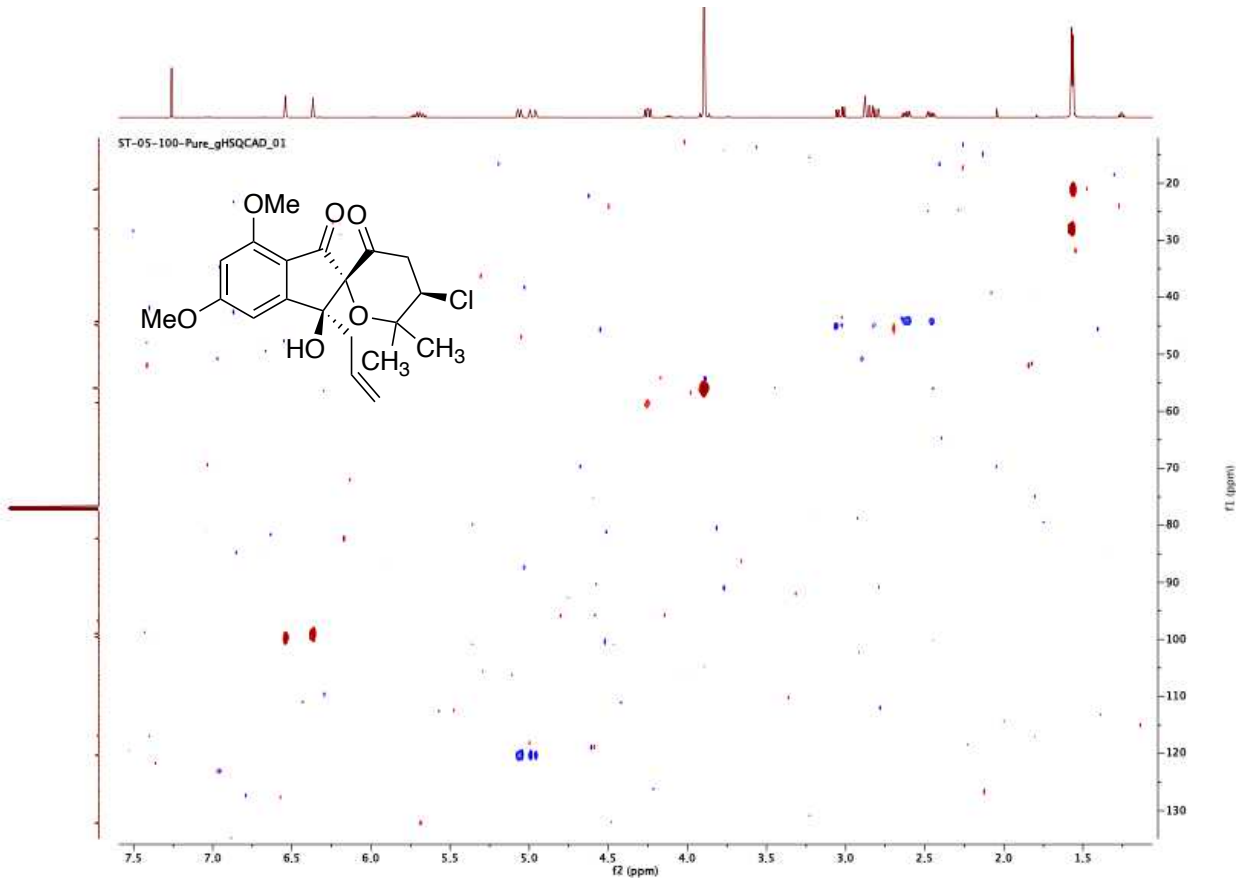


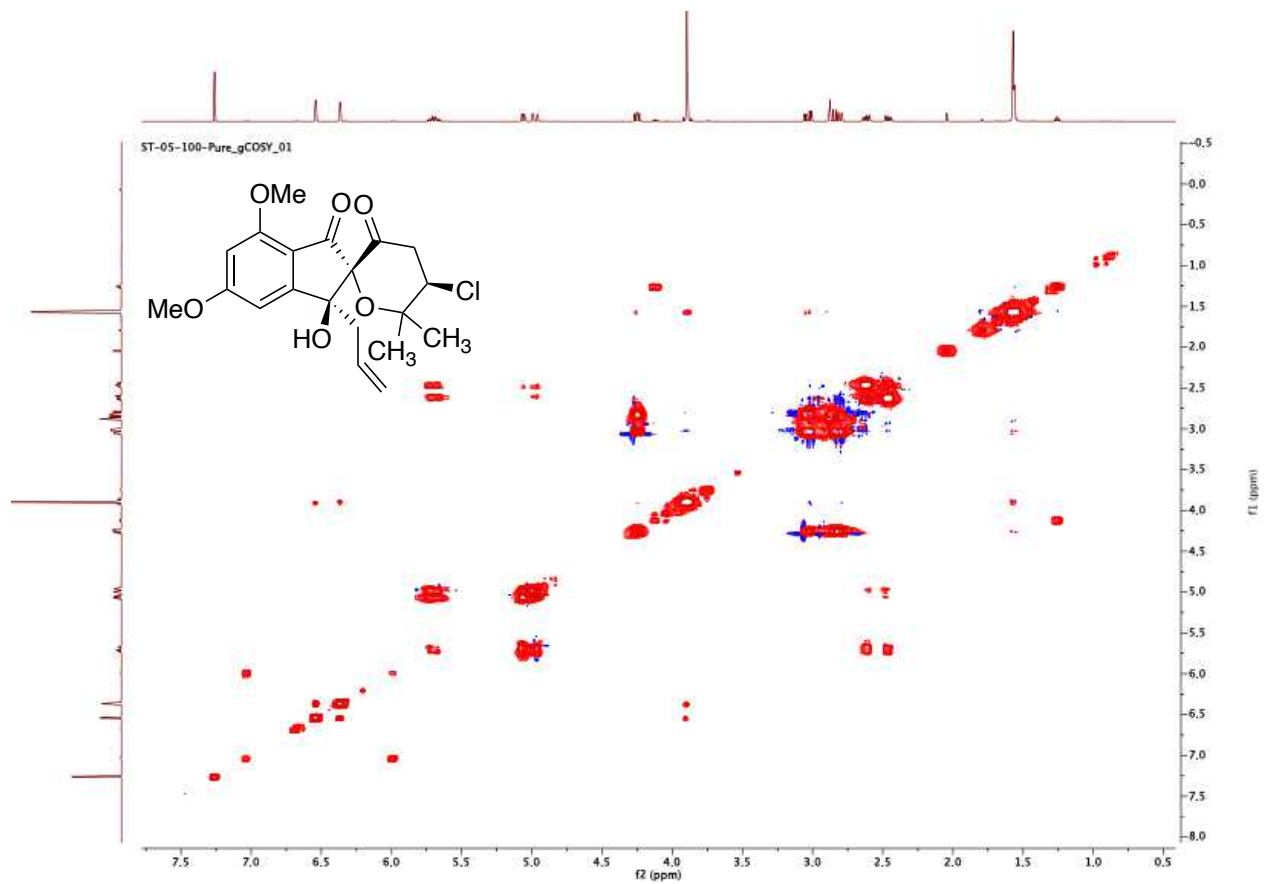


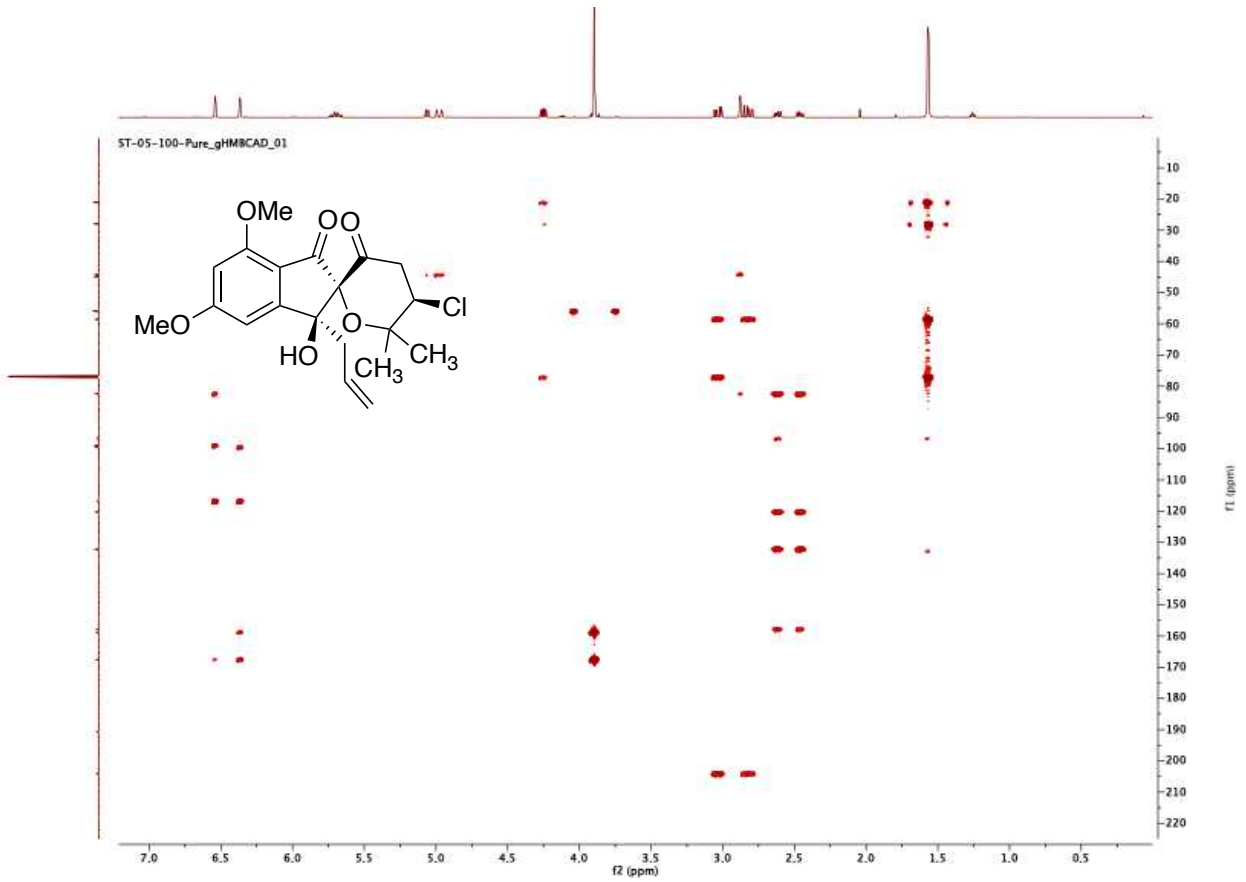


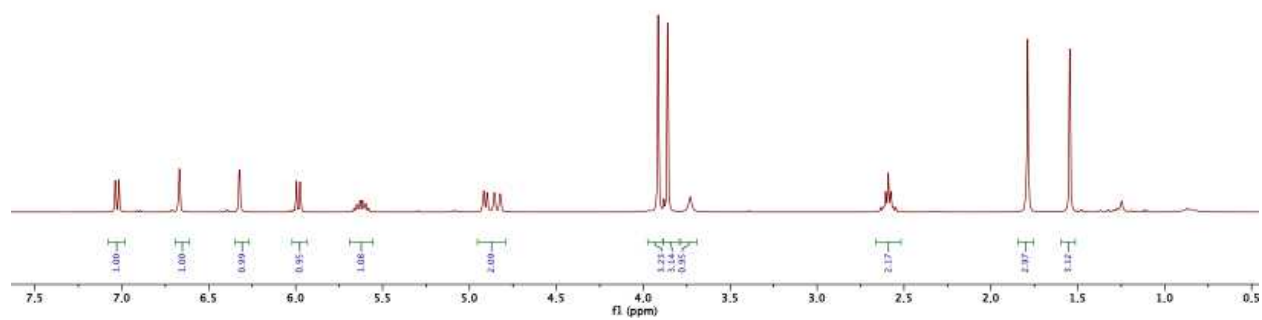
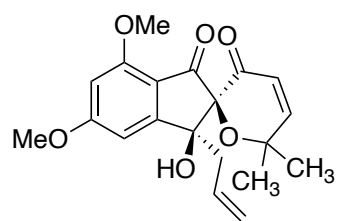




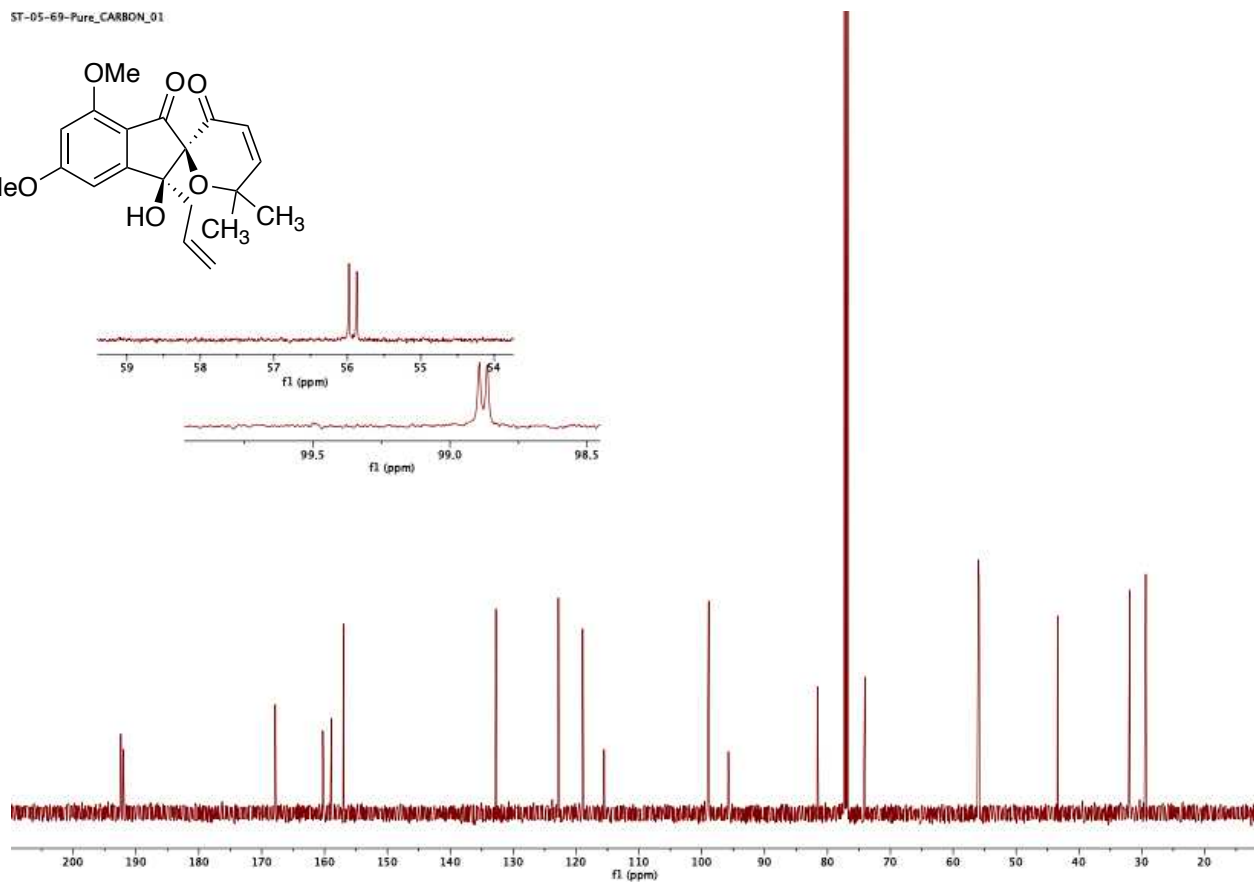
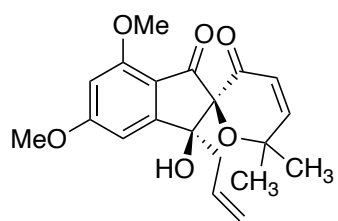


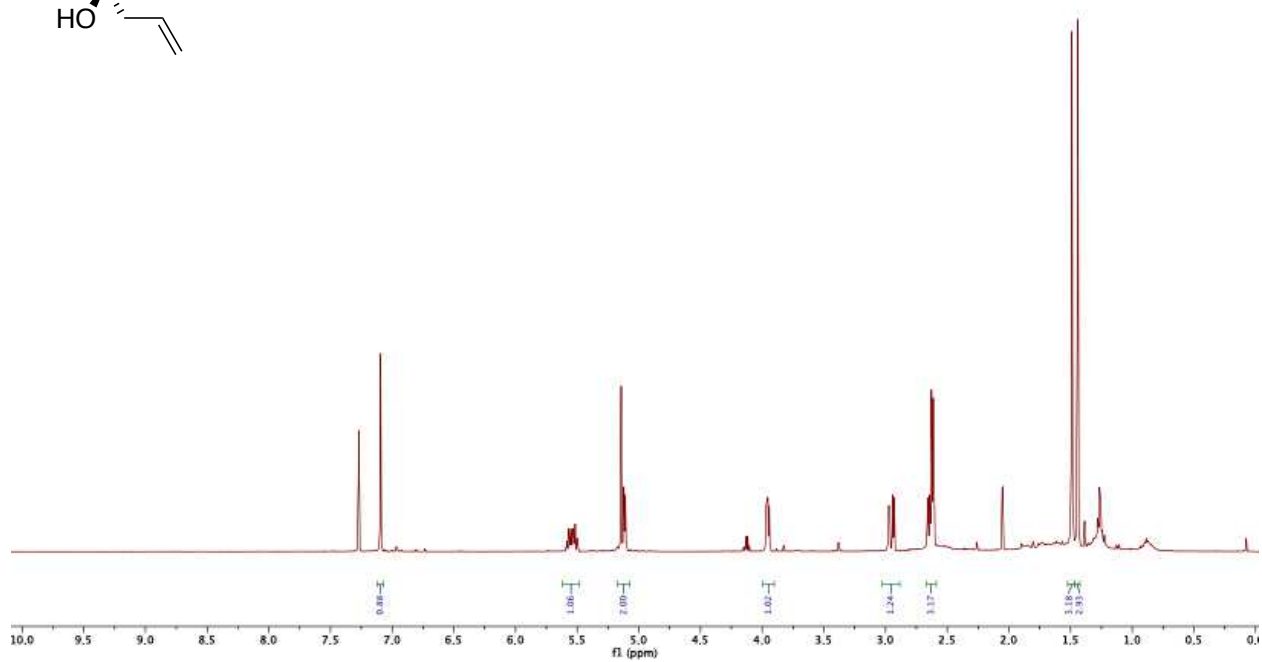
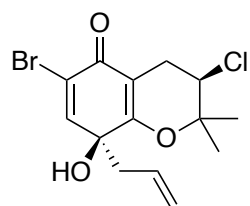




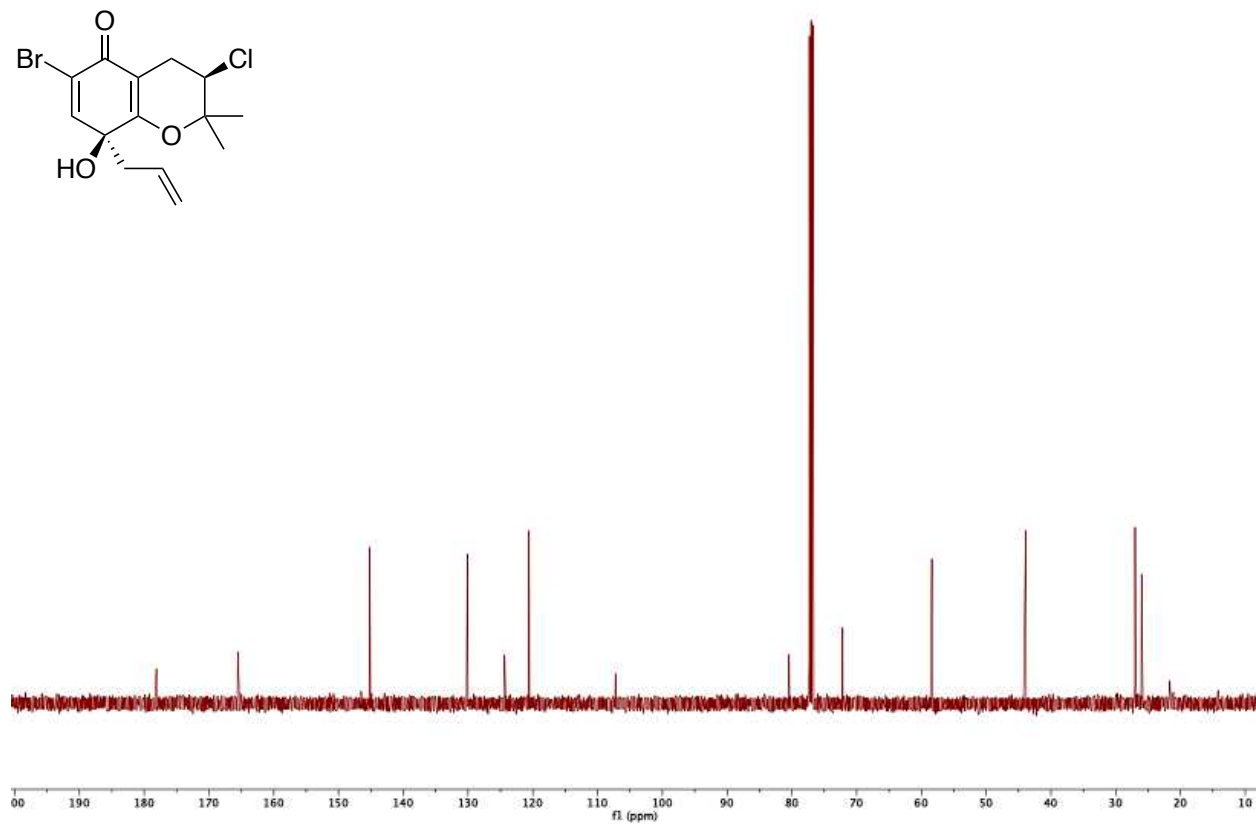
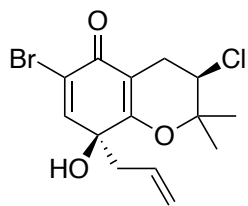


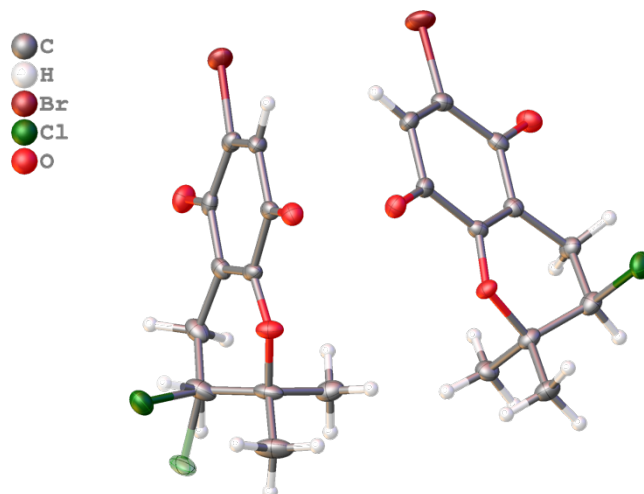
ST-05-69-Pure_CARBON_01





ST-05-531-Pure_CARBON_01





Experimental. Single yellow needle crystals of **II-85** used as received. A suitable crystal with dimensions $0.19 \times 0.13 \times 0.09 \text{ mm}^3$ was selected and mounted on a nylon loop with paratone oil on a XtaLAB Synergy, Dualflex, HyPix diffractometer. The crystal was kept at a steady $T = 99.99(10) \text{ K}$ during data collection. The structure was solved with the ShelXT (Sheldrick, G.M. (2015). Acta Cryst. A71, 3-8) solution program using dual methods and by using Olex2 (Dolomanov et al., 2009) as the graphical interface. The model was refined with ShelXL (Sheldrick, Acta Cryst. A64 2008, 112-122) using full matrix least squares minimisation on F^2 .

Crystal Data. $\text{C}_{11}\text{H}_{10}\text{BrClO}_3$, $M_r = 305.55$, orthorhombic, $P2_12_12$ (No. 18), $a = 21.5399(2) \text{ \AA}$, $b = 19.4791(2) \text{ \AA}$, $c = 5.46090(10) \text{ \AA}$, $\alpha = \beta = \gamma = 90^\circ$, $V = 2291.27(5) \text{ \AA}^3$, $T = 99.99(10) \text{ K}$, $Z = 8$, $Z' = 2$, $\mu(\text{Cu K}\alpha) = 6.965$, 13838 reflections measured, 4631 unique ($R_{\text{int}} = 0.0480$) which were used in all calculations. The final wR_2 was 0.0822 (all data) and R_1 was 0.0322 ($I \geq 2 \sigma(I)$).

Compound	II-85
Formula	C ₁₁ H ₁₀ BrClO ₃
CCDC	2017069
<i>D</i> _{calc.} /g cm ⁻³	1.772
<i>μ</i> /mm ⁻¹	6.965
Formula Weight	305.55
Colour	yellow
Shape	needle
Size/mm ³	0.19×0.13×0.09
<i>T</i> /K	99.99(10)
Crystal System	orthorhombic
Flack Parameter	-0.007(12)
Hoofst Parameter	0.013(11)
Space Group	<i>P</i> 2 ₁ 2 ₁ 2
<i>a</i> /Å	21.5399(2)
<i>b</i> /Å	19.4791(2)
<i>c</i> /Å	5.46090(10)
<i>α</i> /°	90
<i>β</i> /°	90
<i>γ</i> /°	90
<i>V</i> /Å ³	2291.27(5)
<i>Z</i>	8
<i>Z</i> '	2
Wavelength/Å	1.54184
Radiation type	Cu K _α
<i>θ</i> _{min} /°	3.059
<i>θ</i> _{max} /°	76.829
Measured Refl's.	13838
Indep't Refl's	4631
Refl's I≥2 <i>σ</i> (I)	4483
<i>R</i> _{int}	0.0480
Parameters	303
Restraints	0
Largest Peak	0.516
Deepest Hole	-0.593
GooF	1.065
<i>wR</i> ₂ (all data)	0.0822
<i>wR</i> ₂	0.0814
<i>R</i> ₁ (all data)	0.0332
<i>R</i> ₁	0.0322

Structure Quality Indicators

Reflections: d min (Cu) 0.79 | $I/\sigma(I)$ 21.9 | Rint 4.80% | complete 100% (IUCr) 100%

Refinement: Shift 0.001 | Max Peak 0.5 | Min Peak -0.6 | Goof 1.065 | Flack 0.007(12)

A yellow needle-shaped crystal with dimensions 0.19×0.13×0.09 mm³ was mounted on a nylon loop with paratone oil. Data were collected using a XtaLAB Synergy, Dualflex, HyPix diffractometer equipped with an Oxford Cryosystems low-temperature device, operating at $T = 99.99(10)$ K.

Data were measured using w scans of 0.5° per frame for 0.1 s using Cu K $_{\alpha}$ radiation (micro-focus sealed X-ray tube, 50 kV, 1 mA). The total number of runs and images was based on the strategy calculation from the program CrysAlisPro (Rigaku, V1.171.40.81a, 2020). The actually achieved resolution was $\theta = 76.829$.

Cell parameters were retrieved using the CrysAlisPro (Rigaku, V1.171.40.81a, 2020) software and refined using CrysAlisPro (Rigaku, V1.171.40.81a, 2020) on 8719 reflections, 63 % of the observed reflections. Data reduction was performed using the CrysAlisPro (Rigaku, V1.171.40.81a, 2020) software which corrects for Lorentz polarization. The final completeness is 100.00 out to 76.829 in θ CrysAlisPro 1.171.40.81a (Rigaku Oxford Diffraction, 2020) Numerical absorption correction based on gaussian integration over a multifaceted crystal model Empirical absorption correction using spherical harmonics, implemented in SCALE3 ABSPACK scaling algorithm.

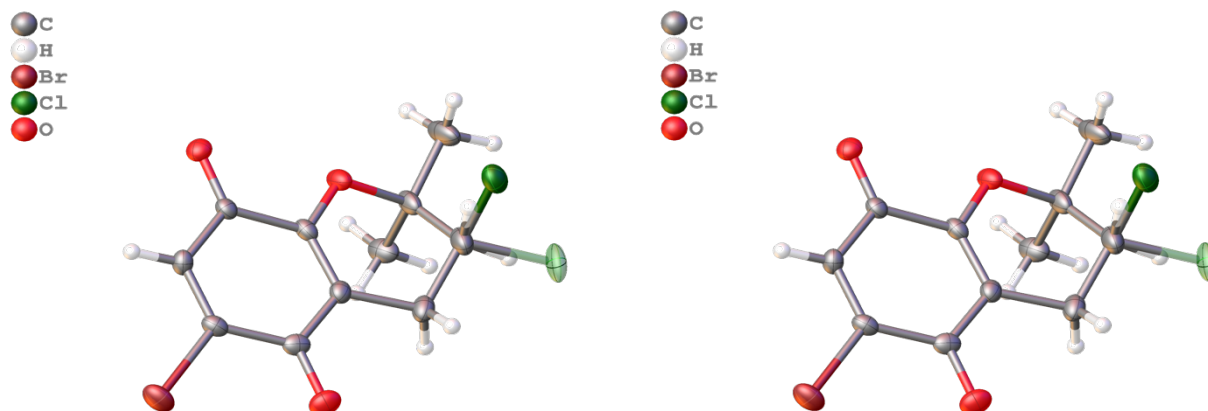
The structure was solved in the space group $P2_12_12$ (# 18) by using dual methods

using the ShelXT (Sheldrick, G.M. (2015). Acta Cryst. A71, 3-8) structure solution program. The structure was refined by Least Squares using version 2014/6 of XL (Sheldrick, 2008) incorporated in Olex2 (Dolomanov et al., 2009). All non-hydrogen atoms were refined anisotropically. Hydrogen atom positions were calculated geometrically and refined using the riding model, except for the hydrogen atom on the non-carbon atom(s) which were found by difference Fourier methods and refined isotropically when data permits.

CCDC 2017069 contains the supplementary crystallographic data for this paper. The data can be obtained free of charge from The Cambridge Crystallographic Data Centre via www.ccdc.cam.ac.uk/structures.

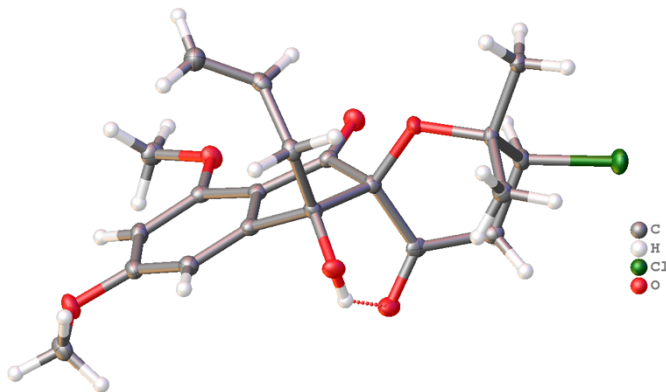
The value of Z' is 2. This means that there are two independent molecules in the asymmetric unit.

The Flack parameter was refined to -0.007(12). Determination of absolute structure using Bayesian statistics on Bijvoet differences using the Olex2 results in 0.013(11). Note: The Flack parameter is used to determine chirality of the crystal studied, the value should be near 0, a value of 1 means that the stereochemistry is wrong, and the model should be inverted. A value of 0.5 means that the crystal consists of a racemic mixture of the two enantiomers.



Reflection Statistics

Total reflections (after filtering)	13885	Unique reflections	4631
Completeness	0.959	Mean I/σ	16.4
hkl_{\max} collected	(25, 24, 6)	hkl_{\min} collected	(-27, -18, -6)
hkl_{\max} used	(27, 24, 6)	hkl_{\min} used	(-26, 0, 0)
Lim d_{\max} collected	100.0	Lim d_{\min} collected	0.77
d_{\max} used	14.45	d_{\min} used	0.79
Friedel pairs	1441	Friedel pairs merged	0
Inconsistent equivalents	0	R_{int}	0.048
R_{sigma}	0.0457	Intensity transformed	0
Omitted reflections	0	Omitted by user (OMIT hkl)	0
Multiplicity	(4109, 1669, 700, 278, 72, 28, 3)	Maximum multiplicity	12
Removed systematic absences	635	Filtered off (Shel/OMIT)	0



Experimental. Single colourless irregular-shaped crystals of **II-141** used as received. A suitable crystal with dimensions $0.24 \times 0.16 \times 0.08 \text{ mm}^3$ was selected and mounted on a nylon loop with paratone oil on a XtaLAB Synergy, Dualflex, HyPix diffractometer. The crystal was kept at a steady $T = 100.00(10) \text{ K}$ during data collection. The structure was solved with the **ShelXS** (Sheldrick, 2008) solution program using direct methods and by using **Olex2** 1.3-alpha (Dolomanov et al., 2009) as the graphical interface. The model was refined with **ShelXL** 2018/3 (Sheldrick, 2015) using full matrix least squares minimisation on F^2 .

Crystal Data. $\text{C}_{20}\text{H}_{23}\text{ClO}_6$, $M_r = 394.83$, orthorhombic, $Pna2_1$ (No. 33), $a = 11.68046(15) \text{ \AA}$, $b = 12.09655(16) \text{ \AA}$, $c = 13.05345(15) \text{ \AA}$, $\alpha = \beta = \gamma = 90^\circ$, $V = 1844.37(4) \text{ \AA}^3$, $T = 100.00(10) \text{ K}$, $Z = 4$, $Z' = 1$, $\mu(\text{Cu } K\alpha) = 2.142$, 10573 reflections measured, 2681 unique ($R_{\text{int}} = 0.0416$) which were used in all calculations. The final wR_2 was 0.0718 (all data) and R_1 was 0.0287 ($I \geq 2 \sigma(I)$).

Compound	II-141
Formula	C ₂₀ H ₂₃ Cl ₆
CCDC	2071120
<i>D</i> _{calc.} /g cm ⁻³	1.422
μ /mm ⁻¹	2.142
Formula Weight	394.83
Colour	colourless
Shape	irregular-shaped
Size/mm ³	0.24×0.16×0.08
<i>T</i> /K	100.00(10)
Crystal System	orthorhombic
Flack Parameter	-0.014(14)
Hooft Parameter	-0.017(13)
Space Group	<i>Pna</i> 2 ₁
<i>a</i> /Å	11.68046(15)
<i>b</i> /Å	12.09655(16)
<i>c</i> /Å	13.05345(15)
α [°]	90
β [°]	90
γ [°]	90
<i>V</i> /Å ³	1844.37(4)
<i>Z</i>	4
<i>Z'</i>	1
Wavelength/Å	1.54184
Radiation type	Cu K α
θ _{min} [°]	4.985
θ _{max} [°]	76.965
Measured Refl's.	10573
Indep't Refl's	2681
Refl's $I \geq 2 \sigma(I)$	2613
<i>R</i> _{int}	0.0416
Parameters	252
Restraints	1
Largest Peak	0.198
Deepest Hole	-0.227
Goof	1.021
<i>wR</i> ₂ (all data)	0.0718
<i>wR</i> ₂	0.0711
<i>R</i> ₁ (all data)	0.0295
<i>R</i> ₁	0.0287

Structure Quality Indicators

Reflections:	d min (Cu λ) 2 θ =153.9°	0.79	<i>I</i> / σ (<i>I</i>)	25.5	<i>R</i> _{int}	4.16%	CAP 133.9° 94% to 153.9°	100		
Refinement:	Shift	0.000	Max Peak	0.2	Min Peak	-0.2	Goof	1.021	Flack	-0.014(14)

A colorless irregular-shaped-shaped crystal with dimensions 0.24×0.16×0.08 mm³

was mounted on a nylon loop with paratone oil. Data were collected using a XtaLAB Synergy, Dualflex, HyPix diffractometer equipped with an Oxford Cryosystems low-temperature device, operating at $T = 100.00(10)$ K.

Data were measured using w scans of $^\circ$ per frame for s using Cu K_α radiation (micro-focus sealed X-ray tube, 50 kV, 1 mA). The total number of runs and images was based on the strategy calculation from the program **CrysAlisPro** (Rigaku, V1.171.41.100a, 2021). The actually achieved resolution was $Q = 76.965$.

Cell parameters were retrieved using the **CrysAlisPro** (Rigaku, V1.171.41.100a, 2021) software and refined using **CrysAlisPro** (Rigaku, V1.171.41.100a, 2021) on 7885 reflections, 75 % of the observed reflections. Data reduction was performed using the **CrysAlisPro** (Rigaku, V1.171.41.100a, 2021) software which corrects for Lorentz polarization. The final completeness is 100.00 out to 76.965 in Q CrysAlisPro 1.171.41.100a (Rigaku Oxford Diffraction, 2021) Numerical absorption correction based on gaussian integration over a multifaceted crystal model Empirical absorption correction using spherical harmonics, implemented in SCALE3 ABSPACK scaling algorithm.

The structure was solved in the space group $Pna2_1$ (# 33) by using direct methods using the ShelXS (Sheldrick, 2008) structure solution program. The structure was refined by Least Squares using version 2018/2 of XL (Sheldrick, 2008) incorporated in Olex2 (Dolomanov et al., 2009). All non-hydrogen atoms were refined anisotropically. Hydrogen atom positions were calculated geometrically and refined using the riding model, except for the hydrogen atom on the non-carbon atom(s) which were found by difference Fourier

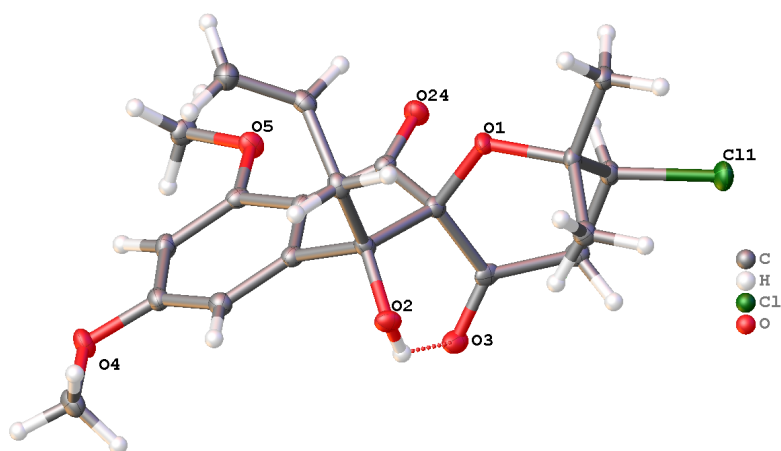
methods and refined isotropically when data permits.

CCDC 2071120 contains the supplementary crystallographic data for this paper.

The data can be obtained free of charge from The Cambridge Crystallographic Data Centre via www.ccdc.cam.ac.uk/structures.

There is a single molecule in the asymmetric unit, which is represented by the reported sum formula. In other words: Z is 4 and Z' is 1.

The Flack parameter was refined to -0.014(14). Determination of absolute structure using Bayesian statistics on Bijvoet differences using the Olex2 results in -0.017(13). Note: The Flack parameter is used to determine chirality of the crystal studied, the value should be near 0, a value of 1 means that the stereochemistry is wrong, and the model should be inverted. A value of 0.5 means that the crystal consists of a racemic mixture of the two enantiomers.



Reflection Statistics

Total reflections (after filtering)	11208	Unique reflections	2681
Completeness	0.687	Mean I/σ	21.86
hkl_{\max} collected	(14, 14, 7)	hkl_{\min} collected	(-14, -14, -16)
hkl_{\max} used	(14, 14, 7)	hkl_{\min} used	(0, 0, -16)
Lim d_{\max} collected	100.0	Lim d_{\min} collected	0.77
d_{\max} used	13.05	d_{\min} used	0.79
Friedel pairs	1004	Friedel pairs merged	0
Inconsistent equivalents	0	R_{int}	0.0416
R_{sigma}	0.0391	Intensity transformed	0
Omitted reflections	0	Omitted by user (OMIT hkl)	0
Multiplicity	(4109, 1669, 700, 278, 72, 28, 3)	Maximum multiplicity	20
Removed systematic absences	635	Filtered off (Shel/OMIT)	0

REFERENCES

REFERENCES

1. Eliel, E. L.; Wilen, S. H.; Mander, L. N., *Stereochemistry of organic compounds*. Wiley-India: New Delhi, 2010.
2. Cahn, R. S.; Ingold, C.; Prelog, V., Specification of Molecular Chirality. *Angew. Chem. Int. Edit.* **1966**, *5*, 385.
3. Lu, H.; Kobayashi, N., Optically Active Porphyrin and Phthalocyanine Systems. *Chem. Rev.* **2016**, *116*, 6184.
4. Nakanishi, K.; Berova, N.; Woody, R. W., *Circular dichroism : principles and applications*. VCH: New York, 2000.
5. Kelvin, W. T.; Kargon, R.; Achinstein, P., *Kelvin's Baltimore lectures and modern theoretical physics historical and philosophical perspectives*. MIT Press: Cambridge, Mass.; London, 1987.
6. Flack, H. D.; Bernardinelli, G., The use of X-ray crystallography to determine absolute configuration. *Chirality* **2008**, *20*, 681.
7. Dale, J. A.; Mosher, H. S., Nuclear Magnetic Resonance Nonequivalence of Diastereomeric Esters of Alpha-Substituted Phenylacetic Acids for Determination of Stereochemical Purity. *J. Am. Chem. Soc.* **1968**, *90*, 3732.
8. Dale, J. A.; Dull, D. L.; Mosher, H. S., Alpha-Methoxy-Alpha-Trifluoromethylphenylacetic Acid, a Versatile Reagent for Determination of Enantiomeric Composition of Alcohols and Amines. *J. Org. Chem.* **1969**, *34*, 2543.
9. Dale, J. A.; Mosher, H. S., Nuclear Magnetic-Resonance Enantiomer Reagents - Configurational Correlations Via Nuclear Magnetic-Resonance Chemical-Shifts of Diastereomeric Mandelate, O-Methylmandelate, and Alpha-Methoxy-Alpha-Trifluoromethylphenylacetate (Mtpa) Esters. *J. Am. Chem. Soc.* **1973**, *95*, 512.
10. Seco, J. M.; Quinoa, E.; Riguera, R., The assignment of absolute configuration by NMR. *Chem. Rev.* **2004**, *104*, 17.
11. Leiro, V.; Freire, F.; Quinoa, E.; Riguera, R., Absolute configuration of amino alcohols by H-1-NMR. *Chem. Commun.* **2005**, (44), 5554.

12. Freire, F.; Calderon, F.; Seco, J. M.; Fernandez-Mayoralas, A.; Quinoa, E.; Riguera, R., Relative and absolute stereochemistry of secondary/secondary diols: Low-temperature H-1 NMR of their bis-MPA esters. *J. Org. Chem.* **2007**, *72*, 2297.
13. Freire, F.; Seco, J. M.; Quinoa, E.; Riguera, R., Challenging the absence of observable hydrogens in the assignment of absolute configurations by NMR: application to chiral primary alcohols. *Chem. Commun.* **2007**, 1456.
14. Sullivan, G. R.; Dale, J. A.; Mosher, H. S., Correlation of Configuration and F-19 Chemical-Shifts of Alpha-Methoxy-Alpha-Trifluoromethylphenylacetate Derivatives. *J. Org. Chem.* **1973**, *38*, 2143.
15. Seco, J. M.; Quinoa, E.; Riguera, R., Assignment of the absolute configuration of polyfunctional compounds by NMR using chiral derivatizing agents. *Chem. Rev.* **2012**, *112*, 4603.
16. Ohtani, I.; Kusumi, T.; Kashman, Y.; Kakisawa, H., High-Field Ft Nmr Application of Mosher Method - the Absolute-Configurations of Marine Terpenoids. *J. Am. Chem. Soc.* **1991**, *113*, 4092.
17. Hoye, T. R.; Jeffrey, C. S.; Shao, F., Mosher ester analysis for the determination of absolute configuration of stereogenic (chiral) carbinol carbons. *Nat. Protoc.* **2007**, *2*, 2451.
18. Kobayashi, N.; Muranaka, A.; Mack, J., *Circular Dichroism and Magnetic Circular Dichroism Spectroscopy for Organic Chemists*. Royal Society of Chemistry: Cambridge, 2011.
19. Solomons, T. W. G., *Organic chemistry*. Wiley: New York; Chichester, 1978.
20. Velluz, L.; Grosjean, M.; Legrand, M.; MacCordick, J., *Optical circular Dichroism*. Verl. Chemie ; Acad. Pr.: Weinheim/Bergstr.; New York, 1965.
21. Lambert, J. B., *Organic structural spectroscopy*. Prentice Hall: Upper Saddle River, N.J., 1998.
22. Hoffmann, S. V.; Fano, M.; van de Weert, M., Circular Dichroism Spectroscopy for Structural Characterization of Proteins. In *Analytical Techniques in the Pharmaceutical Sciences*, Müllertz, A.; Perrie, Y.; Rades, T., Eds. Springer New York: New York, NY, 2016; pp 223-251.
23. Kondru, R. K.; Wipf, P.; Beratan, D. N., Atomic contributions to the optical rotation angle as a quantitative probe of molecular chirality. *Science* **1998**, *282*, 2247.

24. Devlin, F. J.; Stephens, P. J.; Besse, P., Are the absolute configurations of 2-(1-hydroxyethyl)-chromen-4-one and its 6-bromo derivative determined by X-ray crystallography correct? A vibrational circular dichroism study of their acetate derivatives. *Tetrahedron-Asymmetry* **2005**, *16*, 1557.
25. Devlin, F. J.; Stephens, P. J.; Cheeseman, J. R.; Frisch, M. J., Prediction of vibrational circular dichroism spectra using density functional theory: Camphor and fenchone. *J. Am. Chem. Soc.* **1996**, *118*, 6327.
26. Stephens, P. J.; Aamouche, A.; Devlin, F. J.; Superchi, S.; Donnoli, M. I.; Rosini, C., Determination of absolute configuration using vibrational circular dichroism spectroscopy: The chiral sulfoxide 1-(2-methylnaphthyl) methyl sulfoxide. *J. Org. Chem.* **2001**, *66*, 3671.
27. Stephens, P. J.; Devlin, F. J.; Cheeseman, J. R.; Frisch, M. J., Calculation of Optical Rotation Using Density Functional Theory. *J. Phys. Chem. A* **2001**, *105*, 5356.
28. Ribe, S. K., R.K.; Beratan, D.N.; Wipf, P. , Optical rotation computation, total synthesis, and stereochemistry assignment of the marine natural product pitiamide A. **2000**.
29. Harada, N.; Nakanishi, K., *Circular dichroic spectroscopy : exciton coupling in organic stereochemistry*. Univ. Science Books u.a.: Mill Valley u.a., 1983.
30. Chen, S. M. L.; Harada, N.; Nakanishi, K., Long-Range Effect in Exciton Chirality Method. *J. Am. Chem. Soc.* **1974**, *96*, 7352.
31. Harada, N.; Nakanishi, K., Exciton Chirality Method and Its Application to Configurational and Conformational Studies of Natural-Products. *Acc. Chem. Res.* **1972**, *5*, 257.
32. Nakanishi, K.; Kuroyanagi, M.; Nambu, H.; Oltz, E. M.; Takeda, R.; Verdine, G. L.; Zask, A., Recent Applications of Circular-Dichroism to Structural Problems, Especially Oligosaccharide Structures. *Pure. Appl. Chem.* **1984**, *56*, 1031.
33. Harada, N.; Nakanishi, K., A Method for Determining Chiralities of Optically Active Glycols. *J. Am. Chem. Soc.* **1969**, *91*, 3989.
34. Berova, N., *Comprehensive chiroptical spectroscopy. 2 2*. Wiley-Blackwell: Hoboken, N.J., 2012.
35. Pasini, D.; Nitti, A., Recent Advances in Sensing Using Atropoisomeric Molecular Receptors. *Chirality* **2016**, *28*, 116.

36. Wolf, C.; Bentley, K. W., Chirality sensing using stereodynamic probes with distinct electronic circular dichroism output. *Chem. Soc. Rev.* **2013**, *42*, 5408.
37. You, L.; Zha, D.; Anslyn, E. V., Recent Advances in Supramolecular Analytical Chemistry Using Optical Sensing. *Chem. Rev.* **2015**, *115*, 7840.
38. Berova, N.; Di Bari, L.; Pescitelli, G., Application of electronic circular dichroism in configurational and conformational analysis of organic compounds. *Chem. Soc. Rev.* **2007**, *36*, 914.
39. Di Bari, L.; Lelli, M.; Pintacuda, G.; Salvadori, P., Yb(fod)₃ in the spectroscopic determination of the configuration of chiral diols: a survey of the lanthanide diketonate method. *Chirality* **2002**, *14*, 265.
40. Di Bari, L.; Pescitelli, G.; Pratelli, C.; Pini, D.; Salvadori, P., Determination of absolute configuration of acyclic 1,2-diols with Mo-2(OAc)₄. 1. Snatzke's method revisited. *J. Org. Chem.* **2001**, *66*, 4819.
41. Dillon, J.; Nakanishi, K., Absolute configurational studies of vicinal glycols and amino alcohols. I. With ni(acac)₂. *J. Am. Chem. Soc.* **1975**, *97*, 5409.
42. Dillon, J.; Nakanishi, K., Absolute configurational studies of vicinal glycols and amino alcohols. II. With Pr(dpm)₃. *J. Am. Chem. Soc.* **1975**, *97*, 5417.
43. Frelek, J.; Geiger, M.; Voelter, W., Transition metal complexes as auxiliary chromophores in chiroptical studies on carbohydrates. *Curr. Org. Chem.* **1999**, *3*, 117.
44. Superchi, S.; Casarini, D.; Laurita, A.; Bavoso, A.; Rosini, C., Induction of a preferred twist in a biphenyl core by stereogenic centers: A novel approach to the absolute configuration of 1,2- and 1,3-diols. *Angew. Chem. Int. Edit.* **2001**, *40*, 451.
45. Superchi, S.; Casarini, D.; Summa, C.; Rosini, C., A general and nonempirical approach to the determination of the absolute configuration of 1-aryl-1,2-diols. *J. Org. Chem.* **2004**, *69*, 1685.
46. Tartaglia, S.; Pace, F.; Scafato, P.; Rosini, C., A new case of induced helical chirality in a bichromophoric system: absolute configuration of transparent and flexible diols from the analysis of the electronic circular dichroism spectra of the corresponding di(1-naphthyl)ketals. *Org. Lett.* **2008**, *10*, 3421.
47. Li, X. Y.; Tanasova, M.; Vasileiou, C.; Borhan, B., Fluorinated porphyrin tweezer: A powerful reporter of absolute configuration for erythro and threo diols, amino alcohols, and diamines. *J. Am. Chem. Soc.* **2008**, *130*, 1885.

48. Zhang, J.; Gholami, H.; Ding, X.; Chun, M.; Vasileiou, C.; Nehira, T.; Borhan, B., Computationally Aided Absolute Stereochemical Determination of Enantioenriched Amines. *Org. Lett.* **2017**, *19*, 1362.
49. Zhang, J.; Sheng, W.; Gholami, H.; Nehira, T.; Borhan, B., Di(1-naphthyl) methanol ester of carboxylic acids for absolute stereochemical determination. *Chirality* **2018**, *30*, 141.
50. Superchi, S.; Donnoli, M. I.; Rosini, C., Determination of the absolute configuration of 1-arylethane-1,2-diols by a nonempirical analysis of the CD spectra of their 4-biphenylboronates. *Org. Lett.* **1999**, *1*, 2093.
51. Gupta, A. K.; Yin, X. P.; Mukherjee, M.; Desai, A. A.; Mohammadlou, A.; Jurewicz, K.; Wulff, W. D., Catalytic Asymmetric Epoxidation of Aldehydes with Two VANOL-Derived Chiral Borate Catalysts. *Angew. Chem. Int. Edit.* **2019**, *58*, 3361.
52. Nöth, H.; Wrackmeyer, B. In *Tables of ¹¹B-NMR Data*, Berlin, Heidelberg, Springer Berlin Heidelberg: Berlin, Heidelberg, 1978; pp 109-429.
53. Richard, J.; Birepinte, M.; Charbonnier, J. B.; Liautard, V.; Pinet, S.; Pucheault, M., Borinic Acids via Direct Arylation of Amine-Borane Complexes: An Air- and Water - Stable Boron Source. *Synthesis-Stuttgart* **2017**, *49*, 736.
54. Landry, M. L.; Burns, N. Z., Catalytic Enantioselective Dihalogenation in Total Synthesis. *Acc. Chem. Res.* **2018**, *51*, 1260.
55. Chung, W. J.; Vanderwal, C. D., Stereoselective Halogenation in Natural Product Synthesis. *Angew. Chem. Int. Ed. Eng.* **2016**, *55*, 4396.
56. Snyder, S. A.; Tang, Z. Y.; Gupta, R., Enantioselective total synthesis of (-)-napyradiomycin A1 via asymmetric chlorination of an isolated olefin. *J. Am. Chem. Soc.* **2009**, *131*, 5744.
57. McKinnie, S. M. K.; Miles, Z. D.; Jordan, P. A.; Awakawa, T.; Pepper, H. P.; Murray, L. A. M.; George, J. H.; Moore, B. S., Total Enzyme Syntheses of Napyradiomycins A1 and B1. *J. Am. Chem. Soc.* **2018**, *140*, 17840.
58. Tatsuta, K.; Tanaka, Y.; Kojima, M.; Ikegami, H., The first total synthesis of (+/-)-napyradiomycin A1. *Chem. Lett.* **2002**, 14.
59. Landry, M. L.; McKenna, G. M.; Burns, N. Z., Enantioselective Synthesis of Azamerone. *J. Am. Chem. Soc.* **2019**, *141*, 2867.

60. Boger, D. L.; Brotherton, C. E., Total Syntheses of Azafluoranthene Alkaloids - Rufescine and Imeluteine. *J. Org. Chem.* **1984**, *49*, 4050.
61. Jones, S. B.; Simmons, B.; Mastracchio, A.; MacMillan, D. W. C., Collective synthesis of natural products by means of organocascade catalysis. *Nature* **2011**, *475*, 183.
62. Han, J. C.; Li, C. C., Collective Synthesis of Natural Products by Using Metathesis Cascade Reactions. *Synlett* **2015**, *26*, 1289.
63. Serba, C.; Winssinger, N., Following the Lead from Nature: Divergent Pathways in Natural Product Synthesis and Diversity-Oriented Synthesis. *Eur. J. Org. Chem.* **2013**, *2013*, 4195.
64. Anagnostaki, E. E.; Zografos, A. L., "Common synthetic scaffolds" in the synthesis of structurally diverse natural products. *Chem. Soc. Rev.* **2012**, *41*, 5613.
65. Shimokawa, J., Divergent strategy in natural product total synthesis. *Tetrahedron Lett.* **2014**, *55*, 6156.
66. Chen, K.; Baran, P. S., Total synthesis of eudesmane terpenes by site-selective C-H oxidations. *Nature* **2009**, *459*, 824.
67. Pan, G. J.; Williams, R. M., Unified Total Syntheses of Fawcettimine Class Alkaloids: Fawcettimine, Fawcettidine, Lycoflexine, and Lycoposerramine B. *J. Org. Chem.* **2012**, *77*, 4801.
68. Lebold, T. P.; Kerr, M. A., Total synthesis of eustifolines A-D and glycomaurrol via a divergent Diels-Alder strategy. *Org. Lett.* **2007**, *9*, 1883.
69. Shiomi, K.; Nakamura, H.; Inuma, H.; Naganawa, H.; Isshiki, K.; Takeuchi, T.; Umezawa, H.; Iitaka, Y., Structures of new antibiotics napyradiomycins. *J. Antibiot (Tokyo)* **1986**, *39*, 494.
70. Carretero-Molina, D.; Ortiz-Lopez, F. J.; Martin, J.; Oves-Costales, D.; Diaz, C.; de la Cruz, M.; Cautain, B.; Vicente, F.; Genilloud, O.; Reyes, F., New Napyradiomycin Analogues from *Streptomyces* sp. Strain CA-271078. *Mar. Drugs* **2020**, *18*, 1.
71. Garzan, A.; Jaganathan, A.; Marzijarani, N. S.; Yousefi, R.; Whitehead, D. C.; Jackson, J. E.; Borhan, B., Solvent-Dependent Enantiodivergence in the Chlorocyclization of Unsaturated Carbamates. *Chem. Eur. J.* **2013**, *19*, 9015.

72. Jaganathan, A.; Garzan, A.; Whitehead, D. C.; Staples, R. J.; Borhan, B., A Catalytic Asymmetric Chlorocyclization of Unsaturated Amides. *Angew. Chem. Int. Edit.* **2011**, *50*, 2593.
73. Whitehead, D. C.; Yousefi, R.; Jaganathan, A.; Borhan, B., An Organocatalytic Asymmetric Chlorolactonization. *J. Am. Chem. Soc.* **2010**, *132*, 3298.
74. Teitelbaum, A. M.; Scian, M.; Nelson, W. L.; Rettie, A. E., Efficient Syntheses of Vitamin K Chain-Shortened Acid Metabolites. *Synthesis-Stuttgart* **2015**, *47*, 944.
75. Topczewski, J. J.; Neighbors, J. D.; Wiemer, D. F., Total Synthesis of (+)-Schweinfurthins B and E. *J. Org. Chem.* **2009**, *74*, 6965.
76. Epstein, W. W.; Klobus, M. A.; Edison, A. S., Irregular Monoterpene Constituents of *Artemisia-Tridentata-Cana* - the Isolation, Characterization, and Synthesis of 2 New Chrysanthemyl Derivatives. *J. Org. Chem.* **1991**, *56*, 4451.
77. Kitamura, M.; Tashiro, N.; Sakata, R.; Okauchi, T., Synthesis of Diazonaphthoquinones from Naphthols by Diazo-Transfer Reaction with 2-Azido-1,3-dimethylimidazolium Chloride. *Synlett* **2010**, 2503.
78. Snyder, S. A.; Treitler, D. S.; Brucks, A. P., Simple Reagents for Direct Halonium-Induced Polyene Cyclizations. *J. Am. Chem. Soc.* **2010**, *132*, 14303.
79. Jena, B. K.; Reddy, A. V. V.; Mohapatra, D. K., Total Synthesis of Sacrolide A by Following a Nozaki-Hiyama-Kishi Macrocyclization Strategy. *Asian J. Org. Chem.* **2016**, *5*, 340.
80. Ueda, M.; Yamaura, M.; Ikeda, Y.; Suzuki, Y.; Yoshizato, K.; Hayakawa, I.; Kigoshi, H., Total synthesis and cytotoxicity of haterumalides NA and B and their artificial analogues. *J. Org. Chem.* **2009**, *74*, 3370.
81. Schomaker, J. M.; Borhan, B., Total synthesis of haterumalides NA and NC via a chromium-mediated macrocyclization. *J. Am. Chem. Soc.* **2008**, *130*, 12228.
82. Simmons, R. L.; Yu, R. T.; Myers, A. G., Storable Arylpalladium(II) Reagents for Alkene Labeling in Aqueous Media. *J. Am. Chem. Soc.* **2011**, *133*, 15870.
83. Yonezawa, S.; Komurasaki, T.; Kawada, K.; Tsuru, T.; Fuji, M.; Kugimiya, A.; Haga, N.; Mitsumori, S.; Inagaki, M.; Nakatani, T.; Tamura, Y.; Takechi, S.; Taishi, T.; Ohtani, M., Total synthesis of terpenin, a novel immunosuppressive p-terphenyl derivative. *J. Org. Chem.* **1998**, *63*, 5831.

84. Tisdale, E. J.; Kochman, D. A.; Theodorakis, E. A., Total synthesis of atroviridin. *Tetrahedron Lett.* **2003**, *44*, 3281.
85. Bakhoda, A.; Okoromoba, O. E.; Greene, C.; Boroujeni, M. R.; Bertke, J. A.; Warren, T. H., Three-Coordinate Copper(II) Alkynyl Complex in C-C Bond Formation: The Sesquicentennial of the Glaser Coupling. *J. Am. Chem. Soc.* **2020**, *142*, 18483.
86. Tischer, S.; Metz, P., Selective C-6 prenylation of flavonoids via europium(III)-catalyzed Claisen rearrangement and cross-metathesis. *Adv. Synth. Catal.* **2007**, *349*, 147.
87. Trivedi, R.; Tunge, J. A., Regioselective Iron-Catalyzed Decarboxylative Allylic Etherification. *Org. Lett.* **2009**, *11*, 5650.
88. Larock, R. C.; Lee, N. H., Synthesis of Allylic Aryl Ethers Via Palladium-Catalyzed Decarboxylation of Allylic Aryl Carbonates. *Tetrahedron Lett.* **1991**, *32*, 6315.
89. Weaver, J. D.; Recio, A.; Grenning, A. J.; Tunge, J. A., Transition Metal-Catalyzed Decarboxylative Allylation and Benzylolation Reactions. *Chem. Rev.* **2011**, *111*, 1846.
90. Nicolaou, K. C.; Hale, C. R.; Nilewski, C.; Ioannidou, H. A.; ElMarrouni, A.; Nilewski, L. G.; Beabout, K.; Wang, T. T.; Shamoo, Y., Total synthesis of viridicatumtoxin B and analogues thereof: strategy evolution, structural revision, and biological evaluation. *J. Am. Chem. Soc.* **2014**, *136*, 12137.
91. Nakagawa, O.; Shimoda, K.; Izumi, S.; Hirata, T., Facile syntheses of [8,9-H-2(2)]- and [8-H-2]-digeranyl. *J. Labelled. Compd. Rad.* **2000**, *43*, 1301.
92. Komeyama, K.; Itai, Y.; Takaki, K., Practical Stannylation of Allyl Acetates Catalyzed by Nickel with Bu₃SnOMe. *Chemistry* **2016**, *22*, 9130.
93. Lipshutz, B. H.; Ellsworth, E. L.; Dimock, S. H.; Smith, R. A. J., New Methodology for Conjugate Additions of Allylic Ligands to Alpha,Beta-Unsaturated Ketones - Synthetic and Spectroscopic Studies. *J. Am. Chem. Soc.* **1990**, *112*, 4404.
94. Araki, S.; Shimizu, T.; Johar, P. S.; Jin, S. J.; Butsugan, Y., Preparation and Some Reactions of Allylic Indium Reagents. *J. Org. Chem.* **1991**, *56*, 2538.
95. Takeya, T.; Kajiyama, M.; Nakamura, C.; Tobinaga, S., Total synthesis of (+/-)-plumbazeylanone, a naphthoquinone trimer from *Plumbago zeylanica*. *Chem. Pharm. Bull.* **1999**, *47*, 209.

96. Huang, H.; Forsyth, C. J., Complementary regioselective cyclopropyl ring openings of 6-formyl-spirobicyclo[5.2]octane mediated by TMSCl and TBAI. *Tetrahedron* **1997**, *53*, 16341.
97. Clark, R. S. J.; Holmes, A. B.; Matassa, V. G., Synthesis of 4,4-Disubstituted Cyclohexenones .3. The Reaction of 1,3-Bis(Trimethylsilyloxy)Cyclohexa-1,3-Dienes with Dienophiles - an Unexpected Rearrangement of the Adducts from the Reaction with 2-Chloroacrylonitrile. *J. Chem. Soc., Perk. Trans. 1* **1990**, 1401.
98. Gao, A. X.; Thomas, S. B.; Snyder, S. A., Pinacol and Semipinacol Rearrangements in Total Synthesis. *Molecular Rearrangements in Organic Synthesis* **2015**, 3-33.
99. Suzuki, K.; Katayama, E.; Tsuchihashi, G., Asymmetric-Synthesis of Optically Pure "Alpha-Methyl-Beta,Gamma-Unsaturated Ketones Via Triethylaluminum-Mediated Stereospecific Pinacol Rearrangement of Alkenyl Groups. *Tetrahedron Lett.* **1984**, *25*, 1817.
100. Nemoto, H.; Miyata, J.; Hakamata, H.; Nagamochi, M.; Fukumoto, K., A Novel and Efficient Route to Chiral a-Ring Aromatic Trichothecanes - the First Enantiocontrolled Total Synthesis of (-)-Debromofiliformin and (-)-Filiformin. *Tetrahedron* **1995**, *51*, 5511.
101. Corey, E. J.; Ohno, M.; Mitra, R. B.; Vatakencherry, P. A., Total Synthesis of Longifolene. *J. Am. Chem. Soc.* **1964**, *86*, 478.
102. McMurry, J. E.; Bosch, G. K., Synthesis of Macrocyclic Terpenoid Hydrocarbons by Intramolecular Carbonyl Coupling - Bicyclogermacrene, Lepidozene, and Casbene. *J. Org. Chem.* **1987**, *52*, 4885.
103. Reisman, S. E.; Ready, J. M.; Hasuoka, A.; Smith, C. J.; Wood, J. L., Total synthesis of (+/-)-welwitindolinone a isonitrile. *J. Am. Chem. Soc.* **2006**, *128*, 1448.
104. Fan, C. A.; Tu, Y. Q.; Song, Z. L.; Zhang, E.; Shi, L.; Wang, M.; Wang, B.; Zhang, S. Y., An efficient total synthesis of (+/-)-lycoramine. *Org. Lett.* **2004**, *6*, 4691.
105. Liu, J. D.; Wang, S. H.; Zhang, F. M.; Tu, Y. Q.; Zhang, Y. Q., Concise Total Synthesis of (+/-)-Crinine. *Synlett* **2009**, 3040.
106. Angeles, A. R.; Dorn, D. C.; Kou, C. A.; Moore, M. A. S.; Danishefsky, S. J., Total synthesis of peribysin E necessitates revision of the assignment of its absolute configuration. *Angew. Chem. Int. Edit.* **2007**, *46*, 1451.
107. Tanino, K.; Onuki, K.; Asano, K.; Miyashita, M.; Nakamura, T.; Takahashi, Y.; Kuwajima, I., Total synthesis of ingenol. *J. Am. Chem. Soc.* **2003**, *125*, 1498.

108. Wilson, M. S.; Woo, J. C. S.; Dake, G. R., A synthetic approach toward nitinol: Construction of two 1,22-dihydroxynitianes. *J. Org. Chem.* **2006**, *71*, 4237.
109. Gerard, B.; Jones, G.; Porco, J. A., A biomimetic approach to the rocaglamides employing photogeneration of oxidopyryliums derived from 3-hydroxyflavones. *J. Am. Chem. Soc.* **2004**, *126*, 13620.
110. Liu, Y. H.; McWhorter, W. W., Synthesis of 8-desbromohinckdentine A. *J. Am. Chem. Soc.* **2003**, *125*, 4240.
111. Fujii, H.; Ogawa, R.; Ohata, K.; Nemoto, T.; Nakajima, M.; Hasebe, K.; Mochizuki, H.; Nagase, H., Aerobic oxidation of indolomorphinan without the 4,5-epoxy bridge and subsequent rearrangement of the oxidation product to spiroindolinonyl-C-normorphinan derivative. *Bioorg. Med. Chem.* **2009**, *17*, 5983.
112. Rashid, A.; Read, G., Quinone Epoxides .2. Synthesis of (+)-Terreic Acid and Some Related Epoxides. *J. Chem. Soc. C* **1967**, 1323.
113. Reisman, S. E.; Ready, J. M.; Weiss, M. M.; Hasuoka, A.; Hirata, M.; Tamaki, K.; Ovaska, T. V.; Smith, C. J.; Wood, J. L., Evolution of a synthetic strategy: total synthesis of (+/-)-welwitindolinone A isonitrile. *J. Am. Chem. Soc.* **2008**, *130*, 2087.
114. Chen, X.; Ke, H.; Chen, Y.; Guan, C.; Zou, G., Cross-coupling of diarylborinic acids and anhydrides with arylhalides catalyzed by a phosphite/N-heterocyclic carbene co-supported palladium catalyst system. *J. Org. Chem.* **2012**, *77*, 7572.
115. Murakami S, S. T., Methods for Preparing Borinic Acid Derivatives and Novel Borinic Acid Derivatives. *US20150105562A1*, **2015**.
116. Iwao, T.; Kinugasa, T., Reorientation of Styrene Groups in Styreneplatinum(II) and Styrenepalladium(II) Chlorides. *Inorg. Chem.* **1972**, *11*, 3106.
117. Moussou, P.; Archelas, A.; Baratti, J.; Furstoss, R., Microbiological transformations. 38. Clues to the involvement of a general acid activation during hydrolysis of para-substituted styrene oxides by a soluble epoxide hydrolase from *Syncephalastrum racemosum*. *J. Org. Chem.* **1998**, *63*, 3532.
118. Kamal, A.; Chouhan, G., Chemoenzymatic synthesis of enantiomerically pure 1,2-diols employing immobilized lipase in the ionic liquid [bmim]PF₆. *Tetrahedron Lett.* **2004**, *45*, 8801.
119. Superchi, S.; Donnoli, M. I.; Proni, G.; Spada, G. P.; Rosini, C., Induction of Cholesteric Mesophases by Simple Cyclic Derivatives of p,p'-Disubstituted 1,2-

Diphenylethane-1,2-diols: Importance of Shape and Polarizability Effects. *J. Org. Chem.* **1999**, *64*, 4762.

120. Ko, K. Y.; Frazee, W. J.; Eliel, E. L., Asymmetric Reactions Based on 1,3-Oxathianes .3. Secondary Alpha-Hydroxyacids, Rchohco2h and Glycols Rchohch2oh. *Tetrahedron* **1984**, *40*, 1333.

121. Xia, Z. L.; Hu, J. D.; Shen, Z. G.; Wan, X. L.; Yao, Q. Z.; Lai, Y. S.; Gao, J. M.; Xie, W. Q., Enantioselective Bromo-oxycyclization of Silanol. *Org. Lett.* **2016**, *18*, 80.

122. Manzocchi, A.; Fiecchi, A.; Santaniello, E., Stereochemical Control of Bakers-Yeast Mediated Reduction of a Protected 2-Hydroxy Ketone. *J. Org. Chem.* **1988**, *53*, 4405.

123. Cordova, A.; Sunden, H.; Engqvist, M.; Ibrahim, I.; Casas, J., The direct amino acid-catalyzed asymmetric incorporation of molecular oxygen to organic compounds. *J. Am. Chem. Soc.* **2004**, *126*, 8914.

124. Poterala, M.; Plenkiewicz, J., Synthesis of new chiral ionic liquids from alpha-hydroxycarboxylic acids. *Tetrahedron-Asymmetry* **2011**, *22*, 294.

125. Krief, A.; Colaux-Castillo, C., Catalytic asymmetric dihydroxylation of alpha-methylstyrene by air. *Tetrahedron Lett.* **1999**, *40*, 4189.

126. Eliel, E. L.; Bai, X.; Ohwa, M., Enantioselective syntheses of substituted gamma-butyrolactones. *J. Chin. Chem. Soc.* **2000**, *47*, 63.

127. Tsuge, O.; Kanemasa, S.; Hatada, A.; Matsuda, K., Synthetic Versatility of N-(Silylmethyl)Imines - Water-Induced Generation of N-Protonated Azomethine Ylides of Nonstabilized Type and Fluoride-Induced Generation of 2-Azaallyl Anions. *Bull. Chem. Soc. Jpn.* **1986**, *59*, 2537.